Intelligent 3D Seam Tracking and Adaptable Weld Process Control for Robotic TIG Welding

By

Prasad Manorathna

A doctoral thesis submitted in partial fulfilment of the requirements

for the award of Doctor of Philosophy at Loughborough University

September 2015

ABSTRACT

Tungsten Inert Gas (TIG) welding is extensively used in aerospace applications, due to its unique ability to produce higher quality welds compared to other shielded arc welding types. However, most TIG welding is performed manually and has not achieved the levels of automation that other welding techniques have. This is mostly attributed to the lack of process knowledge and adaptability to complexities, such as mismatches due to part fit-up. Recent advances in automation have enabled the use of industrial robots for complex tasks that require intelligent decision making, predominantly through sensors. Applications such as TIG welding of aerospace components require tight tolerances and need intelligent decision making capability to accommodate any unexpected variation and to carry out welding of complex geometries. Such decision making procedures must be based on the feedback about the weld profile geometry.

In this thesis, a real-time position based closed loop system was developed with a six axis industrial robot (KUKA KR 16) and a laser triangulation based sensor (Micro-Epsilon Scan control 2900-25). A National Instruments data acquisition system (NI DAQ) was used to carry out input output control. A Fronius Magicwave welding system was used with a push-pull wire feed system to perform welding. Project planning, selection of equipment, purchasing, designing, system integration and setting up of the complete robotic TIG welding cell is included under the work carried out for the PhD. In this research, a novel algorithm was developed for finding joint profiles and path tracking a three dimensional (*3D*) weld joint. Algorithms were also developed to extract joint features in real-time. Empirical models were developed to predict important weld quality characteristics and to estimate weld machine settings based on the weld joint geometry. The developed robotic TIG welding system, along with the intelligent algorithms, was able to carry out welding of a variable gap weld joint with satisfactory results; closely related to skilled manual welders in visual appearance, weld bead dimensions and mechanical strength.

Although this work is presented in the context of TIG welding, the concept is applicable to any arc welding process and other applications such as robotic sealant application

and spray painting. The work presented in this thesis might interest researchers and application engineers who are interested in automating complex manufacturing tasks.

ACKNOWLEDGEMENTS

This thesis is dedicated my loving mother for her enormous efforts to educate me

PUBLICATIONS

The following publications have been generated from the work presented in this thesis:

- R.P.Manorathna, P.Ogun, S.Marimuthu, L.Justham, M.R.Jackson, "*Evaluation of a 3D laser scanner for industrial applications*", 7th IEEE International Conference on Information and Automation for Sustainability, December 2014, Sri Lanka.

- R.P.Manorathna, P.Phairatt, P.Ogun, T.Widjanarko, M.Chamberlain, S.Marimuthu, L.Justham, M.R.Jackson, "*Intelligent joint feature extraction for adaptive robotic welding*", 13th International Conference on Control, Automation, Robotics and Vision, December 2014, Singapore.

- R.P.Manorathna, S.Marimuthu, L.Justham, M.R.Jackson, "*Human Behaviour Capturing in Manual TIG Welding for Intelligent Automation*", Proceedings of the Institution of Mechanical Engineers, Part B: Journal of Engineering Manufacture, Institution of Mehcnaical Engineers, UK.

- R.P.Manorathna, P.Ogun, S.Marimuthu, L.Justham, M.R.Jackson, "*Control of an industrial robot for 2D path tracking*", Manufacturing the Future Conference, Glasgow UK, 2014.: Poster.

- R.P.Manorathna, S.Marimuthu, L.Justham, M.R.Jackson, "*Intelligent method for weld Quality Characteristic prediction*", Under review, to be submitted to the Journal of Engineering Manufacture, 2015.

- R.P.Manorathna, S.Marimuthu, L.Justham, M.R.Jackson, "*Intelligent and automatic selection of TIG welding process parameters in robotic TIG welding*", Under review, to be submitted to the Journal of Engineering Manufacturing, 2015.

The following publications were contributions from the work presented in this thesis:

- S.Fletcher, W.Baker, R.P.Manorathna, P.Webb, M.R.Jackson, "Human Factors Analysis for the Design of Intelligent Automation: using the Systematic Human Error Reduction and Prediction Approach", Submitted to International Journal of Industrial Ergonomics, 2014.

- S.Fletcher, L.Justham, R.Monfared, Y.M.Goh, R.P.Manorathna "Capturing Human Skill and Process Interactions", Manufacturing the Future Conference, Loughborough University, UK, 2012.: Poster.

TABLE OF CONTENTS

LIST OF FIGURES

LIST OF TABLES

GLOSSARY OF TERMS

2D	Referring to two dimensional space
2M	Class of laser
3D	Referring to three dimensional space
A/D	Analogue to digital converter
Argon	Pure shield inert gas
AVC	Arc voltage control
BOP	Bead-on-plate technique
CAD	Computer aided design
CAM	Computer aided manufacturing
CCD	Charge coupled device
CNC	Computer numerical control
CMOS	Complementary metal oxide semiconductor
CO	Carbon monoxide
CO_2	Carbon dioxide
CPU	Central processing unit
DAQ	Data acquisition system
DC	Duty cycle
DOF	Degrees of freedom
EBW	Electron beam welding
ED	Electrode diameter
EPSRC	Engineering and Physical Sciences Research Council
FSW	Friction stir welding
GUI	Graphical user interface
GMAW	Gas metal arc welding
GTAW	Gas tungsten arc welding
HAZ	Heat affected zone
HF	High frequency
IACIM	Centre for Innovative Manufacturing in Intelligent Automation
IRL	Industrial robot language
JOB	Standard welding parameter programming mode
KRC2	KUKA robot controller version 2
KUKA KR16	KUKA KR16 robot

LAN	Local area network
LBW	Laser beam welding
LED	Light emitting diodes
MATLAB	Mathwork's numerical programming language
MCRL	Manufacturing capability readiness level
ME	Micro-Epsilon
MTC	Manufacturing Technology Centre
MIG/MAG	Metal inert gas/Metal active gas
NC	Numerical control
OLP	Offline programming
PAW	Plasma arc welding
PC	Personal computer
PLC	Programmable logic controller
PTP	Point to point
RR	Rolls Royce Plc
SMD	Shape metal deposition
TCP	Tool centre point
TAST	Through arc seam tracking
TIG	Tungsten inert gas welding
TCP/IP	Transmission control protocol/Internet protocol
SMD	Shape metal deposition
STEP	STandard for the Exchange of Product
WAN	Wide area network
WPS	Welding power source

1 Introduction

1.1 Research background

Most modern high-value manufacturing systems continue to depend heavily on the skill and flexibility of manual work. However, in many cases intelligent automation would be a more advantageous alternative to human work by improving operational efficiency and by removing the need for people to carry out tasks in unhealthy, difficult and dangerous working conditions [1]. Welding is one of the most dynamic and complicated manufacturing processes and, therefore, hard to automate. Automation of welding in industrial based applications is even more challenging because engineers are looking at a particular welding process, material, sizes, thickness and weld geometry. These added constraints can make automation more difficult.

TIG welding is considered to be very difficult to automate since it incorporates more process parameters than other welding processes. TIG welding is also difficult to be replaced by another welding process because of its superior weld quality. Therefore, applications such as welding of aerospace components, which require higher precision and quality, continue to use TIG welding. However, as TIG welding robots still do not have the capability to meet the higher precision and quality as manual TIG welding, skilled manual welders still dominate in the welding of high-end welding of aerospace components. As skilled labour is expensive in developed countries, which are continuously challenged by low salary regions in the world, this has motivated industries to continuously look towards TIG welding automation.

Robots which are used presently in the industry are called "Blind" welding robots as they cannot adapt to changes in geometry [1]. Although sensors have been used extensively, sensor feedback has not been used to satisfactory levels in order to achieve adaptivity [1]. Factors such as speed, size, cost and computational power have been the major limitations for not achieving successful automation. This has also made industrial realization of fully automated welding robots a significantly challenging task [2][3]. Therefore currently, weld trajectory and welding process parameters are pre-programmed by the operator. This method has not returned the required quality for welding of aerospace components [4]. Because, compared to other applications such as

automobiles and white goods, aerospace engine manufacture is a low-volume, high-variety, high-value operation with a high rate of change. This requires an automated solution to demonstrate high capabilities in decision making, intelligence and process adaptivity. One example which demonstrates the requirement for adaptive welding is the welding of civil aerospace-engine (Figure 1-1) in the casings and other complex areas. As can be seen from the figure, welding of such high precision components is a complex task, which is only currently achieved by skilled welders. The expected weld quality is not yet returned with robotic welding.
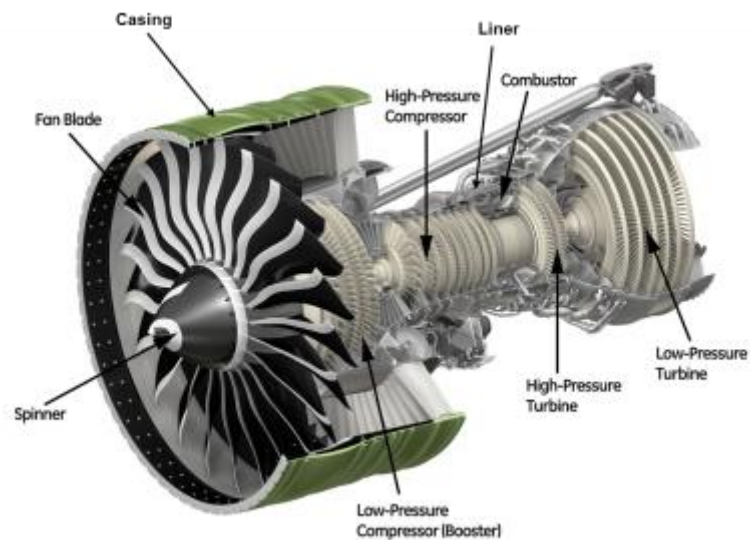
Figure 1-1: An image of an aero-engine section showing important parts[5]

Essential for robotic welding of such complex welding is to have accurate seam tracking, intelligent decision making capability and adaptive weld process control similar to a skilled manual welder. This can be achieved by using feedback about the weld joint geometry and using that to adaptively select the weld process parameters. This leads to controllability over the weld pool shape and can significantly aid in welding complex (*3D*, variable gap/thickness) shapes. Adaptive TIG welding is one of the most discussed topics presently. Paul Gagues at Moog industrial group refer adaptive welding as "*Holy Grail*" of the welding automation industry [6].

Many attempts have been made to achieve adaptive process control and seam tracking which are described in Chapter 2. However, those attempts were not completed to a satisfactory standard to be implemented in the aerospace industry as they have not been able to return the required quality (weld bead shape and welding strength). The work

presented in this thesis describes the research undertaken to demonstrate such a capability, which would be suitable for future use within this industry sector.

Additionally, the use of laser scanners in robotic applications has significantly increased with time and technological advancements. However, laser scanners have not been readily used for aerospace applications due to the shiny surface structure of aerospace components. This results in the laser scanner returning inappropriate data, such as spurious points and noisy data sets, and leads to inaccurate results. Therefore, there is also a research need to investigate methods of reducing the inaccuracies of laser scanners when measuring shinier components and the development of algorithms which can cope with such inappropriate data.

Manufacturing capability readiness levels (MCRLs) are used to describe system maturity of the development of technologies for products in the aerospace and defence industry [7]. In the past, robotic welding solutions were carried out at low MCRL (research level) as shown in Figure 1-2 and fully automated solutions have not been progressed to a satisfactory level (MCRL 3-4) to bring them towards the pre-production stage. This has made it difficult to implement the developments and outcomes of the research at a production level. Hence there is a huge necessity for a robotic welding system which could be transferred in to MCRL 5 so that application engineers can develop the system further with minimum effort and deploy at industrial level.
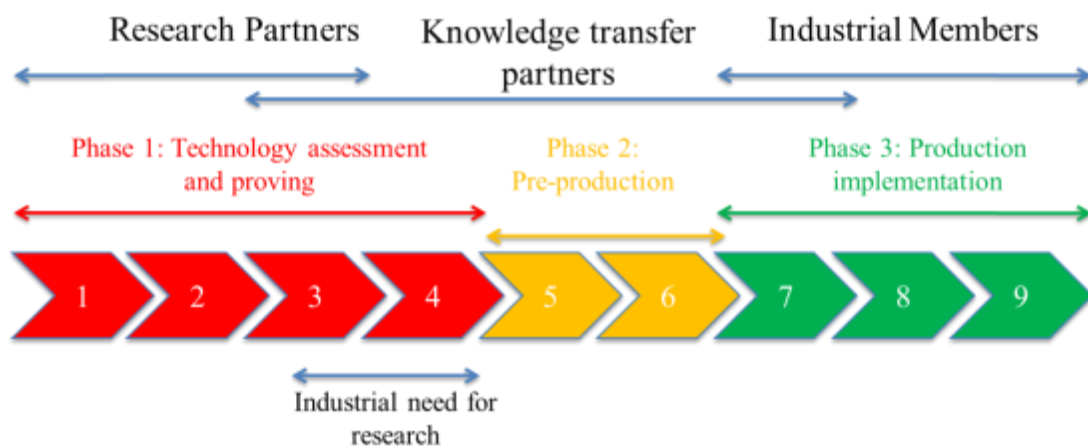
Figure 1-2: Manufacturing capability readiness levels [7]

These factors have led to a renewed interest in creating an intelligent *3D* seam tracking and adaptive weld process, for the control of welding challenging joints.

1.2   Research objectives and novelty

The primary research objective of the work presented within this thesis is the development of a fully adaptable and intelligent TIG welding robot (at MCRL 3) which can perform challenging welding tasks with similar quality to a skilled manual welder.

The research work carried out to achieve this research aim has involved literature and industrial surveys on the current state of the art and formulation and assessment of alternative solutions. The selection of the preferred solution, design and construction of a prototype system and the evaluation and refinement of it has also been included under the work carried out as part of this PhD. This work has included both hardware and software development and complete system integration.

To enable the development of an automated system, which is capable of performing to the same standard as a skilled manual welder, the research within this thesis was initially focussed on developing an approach for understanding the human skills involved in this highly skilled manual task. A system was developed to carry out technical measurements (monitoring process parameter variation) in manual TIG welding by different skilled manual welders and different weld joint types.

Currently data acquisition of information from the shiny components often used in the aerospace industry using laser scanners has been difficult. Therefore, another aim of this research is to understand the capabilities of an industrial laser scanner to perform data acquisition of a shiny component. It is also aimed to find methods to maximize a laser scanner's performance and implement algorithms which are not affected by laser scanner data quality.

To provide a solution which can fulfil the primary research aim, it has also been necessary to develop a method of creating adaptivity in a challenging weld of two thin walled components that are to be welded together in *3D*. This has involved,

- development of an intelligent algorithm for *3D* feature extraction
- development of algorithms for *3D* seam tracking
- novel strategy for robotic welding for aerospace industry
- development of software components for real-time robot and weld machine control
- welding process monitoring and optimization for quality control

4

- empirical model development for quantifying the effect of process parameters on weld quality characteristics
- a strategy for adaptive process control: development of an back-propagation empirical model for the intelligent selection of weld parameters based on joint geometry feedback.

A-priori knowledge generated from theoretical and empirical models and operator experience has been taken advantage of to create an adaptive robotic TIG welding system. A photographic view of the developed system can be seen in Figure 1-3 . Detailed steps involved in the development are described in detail in the following chapters.
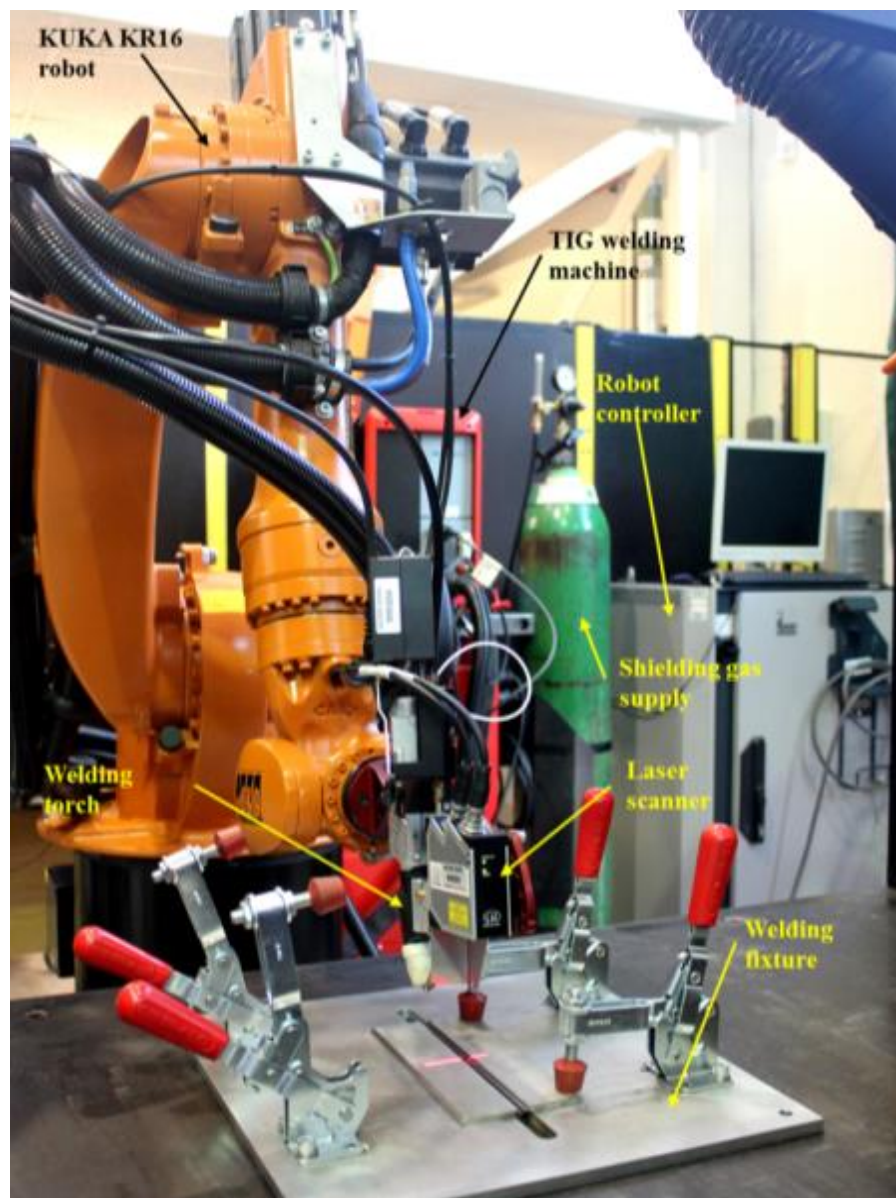
Figure 1-3: Intelligent and adaptable robotic TIG welding system developed by the author

The industrial and research novelties of the work presented in this thesis are listed in Table 1-1.

Table 1-1: Novelties identified

Industrial novelties	Relevant chapter	Research Novelties	Relevant chapter
Development of real-time position based control system for the KUKA KR16 robot	3	Understanding human behaviour in manual TIG welding for intelligent automation	4
Development of PC based control for the Fronius Magicwave 4000 welding machine with capability of setting the welding machine in simulation mode. Feedback control of the welding machine.	3	Performance evaluation of the chosen 3D laser scanner prior to use for data collection. Investigation of data acquisition performance on shiny surfaces.	5
Complete system integration with centralised control and data processing capability	3	Novel algorithm for 3D feature extraction in real time and decision making capability based on the joint fit-up	6
MCRL 3 TIG welding robot	3	3D seam tracking based on joint feature extraction	7
		Empirical model for weld bead dimensions and weld strength prediction	8
		Intelligent back propagation algorithm for selecting machine settings based on the joint geometry	9

	High novelty		Medium novelty		Low novelty

1.3 Project plan

As shown in Figure 1-4, the work was divided in to three stages. Initially, the human skills in manual welding was investigated and studied for intelligent automation. In the second phase, a process parameter monitoring system and *2D* seam tracking along with real-time control of KUKA KR16 was developed. In the final phase, a fully adaptable robotic welding with *3D* seam tracking and adaptive process control was developed. This involved the empirical model development for weld bead shape prediction and the process parameter selection to adapt for variations in joint fit-up.

Figure 1-4: Project plan

1.4 Thesis overview

This thesis contains 10 chapters and they are organized as below.

Chapter 1: The first chapter presents a brief introduction of the topic to be investigated, identifying the motivations which have led to this research. The aims of the research and its objectives are outlined with a clear identification of the proposed novel content of the research. It also contains background information required for the thesis.

Chapter 2: This chapter provides the context for the research and details aspects of existing literature. Focus is placed on the importance of robotic welding, joint feature extraction, *3D* seam tracking, empirical model development for weld bead prediction and adaptable weld process control. An extensive review of the existing methods used in achieving those tasks is also presented.

Chapter 3: Detailed within this chapter is how the system integration was carried out. System specifications of all the equipment used is presented. The method used to integrate the Fronius TIG welding machine, KUKA KR16 industrial robot, National Instruments Data Acquisition System (DAQ), HKS welding sensors, Micro-Epsilon *3D*

laser scanner and IDS *2D* camera. This chapter also presents the software developed using LabVIEW to control the equipment from a single graphical user interface.

Chapter 4: The experiments and results obtained from manual TIG welding is summarised in this chapter. The skilled manual welder's approach to controlling the process parameters is identified. The method of feedback used for decision making and how the complex task of TIG welding is simplified by the skilled welder is also presented. The methodology for adopting the learning from human skill capture in intelligent automation is also discussed.

Chapter 5: In this chapter, the manufacturer specified specifications of a laser scanner are compared with experimentally obtained values. A detailed study was performed to understand the reasons behind the unexpected behaviour of the laser scanner and recommendations where provided to avoid measurement error whilst using it. This is considered to be vital for the validation of seam tracking and gap measurement results.

Chapter 6: A novel algorithm which was developed in Matlab and LabVIEW to extract important features of the joint profile is presented in this chapter. Capabilities such as real-time functionality and functionality to deal with unexpected data from the laser scanner (missing data issue) were achieved by the developed feature extraction algorithm. Performance evaluation results of the algorithm under various weld joint geometries (*U, V* and *I*) and fit-ups are also presented in this chapter.

Chapter 7: Initially the hand-eye calibration methodology is discussed in this chapter which is followed up by *2D* seam tracking using a CMOS camera. The method of using a feature extraction algorithm to estimate the centre of the joint to perform seam tracking is then presented. The seam tracking algorithm was evaluated for performance under various joint geometries and fit-up in *3D*. Results of initial welding trials are also presented.

Chapter 8: The work carried out on development of an empirical model for prediction of the weld bead dimensions and welding strength based on statistical methods is discussed in this chapter. Using the empirical model, the effect of each process parameter on weld quality characteristics was quantified. Validation experiments were carried out and the estimated values are compared with actual values for checking the level of validation of the empirical model.

Chapter 9: The proposed novel methodology of using joint geometry for the intelligent selection of the TIG welding machine settings to control the welding process adaptively is presented in this chapter. The identified most significant process parameters are prioritized to simplify the control problem. Welding of a variable gap butt-joint was investigated as a case study. Four approaches of carrying out welding of a variable gap weld joint were studied; constant parameter approach, industrial approach, skilled welders' approach and the proposed novel approach.

Chapter 10: Conclusions stating what was presented in this thesis and what are the next steps involved is identified.

2   Literature Review

This chapter provides the context for the research and details aspects of existing literature in this area. Focus is placed on the importance of robotic welding, joint feature extraction, 3D seam tracking, empirical model development for weld bead quality prediction and adaptable weld process control.

Section 2.1 provides basic introduction to concepts discussed in the thesis and section 2.2 to 2.7 gives detailed literature review.

2.1   Background

2.1.1   Industrial robotics overview

The main aims of automation in the manufacturing industry are to improve product quality, productivity and uniformity while reducing effort, cycle time and labour cost [8]. Presently robots are used extensively to do this. "*An industrial robot is an electromechanical device, which can be defined as an automatically controlled, reprogrammable, multipurpose manipulator programmable in three or more axes to accomplish a variety of tasks*" [9]. Commercially available robots may be powered by either hydraulic, electric or pneumatic drives [10]. Modern day applications of robots include welding, assembly, painting, packaging, pick and place and inspection. Robots are especially used for tasks which are considered to be hazardous if carried out by humans such as welding, in space and underwater tasks. Robotics is a field which combines mechanical and electrical systems, sensor technology, computers, servo systems and software [11].

A robot can be programmed in many ways [12], such as:

- Lead-through programming: The human operator physically grabs the end-effector and shows the robot exactly what motions to make for a task, while the computer saves the motions (memorizing the joint positions, lengths and/or angles, to be played back during task execution).

- Teach programming: Move the robot to the required task positions via the teach pendant; the computer stores these configurations in memory and plays them

back in robot motion sequence. The teach pendant is a controller box that allows the human operator to position the robot by manipulating the buttons on the box. This type of control is adequate for simple, non-intelligent tasks.

- Off-line programming: Use of computer software, with realistic graphics, to plan and program the motions of robot without use of robot hardware. The robot memory is connected to the offline system so that the programme can be downloaded.

- Autonomous: Controlled by computer, with sensor feedback, without human intervention. Computer control is required for intelligent robot control. In this type of control, the computer may send the robot pre-programmed positions and even manipulate the speed and direction of the robot as it moves, based on sensor feedback. The computer can also communicate with other devices to help guide the robot through its tasks.

- Tele-operation: Human-directed motion via a joystick. Special joysticks that allow the human operator to feel what the robot feels are called haptic interfaces.

- Tele-robotic: Combination of autonomous and tele-operation methods.

In robotics, the term "end effector" is used to describe the gripper or tool that is attached to the wrist of the robot [10]. This can be a welding torch, gripper or any other tool required to perform the task. Industrial robots also comprise communication interfaces to communicate with external devices such as sensors, PLCs and PCs. Robots are capable of receiving signals from external devices and can also be used to control another device. However, this has to be programmed in the software interface.

The robot work volume is the term referring to the space within which the robot can manipulate its wrist end. The work volume is determined by the robot's physical configuration, size (body, arm and wrist components) and the limits of the robot's joint movements [10]. It should be noted that when a tool is fixed to the wrist of the robot, the work volume will be increased. The work volume of the KUKA KR16 robot is shown in Figure 2-1 [13].
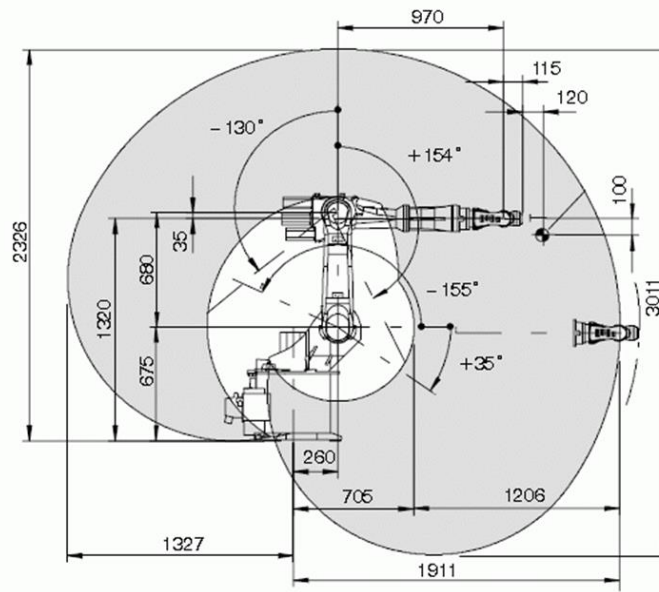
All dimensions are in millimetres

Figure 2-1: Robot work volume[14]

2.1.2 Triangulation-based 3D machine vision techniques

Triangulation is a geometrical calculation method to find the *3D* coordinates of a point using one or more cameras. It takes pixel coordinates of a *3D* point in the images taken at two views and transfers it to the camera frames. From that it is then transformed into the world frame. Triangulation based *3D* vision techniques can be categorized into two groups based on the light used. That is passive vision using ambient lighting and active vision using structured light. The most commonly used *3D* passive vision technique is stereo vision where two images are used to find *3D* information as shown in Figure 2-2. In the case of structured light systems, a projector is used with a single camera as shown in Figure 2-3 [15]. These techniques will be discussed in more detail in Chapter 2.
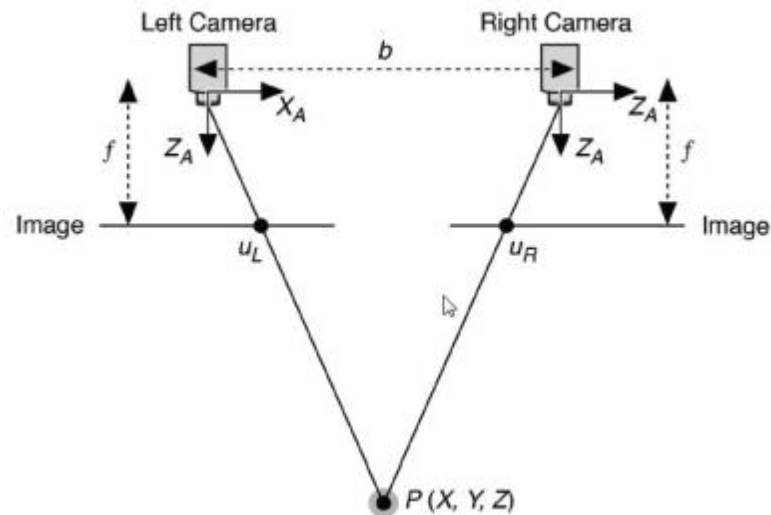
Figure 2-2: Stereo vision principle[16]
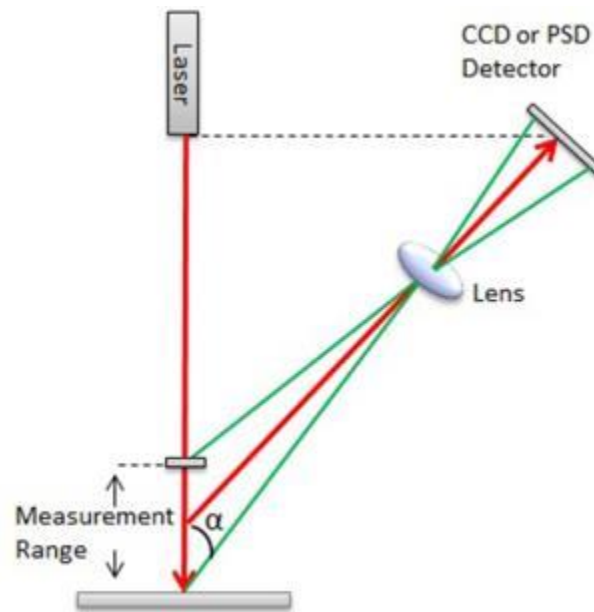
Figure 2-3: Laser scanner principle[17]

2.1.3 Welding

Welding is a process used by metal fabricators for joining similar metals. Joining is achieved by melting and fusing the base metal and also through the application of a filler metal. Welding processes operate at temperature ranges from 800ºC - 1650ºC, depending on the material, welding parameters used, shielding gas and welding process type. Presently welding is popular in the automobile, aerospace, oil and gas industries [18].

2.1.3.1 **TIG welding process**

TIG welding is an arc welding technique in which the arc is maintained by a tungsten electrode in the welding torch and shielded from the ingress of air mostly by an inert gas as shown in Figure 2-4. A filler rod is also used to fill the gap between the sample plates. Usually the filler rod is fed to the front end of the melt pool [18].
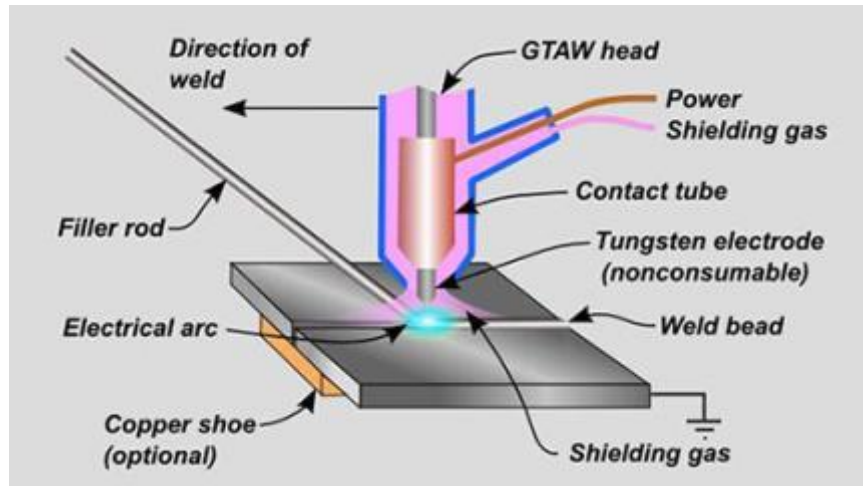
Figure 2-4: TIG welding principle[19]

2.1.4 Stainless steel and its alloys

Stainless steel covers a wide range of steel types and grades, used for corrosion or oxidation resistant applications. Welding is often used for their joining. Stainless steel alloys are made by including Chromium, Nickel, Molybdenum, Titanium, Carbon and Nitrogen. These additions enhance the material properties such as formability, strength and cryogenic toughness [18].

2.1.5 Shielding gasses

Contamination to the welded joint is caused mainly by nitrogen, oxygen and water vapour present in the atmosphere. This can lead to the mechanical properties of the weld being altered in a non-controlled manner. For example, nitrogen in solidified steel can reduce the ductility of the weld and can cause cracking or weld porosity (air traps in the metal). The reason for the porosity is oxygen reacting with carbon to form carbon monoxide (CO). Oxygen also can react with other elements in the steel and form compounds that result in inclusions in the weld. If hydrogen is present the vapour reacts with iron or aluminium and can result in under-bead weld metal cracks. To prevent these defects, the air in the welding zone has to be displaced using shielding gasses. Argon, Helium and Carbon dioxide (CO_2) are the three main gases used for shielding.

Argon and Helium are inert gasses and therefore are used extensively in the welding industry [18].

2.1.6 TCP/IP communication

TCP/IP stands for "Transmission Control Protocol / Internet Protocol" [20]. TCP/IP was developed by the US department of defence. It is a network protocol that defines how data can be sent through network resources such as hubs, switches, adapters and routers. After it was developed by the defence department it was placed in the public domain so that anyone could use it to develop communication networks between different pieces of equipment. Since TCP/IP is the primary protocol used on the Internet, it has become the most popular and is supported by most systems and hardware. The TCP/IP is designed in such a way that each peripheral device connected will have its own address called the "IP address". 65535 ports are available to communicate over each IP address for sending or receiving data [21]. Currently most computers integrated with robots communicate with each other through the TCP/IP protocol. This has significantly benefitted industrial automation.

2.2 Similar work in arc welding automation research in the UK

Apart from the EPSRC-IACIM at Loughborough University, other communities conducting research in the area of arc welding automation in the UK have been identified. They are the Department of Mechanical, Materials and Manufacturing Engineering: University of Nottingham [22], Advanced Manufacturing Research Centre (AMRC): University of Sheffield [23] and Warwick Manufacturing Group (WMG): Warwick University [24]. Similarly to the EPSRC–IACIM, one of the missions of these groups is to conduct research aimed at the welding of challenging components. The work presented in this thesis is novel and notably different to the work being carried out elsewhere in the UK, in the following areas:

- TIG welding automation is considered in this thesis which is harder to automate than other arc welding processes.
- Investigation of the manual skilled welder's behaviour for automation.
- Experimentation of the laser scanner's performance to identify best performance and evaluation of the laser scanner specifications within an unstructured environment.

- Development of the novel feature extraction algorithm whereas other researchers used the software provided with the laser scanner.

- Development of seam tracking algorithms which functions irrespective of the joint profile.

- Development of a 3D seam tracking strategy based on the part fit-up (relative geometrical orientation between the samples in 3D space).

- Use of the actual welding condition (welding of two plates) for experimentation into the effect of the process parameters on the weld quality characteristics. Previous studies have used bead-on-plate technique rather than the actual welding condition.

- Quantification of the effect of the welding process parameters and development of an empirical model for predicting robotic weld quality characteristics (weld bead dimensions and welding strength).

- Development of a back-propagation empirical model to provide adaptation for variable gaps through intelligent control of the welding machine settings.

- Development of a robotic system capable of carrying out scanning and welding automatically. Selection welding parameters in continuous-mode rather than in JOB/Programme mode (where welding programmes need to be pre-stored in the welding machine). No additional programming required at the welding machine.

- Development of a complete solution where the whole adaptive welding process is fully automated (no offline processing needed).

2.3   Welding Automation

Many new challenges exist for the metal fabrication industry in the 21st Century. Fabricators must fulfil the demand for better quality with an overall lower cost and increased yield. Productivity is a major concern with a shortage of skilled workers and the added health and safety concerns [1][25]. The number of existing welders is not enough to satisfy the increasing demand from the industry, According to American Welding Society (AWS) over 500,000 welders are employed in the USA and approximately 200,000 welders are still required to meet demand [25][26][27]. Profitability and sustainability is under continued pressure from strong worldwide competition. As a result welding automation is one of the most discussed topics today.

2.3.1 Evolution of welding robots

Welding became one of the frequently used operations in assembly-line production systems when Henry Ford introduced the assembly line [28]. Automating the welding process was initiated in the mid-20th century [29]. In the 1970s the first trials on robotic welding were carried out with only a small success rate. These traditional robots used hydraulic and air type actuators which made movements difficult in certain directions. In 1973, electric drives were introduced by ABB robotics (Previously ASEA), and the first welding robot was produced in 1975, which is shown in Figure 2-5[30].

Figure 2-5: First welding robot developed by ABB (IRB 6) [19]

Latterly, methods like numerical control (NC) technology have been incorporated with automated welding and with the integration of technology from computers to welding robots, the task has become even more precise and simple [31]. During the last 30 years robots used for welding have become lighter, more compact, more sophisticated and cheaper which creates an ease to accommodate smaller and more complex shapes [32][33].

Rolls Royce was one of the first aero-engine manufacture companies to introduce automation in to their production line in the 1970s [34]. The most recent robotic processes introduced into Rolls Royce are for laser maskant cutting, welding and plasma spraying [34][35]. Robotic Shaped Metal Deposition (SMD) was completed by Rolls Royce in 2004 where the welding process was used as an additive manufacturing process to build up a complex shape [36]. Many more successful projects related to automation of manufacturing processes using robots have been completed by Rolls-Royce. This information is not currently in the public domain.

SimTech, Singapore has developed a robotic system for repair of aero-engine parts using TIG welding [37]. Fraunhofer Institute for Laser Technology (ILT) has also developed a laser metal deposition system with a laser scanning system which measures the wear of gas turbine components and carries out laser cladding processes for repair [38]. Recently GKN Aerospace has also successfully developed a robotic Electron Beam Welding (EBW) system to achieve higher production rates [39]. However, robotic welding in the aero-engine manufacturing industry has not achieved the required level of automation to satisfy the required quality. Therefore this area is still being researched by research institutions and universities to achieve the required confidence levels [22].

Today, robotic welding is performed in many locations from small workshops to underwater and in space. Industrial robots have now been used for resistant spot welding, gas metal arc welding (GMAW) and Laser Beam Welding (LBW), among others, for many years. However, TIG welding has proven to be a difficult welding process to automate and therefore automation has not been realised to a satisfactory level [40]. The most closely to an automated TIG welding system deployed in the industry is by the Advanced Manufacturing Research Centre [23]. Other than this there was no evidence was found in previous literature.

Some of the benefits that industries have experienced recently, when considering robotic welding processes, are improved weld quality, increased productivity, reduced waste, decreased labour costs and improved accuracy. For example, The Mercedes-Benz Corporation and CORSA Performance, Inc. experienced a significant rise in process productivity and product quality with the implementation of robotic welding in the assembly of their auto parts [28]. Jim Bowling, the owner of CORSA, says that the decision making process also eased with the adoption of robot welding systems instead of manual welding [41].

In summary, robotic welding related to the aerospace engine manufacturing industry is still at research level and a complete robotic solution with process and part adaptability is yet to be introduced. Though some welding processes in the automobile industry are being already automated, the TIG welding process has not reached a satisfactory level of automation.

2.3.2 System issues and new technologies in robotic welding

Tool centre point repeatability, part fit-up, low speed, poor wire feedability, contact tip failure, fumes, spatter, equipment reliability and accessibility are some of the challenges faced with the automation of welding [42]. Therefore, achieving controllability during welding has been difficult due to the small size of the weld pool, short interaction times, extreme brightness of the welding arc and the high temperatures achieved during welding. These factors have served to make experimental studies difficult [43]. Among them, the brightness of the arc has been one of the major problems as vision sensors get saturated due to the extreme amount of photons reaching its sensor. Different techniques have been used to overcome this. One such method is to use a band-pass filter with a light source at the same wavelength as the arc light so that the whole spectrum of light is eliminated [44]. This technique has evolved so the vision sensors can be used to observe the weld pool without any disturbance from the arc [45]. Weld pool information can be used to make real-time decisions about the welding process parameters and robot position. For example, by observing the weld pool position relative to the weld joint, small deviations which can occur in weld pool position in 3D (due to gravitational force) can be minimized.

At the start-up of welding, due to the instability of the welding arc, the quality of the weld can be affected. This initiation often creates weld failures due to spatter generation and a discontinuous weld profile. The manual welder has the required experience and capability to react to any disturbance, but, a robot may not have such an instantaneous and unpredictable decision making capability and therefore can produce a poor weld quality at the start. The reaction of the automated system at the start-up of welding must be controlled for a better quality of weld. One such method implemented with MIG welding is discussed in [46]. In this, the authors have studied the wire melting and transporting in relation to the wire feed rate. Different methods, which are used in the power sources during start-up period, were also modelled.

Advanced power supply technology, improved torches and torch gun consumables, feeding systems and the use of a large variety of support robotic peripherals such as cleaners, wire cutters, tool centre point calibrators, seam tracking devices and welding monitoring systems, have provided more opportunities for automation [31]. Welding power supply companies have introduced technology for creating custom pulse waveforms in the welding current signal. This has enabled the operators to select the

waveform according to the challenge of the welding task [47]. This has increased the degree of controllability in automation.

In a manual system the worker can adapt to product variety, whereas it is much harder for a robot. Therefore one of the problems in welding automation is its lower flexibility to job variety which makes it difficult to implement in an assembly line (For example in the automobile industry). However, the introduction of computers has enabled the storage of large numbers of welding programmes and robot programmes. Robotic systems can be programmed in JOB/Programme mode where parameters are stored for different welding tasks. However, this method is an open-loop configuration and does not provide an intelligent feedback control to achieve adaptivity for any sudden changes. Moreover, currently, welding of 3D parts is carried out by separating the component into a set of regions where each region will be programmed with its own set of process parameters. This method can lead to substandard welding quality because any sudden change of process parameters could cause welding defects or weakened joints.

Flexibility of welding cells can be achieved by designing adjustable fixtures which could adjust to product variability. Motoman Robotics has created such an adjustable fixture called Motomount [48]. Yantai Evergreen Precision Machinery Co., Ltd and Puqi Machine Ltd have also produced adaptable chucks with clamps functioning independently [49]. Such flexible fixtures can accommodate product variety and therefore can reduce the need for altering setting up processes in an assembly line.

The productivity of welding robots is another area which has been extensively investigated. According to previous studies such as in [50], robot use has been shown to improve yield compared to humans. However with increasing demand for welding, even robots have to be designed to obtain more and more productivity. One such method is by using dual wires resulting two independent arcs. This has been successful with GMAW and laser welding [33][51][52]. A commercial example of the dual wire technology with MIG welding completed for Garden State Chassis by Lincoln Electric Company is given in [53].

Automation of the end effecter using servo controlled systems called Servoguns with wire feeders have been tested successfully for spot welding. This is one of the recent technologies which has been used successfully in Japan and Europe [32][33]. Smooth

operation with less noise, increased control and continuous monitoring over position and force, faster response, longer tool life, increased accuracy and complete elimination of compressed air and oil are a few of the advantages of Servoguns. A commercialized version of Servoguns is presented in [32].

One inherited problem in automated welding is its extensive use of jigs and fixtures compared to manual welding. Therefore some amount of material distortion due to the stresses encountered from the fixtures and an effect on cooling rate is always present [54]. However, in spite of this, there is very little work which has been found to have been carried out on understanding the effect of using jigs and fixtures on deformation [54]. However, deformation is minimal in welding performed on aerospace components due to the materials used, component size and the use of heavy fixtures [55]. Therefore this thesis does not take in to account deformation during welding.

With the expansion of welding automation in industry, networking has become increasingly important. Information sharing in automated welding through local or wide area networks (LAN and WAN) has been performed using common protocols such as Ethernet, DeviceNet and ProfiNet [33]. This has enabled collaboration between welding robots and now assembly lines are fully automated for carrying out welding (such as arc welding, spot welding) tasks completely automatically (especially in the automobile industry) [56][57]. A method for planning industrial robot networks for automotive welding and assembly lines is described in [58]. A robotic welding production line, where multiple welding robots communicating together to perform welding tasks in the assembly line in an automobile production line, can be seen in Figure 2-6. Recent research work on the development of collaborative welding robots is presented in [22] on the plasma arc welding process. In this the researchers detail the methodology of establishing communication between two robots to perform welding on a complex shape.

Figure 2-6: Collaborative robotic welding[53]

2.3.3 Welding automation in harsh environments

Today, technology has advanced to enable automated welding in various harsh environments; for example underwater and in space [59][60]. However, most existing welding technologies used with atmospheric welding have to be modified to accomplish automated welding in these environments.

Most ship repairing processes are carried out in shallow depth, causing only minor difficulties. The major challenging task lies in undertaking work in deep water such as repairing underwater pipelines. The usual practice in the past has been to take the pipes out from the water and perform repairs which make it costly and time consuming. But today, deep-water welding is carried out with The British Admiralty – Dockyard carrying out the first ever underwater welding task in 1972 [61]. However, high pressure due to the water head, chilling action and risks involved are but a few of the concerns associated with underwater welding [61]. Lack of visibility in water, presence of sea current, difficulties for after weld inspection, ground swells in shallow water and inferior weld qualities are some of the negative results experienced [60]. Automation of TIG welding has also been attempted to a certain extent underwater. One such example is the THOR – 1 (TIG Hyperbaric Orbital Robot) in which a diver performs only the pipefitting and installing the trac and orbital head on the pipe and all the other tasks are performed through an automated setup. Advancements in driverless welding systems over the past decade have eased difficulties in tasks such as pipe preparation, pipe

aligning, automated wire feed and robot operation [61]. A manual welder attempting to carry out repairs using underwater welding techniques is shown in Figure 2-7.

Figure 2-7: Underwater welding[62]

Space is where most technologies are yet to be experimented with and certainly welding is one such area. Repair of orbital debris, fatigue damaged lab modules, radiators, pressurized fluid systems and structures, solar collector arrays, surface vehicles, descent-ascent vehicles, aero-brakes, power plants, antennas and maintenance of various other equipment are some of the tasks which can be assisted by automated welding [59]. According to Dr. Eager, in the mid-1980s the National Aeronautics and Space Administration's (NASA) in-space joining techniques were restricted to mechanical fastening and adhesive bonding [59]. But compared to those techniques, welding has proven to have a higher joint rigidity and strength, lower joint mass, simpler joint design and manufacturing, lower cost, higher joint reliability and wider repair versatility [63]. Therefore exploration into how welding automation may be deployed in space has been researched thoroughly in the past three decades. NASA's tasks such as Space Station Freedom (SSF), the First Lunar Outpost (FLO) and the Manned Mission to Mars (MMM) has forced automation researchers to look into tools for carrying out automated welding in these difficult conditions [59].

2.3.4 Calibration of the robot-welding system

Weld tool calibration

The weld tool calibration is usually performed using a defined point placed in the work area. When the tool centre point makes contact with this point, the pose of the robot hand is stored. Another way of doing this is by using equipment such as theodolite or a laser interferometer [64].

Camera calibration

A camera model comprises the *2D* points in an image of *3D* features outside the camera. Any camera model consists of both intrinsic and extrinsic parameters. Focal length, principal point and distortion parameters are considered as intrinsic parameters whereas camera pose relative to the world coordinate system is considered to be the extrinsic parameter [64]. The traditional way of calibrating a camera is by using a checker board pattern [65][66]. It can be performed by matching the corner points with the image corner points. There are many approaches to do camera calibration such as Tsai's method [67], Heikkila's method [68] and Zhang's method [69]. In [70], a method called the explicit method has been used to obtain camera intrinsic parameters. This can also be done by the camera calibration toolbox provided by Matlab and LabVIEW.

Robot hand-eye calibration

The relationship between the robot base and the end effector can be found using the Denavit-Hartenberg method as presented in [71]. This method has been used frequently in most robotic applications to find the pose of the end effector relative to the base coordinate system. It is vital to find the transformation representing the camera mounting position relative to the robot end effector frame. By observing the resulting motion of the sensor created by moving the robot, this transformation can be found as described in [72]. Over the years, many models have been developed to find the relationship by solving homogeneous transform equations of the form *AX=XB* where, *A* is the transform matrix for the relative motion made by robot, *B* is the transform matrix for the relative motion of the camera and *X* is the unknown camera pose relative to the wrist orientation. A low cost robot hand-eye calibration method is presented in [71] with an accuracy of 1mm. It allowed the camera and object frames to be referenced directly to the robot base co-ordinate frame.

Two ways of solving the homogeneous matrix equation in the form *AX=XB* is presented in [73]. Another example of calibration based on this relationship is presented in [74] for a system with laser vision. In [72] the authors investigate the solution to the above equation and have found that it is not unique and has one degree of rotational freedom and one degree of translational freedom. In [75] a model for obtaining the camera pose related to the base frame is presented. An Ant colony optimization algorithm has been used and the results show that the welding trajectory generated has greater accuracy compared to conventional *PID* and fuzzy controllers. In [65] the authors have also used the *AX=XB* model to obtain the relationship between the robot wrist frame and the camera frame by using a single camera and double position method. Another low cost calibration method is proposed in [66] which allows the object reference frame to be directly related to the robot's base frame without the use of expensive coordinate measuring devices. The accuracy achieved was ±1mm.

Self-calibration

Self-calibration is a feature in modern robots equipped with vision systems which makes the task more simplified for consumers. In such a system no external calibration equipment is required and the camera's intrinsic parameters are determined with a series of images taken. It has been also identified that the minimum images required to find the camera intrinsic parameters in such a system is three [76]. This increases the adaptability of a vision system to be used for real time applications such as robotic welding with reduced difficulty in setting up.

2.4   Human skill capture and its involvement in welding automation

Human behavior and skill capturing is identified as an important aspect in automation of complex manufacturing tasks which are considered difficult to be automated. Also it is also important for introducing continuous improvement to existing automation systems, for example, to simplify the complexity in a particular task in robotic welding.

2.4.1   Human skill capture

Most modern high-value manufacturing systems continue to rely heavily on the dexterity and flexibility of the manual worker. However, in many cases intelligent automation would be a more advantageous alternative to human work by improving operational efficiency and by removing the need for people to carry out tasks in unhealthy and/or difficult/dangerous working conditions [40]. Although technological

advances are increasing, possibilities to develop intelligent automation solutions to replace human work have not been fully implemented. This is because it is not clear exactly what to automate, i.e. to understand which elements of manual welding tasks are most suitable for transfer to automation. It is relatively straightforward to measure physical activity using objective motion capture systems. However, a key obstacle to the development of intelligent industrial automation is that welding tasks often involve a significant amount of unobservable cognitive activity that cannot be captured as easily [77]. Therefore, to successfully develop intelligent automation alternatives, we need to be able to capture the complex and concealed human cognitive skills and knowledge requirements of manual TIG welding as well as the physical elements of the tasks. It is also important to gauge the degree to which these tasks afford human variations [77].

A descriptive study has been completed in [78] on identifying the differences between skilled and unskilled welders by analysing the positional data obtained with a networked *3D* motion capturing system with IR cameras. Movements of the human arm were captured and compared with different skill levels. In [79] and [50] the authors emphasize that the development of adaptive weld process control systems must be approached in a similar way to a skilled manual welder. In [80] the authors have designed a vision sensing and control system which can emulate a skilled welder's intelligent behaviours such as observing, estimating, decision-making and operating. A novel electric welding helmet that uses real-time high dynamic range (HDR) video processing with a small battery-powered device is presented in [81]. This was proposed to aid the manual welder's visibility of the welding area. Authors have found that the developed helmet aided welders and observed increased quality in the welds.

Modelling of the human welder was carried out at the University of Kentucky recently (2014) by Kim and Zhang [77]. The authors have focused upon quantifying the welder's intelligence. This included sensing the weld pool and modelling the welder's adjustments during welding. As an extension to this work the authors also developed a *3D* vision based weld pool viewing system. In this work, the authors have discussed a methodology for transferring the human intelligence model in to a robotic welding system. The work also involved extensive surveys on modelling human dynamics and neuro-fuzzy techniques[1]. Closed-loop control experiments were also carried out to

---

[1] neuro-fuzzy refers to combinations of artificial neural networks and fuzzy logic.

illustrate the robustness of the model-based intelligent controller. The developed human model was compared with welders and presented in [82]. It was observed that the model was adapting to disturbances occurring in the process. The Authors also observed a high robustness in the developed human intelligent model. Although, the relevance of the work at Kentucky for robotic welding is presented, the authors have not implemented their human intelligent model in an actual robotic welding system.

In summary, the work carried out on human skill capture has not been implemented on a robotic welding system. Research on human skill capture should focus more to be carried out to develop a more simplistic control model which can be implemented on robotic systems with reduced difficulty.

2.4.2   Human-robot cooperation in welding automation

Human Machine Interfaces (HMI / Tele-operation) is another growing trend in robotics and automation [83]. This is a method where the operator can virtually present themselves at the actual place of operation and carry out the task with the assistance of a robot. Technologies such as virtual reality, augmented reality, wearable systems and ubiquitous computing are used to create HMIs [83]. An HMI tool is an excellent replacement for jobs that are considered to be dangerous, difficult or tedious for human operators. An interesting project on networking humans and robots is discussed in [84]. The importance of robot-robot and human-robot cooperation in the manufacturing industry is highlighted in [85]. A human-robot collaboration work carried out on teaching the path of a welding torch by the manual operator is shown in Figure 2-8.

Figure 2-8: human-robot collaboration in welding[57]

2.5   Seam tracking in welding automation

Seam tracking sensors are the most frequently used sensor systems in robotic welding. Seam tracking for welding has been performed using various techniques such as mechanical, electrical, sonic, magnetic and optical methods [15][86][87]. However, optical methods are often preferred as they are more accurate, robust and more straightforward to integrate into a system. Moreover, it is a non-contact method [15]. Therefore, in this thesis only the optical based method for seam tracking is presented.

The seam tracker monitors the location of a weld joint and links with the robot control system to track the joint. A good seam tracker should not only consider positional accuracy but also the velocity and acceleration checks that are important in welding and other operations such as spray painting, sealant application and assembly [11][15].

2.5.1   Evaluation of seam tracking

The work carried out on seam tracking in the past can be divided into three generations. The first generation, often called the two-pass approach, surveys the seam along a pre-taught path before performing welding. In the second pass, welding is carried out along the path points found during the first phase. The main problem in this method is the time taken for pre-surveying. This concern was the reason why the second generation was developed, as it delivers real time seam tracking.

Systems belonging to the second generation had to deal with the presence of arc light and spatter. However second generation welding was performed in structured environments more often than not and therefore a major concern was on the adaptability to sudden changes. Hence the third generation of seam tracking systems were focused on achieving adaptable, real time and intelligent control [15]. Ideally in the third generation, the robot should be able to adapt itself to changes occurring from distortions in the work piece shape due to factors such as temperature and variations occurring due to changes in part fit-up and joint preparation. This is achieved by incorporating machine vision to robotic welding systems.

In the aerospace industry, second and third generation solutions are not yet feasible due to several reasons [15]. One such reason for this is that intelligent decisions cannot be made in the second or third generation seam tracking systems as prior knowledge of the weld joint is not available. Such a decision can only be realised if prior knowledge of the joint fit-up is known which can only be obtained in the first generation seam

tracking systems. This is vital in the aerospace industry as a attempting to weld a faulty set-up without prior knowledge can lead to waste, time and high cost.

2.5.2 Seam tracking techniques

Commonly there are two types of seam trackers, namely through-the-arc seam trackers and triangulation based scanners which operate based on vision techniques.

2.5.2.1 Through-the-arc sensing

The through-the-arc measuring technique is based on the fact that changes in the joint geometry will be reflected in corresponding changes in the process parameters such as arc voltage and current. This method has the advantage of directly sensing the local environment at the torch tip. However, the disadvantages of this method are that it cannot provide global information about the area around the joint and also it needs additional motion of the torch (weaving motion). Through-the-arc seam tracking is useful in Submerged Arc Welding (SAW) since optical methods are less effective because the electrode, joint sides, molten pool and the arc are hidden from direct viewing [15]. Commercialized versions of through-the-arc seam tracking are developed by FANUC robotics [88] and ABB robotics [89].

2.5.2.2 3D vision sensing

Vision sensing has been by far the most studied and discussed topic in seam tracking systems. One of the main advantages of this technique is that it is independent of the welding process. Secondly vision sensing has the capability of gathering global information such as part fit up, height mismatch and root gap. It has been proven to be more accurate compared to through-the-arc sensing [15] and the only drawback is the high cost of the equipment. *3D* vision sensing has been used in many industrial applications, including dimensional inspection of white motor body, Printed Circuit Board (PCB) and Integrated Circuit (IC) inspection, *3D* shape re-construction, surface inspection, welding, and drilling [52].

The *3D* position and orientation of an object can be found by monocular vision, stereo vision, dense/sparse range sensing or tactile sensing. Monocular vision uses only one view with pre-defined object dimension while stereo vision uses two views. A dense range sensor scans a region of the world coordinate system with as many scanned points as possible and a sparse range sensor scans only a few points which are adequate to locate any given position. *3D* vision sensing can be classified as stereo vision systems

29

and laser triangulation based systems [15]. Stereo vision systems use two cameras while the laser triangulation systems use one camera and a structured light projector instead of the second camera.

Seam tracking using visual techniques can be undertaken using four different approaches which are,

1. Teaching the seam path with prior knowledge of its geometry. (Eg: CAD data)
2. Teaching an unknown seam trajectory.
3. Real time tracking of a seam with previous knowledge of its geometry.
4. Real-time tracking of a completely unknown seam.

The nominal seam of the first three approaches can be obtained by manual programming, previous seam teaching, from a CAD file or any offline programming method. However the fourth approach is far more complex and difficult since all the parameters and control signals have to be determined in real-time [90].

In previous literature, studies using visual servoing for seam tracking have made use of two control architectures, namely position based control and image based control. In position based control, details are obtained from the camera and used with the geometric data available of the seam. In image based control the use of geometric data is omitted and servoing is done on the basis of the image data directly. However in [90] the investigators state that real-time seam tracking without any prior knowledge is considered to be impractical due to safety reasons. Therefore this thesis will consider position based control which will be discussed in detail in this section. In [90] the authors present an image based system with mathematical models of the seam, real-time seam tracking, orientation correction and noise filtering. The experiments have been carried out to track a planar line and a curve with accuracies of 0.1mm for a line and 0.5mm for a curve.

Stereo vision based sensors

There are many ways of obtaining *3D* information as discussed previously. Among them, stereo vision sensors have a distinct advantage over other methods since they can achieve 3D image acquisition without moving parts [76]. These systems are available with single and multiple cameras. Modern applications of stereo vision range from structure modelling and medical imaging to tracking and obstacle avoiding in mobile

robots [75][91]. The requirement in stereo imaging is to take images from different angles and merge them using a method called stereo matching [91].

The 3D seam of any work piece can be tracked as follows using stereo vision [75].

1. Projection of laser light onto the seam surface (optional).
2. Capturing two images from the cameras placed at different angles.
3. Stereo matching.

The laser stripe is used to ensure the reliability and accuracy of the seam detection and it makes the coordinate detection process far easier. However, for stereo vision to be effective, it is required that the surface being measured has additional features such as edges [15].

In [64] a system which takes images of the weld joint from different positions and orientations and determines the weld seam trajectory using stereo vision is described. A demonstrator was designed as shown in Figure 2-9 with an ABB IRB2400 robot, S4 control system. The camera is from Allied Vision Technologies (Marlin F-131B) with a CMOS 2/3" chip with pixel size of 6.7µm x 6.7µm. The camera was connected to the PC using Firewire and the PC connected with the robot system through RS232. A high accuracy, low distortion machine vision lens from Kowa with infinite depth of field, a minimum working distance of 120mm and a focal length of 8mm was used. With this setup the authors have obtained a mean error of ±0.23mm and a maximum error of 0.7mm which is acceptable for most welding applications. The authors of [64] proposed a sensor which can be mounted away from the weld tool which saves space compared to a conventional sensor. The proposed solution is to re-measure in between each welding sequence with the stereo vision system and to update the weld path accordingly. Some of the issues faced by doing this were the pixel resolution of the image, difficulty in finding edges in *2D* images, poor accuracy of the camera model and its calibration [64].

Figure 2-9: Stereo vision system correcting for path[64]

Stereo vision was realised by using a single camera and double poses method in [65]. This paper describes the importance of recognition and guidance of the initial welding position. A MOTOMAN HP6 robot with a CCD vision sensor integrated with a DH-CG400 image acquisition card was used. The control computer communicated with the vision sensing system through an image acquisition card which communicated with the robot via MOTOCOM, provided by Yaskawa. The mean square error (MSE) obtained in the *x,y* directions was less than ±1mm and less than ±1.5mm in the *z* direction. However the experimental setup was bulky and therefore difficult to be used for the welding of complex trajectories in limited space.

The work presented in [66] also described a stereo vision system. Experiments have been carried out using a Fanuc M6-I, six axis robot with a pointer tool. The stereo vision system consisted of two USB CCD cameras with a resolution of 1280x1024. Results obtained have proven that the robot with the vision system produces an accuracy of ±1mm which the authors concluded was an acceptable value for most robotic MIG welding applications. However, setup was too difficult to be used in the welding of complex welding geometries of different shapes due to its large size.

Stereo vision is discussed as quasi double camera stereovision in [92] which suggest that the double camera stereovision can be approximated to a single moving camera. The Error occurring from the transfer matrices was ±0.3mm and the image processing error achieved was ±0.165mm. In combination, the errors of profile characters for the seam between calculation and measurement are less than ±0.5mm. This method

supports the use of vision technology in welding since the space required for the placement of the camera is less compared to a dual camera stereo vision technology. However, in this method the camera needs relative movement to achieve different poses.

A position based visual servo system for robotic seam tracking which has the ability to automatically detect the seam coordinates also plan the optimal camera angle before welding is presented in [93]. The constructed system consists of the RH6 robot system (developed by Shenyang Institute of Automation), a PIII PC which runs the image processing algorithm and acts as the user interface and two CCD cameras. Only one camera was used to capture the seam image while the other used for post weld quality inspection. This system also can be categorized under the single camera double pose method where the primary camera has the movement capability. Both straight lines and curves were used in experiments for tracking and the overall position accuracy was ±0.5mm. A similar structured light stereo vision system is presented in [94] which produced satisfactory results in the welding of a *V*-groove.

In summary, though a number of attempts have been made on using stereo vision for seam tracking, researchers have not highlighted the adaptability of their system for different kinds of welding processes and various complex weld shapes. Also most work has not evaluated the performance at actual welding conditions. The large size of stereo vision systems and their low accuracy are the main challenges in their implementation in aerospace welding applications. Moreover cameras used in stereo vision systems are not suitable to operate over the long term under extreme welding conditions. There was also no commercial stereo vision systems designed for the welding application.

Laser triangulation based sensors

This technique has been the most widely used method for seam tracking using machine vision due to its fast acquisition time, simple optical arrangement, easiness in feature extraction, low cost, high resolution and robust nature [52] [91]. The basic principle of structured light method is as follows: A narrow band of light is projected on to the *3D* shape and when that light is viewed from another location it appears distorted. The shape of the distorted line is captured by a camera which allows reconstruction of the shape using a triangulation method. An industrial laser scanner extracting seam information for path correction of a robot is shown in Figure 2-10.

Figure 2-10: Laser scanner inspecting prior to welding[83]

Based on the light pattern used, there are four categories of structured light methods [52].

1. Dot structured light
2. Stripe structured light
3. Multi-stripe structured light
4. Grid structured light

The stripe structured light method has been more often used in industrial applications. A structured light system consists of a camera and a projector whereas in stereo systems it contains multiple cameras or multiple views. Therefore, unlike in stereo vision systems, this method does not have the correspondence (Stereo matching) issue [52].

A detailed description on the use of a laser stripe to find *3D* coordinates is given in [95]. A short laser range probe, a 6DOF robot arm with 650mm reach, a 1DOF rotary table (to hold the work piece) and a 4-axis CNC milling machine was used. However, the equations developed are only valid at ideal conditions and the authors have assumed that there is no optical distortion in the camera lens. This is not practical in real operating conditions since there is always a distortion as it is not possible to perfectly align the camera and the laser sensor to give zero optical distortion. With this method the authors have achieved a tracking error of less than 0.1mm.

An application of a laser scanner on a robotic golf club head welding system is presented in [96]. The system consists of a PC, a motion control card, a 2DOF rotary table and a five axis robot called "ReapeR". The accuracy of the vision system is 0.0169mm and is less 0.1mm in the robotic system. Detailed algorithms for edge detection from the point cloud and path generation has been discussed. The overall accuracy achieved was 0.48mm, which was mainly because of the errors from manual teaching of hand-eye coordination. The frame rate used was 60fps which proved to be

slow. The authors suggest that if a better camera with a frame rate of 200fps was used, the processing time could be reduced to less than 2s. However their system was not robust enough for different *3D* shapes.
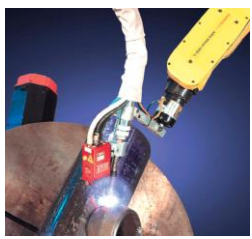
A new vision sensor, based on a circular laser is discussed in [70]. In this paper the projection was a circular laser rather than a beam or stripe. The system consisted of a CCD image sensor and light system based on a rotary lens that generates a circular laser beam. The experiment was carried out using an ABB IRB 2400 welding robot, a CNC platform and a Watec-902H type industrial camera. The authors state that online data from the vision sensor cannot be fed into the robot trajectory pre-set by the robot control because of the characteristics of ABB robots which has not been clearly described. However, the results showed that the seam tracking error is less than 0.5mm along the height tracking direction. However the authors do not prove the applicability of the design to complicated welding challenges.

Another good example of using a laser vision sensor for seam tracking is presented in [97]. The authors were successful in automatic guidance of the robot. Based on the information gathered through vision sensing. A CCD camera and a diode laser were used in [98] for generating 3D coordinates and the experiment was tried for height varying applications. Applications of the same *3D* vision seam tracking system is described in [99]. Another *3D* seam tracking system using a structured light laser is presented in [100]. The authors have proposed and implemented a technique which visually governs offsets in the robot path and controls the welding process factors on the basis of the monitored cross-sectional dimensions with the use of a vision system. A *3D* seam tracking system for sealant application, which is also similar to welding seam tracking, is discussed in [101]. A *6D* seam tracking robot was developed based on laser scanning in [102] with an accuracy of 0.015mm.

2.5.3 Commercial laser scanner product performance overview

There are very few suppliers for laser scanner based seam tracking devices for welding applications. These devices are integrated with industrial laser scanners with customised software. Table 2-1 shows some of the state of the art solutions and their limitations.

Table 2-1: State of art seam tracker specifications [103][104][105][106][107][108][109]

	Name	Reference Picture	Accuracy	Limitations
1	WISE Welding by WISE Technologies Ltd & SICK Ltd		0.5mm	• Large in size • Low accuracy • Needs customization
2	Laser Vision Systems by Servo Robot		0.025mm	• Needs customization
3	6D Seam Tracking form META-VISION Systems		0.05mm	• Large in size • Needs customization
4	Liburdi Seam Tracker		0.5mm	• Needs customization
5	Arc-Eye Vision System from Valk Welding		0.025mm	• Needs customization • Costly
6	Adaptive Welding from FANUC Robotics		0.05mm	• Needs customization • Costly
7	Micro-epsilon Scan-control		0.02mm	• Compact • Low cost • Needs minimal customization

By carrying out an industrial survey, it was found that all these solutions need customization for any particular application. It was also found that most of the state of the art solutions are large in size and expensive. Among them the Micro-epsilon is comparatively compact and low in cost. Compactness can significantly help when carrying out seam tracking in narrow spaces such as between turbine blades in an aero-engine.

Industrial scanners come with a datasheet describing their operating range and other parameters. The information specified in these datasheets has been generated in a controlled environment. Therefore, such datasheets fail to provide a clear overview on the performance of the scanner in the wide range of operating conditions that could be present in an industrial environment [110].

The quality of the data obtained from laser scanners depends on the quality of the signal reflected back from the object surface to the camera sensor [111]. The quality of the reflected signal is influenced by many parameters such as surface reflectivity, stand-off distance, steepness angle of the surface, ambient lighting conditions and incidence angle [112]. Therefore, it is vital to evaluate the performance of a particular laser scanner under actual working conditions prior to its use in any specific application.

Over the past decade, many attempts have been made to understand laser scanner performance under different lighting conditions [111], *3D* geometries [110], materials [113] and surface reflectivity [111]. Past studies show that white and matt surfaces produce better point cloud data compared to black and shiny surfaces [111][113]. However previous attempts do not provide adequate quantitative data and also fail to provide information on the performance of a laser scanner based on the geometry of the surface measured.

In summary, literature suggests that over the years, laser scanners have improved significantly compared to other seam tracking methods and stereo vision systems due to the technological advancement in optical engineering. Presently they are available at low prices (in addition to high accuracy and repeatability) which have made laser scanners very popular among system integrators. However, only minimal work has been carried out to understand the data quality produced by a laser scanner and methods of improving the performance.

2.6 Weld process optimization, empirical modelling and adaptive weld process control for welding automation

TIG welding quality characteristics are strongly influenced by the process parameters. Moreover, those process parameters determine the mechanical and metallurgical parameters of a particular weld [114]. Traditionally, the manual welder selects the desired process parameters based on their experience. Welding current, travel speed, wire feed rate, arc gap and torch orientation are just some of the parameters that a welder can control during the welding process [115]. These parameters are measured using welding sensors and process parameter monitoring software. Over the past two decades process parameter and weld quality monitoring software for welding has been commercially introduced such as ADM IV [116], Arc guard [40], WeldEye [117], Hannover 10.1 [40] and Weldcheck [118]. However, in order to implement new algorithms and control strategies such software has to be modified or new software has to be developed.

While skilled welders have mastered the technique of controlling these process parameters, an automated welding system does not exhibit such capability. Such intelligence or decision making capability can only be programmed into a robotic welding system and it can be realised only by receiving feedback about the welding set-up. For example, material type, size, joint geometry and fit-up [119][120]. Such an intelligent capability is vital for high end welding such as in the aerospace industry. Over the years this has been difficult due to lack of technology advances in sensing technology, robot control techniques and processing power.

A study on the effect of weld process parameters on penetration for the gas metal arc welding process is investigated in [121]. This study also investigates the effect on the micro-structure of the resulting welds. A mathematical model for developing the relationship between the input parameters and weld penetration for submerged arc welding is presented in [122]. The effect of the wire feed rate on the bead geometry of Aluminium sheets with MIG welding is reported in [123]. A detailed sensitivity analysis (effect of process parameters on weld quality) is carried out in [124][125] and [126]. This is further improved by developing mathematical models to predict the weld bead geometry in [127]. Recent advances in automation have introduced pulsing technology to welding. A detailed investigation on the effect of pulsing parameters on weld quality is presented in [128][129] and [130]. Among these studies, authors find

that the most significant process parameter on weld bead shape is the welding current. However it should be noted that most researchers have focused only on welding current, speed and wire feed rate as process parameters.

The design of a process parameter monitoring and control unit for the resistance spot welding process is presented in [131]. A neural network model is presented in [132] and [115] for weld process modelling and control. In [114] the authors present a method of detecting the weld line and a process control methodology for welding automation. They develop an Artificial Neural Network (ANN) solution but there is no evidence that the authors implemented the algorithm in a robotic system. The derived model is significantly complicated and involved lot of computations which makes it difficult to implement in a robotic welding system. This is one of the significant gaps in research related to robotic welding. A simplified mathematical model is essential for real-time process control of welding.

In [130] and [133], the use of the Taguchi's method to control the welding process parameters for obtaining the optimal weld pool geometry is reported. In [134] authors report an application feasibility study of the Grey relation analysis in combination with Taguchi's technique for an optimal parametric combination to yield the best bead geometry of welded joints. The optimization of different welding processes using statistical and numerical approaches is presented in [135]. The authors present a reference guide for statistical methods such as the factorial design method, linear regression, response surface methodology, ANN and Taguchi's method. Characteristics of each method are discussed and presented clearly. In [136], a detailed comparison of statistical models for control of weld bead penetration in the GMAW process is discussed. The authors have found that a polynomial model fits best for predicting the penetration of welds. Another study on a mathematical model for predicting the distortion in welding of thin plates is discussed in [55]. In [137], statistical weld quality prediction methods are compared with a neural network approach. Neural network modelling has also been used for predicting weld joint strength in [138].

Over the years very few attempts have been made to achieve adaptive robotic welding. This was primarily due to lack of sensor, especially vision sensors which are required to understand the weld joint size and shape. Adaptive welding can be realised through joint feature extraction [15]. A robust joint feature extraction for a lap joint is discussed

in [139] using structured light images. Image processing techniques such as smoothing, adaptive thresholding and thinning were used. A vision sensor and a PLC were integrated with a touch screen to build up the mechatronic solution for seam tracking. However, the feature extraction was only performed on a lap joint and different profiles were not attempted. Moreover, the authors have not evaluated the performance of the algorithm.

A laser welding robot developed to achieve adaptive process parameter control is discussed in [140]. The system was developed using a Haas 3006D 3 kW Nd:YAG-laser, a Motoman UP 50 industrial robot and a Servo-robot SMART 20 laser scanner. The gap width was measured continuously, and the data are used to control the welding speed and the wire feed rate. Butt welds in 2mm thick sheet steel with gaps varying from 0.1mm to 0.75mm were welded with this system, by matching the welding and wire speed. However, the attempt was on laser welding which is considered to be easy to automate compared to TIG welding [136]. This is mainly due to the added complexity of wire feeding mechanism in TIG welding. Feeding the wire in to the weld pool from a different axis to the weld electrode is identified to be challenging [136].

A weld pool imaging and processing system along with a robot and automated welding equipment was set up to control the wire feed rate is discussed in [141]. Information from the weld pool was used as the feedback for controlling the welding process. However, the attempt was only carried out in *2D*. The authors have not used empirical modelling techniques to achieve adaptivity in the system. Moreover, the only feedback used was from a *2D* camera about the weld pool which is not adequate to achieve robust control over the weld quality characteristics.

In summary, among the previous attempts, none have been made on developing mathematical models for the control of the robotic TIG welding process whereas most of previous attempts were on MIG welding. Additionally, these investigations have only being carried out to understand the effect of process parameters on the weld quality characteristics. They do not reveal enough information on how the findings can be used to improve the quality of the welds in robotic welding. Moreover, minimal evidence was found on the implementation of any derived mathematical model on a robotic welding system to achieve adaptivity for joint fit-up or variability. However, previous studies suggest that statistical methods are easy to implement in a control

system which this thesis will focus on. Moreover, literature also suggest that Taguchi's method is best suited for obtaining best results with minimum number of experiment and therefore this thesis will use Taguchi method for developing the mathematical model [130] [133].

2.7   Summary

In this chapter, the background of this research was introduced. A detailed investigation was carried out to understand the similar research work carried out before. Previous industrial and research attempts on human skill capturing, laser scanner evaluation, 3D seam tracking, empirical modelling for weld quality prediction and adaptive process control were reviewed.

The review of the literature emphasises the necessity for use of advanced sensor technology for welding automation with industrial robots especially in the aerospace industry. Literature suggests that there has been very limited work on TIG welding automation. It was also found that many industrial applications carry out robotic welding using pre-programmed machine settings and robot paths. This does not assure the required quality for high end applications such as in the aerospace industry. Weld joint feature extraction, tracking and adapting robot path for part fit-up has not been researched to satisfactory levels. Whilst various attempts have been made to understand the effect of weld process parameters on the weld quality characteristics, there are not many attempts that have successfully managed to implement a mathematical model on a robotic system to select the optimum process parameters based on the joint geometry. Moreover, it appears that no work has been carried out on finishing a complete solution to the problem for *3D* seam tracking and adaptive welding.

Research questions and gaps

The key objectives of the work carried out as part of the thesis was outlined in Chapter 1. In order to achieve those, the main research questions to be addressed, which are identified from the literature survey are;

- How can one quantify a manual welder's behaviour in TIG welding for process parameter control and how it can be used for intelligent automation?

- Can the data from a laser scanner be trusted? What are the reasons for inappropriate data from a laser scanner when measuring complex shiny surfaces? How could one overcome this?
- How would one extract joint features for implementing intelligent algorithms?
- Can any algorithm be developed which will function in any 3D orientation of parts?
- Can the algorithm function correctly irrespective of the joint cross-sectional profile?
- What is the effect of process parameters on the weld bead dimensions and welding strength?
- Can a mathematical model be developed to establish the relationship between input and output parameters? What are the most significant process parameters and can their effect be quantified?
- How would one use the joint geometry as a feedback for the intelligent selection of machine settings for carrying out variable gap weld joint?
- What are the differences between the approach of industry, skilled welders and any novel method derived in this thesis in welding of a variable gap butt joint?

These research questions have led to the aim of the PhD being to develop a fully automatic robotic TIG welding system which demonstrates the required intelligence and adaptivity for welding in the aerospace industry. Therefore the following specifications were defined to achieve from the test-rig development.

- Capability to measure robot position.
- Centralised control of all equipment.
- Industrial robot.
- Welding machine and torch with accessories for welding.
- Data acquisition system.
- A personal computer with required processing power to act as the central controller.
- 3D laser scanner for scanning the samples.
- Cameras for monitoring the welding cell for safety purposes.
- Protective shielding between the welding torch and the vision sensors.
- Data display and analysis capability with a graphical user interface.

- Algorithms for seam tracking and process control.

- Protection for electromagnetic interference.

- Extractor unit for fume extraction.

- Guarding system for human safety.

- Sensor systems for weld parameter monitoring.

- Faster response to client-server based commands.

- Position based control strategy in the software.

3   Test rig design and system integration

As explained in Chapter 1 the main objective of this research is to develop an automated TIG welding solution that can work with challenging weld geometries. The selection of suitable equipment and its integration is essential to achieve this task. This chapter presents the detailed description of the selection of the most appropriate equipment for TIG welding experimentation and the methodology used for its integration. The complete mechatronic system was divided into several sub-systems, namely, the welding module, feedback module, motion control module and imaging module. These four systems were linked to each other through a personal computer, which acts as the central controller.

An industrial robot was used to provide the required motion for the welding torch. A TIG welding machine that can be operated in automatic mode was used as the welding source. Automation of TIG welding also requires careful control of all the key process variables, so welding sensors were used to monitor the welding process. Vision sensors were used for seam tracking and to predict the required size of the gap. A data acquisition system was used to send and receive signals from all the equipment. Automation interfaces were used to establish communication between the equipment and the PC. The developed system was also capable of collecting (and displaying) data for further analysis and possible improvement.

3.1   Introduction

On the basis of hardware, the experimental setup can be divided in to four main modules and is shown in Figure 3-1. All equipment was integrated into a workstation (PC) which acts as the main controller. The workstation consists of a HP Intel Xeon 2GHz 6-core processor and 64GB RAM, which is capable of high speed data processing, including real-time image processing and real-time communication with the robot, sensors and welding machine.
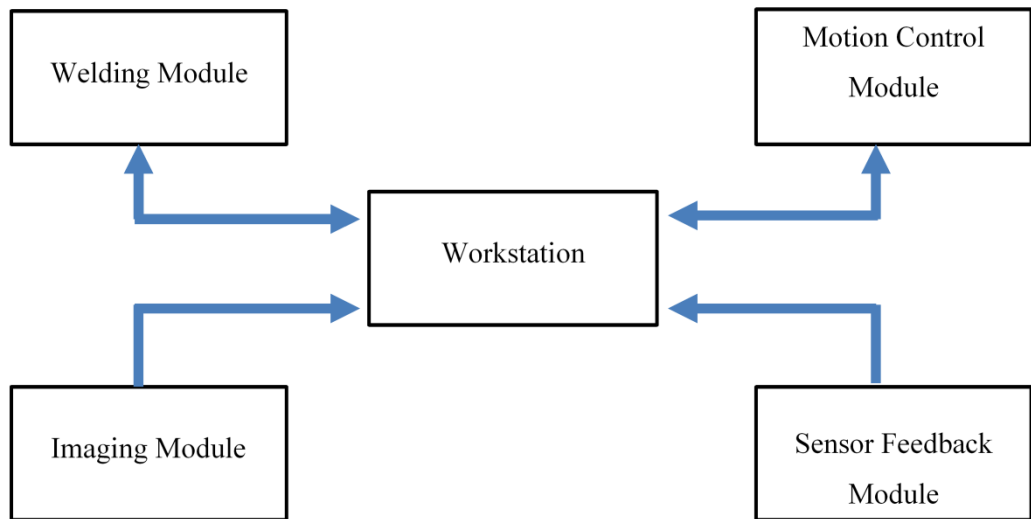
Figure 3-1: Summarized system integration diagram

A descriptive CAD picture of the complete welding cell is shown in Figure 3-2.
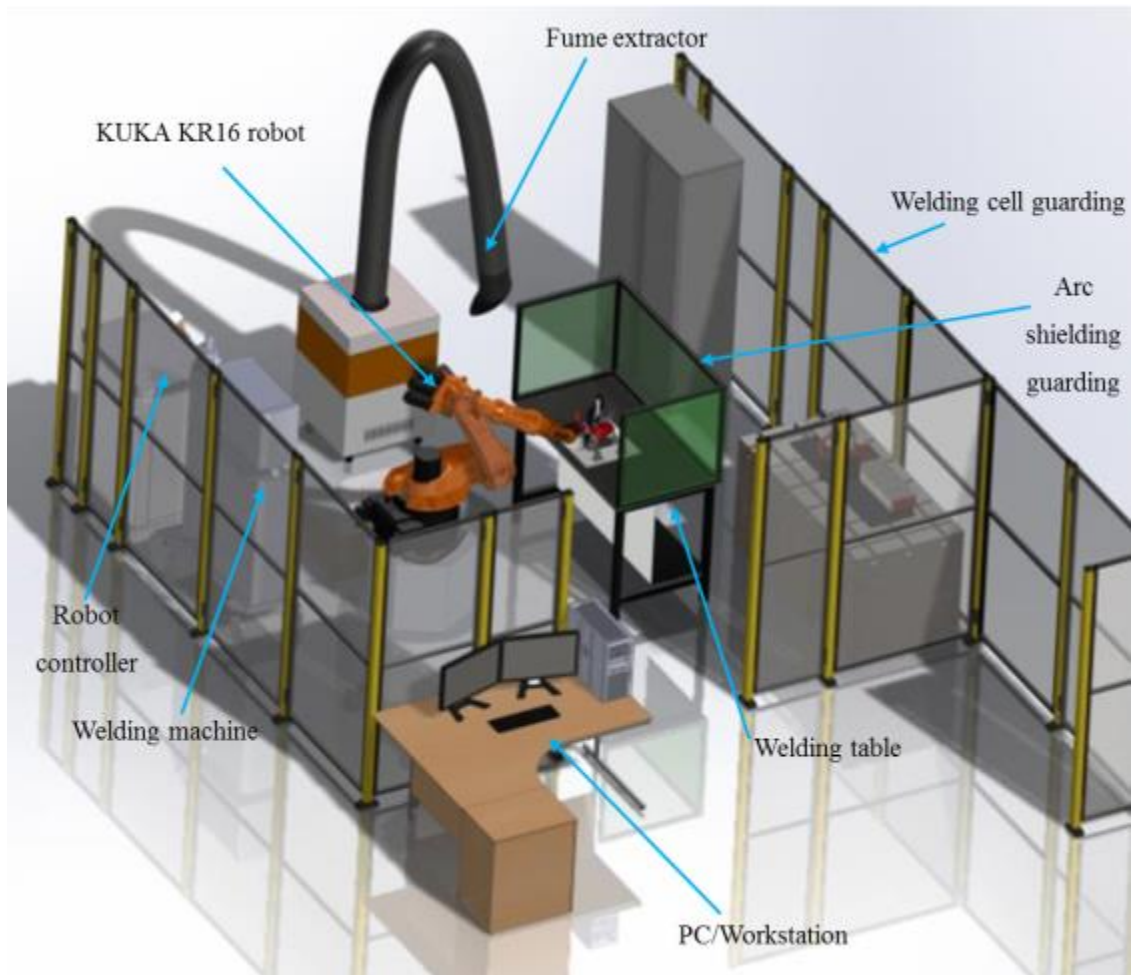
Figure 3-2: CAD design of the welding cell

3.2 Welding module

Initially, various welding equipment from manufacturers, such as Miller, ESAB, Migatronic, Fronius, Lincoln Electric and Dinse were investigated. Considering the need for features such as automation capability, interfacing with a robot controller and the option to control welding parameters, a Fronius TIG/MIG welding machine (Magicwave 4000) was selected. A photographic view of the welding machine is shown in Figure 3-3 (a).

The ratings of the welding equipment are as follows (please refer to Appendix 1 for more specifications of the welding machine),

- Rated Current : 400A
- Voltage Range: 10.1-26V

The Fronius Magicwave 4000 can be operated in JOB/Programme mode where welding programs can be stored in the welding machine. It can also be operated in automation mode (TIG mode), where the welding parameters can be completely controlled from an external system such as a PC. The welding machine is equipped with state of the art technology allowing simultaneous control of multiple parameters including welding current, wire feed rate, pulsing parameters (pulse frequency, base current, duty cycle), filler wire-torch angles and gas flow rate.

The wire feeder used in this study can be operated with a wire-spool of up to 30 mm diameter. It uses cold wire feed technology, in which the filler wire is fed to the melt pool at room temperature. This approach of feeding the wire to the melt pool helps to reduce the heat accumulation and subsequently increase the mechanical properties of the weld. The wire feeder also includes a push-pull system shown in Figure 3-3 (b). The push-pull system functions in a way where the wire is pushed by one motor driver at the welding machine and pulled by another motor driver at the welding torch. It maintains constant tension over the whole length of the wire and helps to maintain uniform wire feed rate all along the robot arm. This assures that the wire feed rate is not affected by the movement of the robot arm.
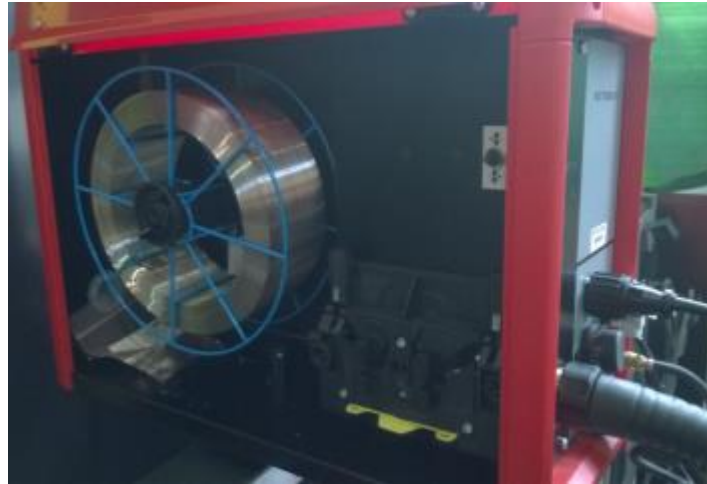
Figure 3.3(a)   Figure 3.3 (b)

Figure 3-3: Photographic view of the welding equipment (a) Fronius Magicwave 4000 welding machine (b) Wire feeder unit [142]

Two different welding torches were used in this study and are shown in Figure 3-4 (a) and (b). The manual welding torch was selected for the initial stages of the research, which was to understand human behaviour in manual TIG welding process. The Robocta TTW 4500 robotic torch shown in Figure 3-4(b) was selected for the automated welding with the robot. As can be seen from Figure 3.4 (b), the Robocta TTW 4500 consists of a motor for pulling the filler wire.

Figure 3.4 (a)   Figure 3.4 (b)

Figure 3-4: Different welding torches used for different phases of the project (a) Manual welding torch, (b) Robocta TTW 4500 robotic torch

3.3   Sensor feedback module

A National Instruments Data Acquisition System (NI DAQ) was selected as the interface to link the PC and other equipment (using Digital and Analogue signals). The NI DAQ card can receive and send digital or analogue signals from the PC. A detailed specification of the NI DAQ system is given in Table 3-1. Figure 3-5 shows a

photographic view of the NI DAQ system. LabVIEW was used as the central software tool for programming.

Table 3-1: Specifications of the data acquisition system

PXIe card	Specifications
NI PXIe 6356	8 Analog Inputs, 2 Analog outputs, 24 Digital IOs, 10V, 1.25MS/s/ch
NI PXIe 6528	48 channel (24 input, 24 output), 60V
NI PXIe 6733	8 Analog output channels, 1MS/s/ch
NI PXIe 6356	798 MB/s, PCI Express

Figure 3-5: NI DAQ card and PXIe chassis system [143]

Appropriate sensors were used for monitoring the welding current and voltage, and their specifications are given in Table 3-2. All the sensors were calibrated and tested at 21˚C and are specifically made for welding applications (refer Appendix 2 for sensor calibration certificates).

Table 3-2: Sensor specifications

Sensor	Range	Accuracy	Bandwidth
Current	0-1000A	±1%	25kHz
Voltage	0-100V	±1%	25kHz

3.3.1 Basic principle of welding Sensors

Current Sensor

The basic principal of a Hall-effect welding current sensor is shown in Figure 3-6(a). As can be seen in the figure, the ground lead of the welding machine passes through the

current sensor. The high current passing through the ground lead will generate a magnetic field around it, which will also travel through the coil wrapped around the core of the sensor. The passage of current produces a potential difference between the opposite ends of the coil, and induces a current which will travel through the coil. The generated potential difference is directly proportional to the welding current. Equation 3.1 is used to find the actual welding current from the sensor reading [144].

$$Actual\ welding\ current = 100\ \times output\ voltage\ from\ the\ sensor \qquad (3.1)$$

<div align="center">
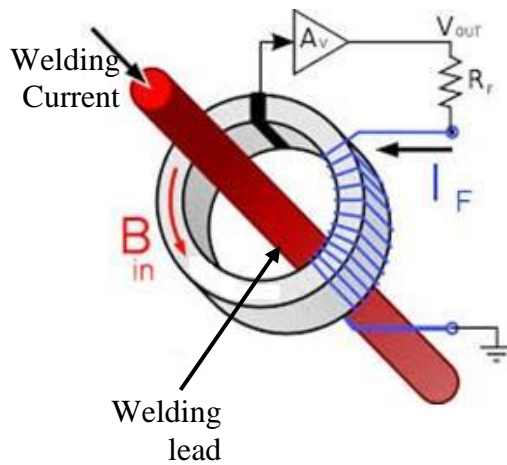
Figure 3.6 (a) Figure 3.6 (b)

Figure 3-6: Hall effect current sensor (a) Hall effect principle, (b) HKS process sensor [144]

</div>

Voltage Sensor

In order to measure the welding voltage, the positive and negative terminal of the welding voltage sensor is connected to the respective terminals of the welding machine. The input voltage (measured actual voltage) is scaled down using the concept shown in Figure 3-7 and an analogue output in the range of 0-10V was generated for measurement. Equation 3.2 is used to find the actual welding current from the sensor reading [144].

$$Actual\ welding\ voltage = 10\ \times output\ voltage\ from\ the\ sensor \qquad (3.2)$$
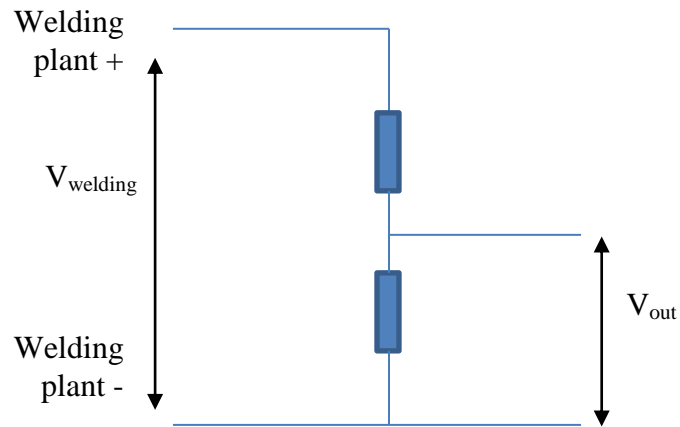
Figure 3-7: Principal of welding voltage sensing

3.3.2 Sensor feedback module integration

All the sensors and the automation interface of the welding machine were integrated to the NI DAQ system through a connector board as shown in Figure 3-8. The DAQ system was capable of acquiring data at 1.25 Mega samples per second per channel. Each channel of the DAQ cards consists of its own analogue to digital converter which assures simultaneous data acquisition. It helps to avoid any time delay between the channels, which is essential for real-time selection and control of the welding process parameters.
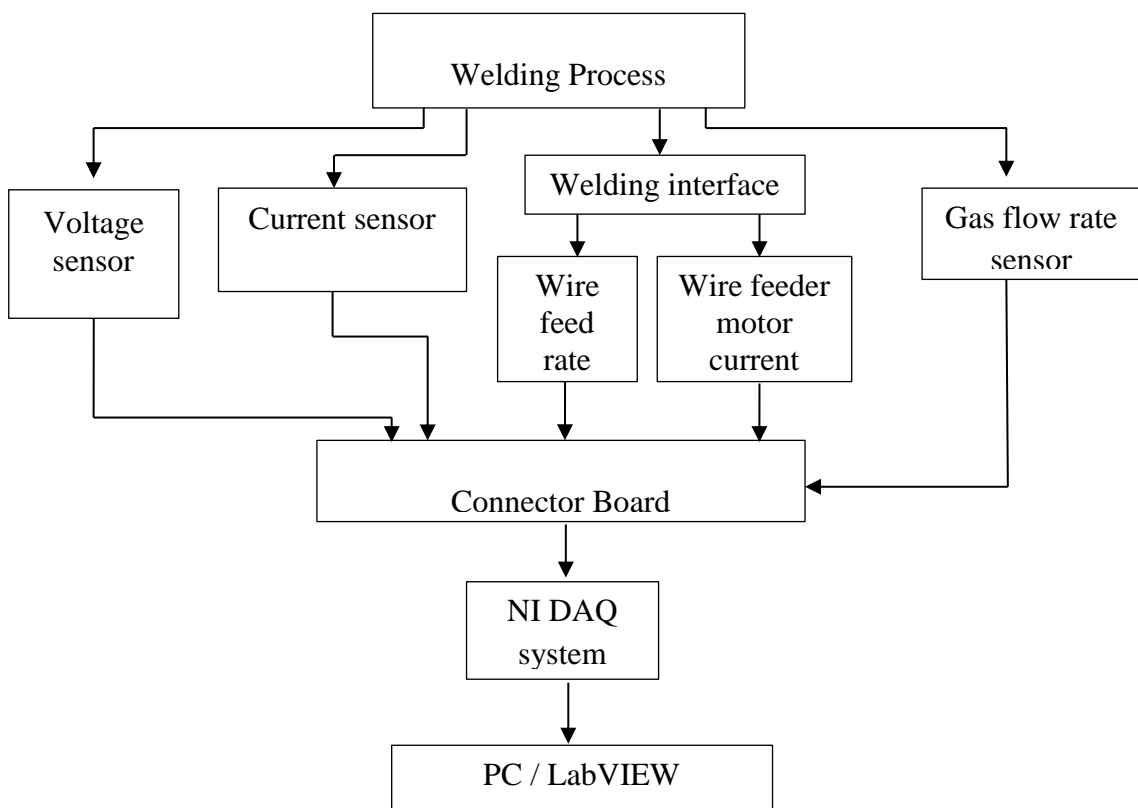
Figure 3-8: Block diagram for NI DAQ system integration with the PC

3.3.3 Signal processing

The welding process data was acquired from all the equipment at a sampling frequency of 1kHz. During the data acquisition, noise was expected due to the interference and disturbance from the welding machine and the robot controller. The raw output (in volts) from the channels of welding current and voltage sensing when the system is at dwell state (no welding) is shown in Figure 3-9 (a) and (b). As can be seen from the figure, the welding current and voltage channels have a maximum noise amplitude of 0.075V (at 375 Hz) and 0.04V (at 135Hz) respectively.
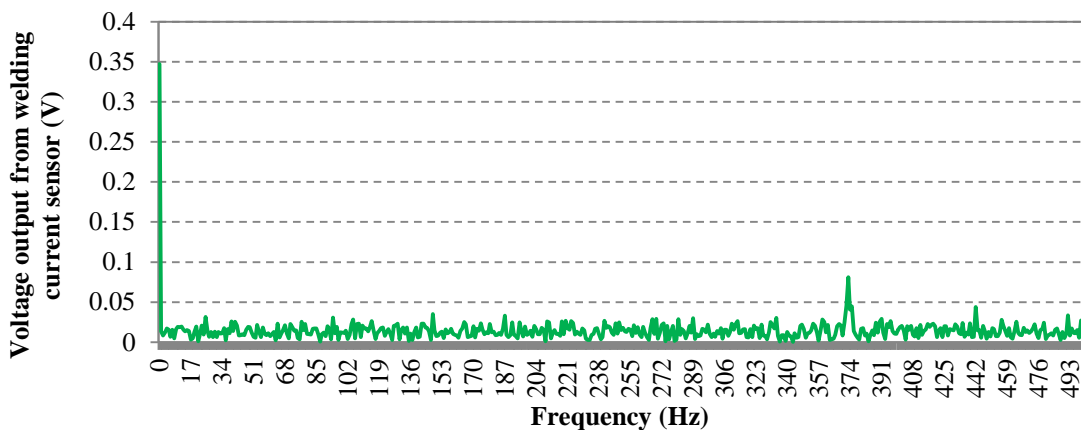
Figure 3.9 (a)
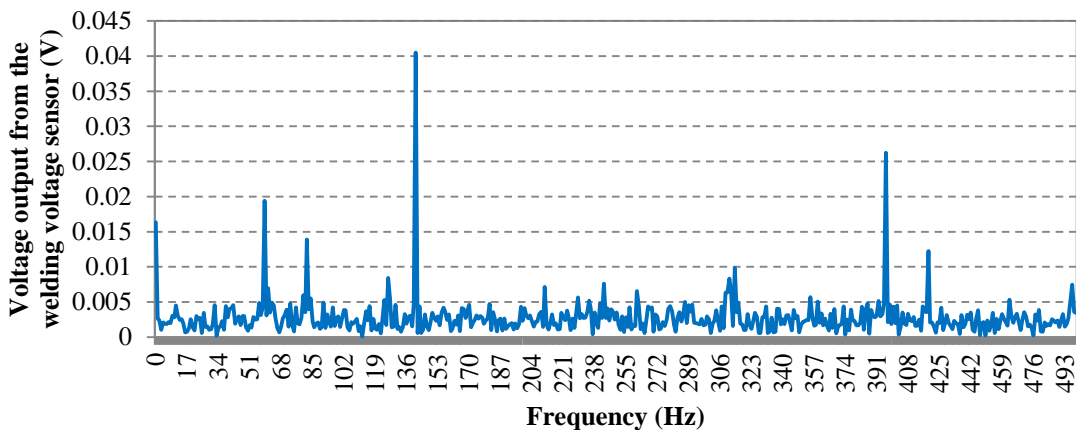
Figure 3.9 (b)

Figure 3-9: Signal channels without noise filtering at dwell state (a) Welding current signal in frequency domain, (b) Welding voltage channel in frequency domain

The actual welding current and voltage at the dwell position (no welding) is shown in Figure 3-10. As can be seen from the figure welding current signal and voltage signal have maximum noise amplitudes of 3A and 0.4V respectively. The amplitude of the welding voltage is not significant (0.4V). However noise amplitude of welding current can significantly affect the weld quality when considering thin sections.
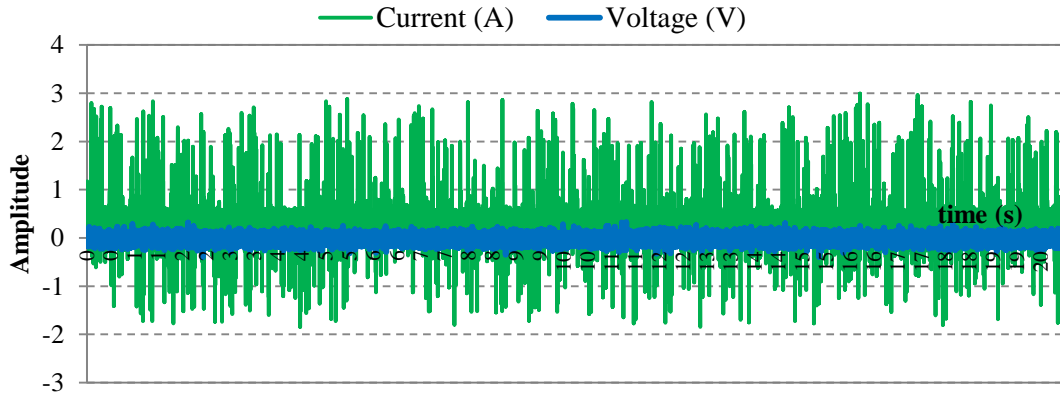
Figure 3-10: process parameters at dwell state

The current and voltage signals, during the welding process are shown in Figure 3-11. As seen from the figure, the welding current signal has both high and low amplitude noise. Comparatively, the welding voltage signal shows uniform reading with low noise.
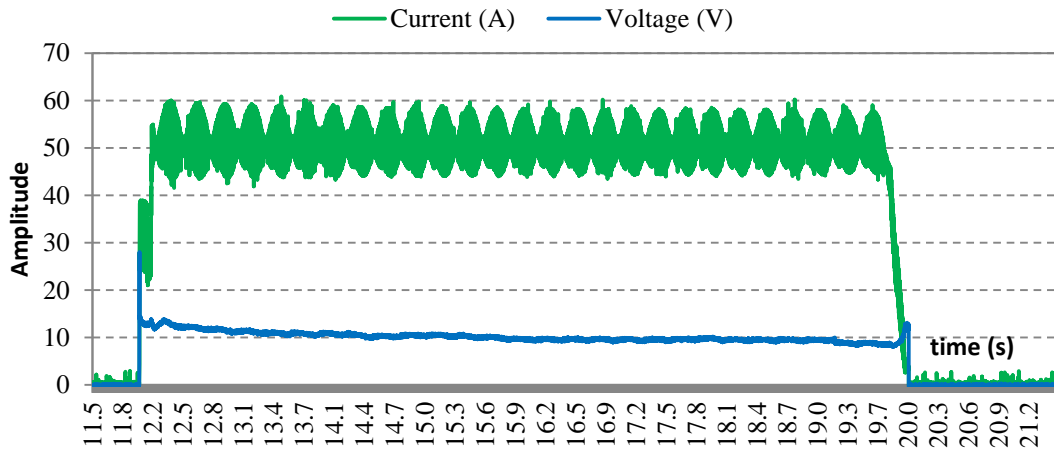
Figure 3-11: process parameters during welding

As can be seen from Figure 3-11, it is essential to remove the noise from the channels, so as to achieve noise-free measurements. In order to do this, the exact frequency of the noise must be established to control it by applying filtering methods. Therefore, the welding current and voltage signals were monitored in the frequency domain during the welding process and the results are shown in Figure 3-12 (a) and (b) respectively. As seen from the figure, two noise frequencies are observed in the welding current channel at 333Hz and 336Hz. No significant noise was observed in the voltage channel. However, low amplitude noise was observed in the voltage channel at dwell condition (Figure 3-9 (b)). In order to remove the noise, a low-pass filter (a filter that attenuates signals with frequencies higher than the cut-off frequency), with a cut-off frequency of

52

250Hz was used with both current and voltage channels to account for the low amplitude noise. This will ensure that signals passing through the filter will have frequencies only below 250Hz. The signals after applying filtering (variation in current signal is only due to the operation of the foot pedal) is shown in Figure 3-13.
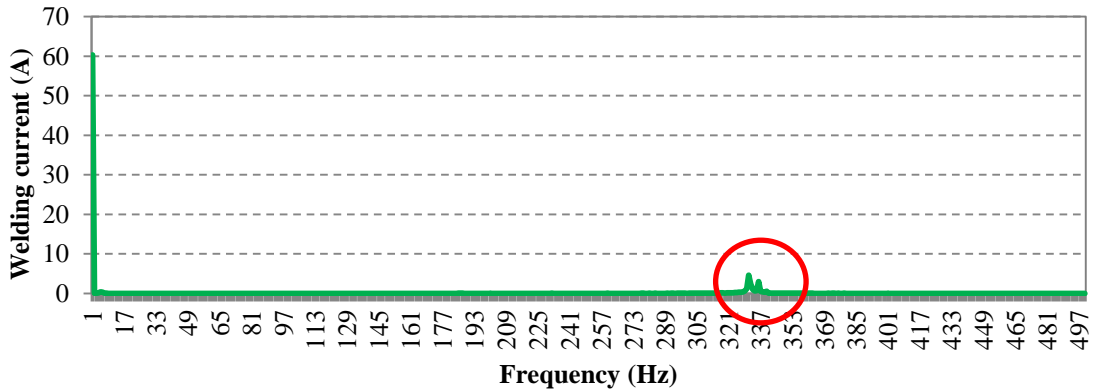
Figure 3.12 (a)
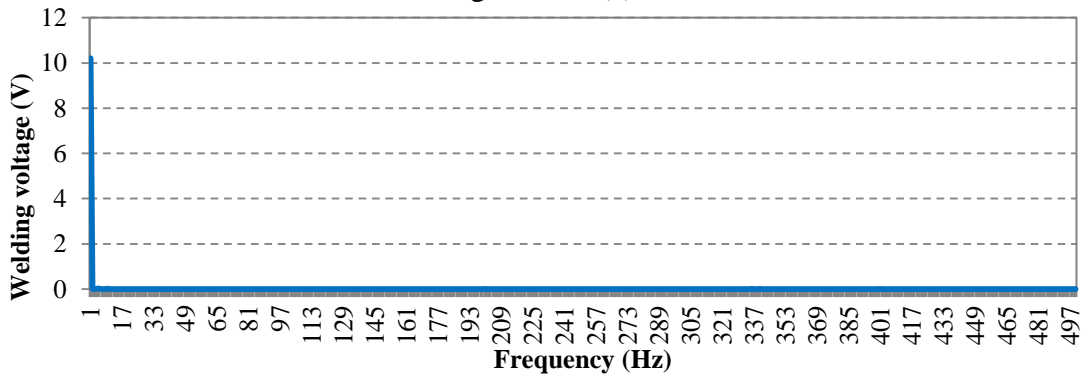
Figure 3.12 (b)

Figure 3-12: Current and voltage signals in frequency domain (a) welding current during welding, (b) welding voltage during welding
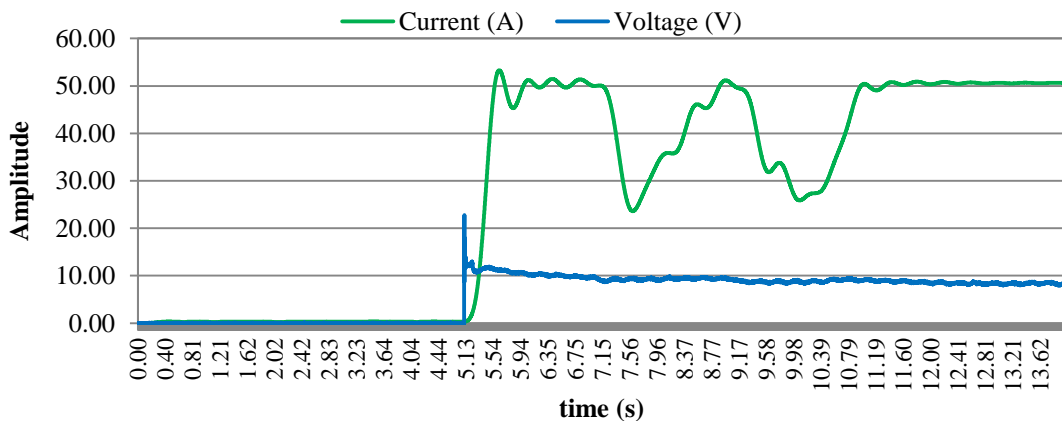
Figure 3-13: Acquired signals after applying filtering

3.4   Imaging module

This section presents the information about the cameras and laser scanner used for the development of the robotic welding system.

3.4.1   Weld area viewing

Currently most automated welding processes are carried out in enclosed areas, without any direct line of sight for the operator. Any fault during the automated TIG welding process, such as sticking of the filler wire to the work piece or inconsistent movement of the robot arm can result in significant damage to the equipment. Therefore, a clear view (indirect) of the weld area is essential to take preventive measures and to avoid any catastrophe during the welding process. During the TIG welding process, high brightness arc, spatter, electro-magnetic radiation and fumes are produced, which complicates the viewing process. High brightness of the arc can saturate the pixels of cameras [145].

In this thesis, a CCD camera based imaging system has been developed to view the weld area. A band-pass filter (notch filter) with an illumination source is used with the camera. The band-pass filter allows only a small spectrum of light to reach the camera, and therefore eliminates the welding arc wavelength. The illumination source used is a LED array (16W) and was used at the same wavelength of the band-pass filter. The selection method of the wavelength of the filter and illumination source can be described as follows:

Initially, an Oceanoptics spectrometer was used to investigate the spectrum range of the welding arc. Figure 3-14 shows the typical spectrum (from 200-1200nm) observed during the TIG welding of a stainless steel material with pure shield Ar gas. As can be seen from the figure, the welding arc produces a high brightness in the range of 350-920nm. Therefore, a wavelength above this threshold should be ideal for viewing the TIG welding process. Therefore a wavelength of 950nm (±10nm spectral width) was selected as the viewing wavelength. The selected band-pass filter and the selected camera (Stemmer IDS UI-5240SE-NIR-GL) with a 14mm lens are shown in Figure 3-15. The photographic view of the imaging system is shown in Figure 3-16.
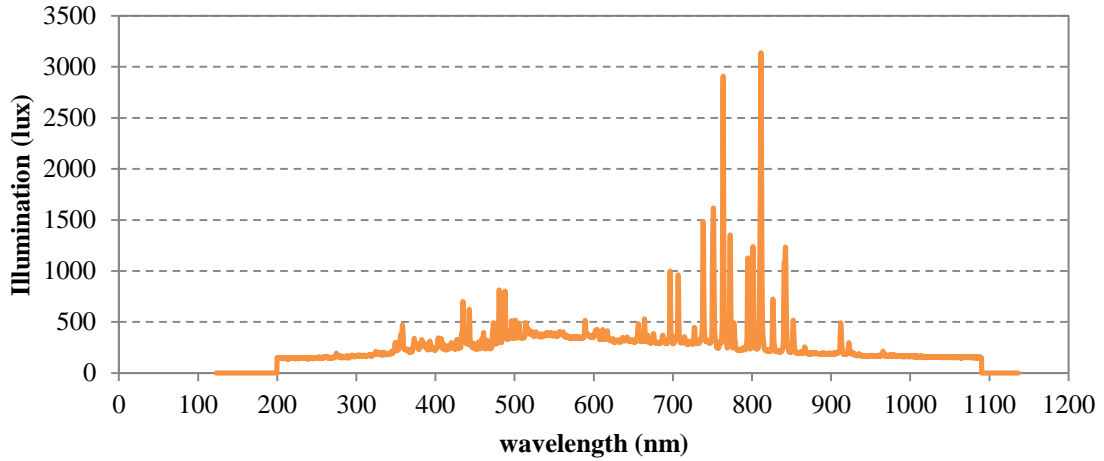
Figure 3-14: Welding spectrum

Figure 3.15 (a)   Figure 3.15 (b)

Figure 3-15: (a)Band-pass filter, (b) lens and camera[146]
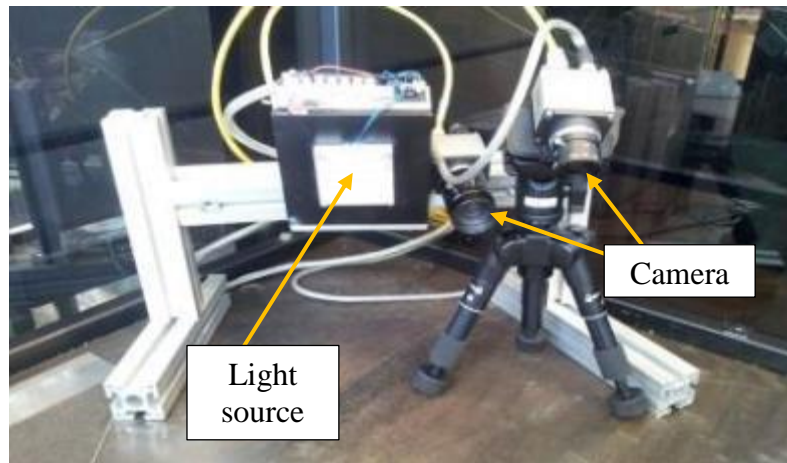
Figure 3-16: Camera with illumination source for weld area viewing

3.4.2   Laser scanner for 3D seam tracking

Gap measurement and seam tracking is an essential part of the proposed automated welding system. Seam tracking helps to account for any variations in the weld seam position, caused by part fit-up. As mentioned in Chapter 2, laser based triangulation sensors are increasingly used [15] for welding gap measurement and seam tracking. A

schematic view of the triangulation principle used in laser scanners is shown in Figure 3-17. Triangulation refers to the process of determining the location of a point by measuring angles from known points [147].
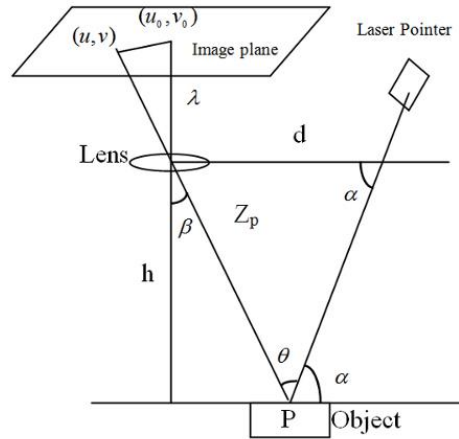
Figure 3-17: The triangulation principle of laser scanners[147]

Commercial laser scanners are available as open configuration or as confined configuration. In open configuration, the camera and the laser source are attached to a movable mounting structure that offers flexibility over the resolution of the system (by controlling the angle between laser and camera). However, this can also be a disadvantage, as there can be positional deviation due to vibrations or environmental temperature, which is not ideal for most industrial TIG welding [148] applications.

Confined configuration systems, confine the camera and the laser source within an enclosed housing, which protects the system from external disturbances and makes it more suitable for industrial applications. Therefore, a confined system was selected for this study. Among the available confined configuration laser scanners Micro-epsilon suits best for the research objectives in this thesis as it is compact and low cost. Moreover it is easy to integrate with robotic systems.

The Micro-epsilon laser scanner uses a laser source and a CMOS sensor to capture the image as shown in Figure 3-18. The laser scanner comprises a 690nm (class 2M,) 8mW laser source, with a band-pass filter. The laser source helps to illuminate the geometry providing distinctive contrast from the surroundings. The reflected light from the laser line is captured by a receiver and projected onto the CMOS sensor in the camera. The laser scanner information can then be transferred to an external system through

EtherNet TCP/IP (Transmission Control Protocol/Internet Protocol) or a Firewire network.
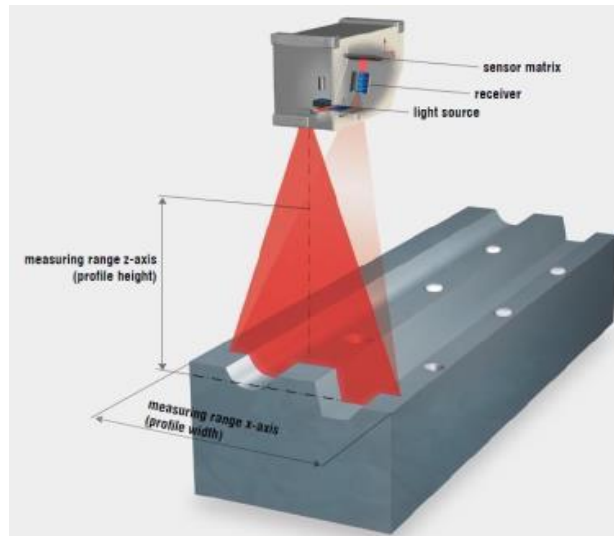
Figure 3-18: The triangle shape of the scanning beam [149]

The laser scanner's firmware (Scan-Control) is equipped with various profile measuring functions such as width, depth, height and angles. It also comes with software development kit (SDK) interfaces for customised development in C/C++ and the LabVIEW environment [149]. The LabVIEW SDK was preferred for this thesis to develop customized measurement functions. Specifications of the laser scanner are given in Table 3-3. A series of experiments, which were performed to evaluate the laser scanner's capability, are detailed in chapter 5.

Table 3-3: Performances of the selected Micro-Epsilon Scan-control 2900-25 laser scanner [149]

Lateral measurement range (resolution)	Depth meas. Range (resolution)	Profile freq.	Point measuring rate	Min. Standoff distance	Dimensions /weight
Up to 143 mm /1280 points	Up to 265 mm/2 µm	Up to 4 kHz (4,000 profiles/sec)	Up to 2.56 M points/sec	54 mm	96x85x33 mm/380 g

3.5   Motion control module

Automated welding processes require accurate positioning and controlled movements, so as to achieve the required weld quality. Robot-based welding torch movement in automation is expected to increase the efficiency of welding processes while increasing the weld quality. In this project, the movement of the welding torch and laser scanner is realized through a six axis industrial robot (KUKA KR16). A photographic view of the KUKA KR16 is shown in Figure 3-19. Specifications of the KUKA KR16 robot are given in Table 3-4.

Figure 3-19: KUKA KR16 robot and robot coordinate systems [150]

Table 3-4: Robot specifications [13]

Specification	Value
Maximum Payload	16 kg
Reach	1611 mm in axes 1 to 5
Repeatability	0.05 mm ISO9283
Degrees of Freedom	6
Robot Weight	235 kg
Controller	KRC2, 2005 (KSS v5.7)

The robot can be programmed either from the control panel (with the hand programming facility (teach pendent)) or from an external PC. The KRC2 controller can provide various motions including continuous, linear and point-to-point motion [13]. The controller also has options for direct input/output communication, which can be used for communication with external systems such as weld power supplies, PLCs or PCs. Communication with any external system can be achieved via the EtherNet TCP/IP interface or by standard Analogue/digital I/O. The robot has two operating systems; Microsoft Windows and VxWorks. External systems can communicate with the robot through the robot controller's PC (windows OS) or directly with the robot's in-built real-time system (VxWorks) in the robot controller. However, it was understood that communication with the windows PC is slower compared to VxWorks [151]. Therefore in this study, the communication between robot and external systems is performed through an external PC-VxWorks link (through EtherNet TCP/IP) as shown in Figure 3-20.
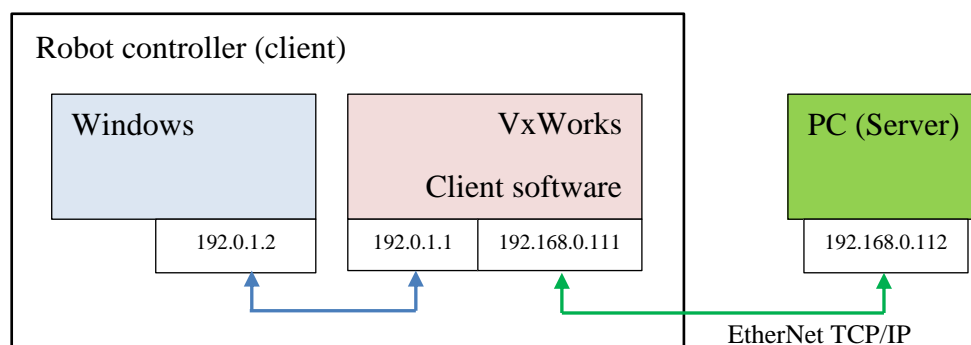
Figure 3-20: Network connection diagram

The KUKA.Ethernet.KRL.XML [151] protocol enables communication and data exchange between the real-time operating system of the KUKA robot and an external system (PC or sensors) and vice versa. It includes a real-time Ethernet network card installed in the robot controller. The client software (KUKA Ethernet.KRL.XML) is installed in the VxWorks operating system for real time data transmission. The server application software was developed in the PC running on LabVIEW which communicates to the client (the robot) via the TCP/IP protocol to transfer data in XML format.

The data transmission sequence is as follows:

1. The PC evaluates and determines the data to be sent to the robot.

59

2. The data to be sent are patched into an XML string.

3. The packed XML string is transmitted to the robot controller via the EtherNet TCP/IP protocol.

4. The XML parser contained in KUKA.Ethernet KRL XML extracts the data from the XML string.

5. The extracted data are stored in an intermediate buffer.

6. The robot program written in KRL at the robot controller executes the functions to access the data stored in the intermediate buffer.

The data transmission sequence can be given in following steps.

1. The robot receives data from the PC.

2. The data is checked for XML conformity and well formness.

3. Received data is copied into appropriate buffer and held there for further processing.

4. The value read from the buffers are then copied to KRL variables.

A sample of the XML files sent and received from the robot is given in Appendix 3.

The communication within the KRL programme is executed as follows.

1. Open connection (at the real time network card).

2. Send a trigger signal to the PC via EtherNet TCP/IP.

3. Wait for data from the PC.

4. Read data from the variables.

3.6   System integration

3.6.1   Hardware integration

As mentioned at the start of this chapter, the complete system has four different modules that need to be integrated together. TIG welding machine, KUKA KR16 robot, laser scanner (3D Scan-control) and welding sensors are to be connected to a PC which will act as the central controller running on LabVIEW. The PC will also possess all the algorithms required for robotic welding. A summarized system integration diagram of the robotic welding system is shown in Figure 3-21.
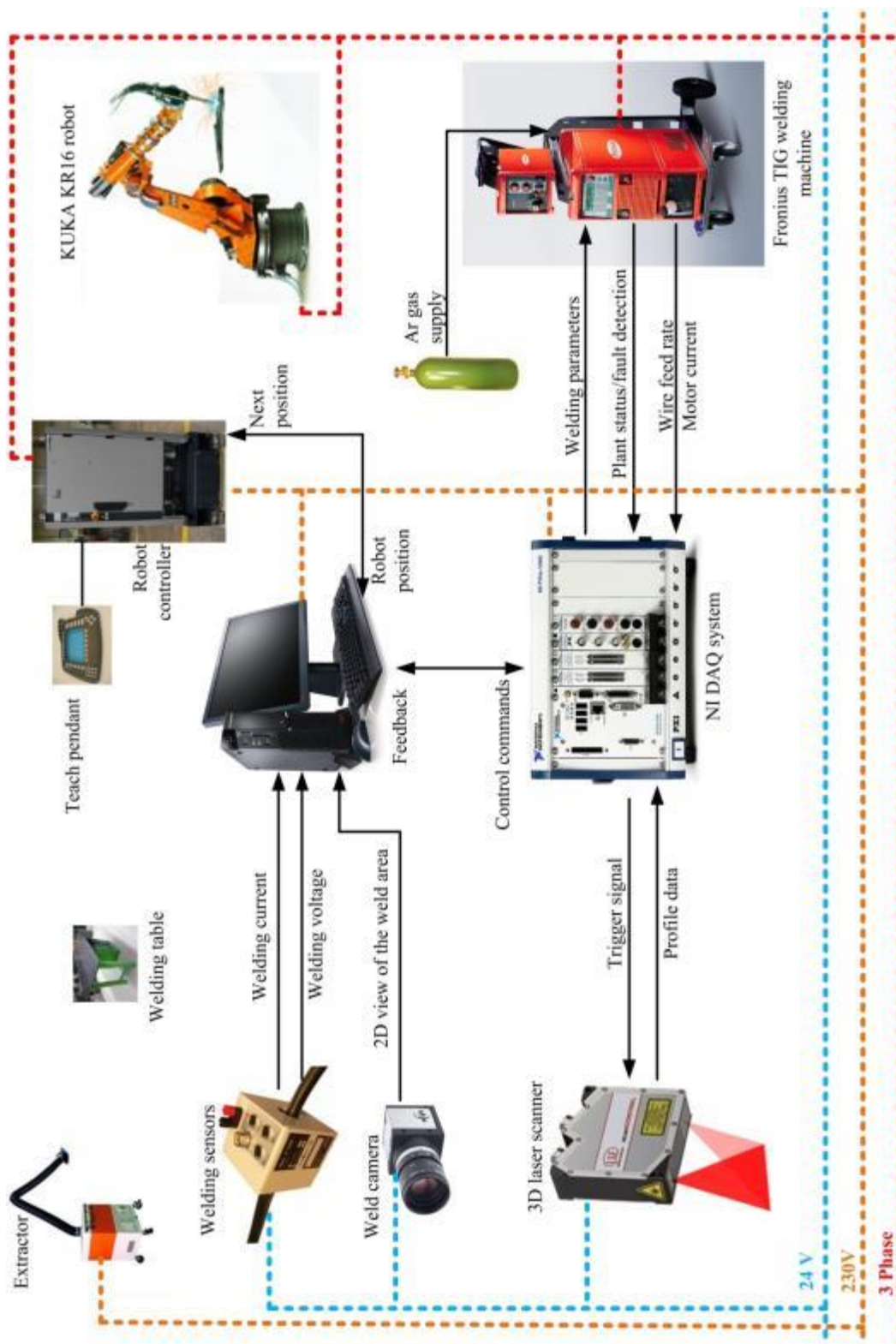
Figure 3-21: System integration diagram

Communication from the PC to the sub-modules is realized as follows.

- Welding machine : Analogue/Digital IO
- Robot : Ethernet TCP/IP
- Laser scanner : Ethernet TCP/IP
- Weld camera : Ethernet TCP/IP
- Welding sensors : Analogue/Digital IO

The control diagram of the system developed is shown in Figure 3-22. Initially the robot is provided with its nominal path to follow and the start parameters (welding current, pulse frequency, duty cycle, base current and wire feed rate) of the welding machine. The robot will first move along the nominal path and collect profile data and process it to find the joint centre positions, joint fit-up and cross sectional area variation along the joint. In the welding-run this information will be used to adjust welding machine settings.
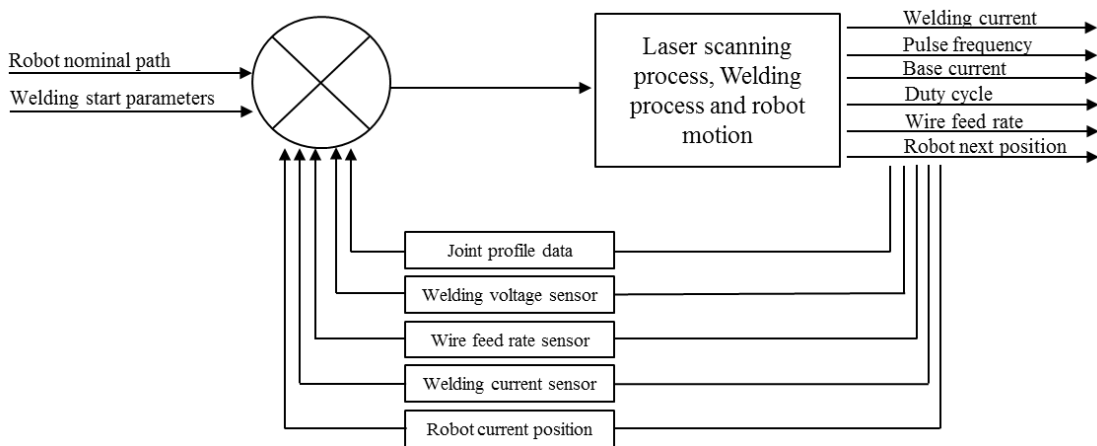
Figure 3-22: Control diagram of the system

A welding table with a guarding system was designed and fabricated for safe automated robotic welding. The guarding panels were selected so as to absorb the arc light or ultra violet rays (UV) generated during the welding process. A Kemper extractor was used with the system to extract the fumes generated during the welding process. A welding fixture was also designed and fabricated which is shown in Figure 3-23.

62

Figure 3-23: Welding fixture

3.6.2 Software integration

To achieve successful automation of the TIG welding process, several intelligent algorithms were developed in this thesis including a *3D* feature extraction algorithm (Chapter 6), a seam tracking algorithm (Chapter 7), a process parameter optimization algorithm (Chapter 8), and an intelligent parameter selection algorithm (Chapter 9). These algorithms are discussed further in the following chapters.

As part of the work carried out in this thesis a novel software tool was developed for TIG welding automation, which is capable of controlling the robot, initiating the laser scanner, optimising the welding process parameters by processing the data received from the sensors (including the laser scanner), performing seam tracking in *3D* (Chapter 7), predicting weld bead geometry (Chapter 8), intelligent selection of welding machine settings (Chapter 9) to obtain desired weld bead shape and *3D* robotic welding. The system software can be divided into four sub-modules and is shown in Figure 3-24.
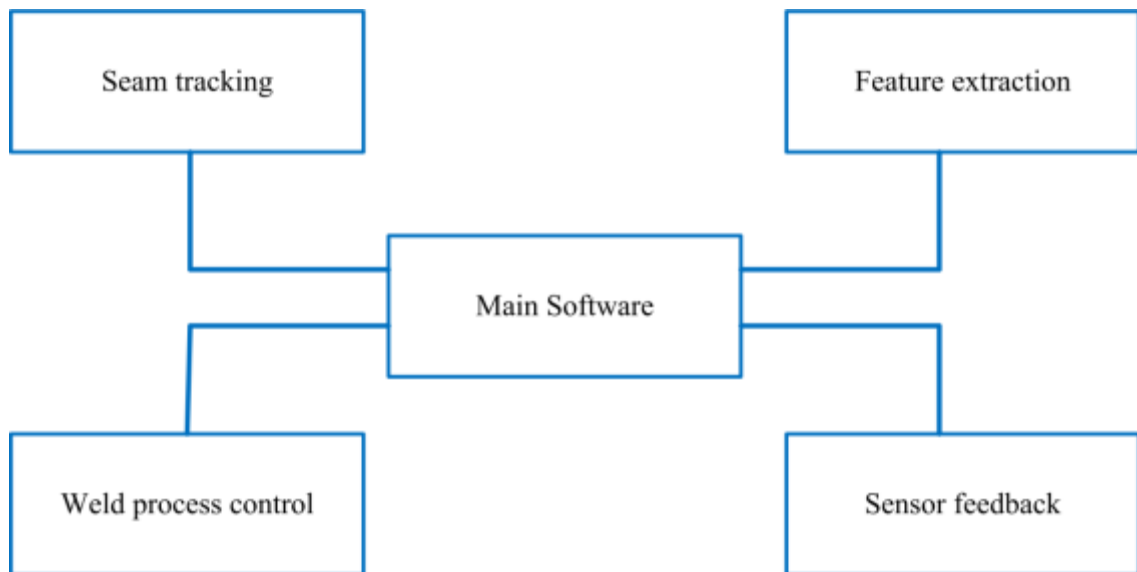
Figure 3-24: Software integration diagram

The photographic views of the software sub-modules developed using the LabVIEW environment is shown in Figure 3-25 to Figure 3-28. Detailed descriptions of these modules are discussed in subsequent chapters.
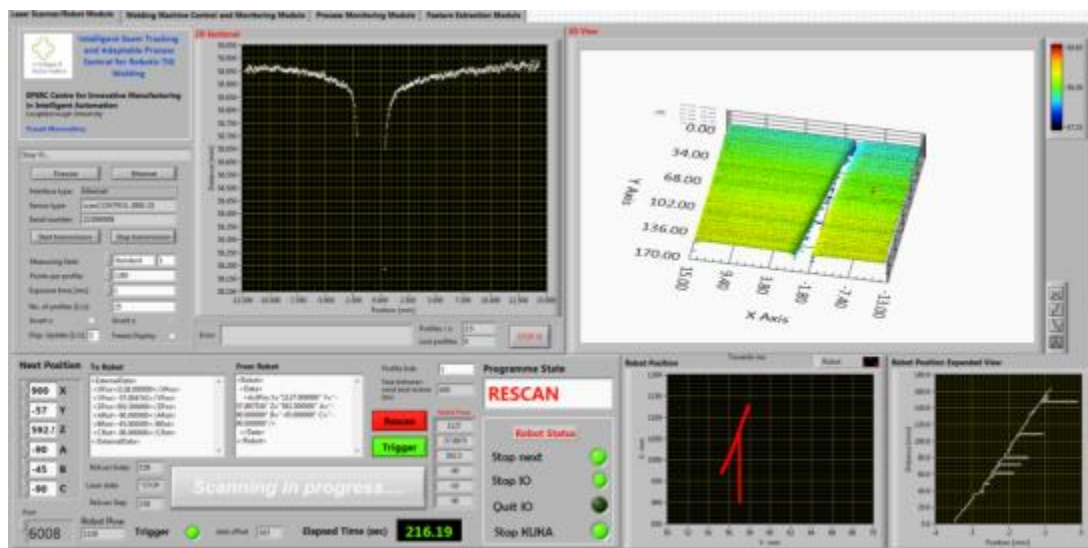
Figure 3-25: 3D Seam tracking software module
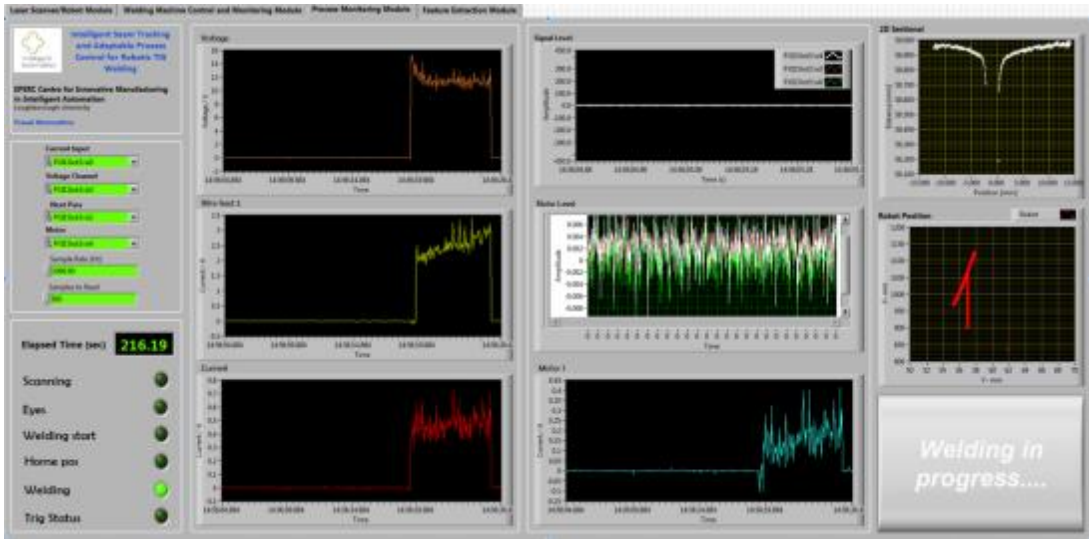
Figure 3-26: Sensor feedback software module
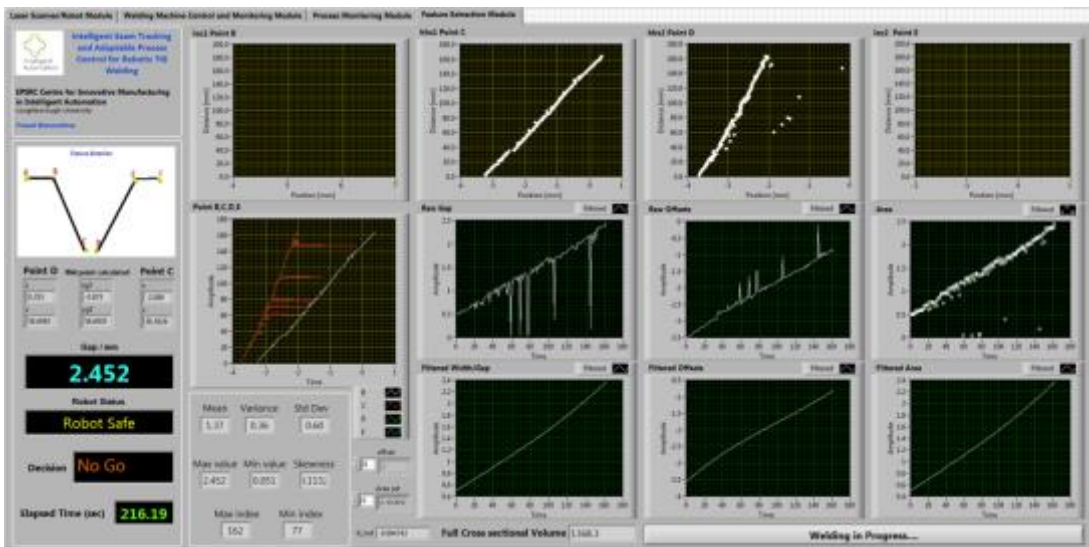
Figure 3-27: 3D Feature extraction software module

Figure 3-28: Weld process control software module

The methodology for carrying out *3D* seam tracking and robotic TIG welding using the above mentioned hardware and software modules with intelligent algorithms are discussed in detail in later chapters.

3.7   Summary

The work presented in this chapter discussed the approach used to select and set-up the robotic TIG welding cell. Detailed discussion of the equipment and their technical specifications were presented. The Fronius Magicwave 4000 welding machine was selected for the automated TIG welding process due to its robust integration capabilities. The Micro-Epsilon Scan-control was selected as the laser scanner because of its compact size and low cost. It suits well for automated seam tracking. Hardware integration and software development were also discussed.   The data processing algorithms, which were used to remove noise from the data obtained from the welding sensors, were discussed. Visualisation of the TIG welding process using a CCD camera, which requires a band-pass filter and an illumination source at a wavelength of 950nm (±10nm spectral width), was also discussed.

A novel software tool was developed to control all the modules of the automated system (laser scanner, welding machine, robot, camera, welding sensors and NI DAQ system) from a PC which was used as the central controller. The robotic welding system was capable of performing automated TIG welding and its intelligent algorithms and system performance is discussed in detail in the following chapters.

4 Human Knowledge and Skill Capture in TIG Welding

This chapter presents the work carried out to understand how experienced human welders approach the difficult and complex task of TIG welding. A novel study on quantifying manual TIG welding, which will ultimately help intelligent automation of TIG welding is discussed. Through manual TIG welding experimentation, the study identifies the key process variables, critical tasks and the strategies adapted by manual welders. Controllability of the welding process parameters and human actions in challenging welding situations (different weld joint types) were studied both qualitatively and quantitatively. Results show that welders with better process awareness can successfully adapt to variations in the geometry and the TIG welding process. Critical decisions taken to achieve such adaptations are mostly based on visual observation of the weld pool. Results also reveal that skilled welders prioritise certain process parameters to simplify the complexity of the TIG welding process.

4.1 Introduction

Despite the merits of the manual TIG welding process in the manufacture of aerospace components in general, a negative aspect with it is the shortage of skilled manual welders and more importantly health and safety concerns [27]. Attempts to develop a straightforward robotic TIG welding solution for aerospace components in the last decade have failed to achieve the desired weld quality. Studies indicate that the lack of process knowledge and adaptability are the major weaknesses of robotic TIG welding [6]. Most of the existing welding robots (such as spot welding robots) perform pre-programmed tasks in assembly lines which have less variation within the parts and the processes [53][152]. Such operations do not require much intelligence and adaptability as the decisions can be pre-programmed. However, applications such as TIG welding of aerospace components involves complex *3D* shaped components [40] and require considerable real-time attention to any minor process variation. This is an issue with the existing robotic welding systems, as their capabilities are limited in real-time sensing and decision making. Furthermore, for any successful automation, the process fundamentals need to be understood in the context of automation.

Some of the previous research carried out in this area have attempted to duplicate human behaviour in to an automated solution [152]. However, intelligent automation is not about producing complete like for like automation solutions to replace a human worker. The Best automation solutions can be produced by understanding the methodology used by a human worker, and using that information for better automation. Prior to any automation, it's important to understand which tasks should be considered for automation and how they should be automated, without which the automation solution may not be economically or practically viable. As shown in Figure 4-1, this research work aims to understand the methodology adopted by a human welder to achieve a good weld, and use the best automation technique to incorporate this methodology into an automated solution.
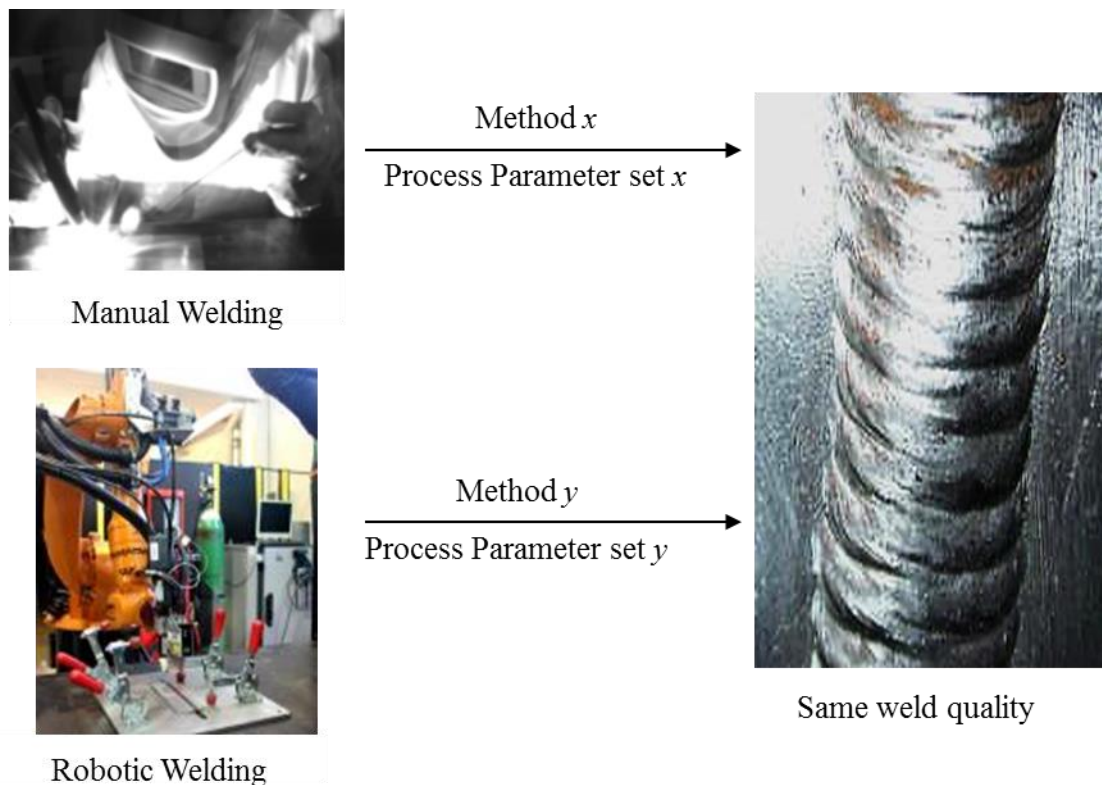
Figure 4-1: Output of manual and robotic welding

4.2 Methodology for human knowledge capturing in TIG welding

Quantitative data was collected from the manual TIG welding process, and statistical techniques were used to analyse the data. Interviews were carried out to collect qualitative data and were correlated with the quantitative data.

4.2.1 Sampling Method

To get a better understanding of human behaviour during TIG welding, manual welders with various skill levels were chosen (as shown in Table 4-1).

Table 4-1: Criteria for defining skill levels for testing

Skill Level	Selection Criteria
Novice	No experience in welding.
Semi-Skilled	Have experience in other welding types but no experience in TIG welding.
Skilled	Years of experience in TIG welding

The study of TIG welding with novice skill levels will elucidate the types of defects and errors that could occur during initial robotic TIG welding (i.e. without any process knowledge or adaptive control sensors). Semi-skilled welders were selected to identify the extent of knowledge that is required for producing good TIG weld samples. TIG welding experts are expected to produce the best quality welds and the methodology used by them is expected to provide the key information for automation. Moreover, their behaviour at challenging welding conditions could be used to correlate to the errors that an automated system could fail under when facing a similar challenge.

4.2.2 Participants

Due to individual differences between operators, more than one operator representing each knowledge level was recruited to the study. All the experiments were performed according to the ethics guidelines set out in the Code of Ethics and Conduct of the British Psychological Society (2009) [153]. Welders were given prior introduction to the welding equipment and the risks involved in welding. Selected participant profiles are described in Table 4-2.

Table 4-2: Description of manual welders

Welder	Experience
N1	No experience in welding
N2	Have very small experience in welding
N3	No experience in welding
SS1	Good experience with manual metal arc welding but only one instance has done TIG welding. Has experience with welding automation with an x-z linear rail.
SS2	Good experience with all types of welding processes except TIG welding.
SS3	Has some experience in TIG welding.
S1	Has a background in aircraft maintenance with the Royal Air Force and currently teaches a range of welding techniques to undergraduate students.
S2	Has a background in high quality welding and routinely undertakes a range of bespoke manual TIG welding projects.
S3	Over 40 years' experience in TIG welding.

N : Novice
SS : Semi-Skilled
S : Skilled

S 1

Skilled   Welder 1
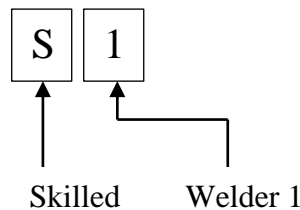
4.2.3 Experimental setup and materials

A block diagram of the experimental setup is shown in the Figure 4-2(a) and images of the setup are shown in Figure 4-2(b). The TIG welding equipment used for the task include: Fronius Magicwave 4000 welding set with welding torch, argon inert gas supply, earth cable, a steel covered work bench, a stool for the operator, pre-cut base metal practice pieces and filler rods. The experimental samples are of size 200mm x 50mm x 1.5mm (stainless steel 316l) with 1.6mm filler rods. Standard personal protective equipment (PPE) was used during the experiment including, welding masks, lab coats and protective boots. Before each experiment, the work pieces were cleaned using a wire brush to assure better weld quality and to avoid defects due to oxides on the surface. A file was used for edge preparation of the part.
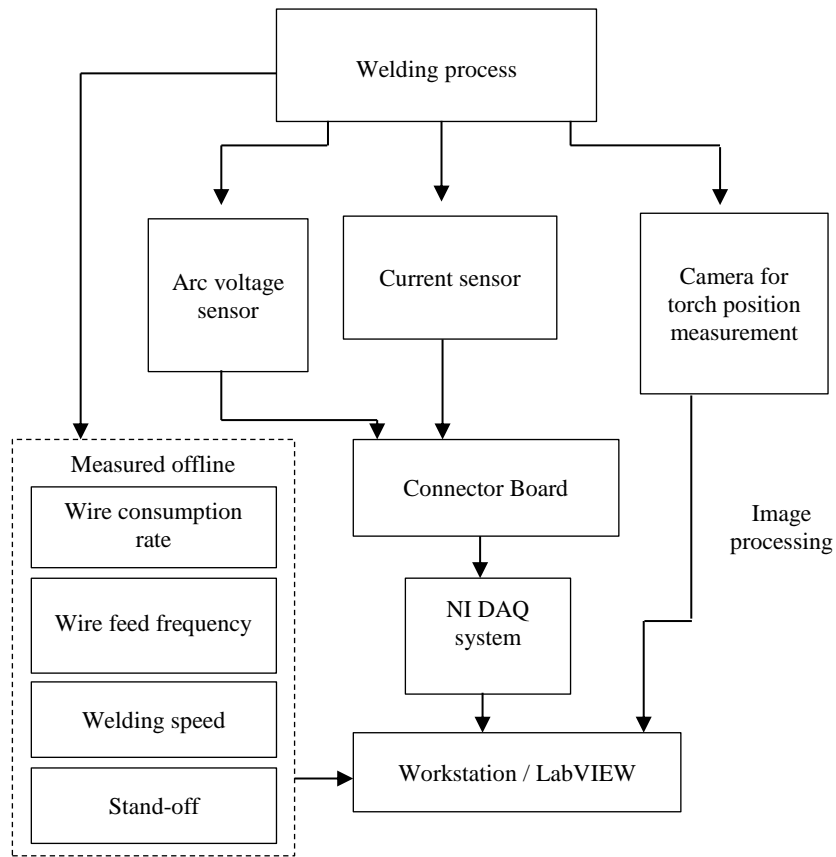
Figure 4.2(a)
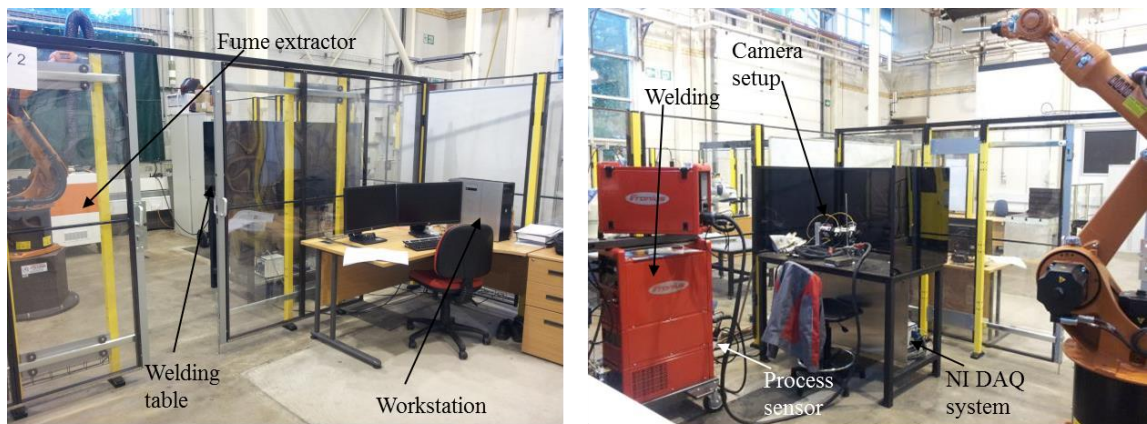
Figure 4.2(b)

Figure 4-2: System diagram of the experimental setup (a) block diagram, (b) image of the physical set-up

Three different types of weld joints (butt, lap and fillet joint) were selected as shown in Figure 4-3. A butt weld is considered to be more difficult according to the experts, followed by the fillet and finally the lap joint. More defects are expected to be present in a butt joint, due to the gap between the parts. A lap weld joint is expected to be more easily weldable than the fillet weld, as the assessment of the weld seam is difficult in a fillet weld.
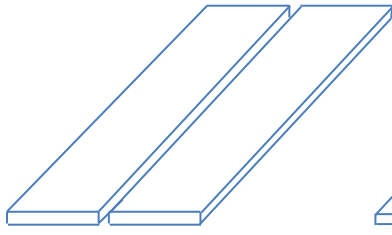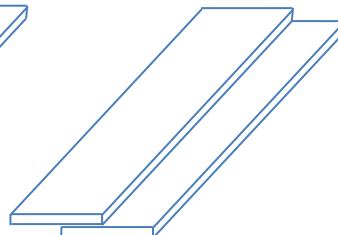
| Figure 4.3(a) | Figure 4.3(b) | Figure 4.3(c) |
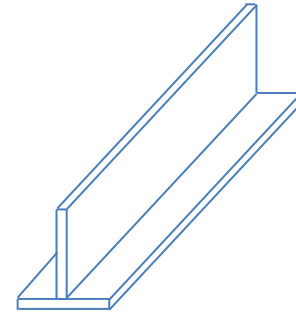
Figure 4-3: Three weld joint selected for testing (a) Butt joint, (b) Lap joint, (c) Fillet joint

4.2.4 Testing method

All the welders were provided with an introduction to health and safety and also the operating procedure of the equipment prior to the experiments. One practice run was performed for all the novices to make sure they felt comfortable during the experiments.

The following four joint configurations were then experimented with for each welder:

1. Butt weld with a constant, 1mm, gap
2. Butt weld with a varying gap from 1mm to 3mm
3. Lap weld with zero gap
4. Fillet weld with zero gap

The varying gap joint was selected to study the adaptability of the welders for geometry variations and to understand human adaptation for successful automation. Four runs for each welder were carried out, which lasted between 1 to 2 hours. Each weld was followed by a discussion session to investigate the experience of the welder during the laying of the weld. All important points raised during the discussion were noted down for further analysis.

Welding current was measured using a Hall Effect current sensor and the welding voltage was measured between the opposite polarities of the welding machine. All the data were logged simultaneously into a PC through the National Instruments Data Acquisition (NI DAQ) system at a sampling rate of 1 kHz. A low-pass filter was designed to filter any noise generated within the data acquisition system.

The Stemmer IDS UI-5240SE-NIR-GL camera was used to measure the weld angles of the torch and filler wire as shown in Figure 4-4. Videos of each weld were recorded and weld angles were calculated using the LabVIEW Image processing toolkit (Edge detection). Typical torch-wire orientation is shown in Figure 4-5. Angles were only

considered in the *x-z* plane as the movement of torch and filler wire in the *y* direction (perpendicular to travel direction and normal of work piece plane) is insignificant and could not be measured accurately using the single camera system.

Figure 4-4: An image of the camera setup for testing a welder
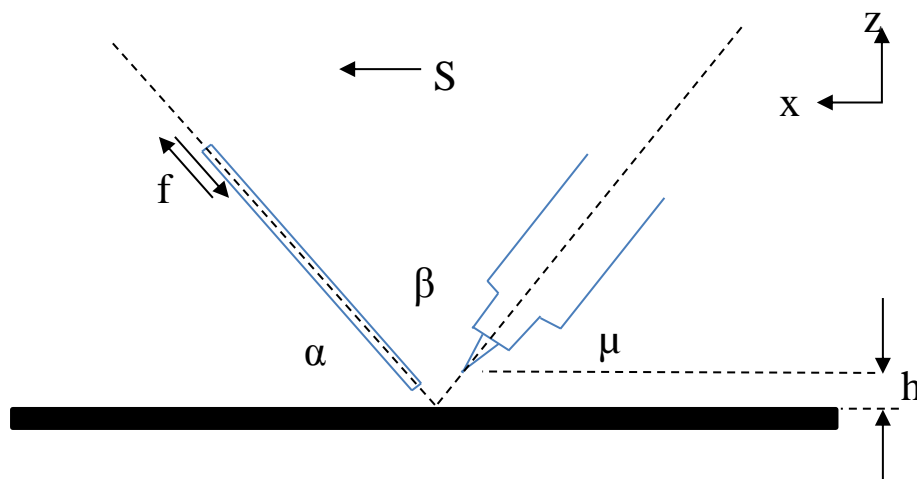
α	:	Forward angle	*f*	:	Filler wire feed frequency
β	:	Weld angle	*h*	:	Stand-off distance
μ	:	Back angle	*c*	:	Filler wire consumption rate
s	:	Welding Speed			

Figure 4-5: Torch and filler wire position definition

The lliterature recommendation is to maintain weld angles in the range of α: 60-85°, β: 80-90°, μ: 15-30° [126]. Stand-off is the distance between the welding torch tip and the work piece surface. This is also referred to as the arc length. It is difficult to extract this information from the video as the bright light saturates the area around the point of arc. But since voltage is directly proportional to the stand-off, the equation presented in Appendix 4 will be used to estimate the stand-off distance. Average welding speed was calculated from equation 4.1, using the welding time obtained through the offline video.

Welding speed was assumed to be uniform along the weld and varying only among different joint configurations.

$$Average\ welding\ speed = \frac{Length\ of\ the\ weld}{Weld\ time} \tag{4.1}$$

The average filler wire consumption rate was calculated using equation 4.2.

$$Filler\ wire\ consumption\ rate = \frac{(l_1 - l_2)}{Weld\ time} \tag{4.2}$$

where l_1 and l_2 are the length of the filler wire before and after welding respectively.

Total number of filler wire movements in to the weld pool was counted from offline videos and the filler wire feed frequency was calculated using equation 4.3.

$$Filler\ wire\ feed\ frequency = \frac{Number\ of\ filler\ wire\ dippings}{Weld\ time} \tag{4.3}$$

A typical welding current and voltage diagram is shown in Figure 4-6. The following parameters could be obtained from it.
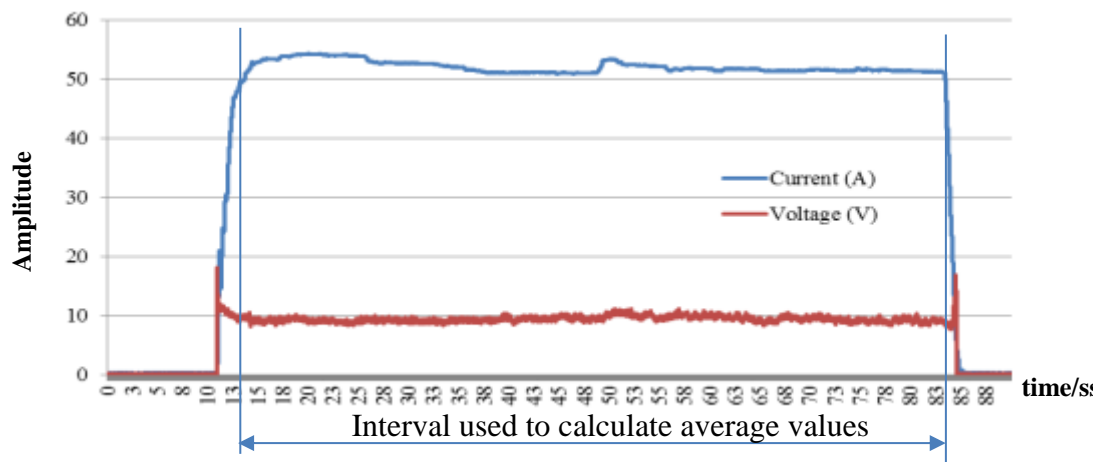
Figure 4-6: Typical welding diagram

- Average welding current (I_{avg}): This is the mean value of current signal between where the welder starts and stops moving the welding torch.
- Standard deviation in current: This describes the average deviation in welding current from its mean value.
- Average welding voltage (V_{avg}): Average voltage is the mean value of the voltage signal and is measured between the start and stop of torch movement.

74

- Standard deviation in voltage: This is the average deviation in voltage from its mean value. Standard deviation in voltage is an indirect measurement of the amount of control the welder has on torch positioning.

An INSTRON 8801 tensile testing machine was used for carrying out the tensile tests to find the breaking strength of the welds. In addition to these quantitative measures, qualitative measures were also recorded. Notes were taken after each weld and experience of the welder was noted down. Videos were recorded for further analysis.

4.3 Results and discussion

Process parameter variations for different weld joint types were measured. Parameters such as voltage, current, speed, wire feed frequency and wire consumption rate used by various welders for various joint configurations are presented in this section. All these parameters are compared against the different skill levels. Qualitative results from the interview sessions are also discussed in this section.

4.3.1 Effect of skills on weld appearance

To study the significance of skill level on the weld bead quality, the weld produced by various manual welders (constant gap butt weld) were assessed for visual imperfections. A weld produced by novice (N1) welder is shown in Figure 4-7.
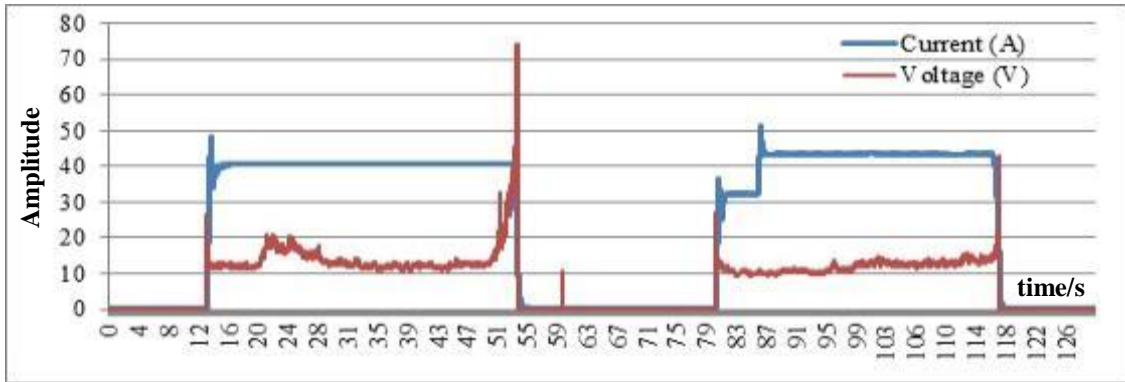
Figure 4.7 (a)

Figure 4.7 (b)
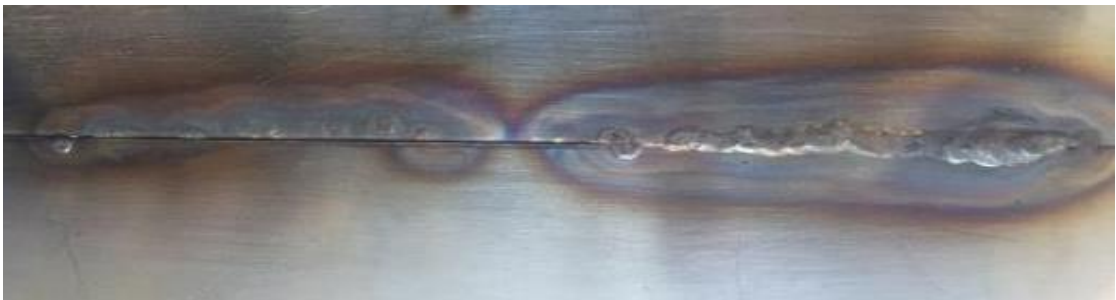
Figure 4.7 (c)

Figure 4-7: Butt weld completed by a novice welder (a) welding current and voltage variation against time, (b) top view of the weld, (c) bottom view of the weld

As can be seen from the figure, the welding was not of good quality and was stopped at the middle (due to contamination of the electrode). During the first half of the weld, the novice faced difficulties in establishing the weld pool which resulted in poor quality. Weld ripples noticed in the first half of the weld is predominantly due to melting of the filler wire by the arc, rather than melting created by the heat of the weld pool. A decent weld pool was established in the second half of the weld which resulted in better quality weld than the first half. This result demonstrates the importance of establishing the weld pool before the movement of the welding torch, which has to be taken into account in welding automation.

76

It can also be seen from figure 4.7(b) that heat affected zone (HAZ: shown in the figure) is not consistent. For a good weld it is vital to maintain constant heat input throughout the length of the weld. As can also be noted from Figure 4.7(a), the welding voltage varies significantly, which indicates the welder's inexperience in maintaining the torch height at a constant level. In addition, it can be seen from Figure 4.7 (b) that a good penetration can only be achieved once the weld pool is established.

A butt weld performed by a semi-skilled welder (SS1) is shown in Figure 4-8.
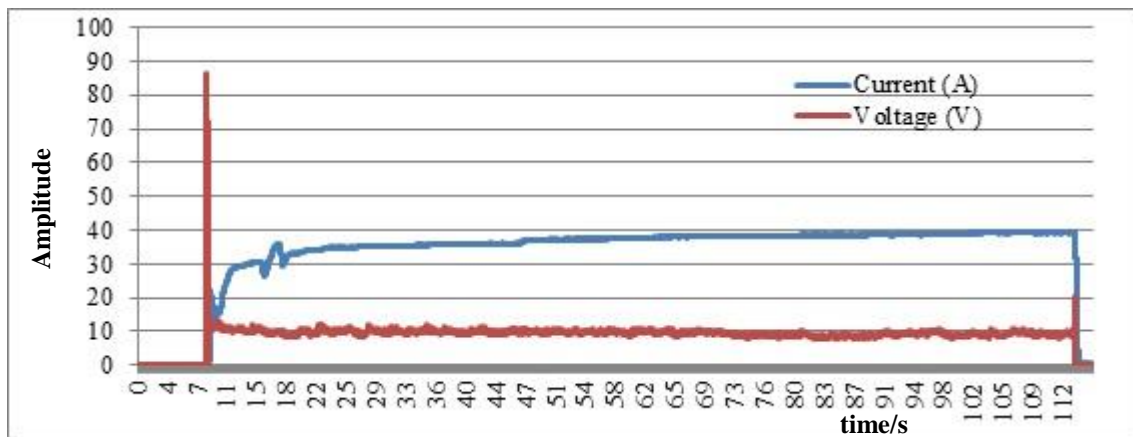
Figure 4.8(a)

Figure 4.8(b)

Figure 4.8(c)

Figure 4-8: Butt weld completed by a semi-skilled welder (a) welding current and voltage variation against time, (b) top view of the weld, (c) bottom view of the weld

As expected and as shown in Figure 4.8 (a), the welder has maintained a constant voltage (constant stand-off is maintained). However, the welding current has been

reduced rapidly at the end of the weld which may affect the mechanical strength of the weld at that point (comment from skilled welders). As seen from the figure 4.8 (b), the weld ripples were not uniform (weld width varies along the length of the weld), even though the HAZ is consistent along the weld. It was also noted from the sample that the weld contains excessive reinforcement with inadequate penetration shown in figure 4.8 (c).

Data obtained for a skilled welder is shown in Figure 4-9.
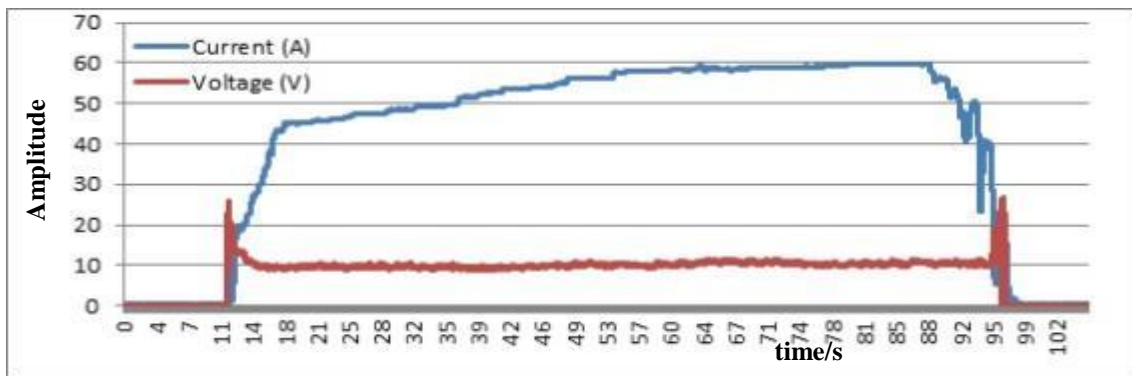
Figure 4.9 (a)

Figure 4.9 (b)
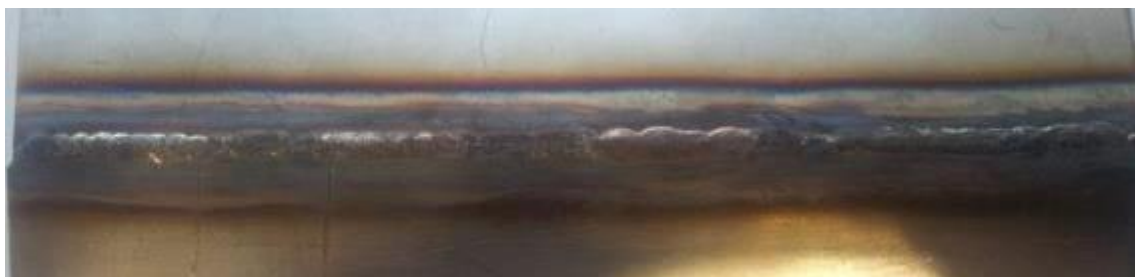
Figure 4.9 (c)

Figure 4-9: Butt weld completed by a skilled welder (a) welding current and voltage variation against time, (b) top view of the weld, (c) bottom view of the weld

As seen from the figure 4.9 (b), it is evident that the welder has maintained a constant ripple frequency, bead width, HAZ and acceptable reinforcement. Welding current was reduced gradually at the end compared to other two skill levels as shown in figure 4.9 (a). Voltage is consistent which suggests the welding torch was maintained at a constant

stand-off. As seen in the bottom view in figure 4.9 (c), the welder has achieved acceptable penetration as well.

Images of the welding results of the other welders are presented in Appendix 6.

4.3.2 Effect of welding skills on process parameter control

This section presents the results and discusses the effect of the selected skill levels on process parameter control.

4.3.2.1 Welding current

The average welding current and respective standard deviation maintained by the welders is shown in Figure 4-10 and Figure 4-11. As noted, all the welders have used a similar range of welding current; however the standard deviation shows significant variation between the skill levels. This variation can be explained on the basis of the need for simultaneous control of more than one process parameter during the welding process, such as control of welding current and wire feed rate. Novice welders have used constant current during the welding process (lower standard deviation) and may have focused on controlling other parameters (such as torch position). However, the skilled welders have controlled most of the parameters (S1-varying current, constant gap, optimal torch position) and have demonstrated the need for simultaneous control of more than one parameter. This result confirms that the TIG welding is a complex process and any automation attempt should consider simultaneous control of multiple parameters.
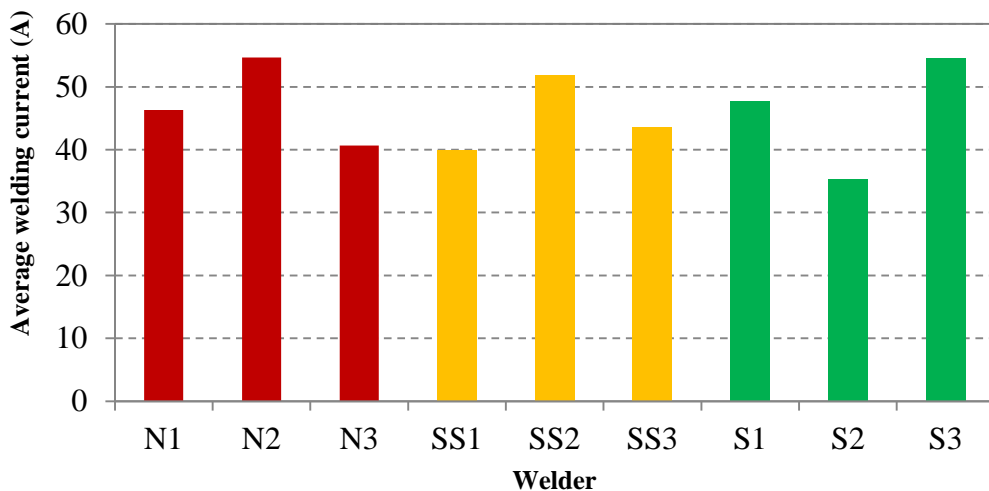
Figure 4-10: Average welding current used by different welders

79
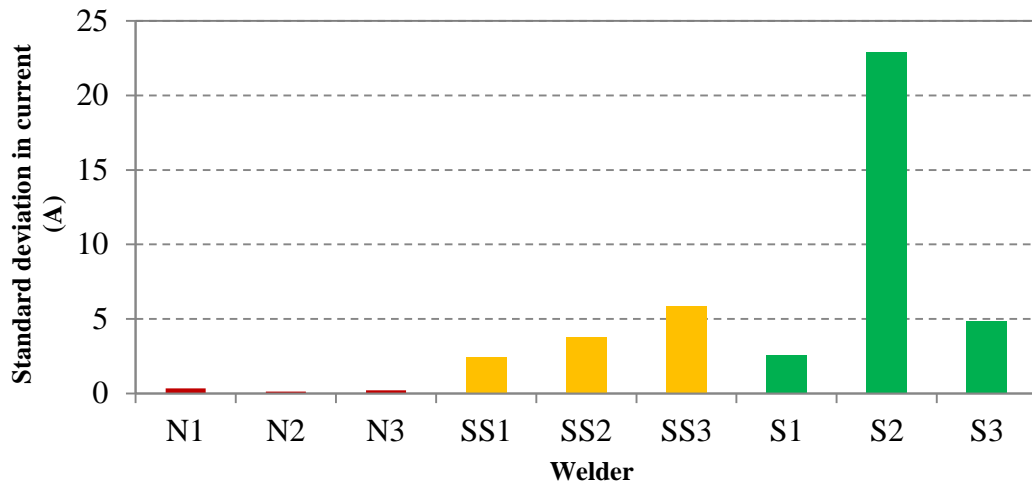
Figure 4-11: Standard deviation in welding current for different welders

Different techniques used by welders in welding current control are shown in Figure 4.12.
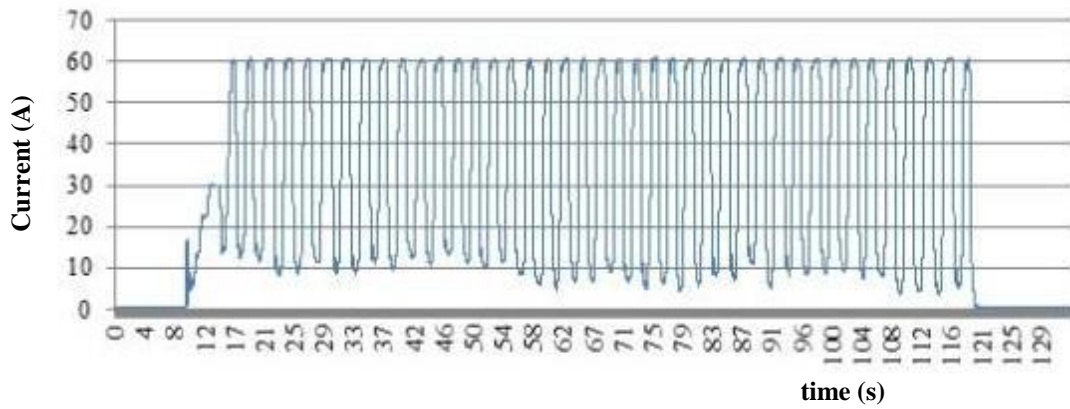
Figure 4.12(a)
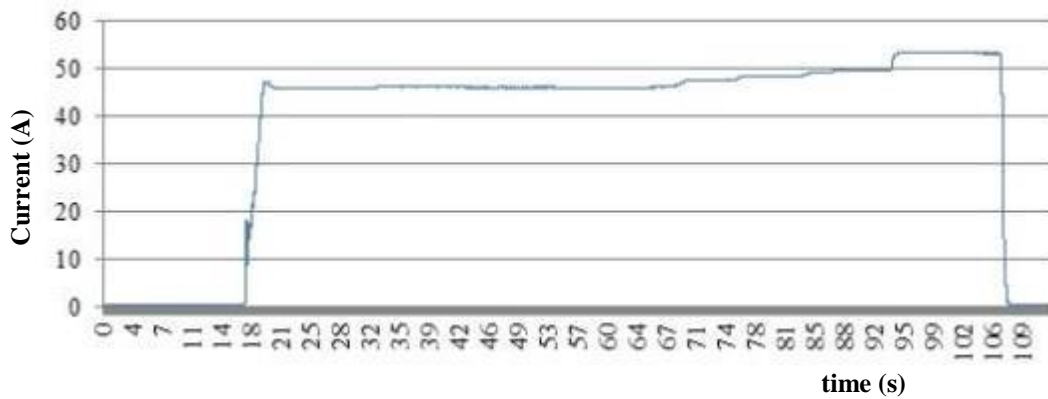
Figure 4.12(b)

Figure 4-12: Different manual welding techniques (a) pulse created by the manual welder from the foot pedal, (b) normal welding technique used by welders

According to Figure 4-11, S2 show a significantly high standard deviation because S2 deliberately used a special technique of oscillating the foot pedal to create a pulse in welding current signal. Post study interviews suggested that S2 believes he can reduce

the heat input to the work piece by using this pulsing method and therefore he can achieve less deformation. As seen in Figure 4-12 (a) S2 has managed to achieve a lower average current (35A) compared to the other welders (48A) in Figure 4.12 (b). Presently this technique is adopted in automation for welding thinner work pieces so that the deformation can be minimized.

A photographic view of the welded sample with pulsed current is shown in Figure 4-13. As can be noticed, the pulsing technique shows good penetration, however the weld appears to be grey from the bottom side. This is not attributed to pulsing, but the ineffectiveness of human welder in simultaneous control of multiple tasks. During the oscillation of foot pedal (to generate pulsed welding current), the oscillating effect indirectly affects the voltage signal as shown in Figure 4-14. It seems, even a skilled human welder faces difficulty to synchronize two motions together (in this case hand and foot movement).
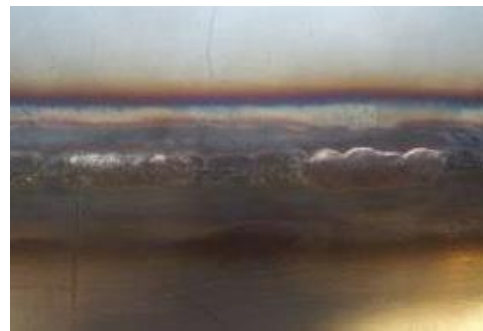
| Figure 4.13 (a) | Figure 4.13 (b) |

Figure 4-13: Pictures of bottom side for different weld techniques (a) pulsed current, (b) constant current
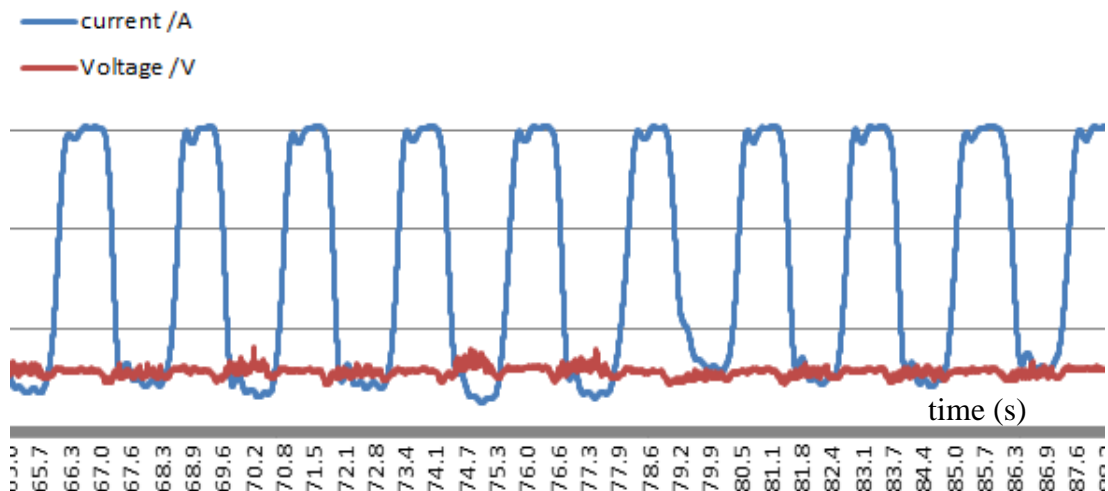
Figure 4-14: Indirect effect of pulsing on the voltage signal

4.1.1.1 **Welding voltage**

The average voltage and standard deviation in voltage respectively are shown in Figure 4-15 and Figure 4-16. As noticed from Figure 4-15, novices have a higher average voltage compared to the other two skill levels. This should be attributed to novice's unawareness of the importance of holding the torch at an appropriate stand-off distance. At higher stand-off distances the weld pool fails to get the required gas shielding and consequently a poor weld quality is seen. This result indicates that it is important in automation to control the robot path in a way that the stand-off distance is always maintained within an acceptable range.
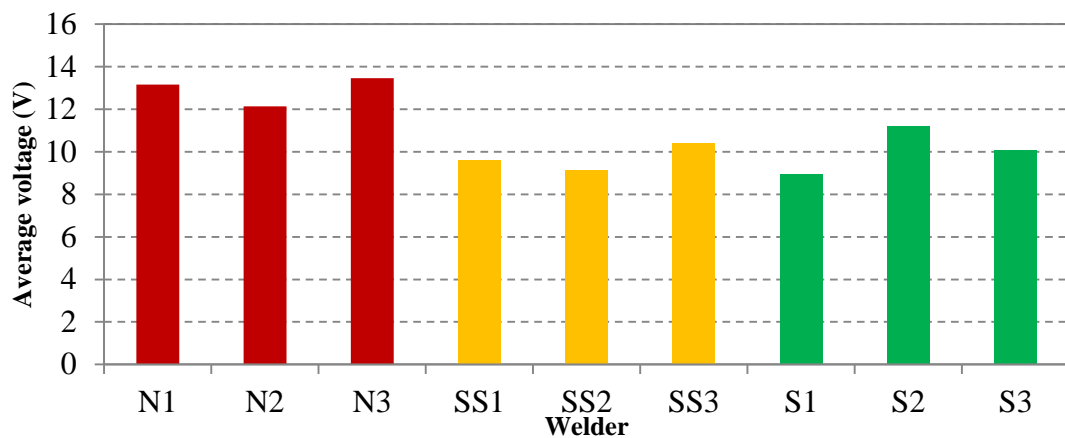
Figure 4-15: Average voltage measured for different skill levels

The standard deviation in the voltage provides an indication of the welders' control over the torch positioning. As observed in Figure 4-16, novices have a higher standard deviation in voltage compared to the other two skill levels. This could be due to their inexperience or lack of knowledge of the importance of maintaining a constant voltage throughout the weld. Post-weld interviews indicated that novice welders had difficulty in the simultaneous control of both the torch positioning and the foot pedal control which may have been the reason for their higher standard deviation in voltage. However, post-weld interviews with skilled welders shows that the torch movement (vertically) should be kept to minimum, which is reflected from the voltage readings. As mentioned earlier, the welder S2 used a unique technique of oscillating the current by using the foot pedal, which has affected his performance on maintaining consistent stand-off distance. This has resulted in a relatively higher standard deviation in voltage for S2 compared to other two skilled welders (S1 and S3). These results also suggest that any voltage variation which can occur in robotic welding should be kept at minimal.
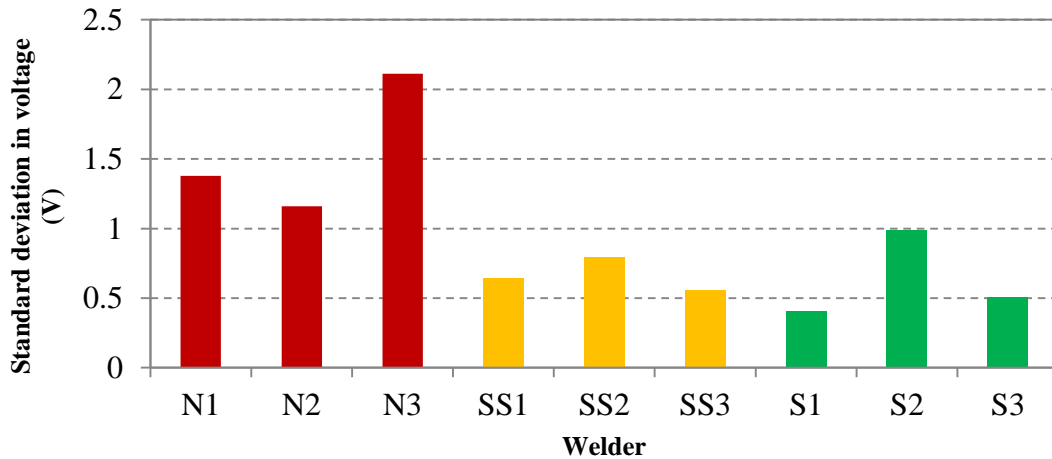
Figure 4-16: Standard deviation in voltage for different skill levels

4.3.2.2 Welding speed

The average welding speed maintained by the welders is shown in Figure 4-17.
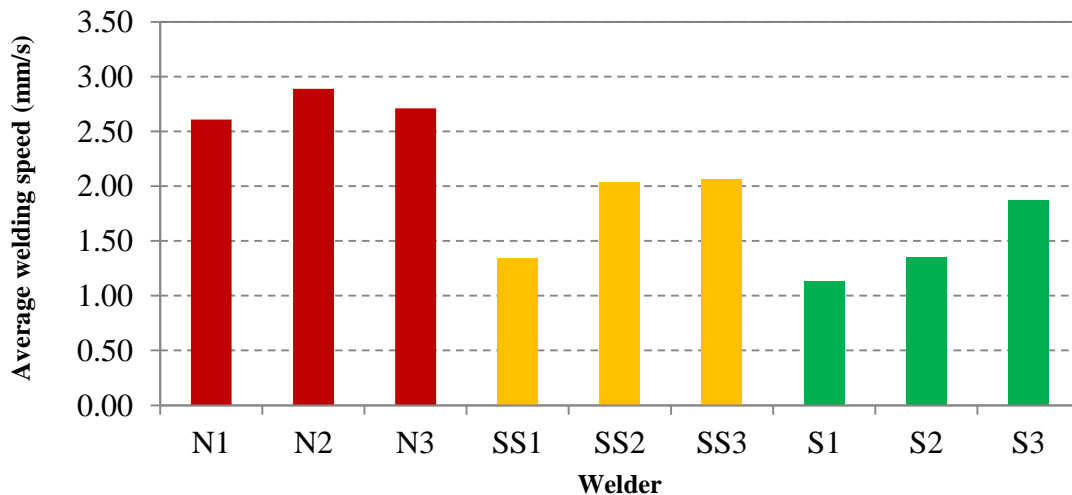
Figure 4-17: Average welding speed maintained by different welders

According to the figure, novice welders attempt to move faster than the other welders. Post weld interviews suggested that this is because it is difficult for the novice to hold the torch for a long period of time. Novices also came across difficulties in feeding filler wire and therefore ran-out of filler wire before completing the weld. As a result, novices attempted to complete the weld as quickly as possible. It was observed from the captured welds that attempting to move faster can result in losing the weld pool and therefore poor quality as shown in Figure 4-18.
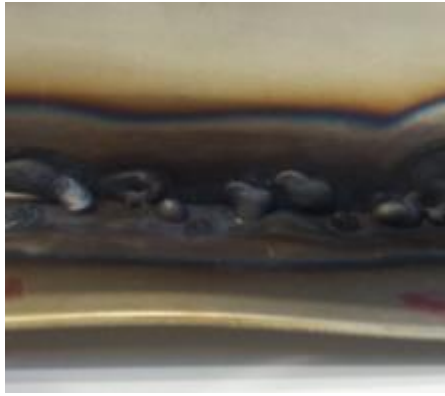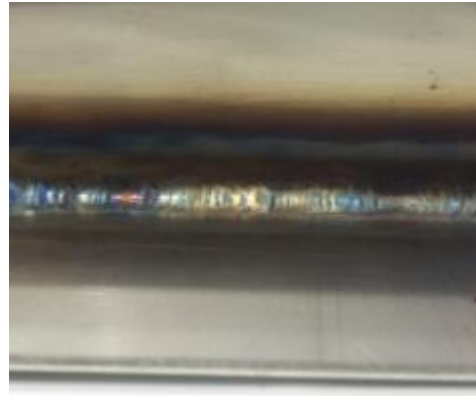
Figure 4.18(a)   Figure 4.18(b)

Figure 4-18: Effect of welding speed on weld finish (a) Higher speed (b) average speed used by a skilled welder

4.3.2.3 Filler wire frequency and consumption

The filler wire feed frequency and consumption rate observed for different welders are shown in Figure 4-19.
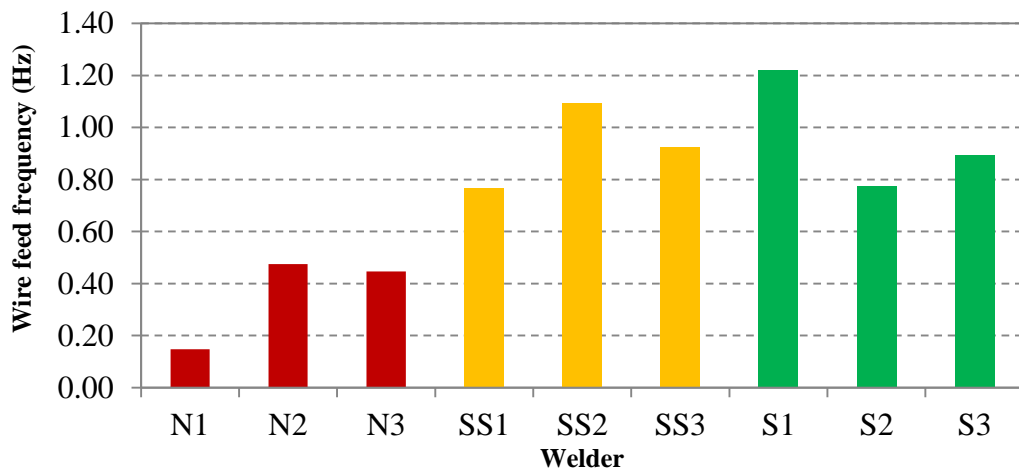
Figure 4.19 (a)
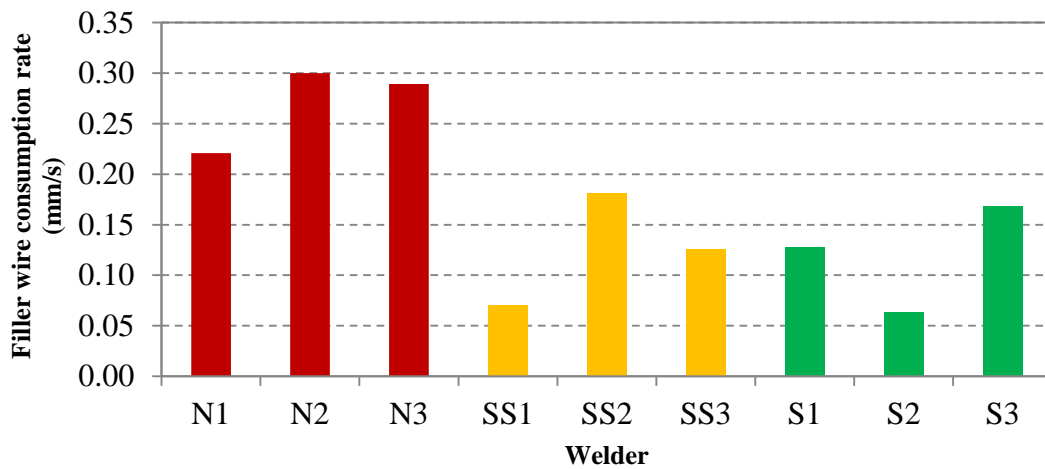
Figure 4.19 (b)

Figure 4-19: Filler wire feed frequency and consumption rate for different welders (a) filler wire feed frequency, (b) filler wire consumption rate

As noticed from Figure 4-19(a), novice welders used a lower wire feed frequency compared to the semi-skilled or skilled welders, however the novice welders have consumed more filler wire than other welders (Figure 4-19(b)). This is contradictory since it was expected that the filler wire consumption should increase with higher feed frequencies (it was observed from videos that the feed amount does not vary significantly).

Analysis of the offline weld videos showed that the novices feed the filler wire into the arc, whereas the skilled welders feed the filler wire into the melt pool. Feeding the filler wire to the weld pool is a very important factor in TIG welding because it assures continuity and consistency of the weld bead. This is reflected in the weld images in Figure 4-20 where the novice has failed to achieve a continuous weld compared to the more experienced welder. Feeding of the filler wire into the melt pool results in a more uniform weld bead and should be considered as a critical task in TIG welding automation.

| Figure 4.20 (a) | Figure 4.20 (b) |

Figure 4-20: (a) Globular droplets from melting the wire from the arc (b) a weld performed by feeding the wire in to the melt pool

4.3.2.4 Stand-off distance

The Stand-off distance for the different welders is shown in Figure 4-21.
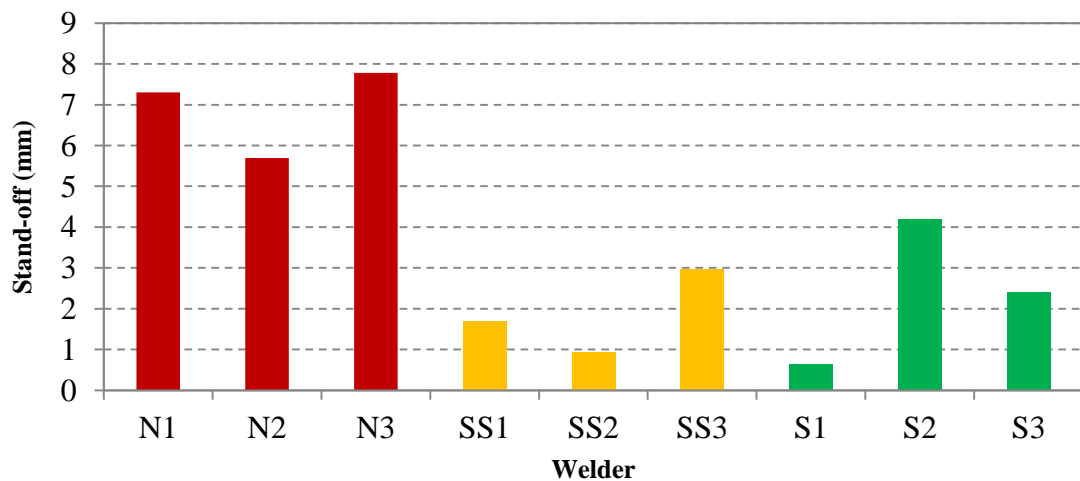
Figure 4-21: Torch stand-off distance for different welders

As can be seen in the figure, novice welders have higher stand-off distances compared to welders of other skill levels. Higher stand-offs will reduce the gas shielding around the welding arc and can result in poor weld quality. Also, an increase in stand-off will result in an increase of the voltage and subsequently more thermal deformation of the part. Therefore it is vital in automation to understand and maintain the stand-off distance to achieve the required weld quality.

4.3.2.5 Torch / Filler-Wire Orientation

Example photographic views of the welders with different skill levels are shown in Figure 4-22(a), (b) and (c).
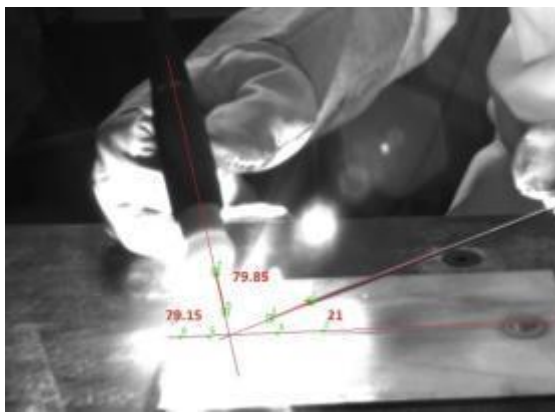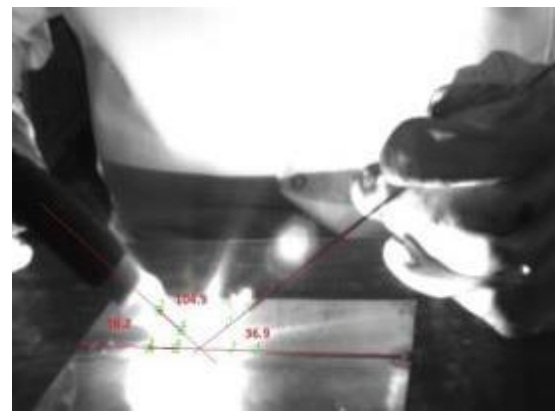
Figure 4.22(a)   Figure 4.22(b)
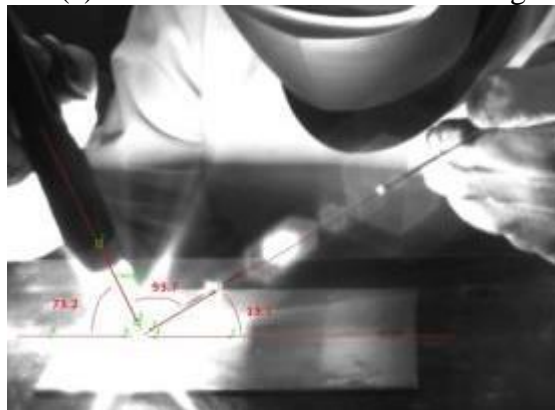
Figure 4.22(c)
Figure 4-22: Images taken for different skill levels (a) novice welder, (b) semi-skilled welder, (c) skilled welder

As seen from Figure 4-22(c), the skilled welder is monitoring the process very closely (head position much closer to the weld zone) and maintains a comfortable position to visualize the weld pool compared to the other welders. Visualisation of the weld pool and subsequent adaptive control of the process parameters is significant in TIG welding and should be considered in automation. Weld angles are also important in maintaining

a the required weld pool shape and better gas shielding around the weld. As mentioned in Section 1.5.3, For a good weld, it is recommended to have the weld angles; α: 60°-85°, β: 80°-90°, μ: 15°-30° [126]. As noted from Figure 4-23, only the skilled welder maintains the weld angle within this acceptable range.
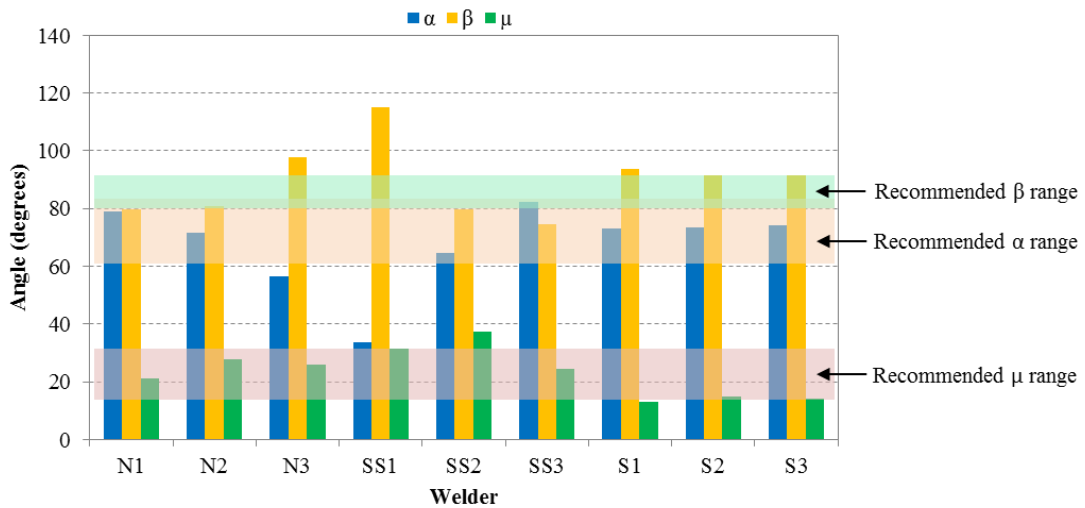
Figure 4-23: Torch/filler wire orientation

4.3.3 Process Parameter Variation for Weld Shapes/complexity

This section presents the results of the manual welder's behaviour in process parameter selection for the different joint types[2].

4.3.3.1 Average welding current

The average welding current used by the welders for the various joint types is shown in Figure 4-24.
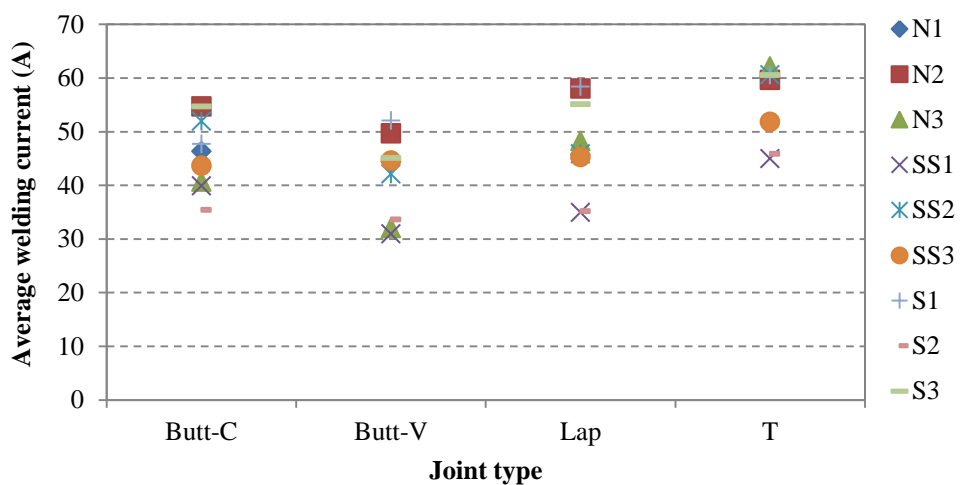
Figure 4-24: Average current variation against joint type

---

[2] Fillet joint is also referred to as 'T'joint

As can be seen from figure, the average welding current is lower for the butt joint compared to the other joints. The reason is that a lap or T-joint doesn't have any gap between the plates (zero gap condition) and therefore requires a higher power to melt the plates which is achieved by a higher current. Also noted from the figure is that the butt weld with a varying gap would require a lower welding current compared to the butt weld with a constant gap. This is due to the fact that, an increase in the gap results in the rapid melting of the work pieces, which then requires a lower welding current to reduce the heat input.

4.3.3.2 Average welding voltage

Average welding maintained for the different joint types by the welders is shown in Figure 4-25. As can be seen from the figure, there is no significant variation in the average welding voltage for the different weld joints. This implies that the welders do not change the stand-off to adapt for joint type.
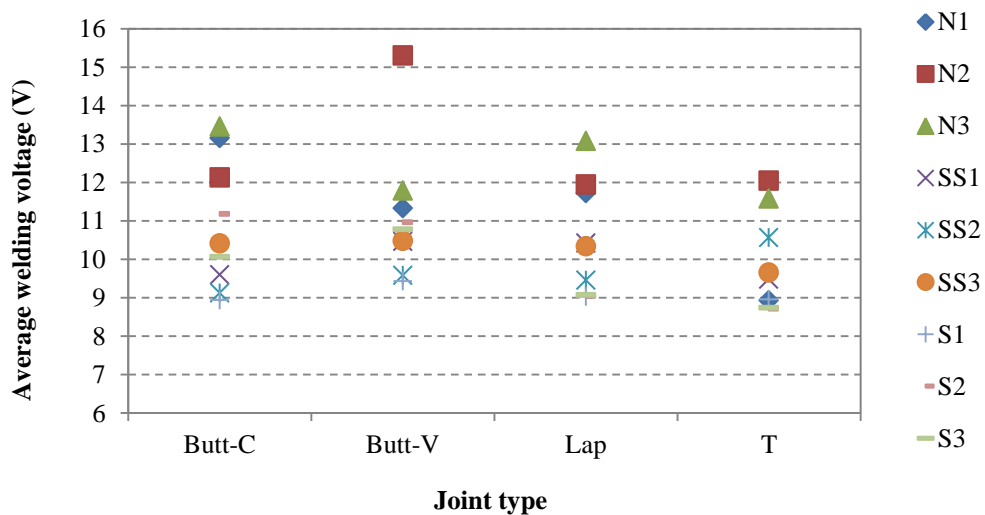
Figure 4-25: Average voltage against joint type for different welders

4.3.3.3 Filler wire consumption/feed frequency

The filler wire consumption rate for the different joint types is shown in Figure 4-26.
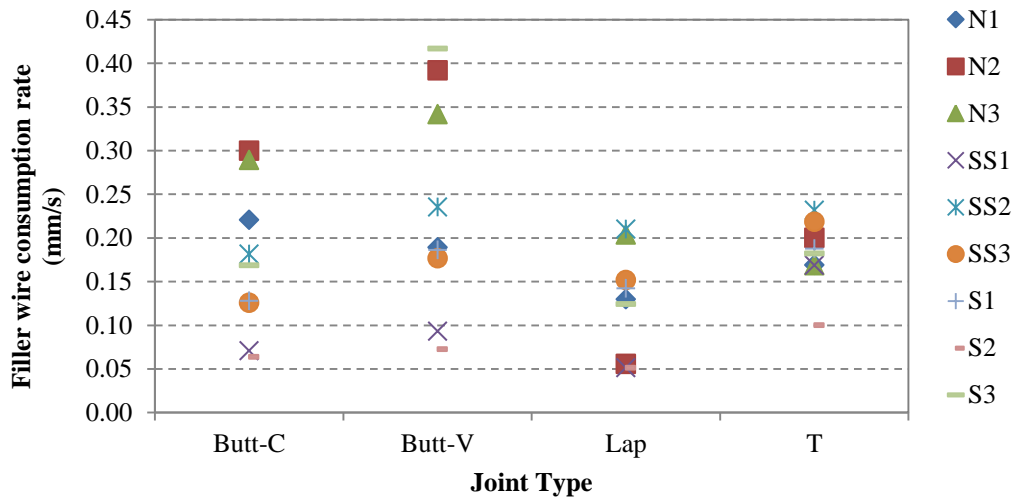
Figure 4-26: Filler wire consumption rate for different weld joints

According to the figure, more filler wire was used for the Butt-weld-varying gap joint than the other joints. This is related to the high volume of filler required to fill the varying gap joint compared to the other joints. The amount of filler wire used in the Lap and T-joints are low due to the zero-gap-fit-up. Also noted from the figure is that more filler was used with T-joint than Lap joint. This is attributed to the rapid melting of the edge of the lap joint compared to the T-joint. The filler wire feed frequency showed a similar pattern as the filler wire consumption.

4.3.3.4 Welding speed

The average welding speed used for each joint type is shown in Figure 4-27.
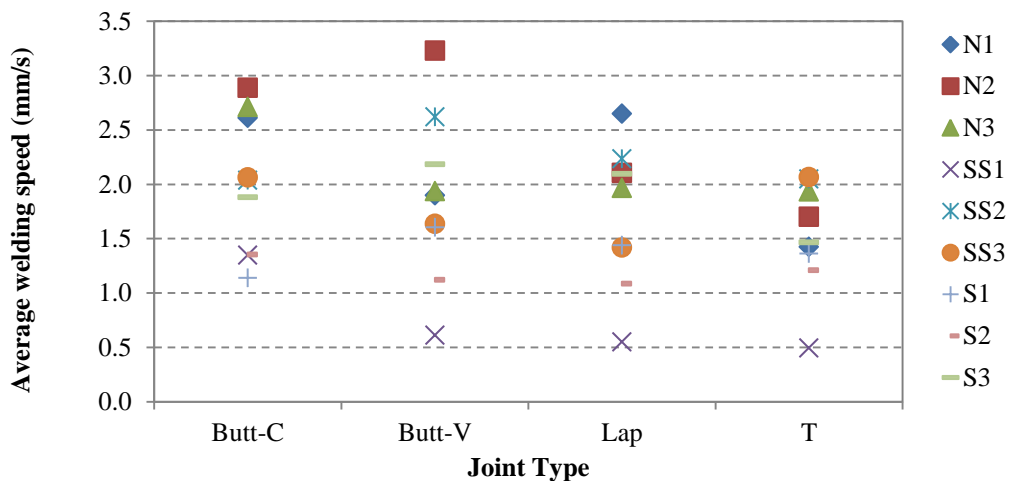
Figure 4-27: Welding speeds used for different weld joint types

According to the figure, most of the welders use lower speeds for Lap and T-joints compared to Butt joints. This is due to the zero-gap-fit-up for Lap and T-joints, which require a higher heat input and consequently lower speeds. However, novice welders

tend to move faster compared to other welders, as they attempt to complete the weld as soon as possible (explained in section 4.3.2.2).

4.3.4   Analysis based on post-weld interviews

To interpret the data observed during welding, interviews were carried out after each welding run. Videos were also observed offline and compared with the experimental results. Critical tasks, important decisions and actions were identified from the post-weld interviews through a questioner to the welders (Refer Appendix 7). Table 4-3 shows the number of welders who were successful in each critical task, and, as expected, the skilled welders were successful in most of the tasks. The novice welders were not successful in most of the tasks, due to a lack of process knowledge and therefore could not make the right decisions, which is also evident from the experimental samples (as seen in Figure 4-7).

Table 4-3: Results of the post-weld interview – Welder task competency

	Critical Task	Novice (Out of three)	Semi-Skilled (Out of three)	Skilled (Out of three)
1	Holding torch and filler rod at correct place before striking the arc	2	3	3
2	Pressing the foot pedal to the right amount to strike the arc	2	3	3
3	Establish the weld pool before moving	1	3	3
4	Start moving the torch and filler wire gradually with the weld pool	1	3	3
5	Feeding the filler wire to the weld pool	0	2	3
6	Controlling the process parameters in appropriate levels	0	2	3
7	Maintaining a constant weld pool size and ripple frequency	0	2	3
9	Maintain a constant stand-off distance	0	2	3
10	Maintaining weld angles in the specified range	0	0	3
11	Release of the foot pedal gradually at the end of welding	0	1	3
12	Holding the torch at the end until gas flow finishes	0	0	2
	Weld quality by visual inspection	**0/3 Good**	**2/3 Good**	**3/3 Good**

Failure to accomplish the critical tasks (as can be seen from Table 4-3, the Novice fails to accomplish 5 of the12 tasks) can significantly affect the weld quality (Figure 4-7). These results demonstrate the need for the successful completion of each critical task to

achieve a good weld quality. Methodologies should be adopted in the robotic welding system to for the successful completion of all the critical tasks.

The typical feedback methods used by the welders obtained from post welding interviews are given in Figure 4-28.
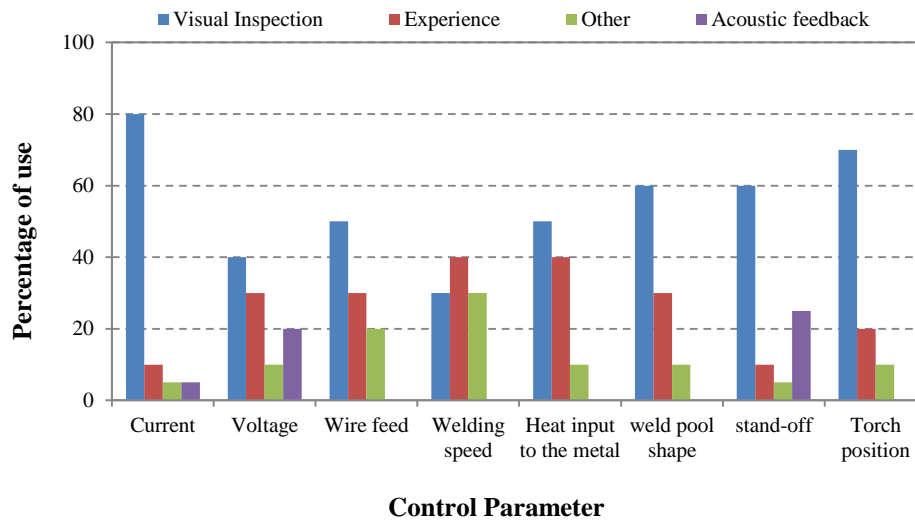
Figure 4-28: Decision making criteria for critical tasks identified in TIG welding

As can be seen from the figure, most of the welding parameters are predominantly controlled based on visual observation of the weld pool. A few welders have also used the acoustic feedback from the welding arc to control the voltage and therefore the stand-off distance. However, these results confirm the significance of visual feedback in TIG welding automation.

4.3.5 Manual welder's behaviour at a challenging welding task

Automation of welding has been attempted numerous times in the past, and the solutions are quite successful on simple geometries. However, most automation processes fail to produce the required weld quality with complex geometries. In this section, a complex geometry (corner of a plate) was welded by manual TIG welding to understand the methodology adapted by the human welders control the weld pool at the corners. A lap joint configuration (L-shape weld) was used as shown in Figure 4-29 for the experimentation.
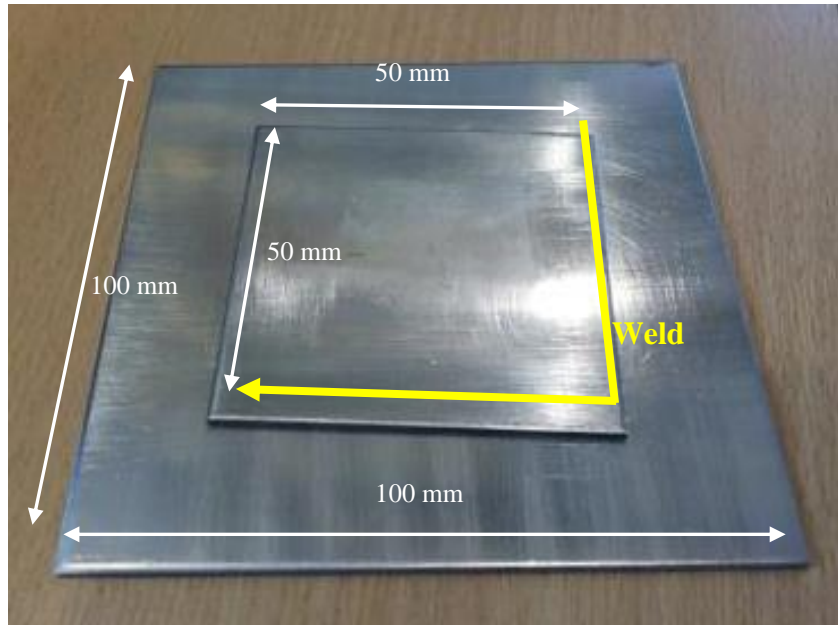
Figure 4-29: Sample weld joint to check human adaptability

A sample weld completed by a skilled manual welder is shown in Figure 4-30 (a). As can be seen the width of the weld bead and HAZ was uniform throughout the weld. Figure 4-30 (b), (c) and (d) shows the welding current used for three trials.

Figure 4.30(a)
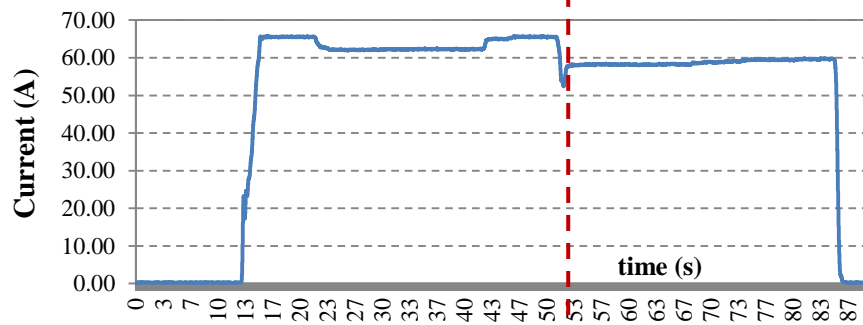
Figure 4.30(b)
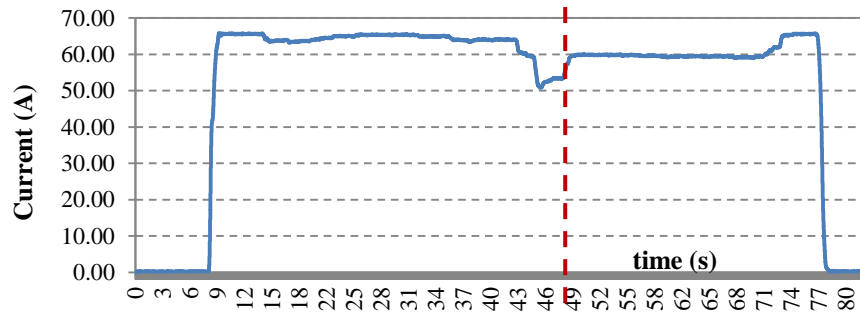
Figure 4.30(c)
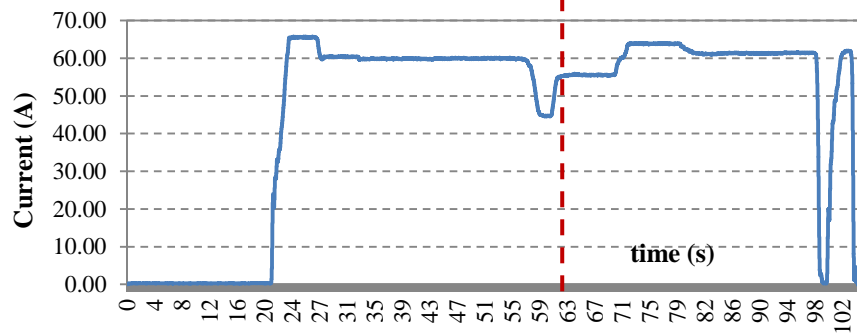
Figure 4.30(d)

Figure 4-30: Experimental results of welding corners (a) welded sample, (b) trial-1, (c) trial-2, (d) trial-3

As can be seen from the figures, the manual welder has reduced the welding current at the corner. By reducing the current the total heat transferred to the work piece is reduced and therefore the consistency of the weld bead is assured.

This is a single case study carried out to understand the methodology used by manual welders in a challenging weld shape. A similar method could be used for any challenging situation and a similar methodology could then be implemented in an automated solution for all the measured process parameters.

4.2   Summary

The work reported in this chapter was focused on understanding the manual TIG welding process, in the context of TIG welding automation. The methodology adopted by human welders to control the process parameters for complex geometries with challenging welding situations was investigated. TIG welding is complex and human welders without process knowledge failed to produce a good weld. Experienced welders achieved good weld quality even for complex geometries. Human welders use different techniques during the welding process, and each technique has its own advantages and disadvantages. Welding current and wire feed rate are the most significant parameters that need to be controlled and prioritised to account for variations in geometry and heat input. Results indicate that the adaptive control of parameters is vital for successful TIG welding automation. Critical tasks in TIG welding includes, establishing the weld pool, feeding filler wire to the weld pool and maintaining constant weld pool shape. The human welders control most of these critical tasks using visual observation of melt pool. Feedback control on the basis of visual information from the weld pool is essential for successful automation of TIG welding. The methodology adopted by human welders to control the welding was established and will be used in the chapters on automation of TIG welding.

5 Performance evaluation of the 3D laser scanner

Work presented in this chapter attempts to establish the performance of the *3D* laser scanner (Micro-Epsilon:Scan-Control). A novel definition of the best strategy for testing prior to its use is proposed. A similar testing approach can be applied to any industrial laser scanner prior to its application to minimize any ambiguity in measurements.

5.1 Introduction

Laser scanning results must meet specifications (for example: accuracy) in order to provide the necessary performance standards for an industrial application. On the other hand, if instruments and methods yield performance far above the needed standard, it will result in unnecessary cost and expenditure. Therefore, any scanning task should carry not only the derivation of the relative positions of points and objects but also an estimation of the accuracy of the results. Moreover, the specifications given by the laser scanner manufacturers are not standardised and hence not comparable. During initial experiments it was also found that laser scanners return unexpected results (such as noisy data points) at different operating conditions.

Laser scanners are built in small batches and their accuracy varies depending on the calibration and handling of each individual instrument. Environmental conditions, surface reflectivity, angle of viewing, surface roughness and stand-off distance are some factors which could also affect the measurement performance. Therefore, it was very important to evaluate and establish the performance specifications of the laser scanner, as this specifies the accuracy of any measurements taken during its application.

This chapter presents a set of experiments to evaluate a compact red-light laser scanner to understand its performance in challenging conditions such as variable illumination, viewing angle, stand-off height and surface reflectivity. The best working range was established and regions where the laser scanner produces noisy and missing data was identified and quantified. Reasons for any inadequate results were identified and discussed. Finally, recommendations are made for minimizing the error in the data acquired from any laser scanner. A similar approach could be taken on any industrial

laser scanner to check its performance before use in an actual application so that the users understand the limitations and take any necessary actions to overcome them.

It should be noted here that parameters such as the electrical interference was not considered in the work presented in this thesis as it was out of scope of the thesis. Also the sensor performance is not affected while it is welding since this thesis considers two-pass approach (First scanning and then welding).

5.2   Experimental setup

In Figure 5-1, the photographic view of the experimental set-up is shown with the Micro-Epsilon Scan-control 2900-25 laser scanner mounted on the end effector of the KUKA KR16 robot. The KUKA robot provides relative motion which allows *3D* data to be obtained.

Figure 5-1: Photographic view of the experimental set-up

The laser scanner comes with software, called Scancontrol, which could be used to measure surface features such as gap width, depth and height. Figure 5-2 shows a screenshot of the software display used to measure the width of a feeler gauge. Similar methods were used for all the measurements carried out for the tests presented in this chapter.
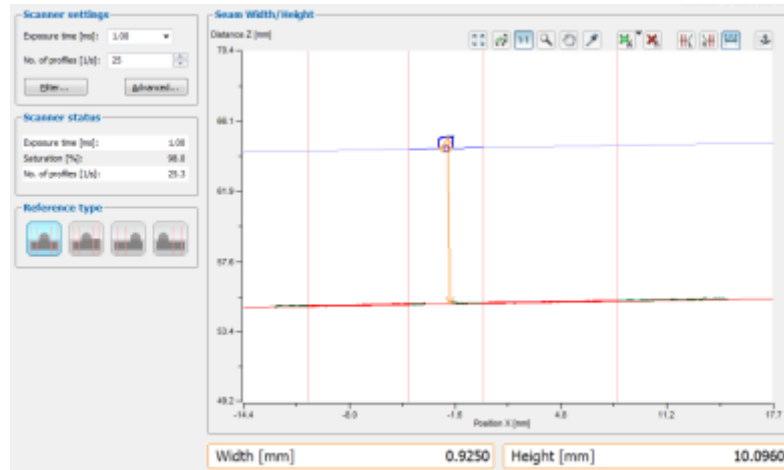
Figure 5-2: Photographic view of the Scan-control software

The manufacturer specified technical parameters of Scancontrol 2900-25 used in this study are given in Table 5-1.

Table 5-1: Manufacturer specified data of the Micro-epsilon Scancontrol 2900-25 laser scanner[149]

Measuring range Z-axis extended	26mm (53-79mm)
Spatial resolution	20µm
Depth resolution	20µm
Laser line width	23.2-29.3mm

5.3 Methodology, results and discussion

As shown in Figure 5-3, a set of metric feeler gauges (0.05-1mm: 20 Blatt) and a set of slip gauges (M&W 700 Series) were used as the calibration samples for the experiments. All the experiments were carried out at room temperature between 16-19˚C. Each measurement was repeated three times to assure repeatability.

Figure 5.3 (a)   Figure 5.3 (b)

Figure 5-3: Calibration samples (a) feeler gauge set, (b) slip gauge set

Section 5.3.1 compares the manufacturer specified specifications with the actual data obtained during testing. Performance evaluation tests were designed to find the optimal operating range for the *3D* laser scanner, including;

- working span
- vertical and horizontal resolution
- repeatability
- measurement accuracy at different exposure levels
- illumination conditions

Factors affecting the data acquisition performance of the laser scanner are presented in Section 5.3.2. These are;

- stand-off height
- steepness angle
- angle of incidence
- surface reflectivity
- exposure time
- threshold value

While measuring the effect of one parameter, the other parameters were maintained at a constant value. Within each of the following sections, the methodology for the tests is described before the test results are presented and a relevant discussion is carried out.

5.3.1   Laser scanner performance check

5.3.1.1   Evaluation of the working span

The working span of a laser scanner gives information on the working range within the laser line projection. It is vital to know the actual working range prior to its use so the user has prior knowledge about how the robot should be moved in order to collect the most complete set of data. The working range is the combination of vertical and horizontal ranges. In order to estimate the horizontal and vertical range, the laser line was projected perpendicularly on to a flat surface. The resulting laser line length was measured and the relevant stand-off height was also recorded. This was repeated for increments of 0.2mm in the stand-off distances from 45-85mm.

In Figure 5-4(a), the schematic laser span for a typical line laser is shown and in Figure 5-4(b) the measured results can be seen. As noted from the figure and the results shown in Table 5-2, there is a significant (2-16%) difference between the specified and actual values in the horizontal (b1 and b2) and the vertical (h) ranges of the scanner. The deviation could be due to the changes in the ambient lighting conditions (discussed in section 5.3.1.5) because the manufacturer specified values are obtained in a controlled environment.
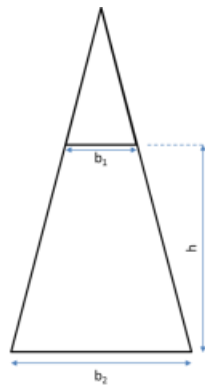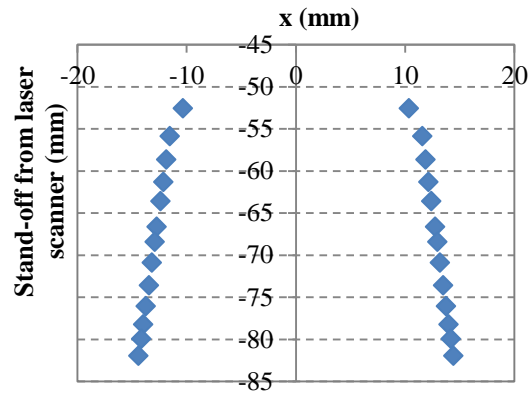
Figure 5.4(a)   Figure 5.4(b)

Figure 5-4: Specified and measured working ranges of the laser scanner (a) specified laser scanner span, (b) actual span

Table 5-2: Specified and actual values of the range

Parameter	Specified Value (mm)	Actual Value (mm)	Percentage difference (%)
b1	23.2	20.71	10.7
b2	29.3	28.81	1.7
h	26	30.21	16.2

5.3.1.2 Finding vertical and horizontal resolution

As specified by the manufacturer, the laser scanner's vertical and horizontal resolution is ±20μm. However the measurement accuracy of the scanner may not be uniform over the whole vertical (53-79 mm) and horizontal range (25mm). Therefore it is important to assess the measurement accuracy of the scanner along its vertical and horizontal range. A 20mm slip gauge was used as the test piece, and its width was measured at various heights (52-83mm) from the laser scanner as shown in Figure 5-5.

Figure 5-5: Setup for vertical resolution measurement

The sample was placed at the middle of the laser scanner line to minimize any effect which may occur due to the horizontal point of measurement in the laser line. In Figure 5-6, the percentage error (calculated using equation 5.1) in measurements for various stand-off distances is shown. As can be noted from the results, the accuracy of the scanner varies along its z-axis. The best performance was noticed around a stand-off height of 65mm, which is at the middle of the laser scanner's vertical range. This is because the sensitivity of the camera sensor is at its maximum at the middle of the sensor.

$$Percentage\ error = \frac{(Set\ value - Measured\ value)}{Set\ value} \times 100\% \qquad (5.1)$$
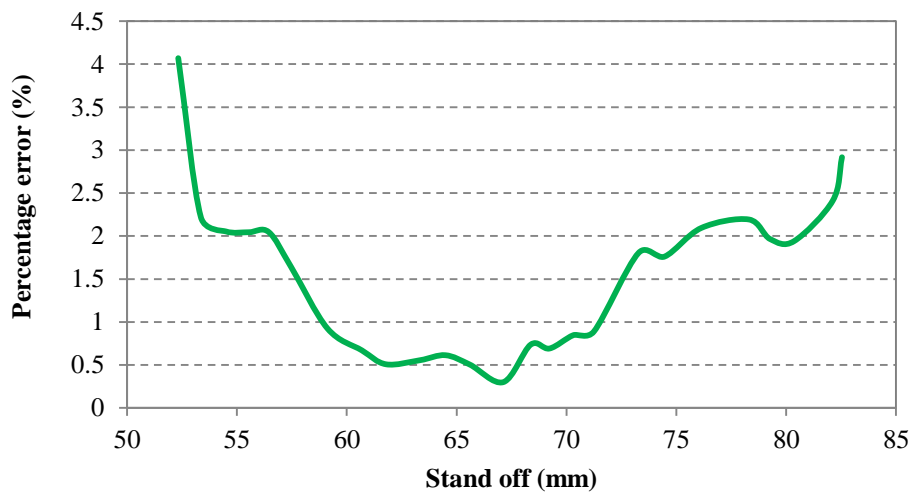
Figure 5-6: Percentage error in measurements along z-axis

To evaluate the horizontal accuracy of the laser scanner, the width of a metric feeler gauge (1mm) was measured at various positions along the laser line as shown in Figure 5-7. The stand-off distance was kept constant at 65mm.

Figure 5-7: Setup measuring a metric feeler gauge and percentage error in measurements

In Figure 5-8, the measured values and percentage error (calculated using equation 5.1) of the measurements along the laser line are shown.
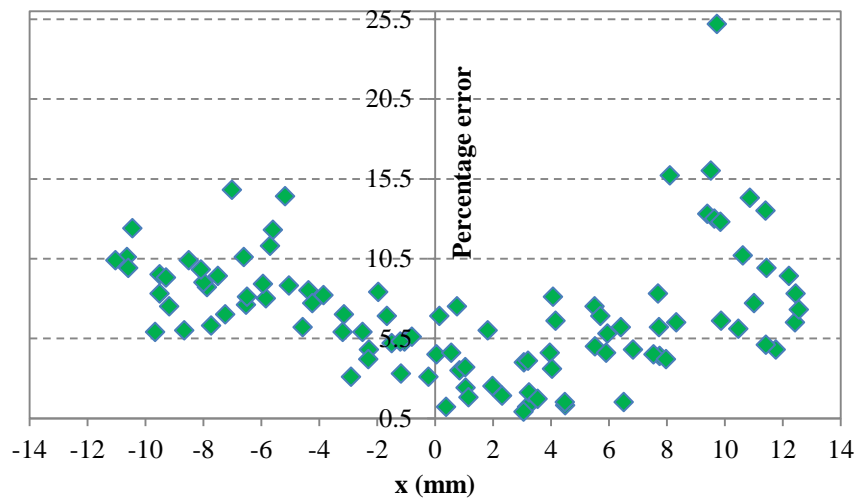
Figure 5-8: Percentage error along the x-axis of the laser scanner

These results show that the laser scanner produces accurate measurements at the middle of its working span. To avoid any uncertainty in measurements, it is therefore advisable to orient the laser scanner so that the area being measured is close to the centre of the laser span.

5.3.1.3 Laser scanner performance evaluation at different exposure levels

In order to find the accuracy of measurements against exposure time, a 20mm slip gauge was measured at different exposure times ranging from 0.01 to 40ms. The results obtained are shown in Figure 5-9.
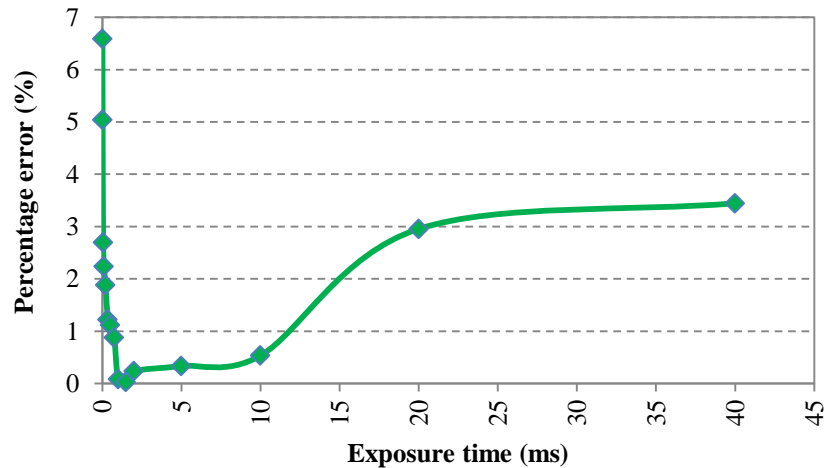
Figure 5-9: Percentage error against exposure time

As can be seen from the figure, the measured value varied depending upon the exposure time setting. The error is at a minimum around 1ms exposure time.

5.3.1.4 Repeatability test for gap measurements

The repeatability of the scanner was evaluated by measuring a 1mm gap between two stainless steel samples. The laser scanner was set at 68mm (middle of its working range) stand-off distance from the work piece. 1ms exposure time was used for the experiment. Twenty six measurements were taken at an interval of five seconds and all measurements were obtained close to the centre of the laser working span. Figure 5-10 shows the percentage error (percentage deviation from 1mm) for each of the twenty six scans. As noted from the figure, the maximum percentage error is 3.6% (36µm) and the mean error is ±28µm. The laser scanners reported accuracy is ±20µm. The results mean the scanner performance in not consistent with the specification. However, it is close to the specification and adequate for the task of seam tracking.
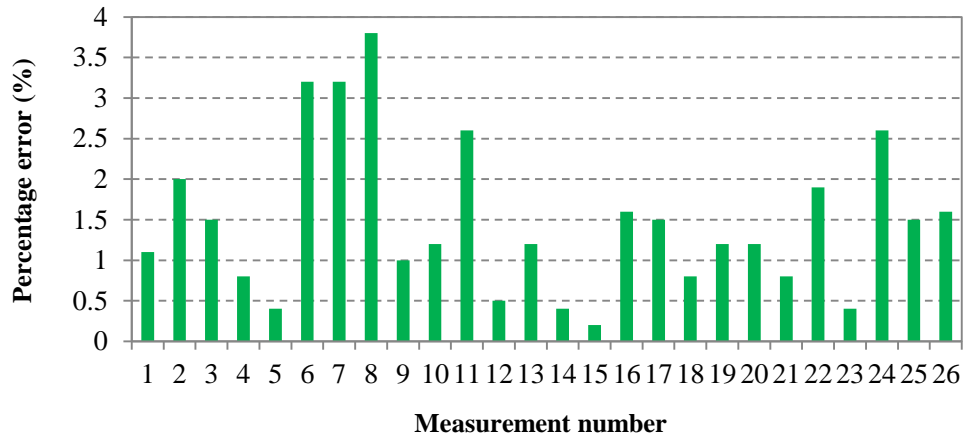
Figure 5-10: Percentage error in measurements for checking repeatability

5.3.1.5   **Laser Scanner Performance at Different Illumination Conditions**

External lighting is expected to significantly affect any vision sensor. Therefore, experiments were conducted to assess the performance of the laser scanner at three different lighting conditions as given below;

- Ambient lighting

- Partially controlled – some ambient light can reach the sensor

- Fully controlled – no ambient light reaches the sensor (achieved by covering the area surrounding the laser scanner). No sun light can reach the sensor

The tabulated data in Table 5-3 gives the laser scanner's performance in measuring different sizes of feeler gauges at three different lighting conditions. As noted from the table there are fluctuations (fluctuations were monitored for 5s before recording the range of values) in the reading when measuring smaller widths. Also the fluctuation occurs when the sun is present (which changes the illumination level). However, no fluctuations were detected in readings when measuring widths higher than 0.4mm even when the sun was present (ambient). This result reveals that the laser scanners do not return the same readings when the lighting condition varies.

Table 5-3: Measured values of feeler gauge

Feeler gauge size (mm)	Ambient (mm)	Fluctuation in reading	Presence of the Sun	Partially controlled (mm)	Fluctuation in reading	Presence of the Sun	Fully controlled (mm)	Fluctuation in reading	Presence of the Sun
1.00	0.992	×	√	0.996	×	√	1.003	×	√
0.95	0.942	×	×	0.942	×	×	0.944	×	√
0.90	0.88	×	√	0.891	×	√	0.898	×	√
0.85	0.816	×	√	0.836	×	√	0.852	×	√
0.80	0.785	×	×	0.791	×	√	0.794	×	√
0.75	0.711	×	×	0.72	×	×	0.742	×	×
0.70	0.692	×	√	0.698	×	×	0.698	×	√
0.65	0.641	×	√	0.652	×	√	0.653	×	×
0.60	0.594	×	×	0.594	×	×	0.611	×	×
0.55	0.542	×	×	0.542	×	×	0.52	×	√
0.50	0.497	×	×	0.498	×	√	0.497	×	√
0.45	0.464-0.541	√	√	0.439	×	√	0.506	×	√
0.40	0.397	×	×	0.397	×	×	0.396	×	√
0.35	0.377-0.420	√	√	0.358-0.376	√	√	0.359	×	√
0.30	0.299-0.317	√	√	0.337	×	×	0.337	×	×
0.25	0.23-0.245	√	×	0.231	×	√	0.253	×	×
0.20	0.254-0.274	√	√	0.215	×	×	0.214	×	×
0.15	0.201-0.233	√	√	0.193	×	×	0.181	√	×
0.10	0.117-0.150	√	√	0.89-0.134	√	√	0.68-0.113	√	√
0.05	0.046-0.126	√	√	0.067-0.087	√	√	0.067-0.088	√	√

The error (calculated using equation 5.1) in measurements against the gauge size under different illumination conditions is shown in Figure 5-11. As noted from the Figure the error is higher when measuring small widths irrespective of the illumination condition. However it is also evident that the percentage error in measurements is higher at ambient lighting conditions. This indicates that the laser scanners should be used at controlled lighting conditions for best performance.
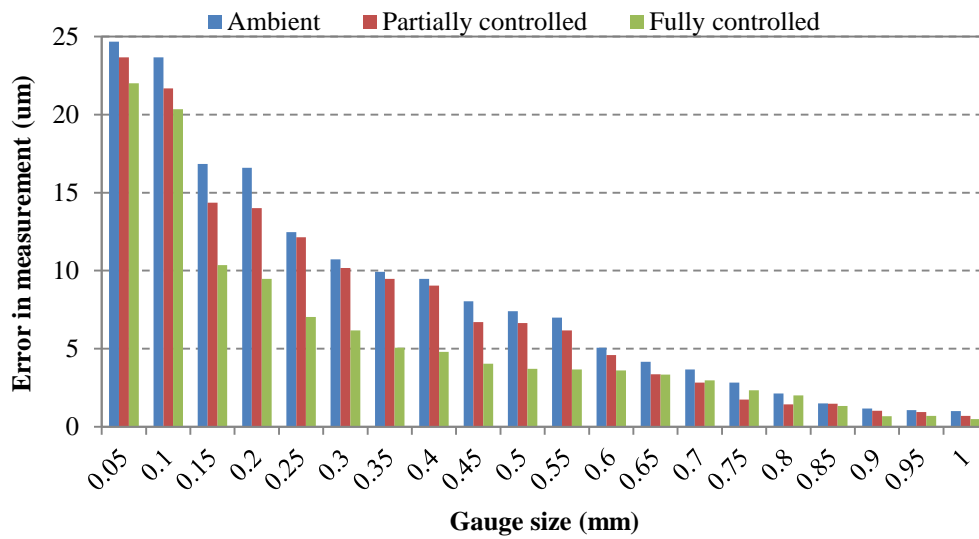
Figure 5-11: Measurement error at different illumination conditions

5.3.2 Understanding reasons for faulty data issue of laser scanners

Noisy data are the data points present in unexpected positions and missing data are the points where the expected data are not present.

During the initial experiments, noisy and missing data were observed at some positions (see Figure 5-12 showing inappropriate data while scanning a flat surface). Literature also suggests that the noisy data and missing data points can be associated with many parameters including the viewing angle, stand-off distance and surface reflectivity [111]. In Figure 5-12, a typical example of raw data observed on a flat surface can be seen. The expected result is a horizontal line since the surface being measured is flat. However, as can be seen from the figure, a number of noisy and missing data points were observed in the resulting data. This section identifies the reasons for this behaviour of laser scanners.
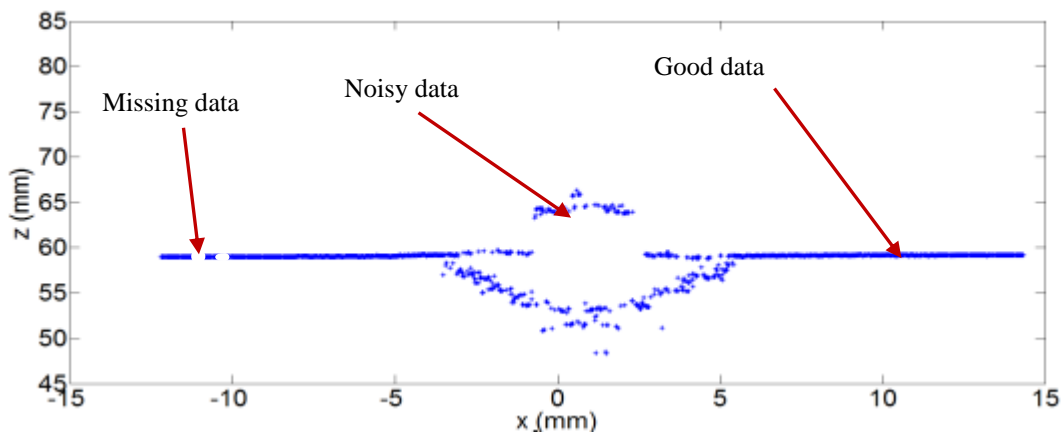
Figure 5-12: Inappropriate data from a laser scanner

To investigate this, experiments were carried out to understand the effects of the following parameters on the data quality:

1. Stand-off distance
2. Steepness angle of the surface being measured
3. Angle of incidence that the laser scanner makes with the surface being measured
4. Surface reflectivity (albedo)
5. Exposure time
6. Threshold value
7. Laser power

5.3.2.1 Effect of Stand-off Distance on Data Quality

As described in section 5.3.1.2, there is a particular stand-off distance that the laser scanner produces its best accuracy. In addition to accuracy related issues, laser scanners also produce missing data points based on the stand-off distance. In order to examine this, measurements were performed on a 20mm slip gauge to assess the number of missing data points at various stand-off distances (53-83mm). The number of data points acquired against stand-off distance was calculated at each stand-off height. According to the manufacturer, the laser scanner produces 1280 laser points along its laser line. However, the amount of laser points falling on the 20mm block is less than 1280 and also varies based on the stand-off distance as given in equation 5.2 where h is the stand-off distance. Therefore the missing number of data points can be found using equation 5.3.

$$Expected\ number\ of\ points = \frac{1280}{0.38\ x\ h} x\ 20 \qquad (5.2)$$

$$\begin{aligned} Number\ of\ missing\ data\ points \\ = Expected\ number\ of\ points \\ - Acquired\ number\ of\ points \end{aligned} \qquad (5.3)$$

The number of missing data points against the stand-off distance is shown in Figure 5-13. From the figure, it can be seen that the laser scanner produces the minimum number of missing data points at a stand-off distance of 68mm which is the middle of the vertical range. It is important to take this in to account to maintain the optimum stand-off distance whilst taking measurements.
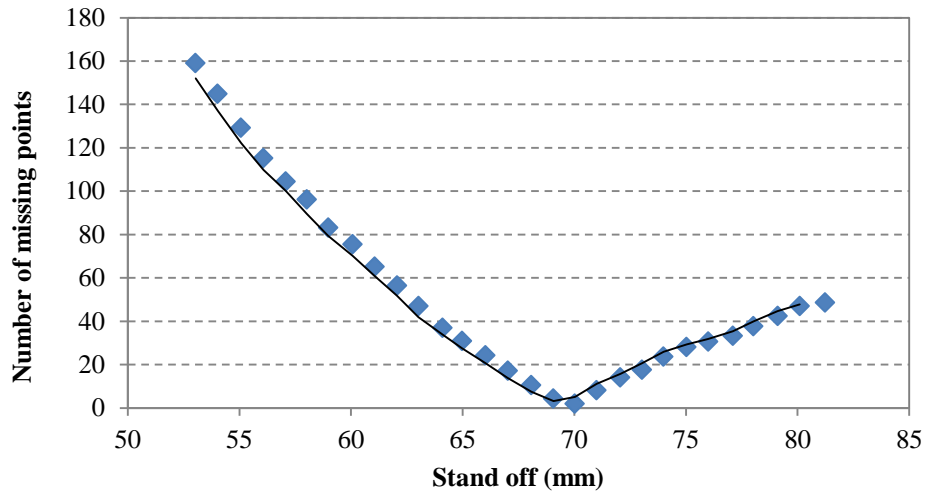
Figure 5-13: Number of missing data points against stand-off distance

5.3.2.2 **Effect of surface steepness on data acquisition**

The angle of interaction between the laser scanner and the surface being measured can affect the quality of the data acquisition process. A 50mm x 200mm size stainless steel work piece was measured at different steepness angles (α) as shown in Figure 5-14.
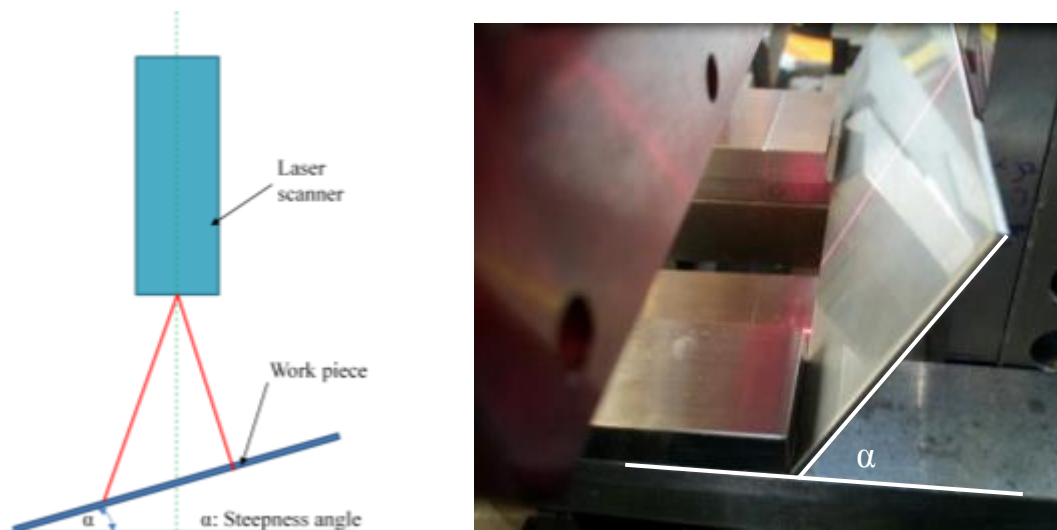
Figure 5-14: Arrangement for measurements at different steepness angles

It should be noted that during the experiments it was always ensured that the laser line fell completely on the surface being measured, which assured that for each measurement the full 1280 points was expected to be recorded. The number of data points acquired from the laser line was calculated for each steepness angle (from $0°$-$85°$). As seen from Figure 5-15, there is a threshold at $37°$, above which the performance of the laser scanner starts to deteriorate. At higher steepness angles, the number of laser points falling on to the sample per unit length reduces, which affects the data acquisition performance. To minimize this, users should orient the scanner in a

107

way to maintain the steepness angle below the threshold of 37˚. It should be noted that, stand-off height was maintained at 68mm (selected based on interviews with skilled welder and also initial bench testing of the laser scanner) was not changed during the experiment.
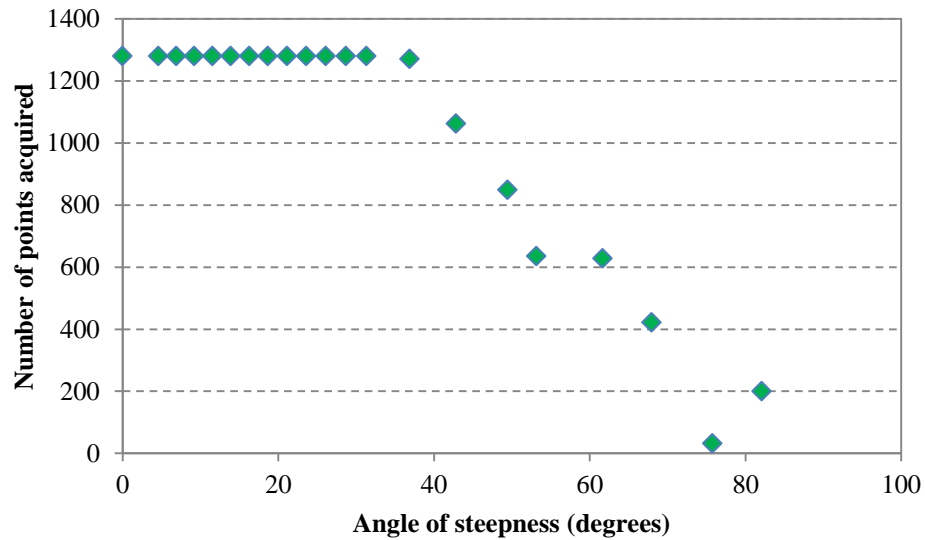
Figure 5-15: Results of number of missing data points measured against steepness angle

The data obtained for the different steepness angles is shown in Figure 5-16. The scanner failed to return any data above 82˚ which could be defined as the critical steepness angle for the selected laser scanner. This suggests that any object which has surface features above the critical incidence angle cannot be visualized from the laser scanner. Therefore, alternative methods, such as moving the robot in such a way that the steepness angle of a surface at any given position is less than the critical steepness angle, is required for visualisation.
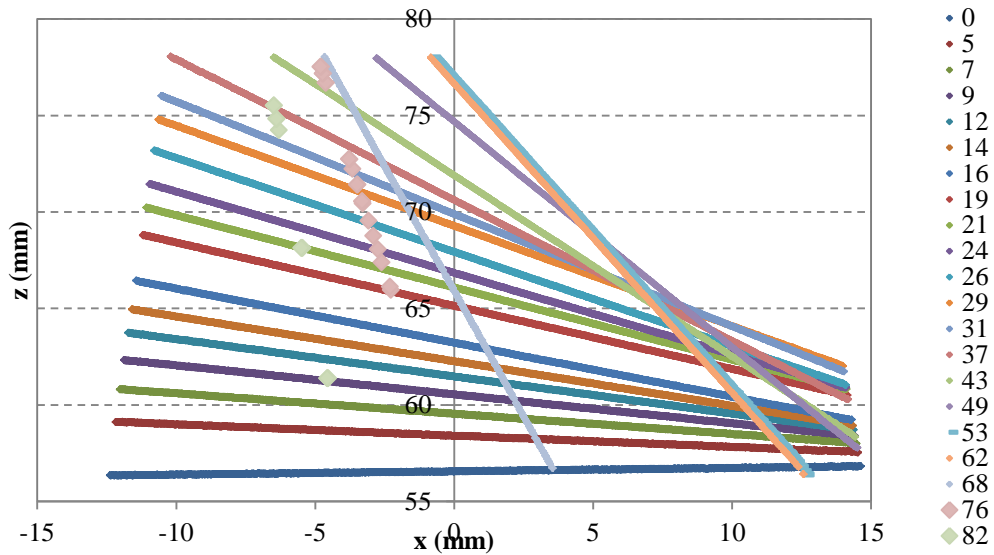
Figure 5-16: Data at various steepness angles

5.3.2.3 **Effect of angle of incidence on data quality**

To study the effect of the angle of incidence (angle between the horizontal and the surface being measured) on the data acquisition performance, an experiment was carried out by setting known incidence angles from 0° to 85°. A 50mm by 200mm stainless steel work piece was used for this test as shown in Figure 5-17.
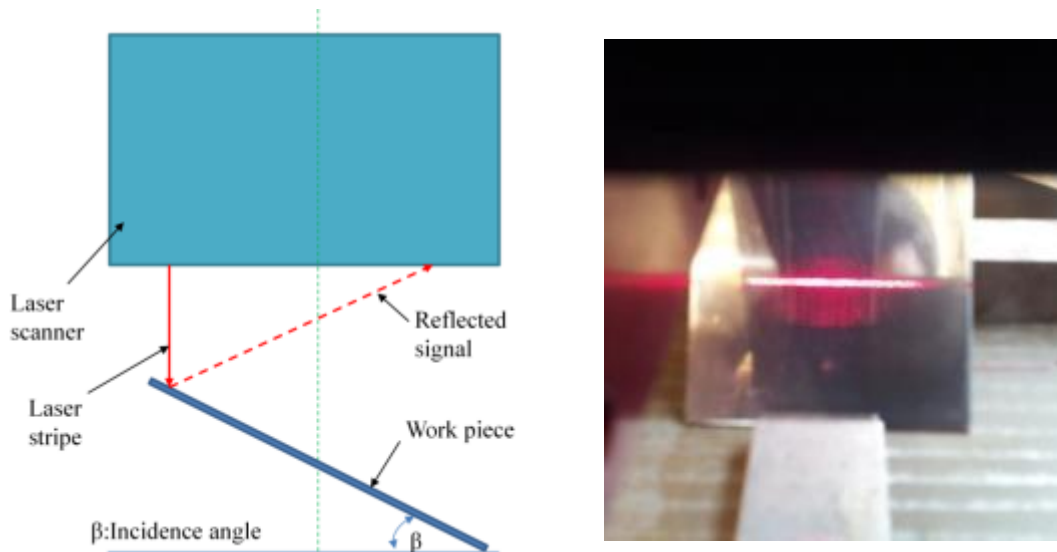
Figure 5-17: Arrangement for measurements at different incidences angles

The raw images obtained from the laser scanner at different incidence angles can be seen in Figure 5-18 (Please note that these angles were set using slip gauges on one side of the stainless steel piece). As seen from the figures the laser scanner returns images containing areas of noise between 14°-25°.

In order to examine this further, the raw data obtained from the laser scanner between these angles was studied in more detail as shown in Figure 5-19. As can be seen from the figure, the noisy data is mostly deviations from the expected linear output. Upon further investigation, this is because the reflected laser signal coincides with the camera axis of the laser scanner. In this range, the camera sensor gets saturated because of the number of photons reaching the camera sensor.
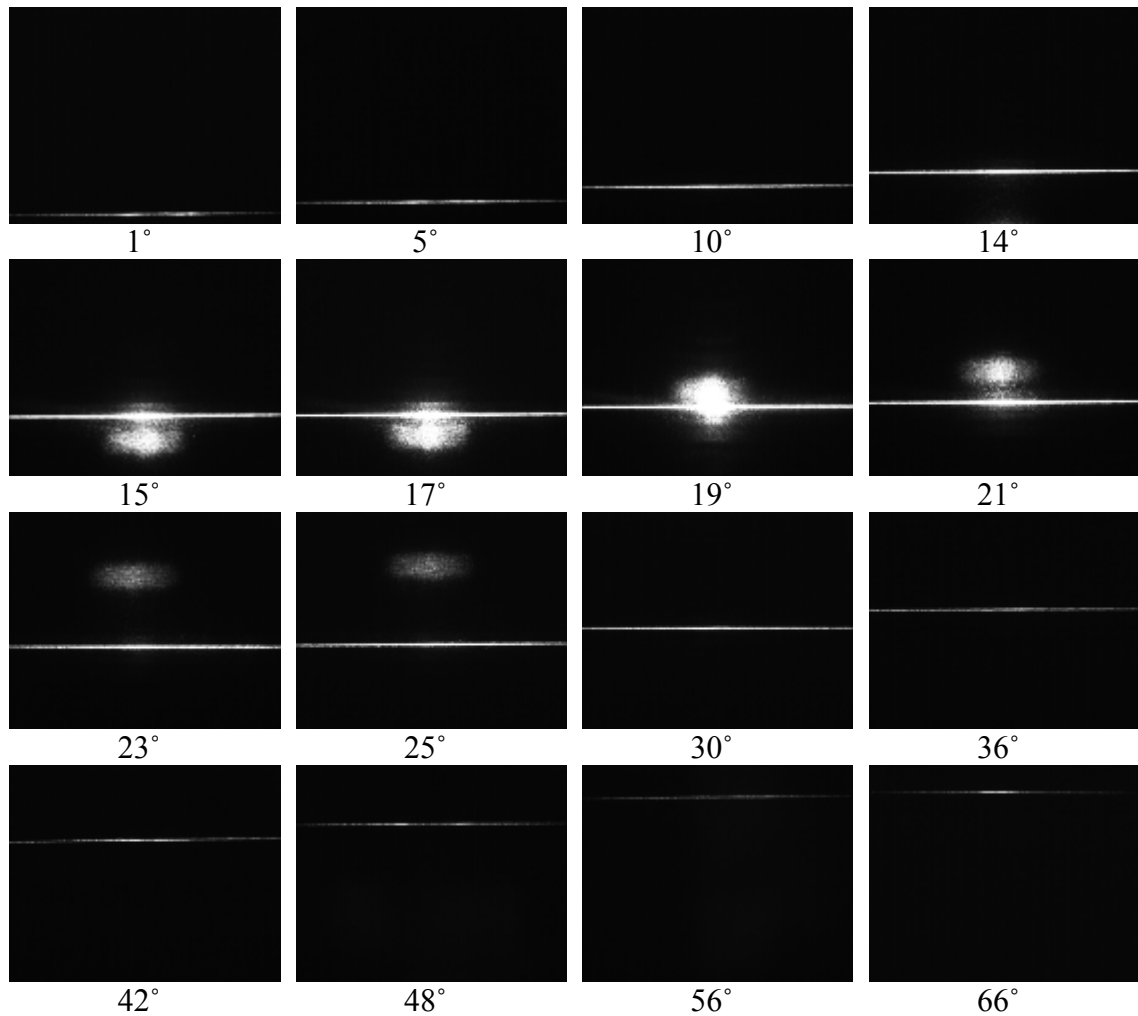
Figure 5-18: Raw images obtained from the laser scanner at different incidence angles
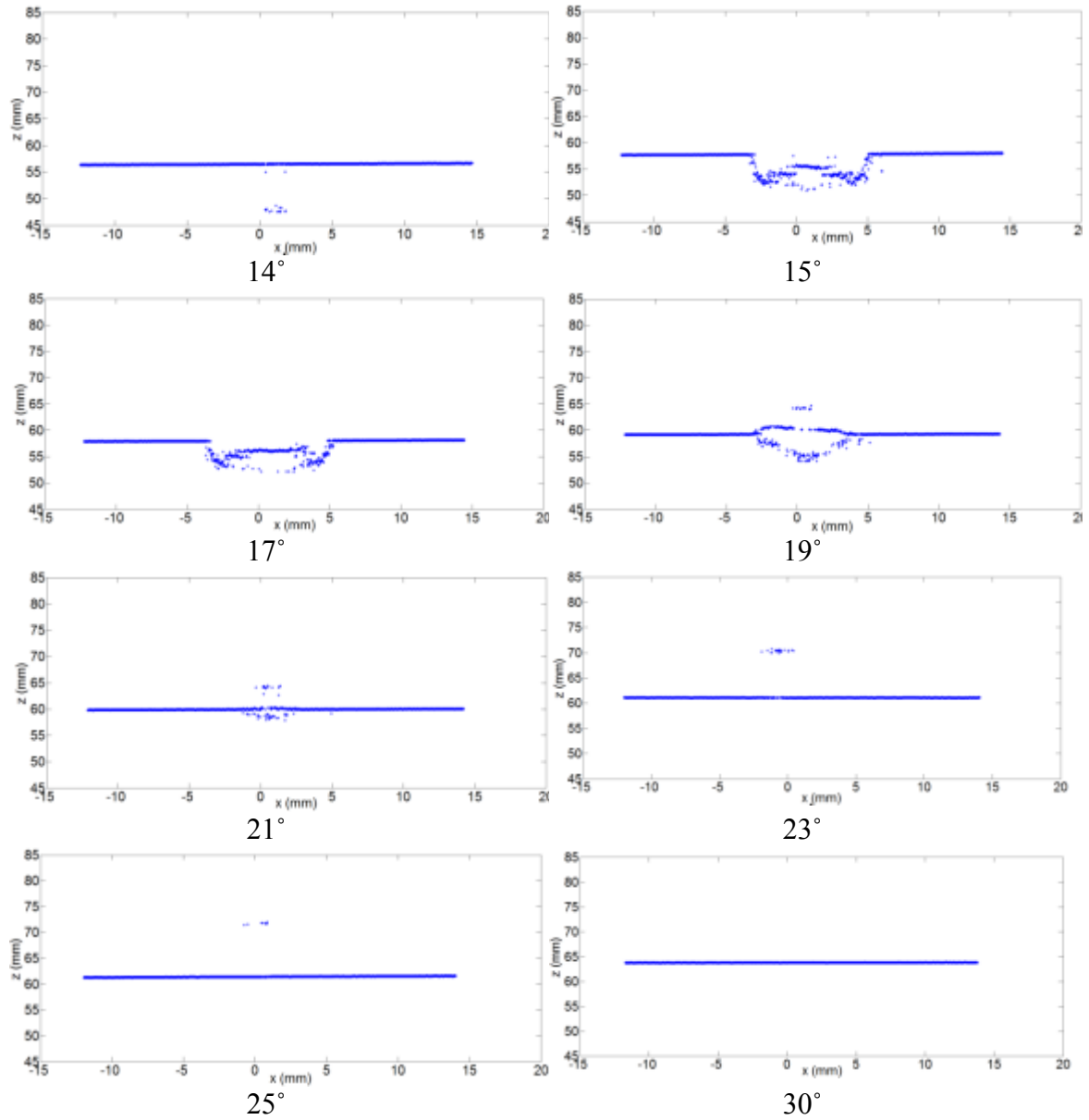
Figure 5-19: Effect of incidence angle on data acquisition

In Figure 5-20(a), the number of noisy data against the incidence angle is shown and the respective noise percentage (calculated using equation 5.4) is shown Figure 5-20(b). As noted from the figure, the laser scanner has a higher percentage of noisy data between 15˚ and 25˚ and the maximum noise was noticed at 19˚. This is an unexpected behaviour of the scanner and not stated by the manufacturer in their datasheet. These factors should be examined before using any laser scanner for measurements to avoid critical incidence angle range by controlling the robot pose.

$$Noisy\ data\ percentage = \frac{(Total\ data\ points - noisy\ points)}{Total\ data\ points} \times 100\% \quad (5.4)$$
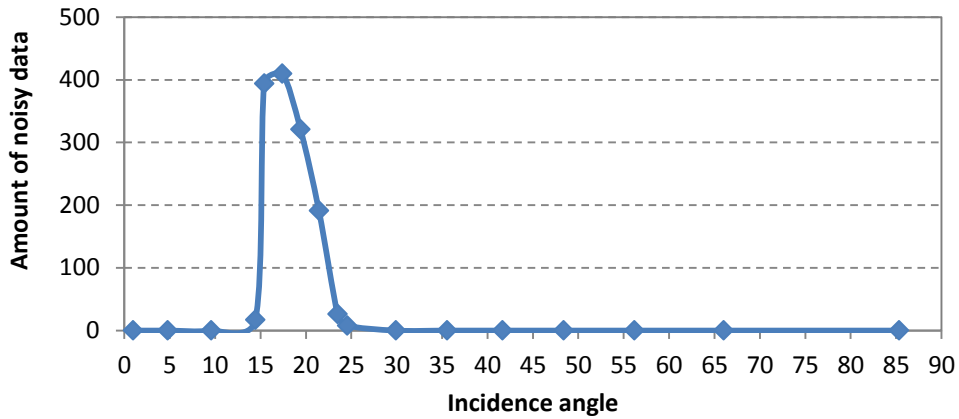
Figure 5.20(a)

Figure 5.20(b)

Figure 5-20: Effect of incidence angle on data acquisition (a) number of noisy data points (b)noisy data percentage

5.3.2.4 **Effect of surface reflectivity/finish on data quality**

To understand the effect of surface reflectivity on data quality, three samples (normal, shiny, matt) with different surface reflectivities were selected, which are shown in Figure 5-21. All three samples were then tested with the laser scanner by keeping them at the peak critical incidence angle of 19˚. In Figure 5-22, the raw image results obtained are shown. As can be noted from the figure, the matt-finished surface did not saturate the camera at the critical incidence angle whereas the other two surface finishes produced a high percentage of noisy data. This suggests that the surface reflectivity affects the data acquisition performance of a laser scanner and users should consider the surface quality of the object being measured when selecting a laser scanner.

(a) Normal   (b) Matt   (c) Shiny

Figure 5-21: Different surface finished samples
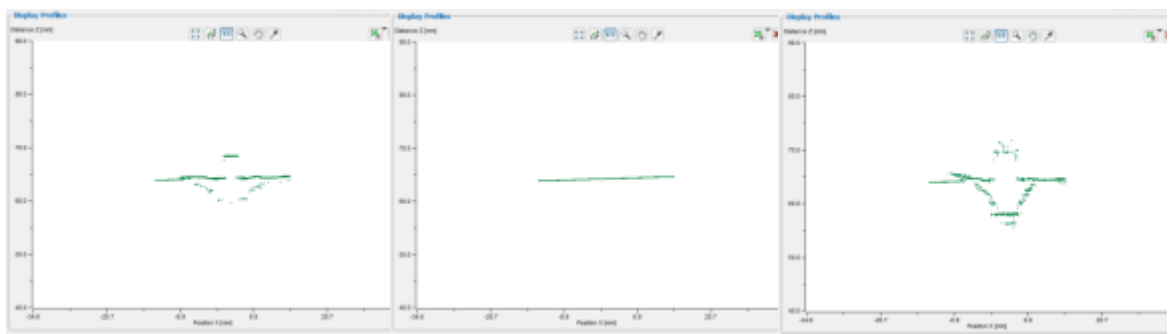
(a) Normal   (b) Matt   (c) Shiny

Figure 5-22: Results obtained for different surface finish

5.3.2.5 **Effect of exposure time on data quality**

In order to examine this, the shiny sample was used and the exposure time was varied from 0.01ms to 40ms and the number of noisy points was calculated from the resulting data. The raw images obtained from the camera at different exposure times are given in Figure 5-23. As noted from the images, they become saturated at higher exposure times due to the number of photons reaching the sensor being beyond its maximum.

0.01s	0.02s	0.05s	0.1s
0.2s	0.35s	0.5s	0.75s
1s	2s	5s	10s
20s	40s		
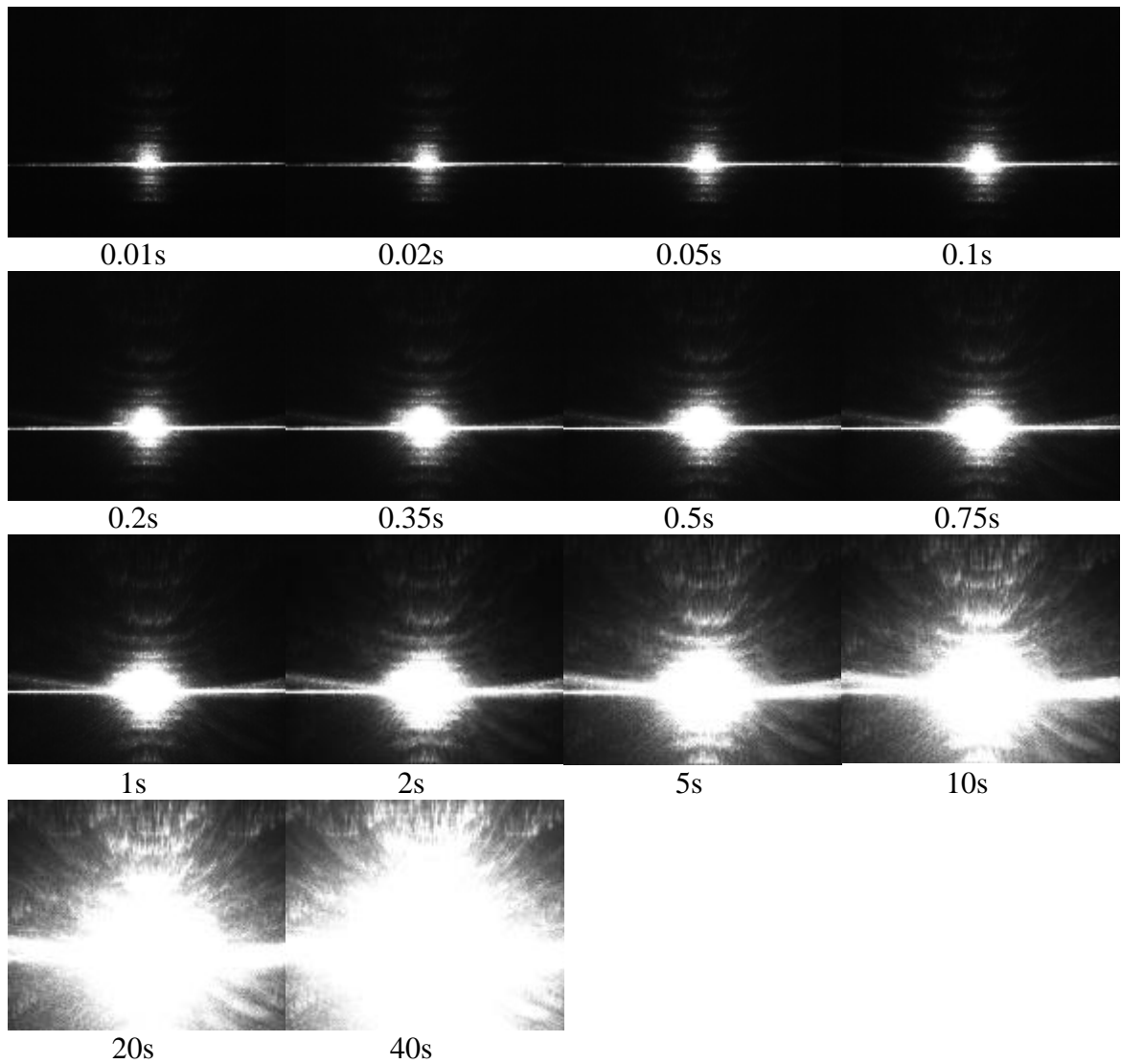
Figure 5-23: Raw images captured at different exposure levels

In order to quantify the effect of exposure time on data quality, the percentage of noisy data points was calculated using equation 5.4 for each exposure time which is graphed in Figure 5-24(b). Its respective absolute number of noisy data points is shown in Figure 5-24(a).
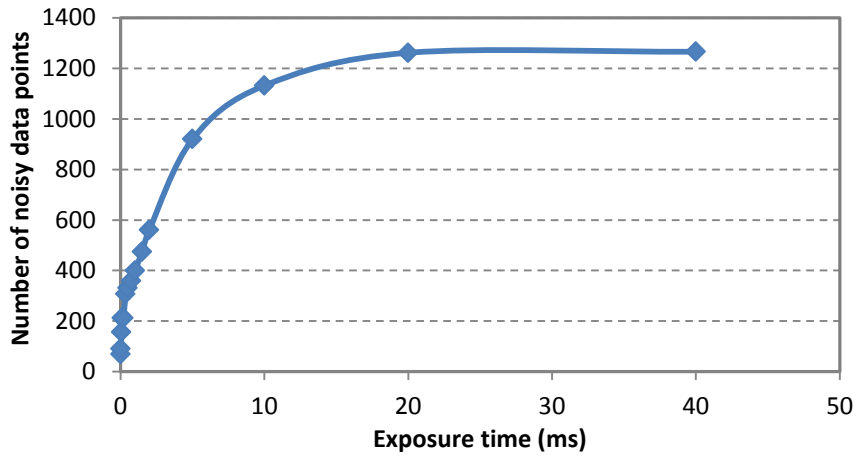
Figure 5.24(a)
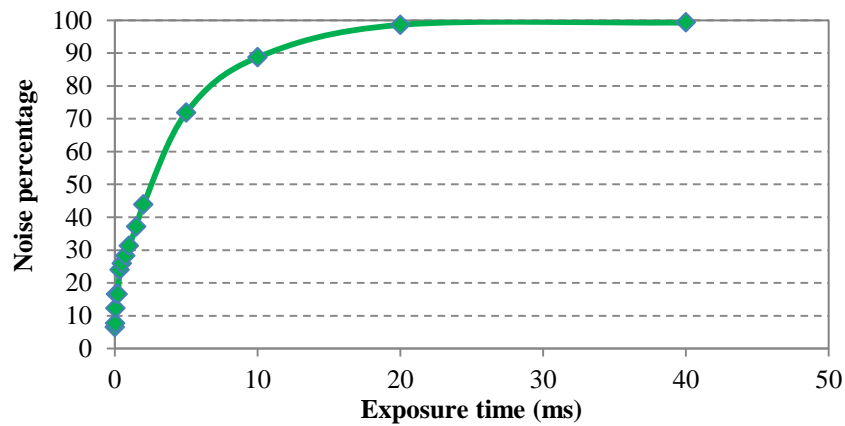
Figure 5.24(b)

Figure 5-24: Effect of exposure time on data acquisition (a) number of noisy data points (b) noisy data percentage

It was understood from the results that a high exposure time leads to more noisy data points and a low exposure time leads to missing data points. Therefore it is important to find out an optimum exposure time for a "shiny" surface such as the stainless steel samples used for welding in the later chapters of this thesis. In order to investigate the optimum exposure time a shiny *U*-groove was created (see Figure 5-25) from stainless steel. This shape was chosen because it has both high and low steepness angles along its cross-section.
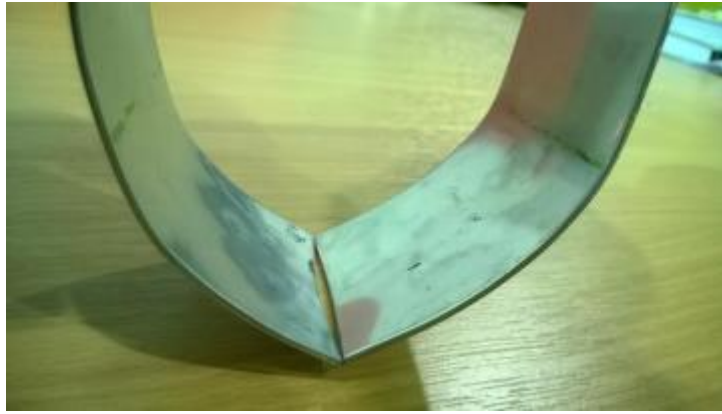
Figure 5-25: U-groove for finding optimum exposure time

The noisy and missing data percentage at different exposure times is given in Figure 5-26. As noted from the figure, data with the lowest noise and missing data percentage could be acquired between 1ms and 2ms of exposure time.
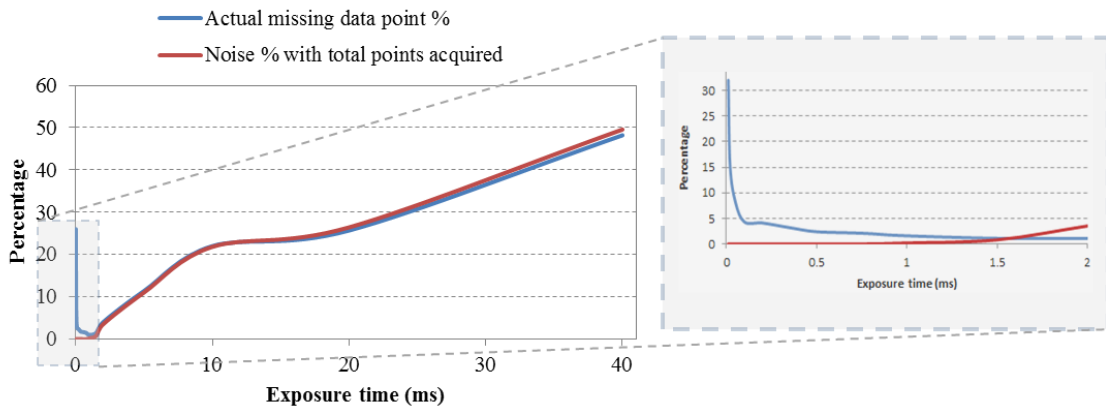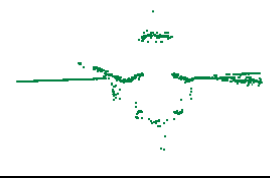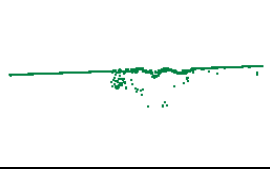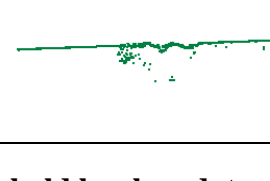
Figure 5-26: Missing and noisy data percentage against exposure time

5.3.2.6 Effect of Laser Power on Data Quality

The Micro-epsilon laser scanner contains four different laser power options, these are standard, standard-pulsed, reduced and reduced-pulsed (the actual power ratings are not specified by the manufacturer). In order to find the effect of the laser power on data acquisition, the "shiny" stainless steel sample was oriented in such a way that it makes 19˚ incidence angle with the laser scanner. Data were then acquired at different laser power levels and the results are tabulated in Table 5-4. Ideally the laser scanner should return a straight line in the resulting data. From the images it can be seen that the lower laser power assures more linearity in the results obtained. However the number of data points acquired did not vary significantly for the different laser power levels, which suggests that laser power is not a factor causing missing data but noisy data. Therefore it can be recommended to use a lower laser power for *3D* shiny objects especially in the aerospace welding industry which involves complex shiny parts.

116

Table 5-4: Data acquired at different laser power levels

Configuration	Raw image	Number of data points acquired	Noise percentage (%)
Standard		1277	23
Standard-pulsed		1275	20
Reduced		1278	7
Reduced - pulsed		1277	6

5.3.2.7 Effect of threshold level on data quality

Every laser scanner operates to find the laser line from raw images and separates it from the background. The separation is accomplished by defining a threshold value so that any point beyond the specified threshold can be acquired as a data point and the rest is filtered out. This directly affects the obtained data quality because inappropriate threshold values can lead either to inappropriate (noisy) or missing data points.

In order to investigate this, the shiny sample was placed at an incidence angle of 19° and the in-built threshold value was varied from 1 to 800. Figure 5-27(a) shows the number of noisy data points against the threshold value and Figure 5-27(b) shows its respective percentage values. As can be seen from the figure, there is a reduction in the percentage of noisy points at higher threshold values. This result also reveals that the selection of the optimum threshold level can enhance data quality and therefore will help provide better performance in measurements.
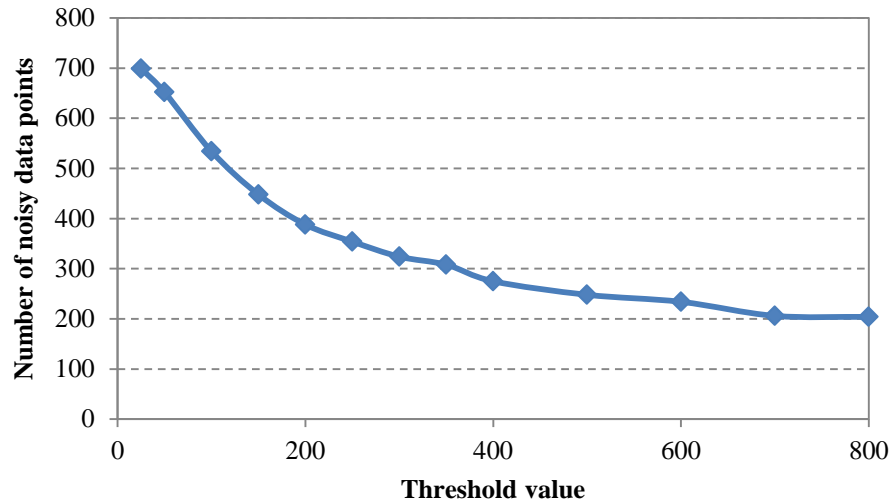
Figure 5.27(a)
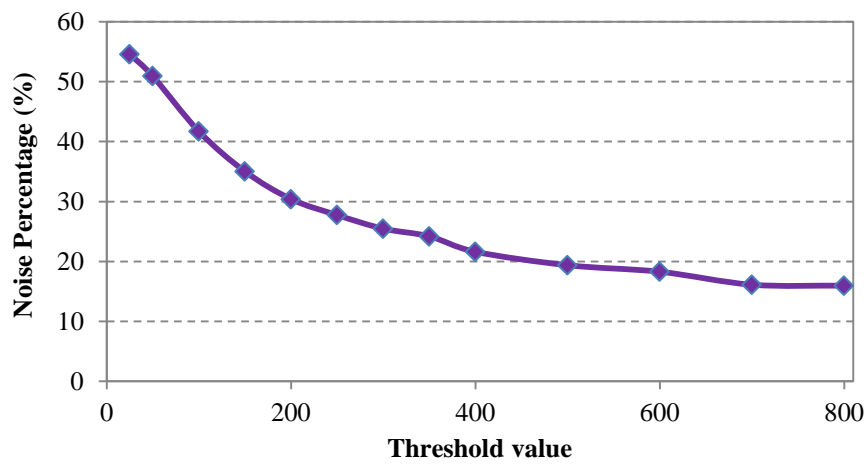
Figure 5.27(b)

Figure 5-27: Data acquisition performance against specified threshold value (a) number of noisy data points (b) noisy data percentage

5.4   Summary

The work reported in this chapter was focused on understanding the performance of a *3D* laser scanner and establishing the optimum set of parameters for enhancing data acquisition performance.

The work-span of the laser scanner was found and the results obtained show the actual values are different from the specified values in the manufacturer's datasheet. It was also found that the vertical and horizontal resolution of the laser scanner varies along its z and x axes respectively. Measurement accuracy reaches its maximum at the middle of the laser line span (67mm stand-off). The relationship between the sensor resolution against the stand-off distance was also established. The accuracy of measurements at different exposure levels was also measured and, according to the results obtained, the

118

variation from the expected linear output is minimal around 1-2ms exposure time. The repeatability of the sensor was measured and the mean-error was found to be ±28um whereas the standard deviation in readings was ±36um. The laser scanner performance at different illumination conditions was investigated. Results show that ambient lighting affects the measurements where the laser scanner fails to settle at a particular reading. This effect was significant when measuring smaller dimensions. Controlled lighting conditions result in better performance. The error in the readings obtained is higher when measuring small objects.

Stand-off distance, steepness angle, angle of incidence, surface reflectivity, exposure time, threshold value and laser power are the attributes which affect the data acquisition performance of a laser scanner. The number of missing points is minimal around 67mm stand-off distance. High steepness angles above a threshold steepness angle of 40˚ resulted in more missing data points. It was found that there is a critical incidence angle range (15˚-25˚) in which the laser scanner gets saturated due to the number of photons reaching the sensor. This effect was significant on shinier surfaces. Surfaces with a matt-finish resulted in good point cloud data at any angle. Results also revealed that the percentage of noisy data increases with exposure time. However it was also shown that more data points could be acquired if the exposure time is high. Exposure times between 1s and 2s resulted in the minimum number of missing and noisy points. The effect of laser power on data acquisition was also investigated. Results showed that for a shiny object the number of noisy data points increases with laser power. However it should be noted that laser power did not affect the percentage of missing data points. The effect of threshold value was also studied which resulted in more noisy data points at lower threshold values for a shiny surface. From the results it was understood that for best results,

- Stand-off height to needs be maintained at 67-68mm
- Exposure time at 1-2ms
- Angle of incidence should not be between 15˚ and 25˚
- Angle of steepness is not above 40˚
- Laser scanner uses optimum power and threshold value.

These settings have been be used for the data collection which is presented in the following chapters to perform *3D* seam tracking and *3D* feature extraction. Enhanced

data quality is expected to return better performance in the developed algorithms for point cloud processing. A similar experimental procedure is proposed for evaluating the performance of any laser scanner prior to its use so that the errors in measurements can be minimized.

6　3D Feature Extraction and Quantification of Joint Fit-up

In Chapter 5 the most suitable laser scanner settings for the best performance of the laser scanner was identified for this type of application and these settings have been used for data collection in this Chapter and the following Chapters.

Recent advances in automation and sensor technology have enabled the use of industrial robots for complex tasks that require intelligent decision making. Vision sensors have been the most successfully used sensor in many high value industrial applications. Over recent years, weld seam tracking has been a topic of interest, as most of the existing robotic welding systems operate on the basis of pre-programmed instructions. Such automated systems are incapable of adapting to unexpected variations in the seam trajectory or part fit-up. Applications such as TIG welding of aerospace components require tight tolerances and need intelligent decision making. Such a decision making procedure has to be based on the weld groove geometry at any instance. In this chapter a novel algorithm along with an automated system is described for estimating the joint profile of three *3D* weld grooves. A real-time position based closed-loop system was developed with a six axis industrial robot and a laser triangulation based sensor. The system was capable of finding the *3D* weld joint profile and making intelligent decisions accordingly. Raw data from a vision sensor was processed through the novel algorithm to obtain important features of the weld groove at an accuracy of $\pm 8.3 \mu m$ and $\pm 43 \mu m$ in the x and z co-ordinates respectively. A detailed description of the novel algorithm developed and the results of performance tests carried out are presented in this chapter.

6.1　Introduction

A successful *TIG* welding automation system should be capable of adapting to any variations in the weld seam position, caused by part fit-up or distortions. Over the past few decades, extensive research has been carried out on the use of weld seam tracking [154][155][156]. However, not enough work has been carried out on finding the geometry of a weld groove. Conventional seam tracking has only been used to estimate the weld seam coordinates for path correction of the robots. This process alone could be adequate for a simple geometry, but some advanced applications (e.g. aerospace,

welding of vanes to a hub in an aero-engine) require in-process control of the weld parameters [121] to accommodate for complex geometries and part fit-up. Such a requirement can only be realized by the identification of geometrical features which will enable intelligent decision making and therefore control of the welding process (path and process parameters) [132].

Requirement for joint fit-up quantification and seam tracking under this thesis are listed as below.

- Finding joint centre position with an accuracy of ±0.5mm.
- Determination of a coordinate in x,y or z axis with an accuracy of ±100µm.
- Tracking path to be determined correctly irrespective of the joint fit-up orientation and joint profile type.
- The feature extraction or seam tracking algorithm should function irrespective of the joint profile type.
- The feature extraction and seam tracking algorithm should function irrespective of the point cloud quality.
- The algorithms should be capable of eliminating any spurious outliers detected.

6.2 Experimental setup and methodology

The experimental setup (Figure 6-1) used for the feature extraction consists of the KUKA KR16 six axis industrial robot, Micro-epsilon laser scanner, workstation and the external digital pulse generated from the NI DAQ system used for triggering the laser scanner. The arrangement of laser scanner at the end effector of the robot can be seen in Figure 6-2.
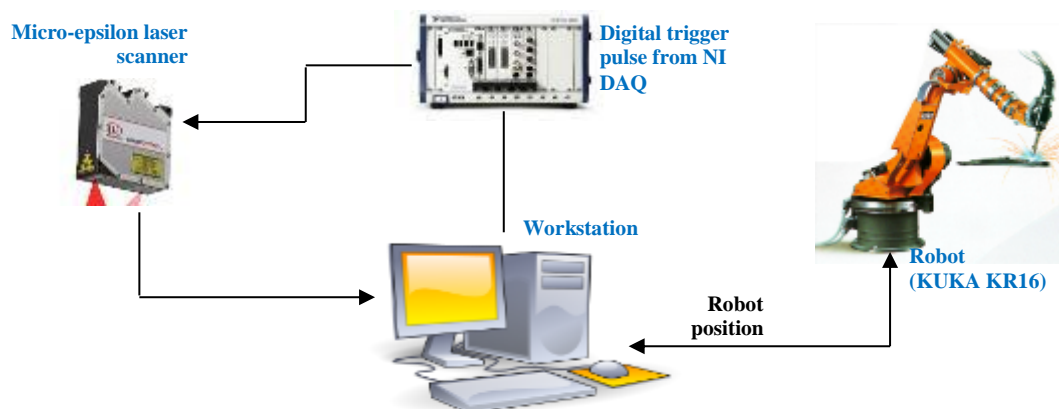
Figure 6-1: Experimental setup used for joint feature extraction

122
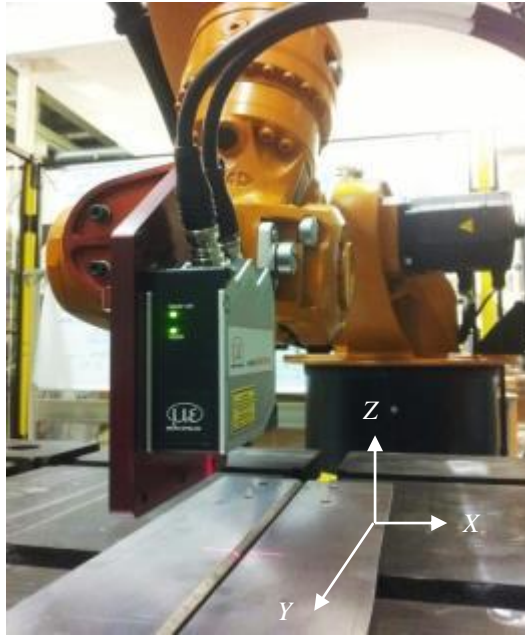
Figure 6-2: Photographic view of the experimental setup

A position based control system (with a sequence of operations as shown in Figure 6-3) software was developed using LabVIEW to control the overall process. Initially, the robot requests positional data from the computer, which is also used as a command to trigger the laser with a 5V digital pulse. Once triggered, the laser scanner acquires a single profile (*2D* data) and sends it to the computer through an Ethernet connection within 20ms.

```
┌─────────────────────┐
│   System start-up   │
└─────────────────────┘
           │
           ▼
┌─────────────────────────────────────┐      ┌──────────────────┐
│ Set operating parameters on the     │◄─ ─ ─│ Manual input from│
│ laser scanner                       │      │   the operator   │
└─────────────────────────────────────┘      └──────────────────┘
           │
           ▼
┌─────────────────────┐
│ Initiate laser      │
│ scanner             │
└─────────────────────┘
           │
           ▼
┌─────────────────────┐
│ Guide to seam start │◄──────────┐
└─────────────────────┘           │
           │                       │
           ▼                       │
        ╱        ╲                 │
       ╱ Got to the ╲    No        │
      ╱    start?    ╲─────────────┘
       ╲           ╱
        ╲         ╱
           │ Yes
           ▼
┌─────────────────────┐
│ Trigger laser       │◄──────────┐
│ scanner             │           │
└─────────────────────┘           │
           │                       │
           ▼                       │
┌─────────────────────┐           │
│ Transfer data to    │           │
│ the PC              │           │
└─────────────────────┘           │
           │                       │
           ▼                       │
┌─────────────────────┐           │
│ Extract features    │           │
│ from the data       │           │
└─────────────────────┘           │
           │                       │
           ▼                       │
        ╱        ╲                 │
       ╱ Features  ╲     No        │
      ╱ extracted?  ╲──────────────┘
       ╲           ╱
        ╲         ╱
           │ Yes
           ▼
┌─────────────────────┐
│ Move robot to next  │
│ position            │
└─────────────────────┘
```
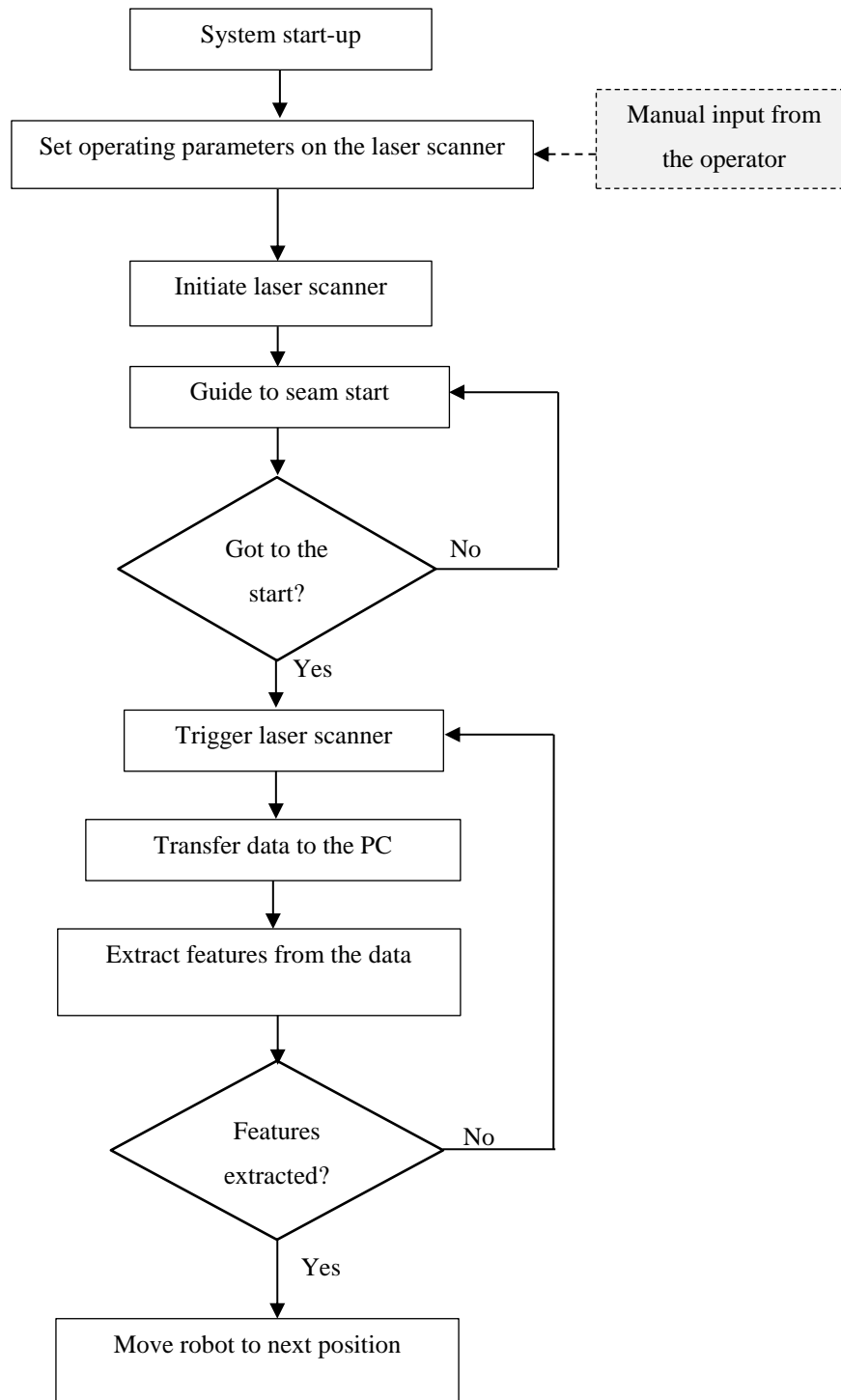
Figure 6-3: Sequence of operations for robotic scanning and feature extraction

The obtained *2D* data is processed to find the important features such as the edges of the weld joint (welding joints used for the study are shown in Figure 6.4(a)-(c)). Please refer to Figure 6.5 for more information. Once the features are extracted, the computer sends a command to the robot, to move to the next position (in this study the robot step is 1mm along the scan direction). After moving to the next position, the robot sends its *3D* coordinates back to the computer which is used again as a command to trigger the

laser scanner. The cycle is repeated until the scan is completed. The extracted feature points are then plotted in *3D* for visualization and further analysis.

Figure 6.4 (a)
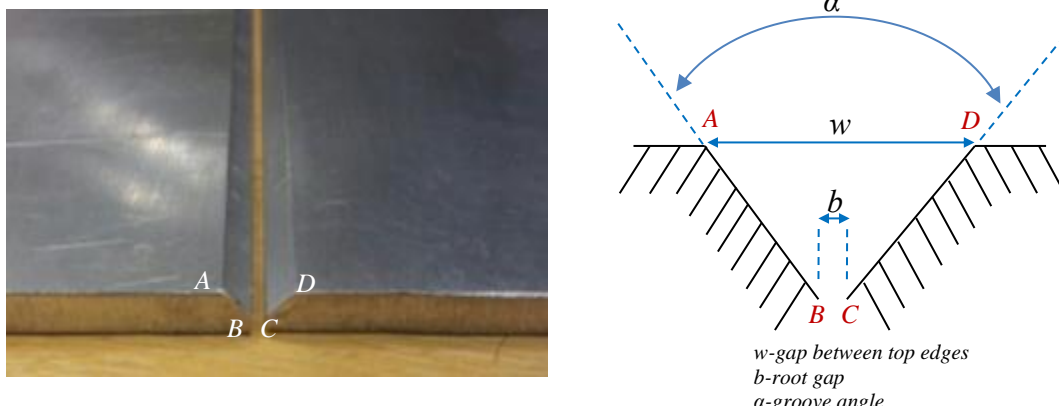
Figure 6.4(b)
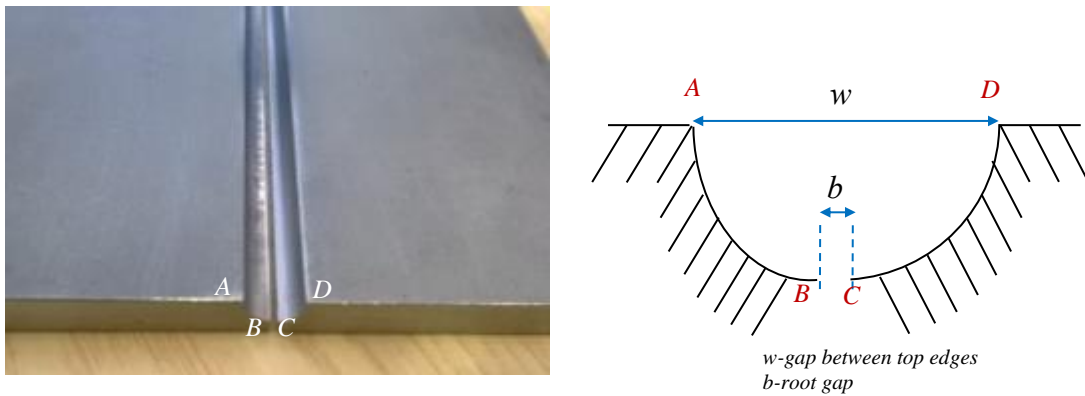
Figure 6.4(c)

Figure 6-4: Sample weld groove types used for feature extraction (a) I groove, (b) V groove, (c) U groove

The weld geometry measurements were carried out on samples with standard *I*, *V* and *U*-groove profiles. These joints were selected as they are the most common type of joints found in the welding industry [40][157].

6.3 Real-time feature detection of 2D profile

Feature detection and extraction was performed on *I*, *U* and *V* grooves. The steps involved in detecting the feature points of a *V* groove are described within this section in detail. A similar method has been applied for both the *I* and *U* grooves and the results are presented at the end of this section.

The important points to be extracted from the weld joint are shown in Figure 6-5. These features are point *A, B, C* and *D* respectively. A two stage extraction process is undertaken for each sample. The first stage is the application of filtering techniques, such as a low pass filter, which has been applied in LabVIEW to eliminate any outliers and the second stage is an edge detection method, generally the gradient method, which is implemented to find the features. Data processing is carried out in real-time via the Ethernet connection with the PC and the extracted points are stored for further analysis and improvement after combining the data set into *3D* space (described later in this chapter).
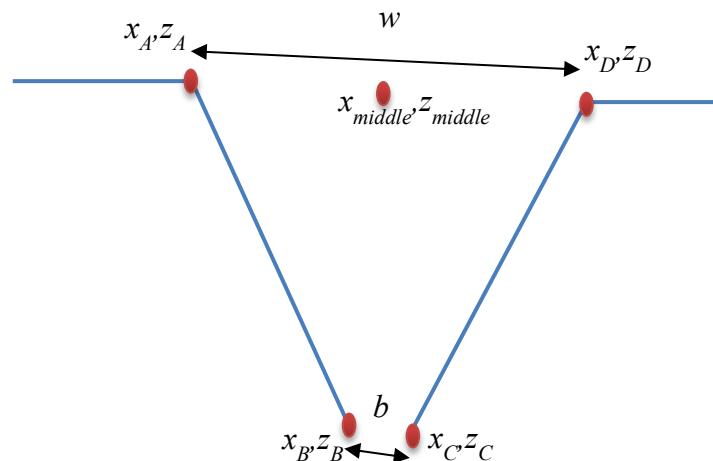
Figure 6-5: Features to be extracted from a weld joint

6.3.1 Feature extraction of a *V*-groove

The raw data obtained from the laser scanner has noise and missing data due, predominantly, to specular reflection. This noise needs to be removed prior to data processing. As shown in Figure 6-6(a), which is a representative dataset collected during the experimental process, most of the noise was observed at the ends of the laser line. This is attributed to the reduced sensitivity of the scanner at these points. To remove these outliers, the raw data was cropped by five percent from both ends, which results in the dataset displayed in Figure 6-6(b).

126
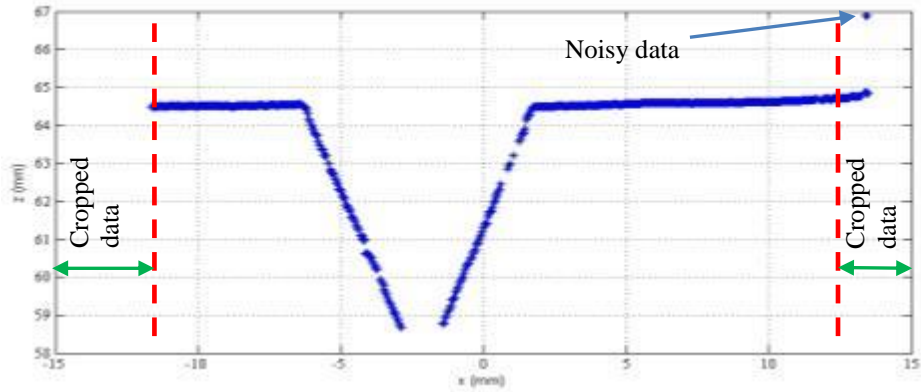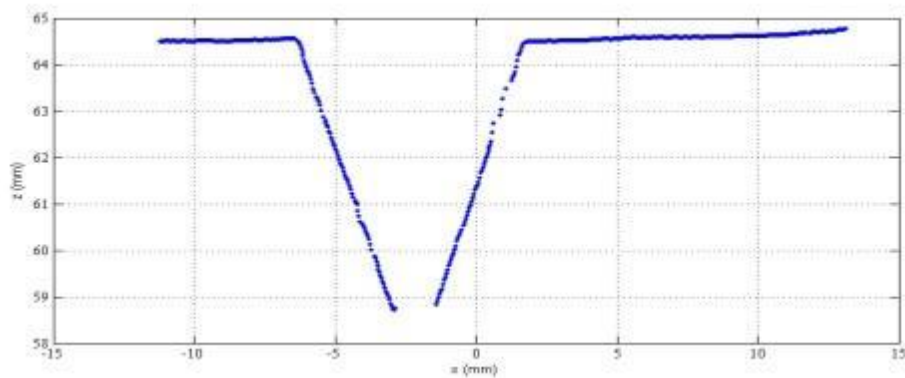
Figure 6.6(a)

Figure 6.6(b)

Figure 6-6: Data cropping process for outlier removal (a) data cropping process (b) resulting data

An edge is defined as a point where there is a sharp change in gradient [91]. Hence the gradient method was used for edge detection. By calculating the gradient (Gi) between each successive laser point (using equation 6.1), point A and D were recognized. The obtained gradient values can be seen in Figure 6-7, the start of the positive peak is related to point A and the fall of the negative peak is related to point D.

$$G_i = \frac{y_i - y_{i-1}}{x_i - x_{i-1}} \tag{6.1}$$

where, x_i and x_{i-1} are the x coordinates of two adjacent laser points.

$$dx_i = x_i - x_{i-1} \tag{6.2}$$

where, dx is the offset (along the x axis) between two consecutive laser points.
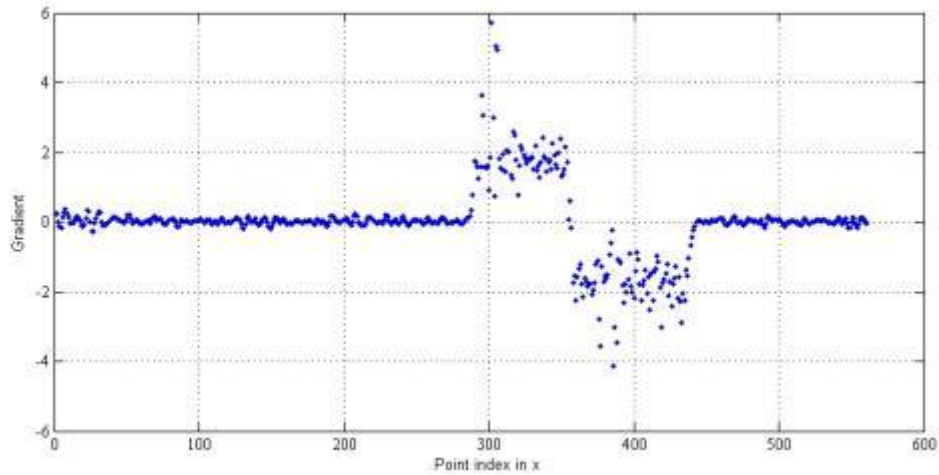
Figure 6-7: Gradient values along the 2D point cloud (*dy/dx*)

According to the manufacturer the lateral resolution of the laser scanner is 20μm [149]. Therefore, it was ensured that the gap between point *B* and *C* was always more than the sensor resolution (>20 μm). Points *B* and *C* were established on the basis of the maximum horizontal offset between two successive laser points. Equation 6.2 was then used between all the adjacent laser points in a single *2D* cross sectional profile to find when the maximum value occurred, which resulted in the data displayed in Figure 6-8. Points *B* and *C* are present where the spike is detected.
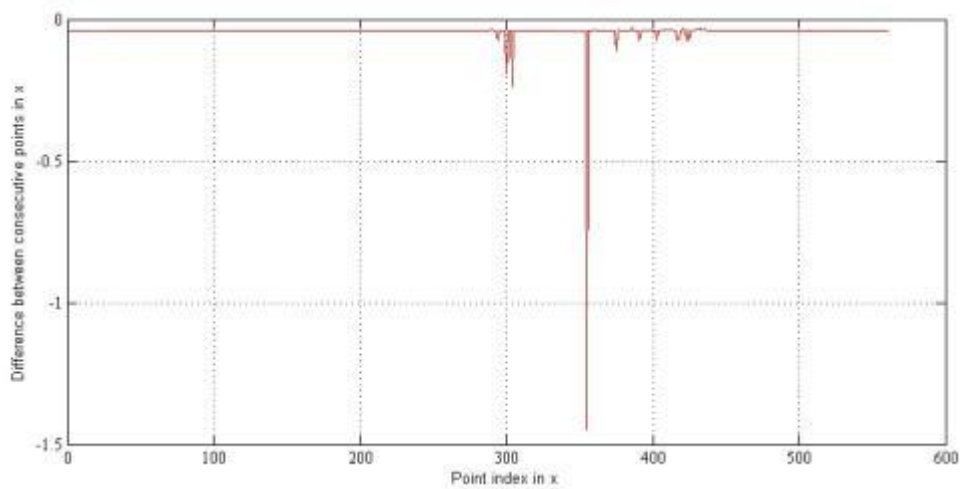
Figure 6-8: horizontal offsets between two consecutive laser points (*dx*)

Figure 6-9 shows the extracted points plotted on the raw data.
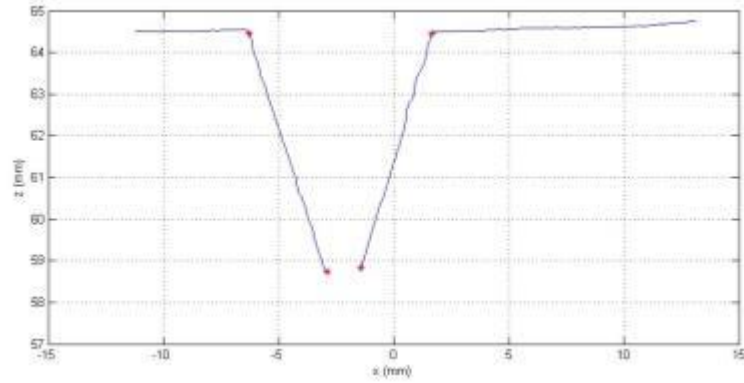
Figure 6-9: Extracted feature points (●)

The points identified using this method was then used to calculate the coordinates of the middle point of the seam using equation 6.3 and 6.4. The values of x_{middle} and z_{middle} were then used for guiding the welding torch during the welding process (as detailed in Chapter 7).

$$x_{middle} = \frac{x_A + x_D}{2} \tag{6.3}$$

$$z_{middle} = \frac{z_A + z_D}{2} \tag{6.4}$$

The root gap (*b*) and the gap between the top edges (*w*) (shown in Figure 6-4) were calculated using equations 6.5 and 6.6. The outcomes of these calculations were used to inform decisions being made on the joint geometry. For example, if the root gap were above a certain tolerance value (1mm), a decision could then be made about whether it is possible to weld the joint.

$$b = \sqrt{(x_B - x_C)^2 + (z_B - z_C)^2} \tag{6.5}$$

$$w = \sqrt{(x_A - x_D)^2 + (z_A - z_D)^2} \tag{6.6}$$

The method of using the derived centre points for seam tracking is discussed in detail in Chapter 7 and the method of using the extracted points for joint volume calculation (for adaptive weld process control) is discussed in Chapter 9

6.3.2 *U*-Groove

The steps used to extract the features in the *V*-groove are also used for the *U*-groove and the results are shown in Figure 6-10.

129
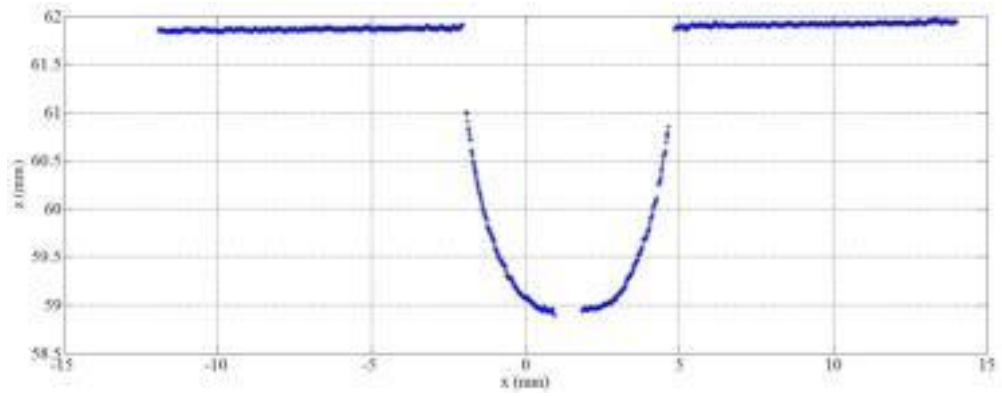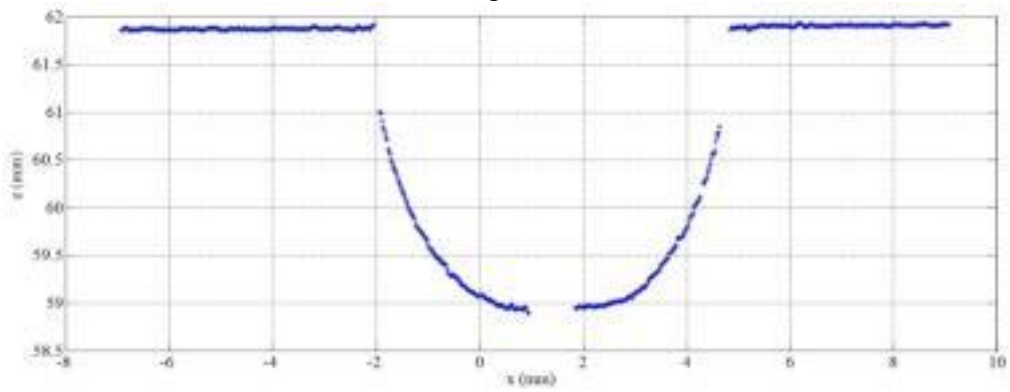
Figure 6.10 (a)

Figure 6.10 (b)
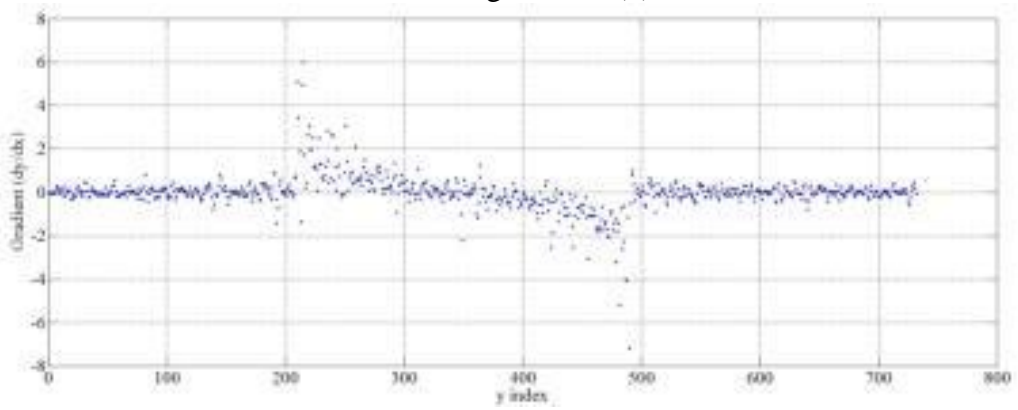
Figure 6.10 (c)
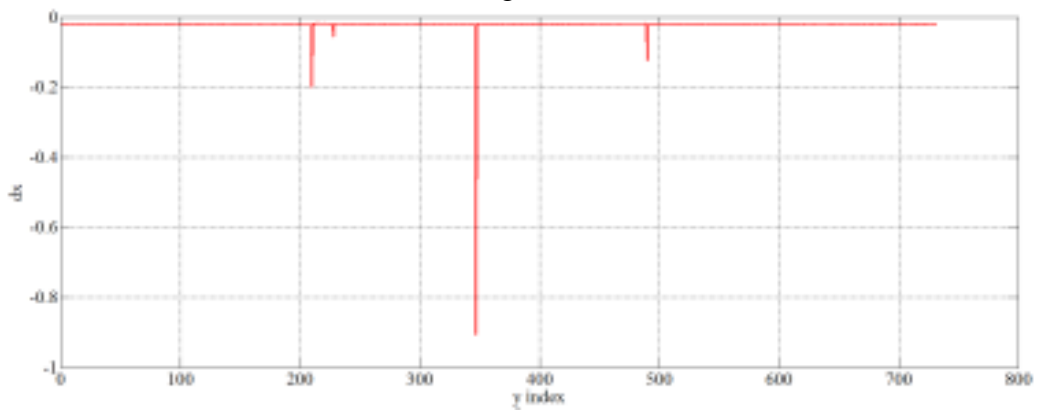
Figure 6.10(d)
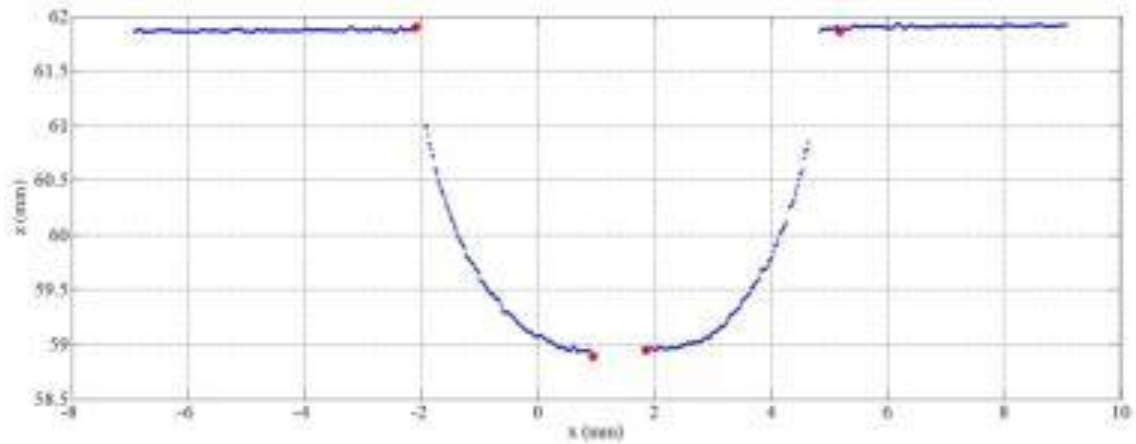
Figure 6.10 (e)

Figure 6-10: Feature extraction steps for the U-groove (a) raw data, (b) cropped data, (c) gradient

(dy/dx), (d) Offset between consecutive laser points (dx), (e) extracted feature points (•)

As can be seen from Figure 6-10(a) there are a large number of missing data points, approximately 200 points, due to the high steepness angle in a *U*-groove at the start of the *U* shape. It can be seen in Figure 6-10(d), that point *D* has slightly deviated from the actual edge. However this error is measured to be 30um which does not affect the performance significantly. Therefore it can be concluded that the algorithm overcomes the effect from the missing data regions and extracts the feature points to a satisfactory level.

6.3.3 *I*-Groove

The data processing sequence for an I-groove is shown in Figure 6-11.
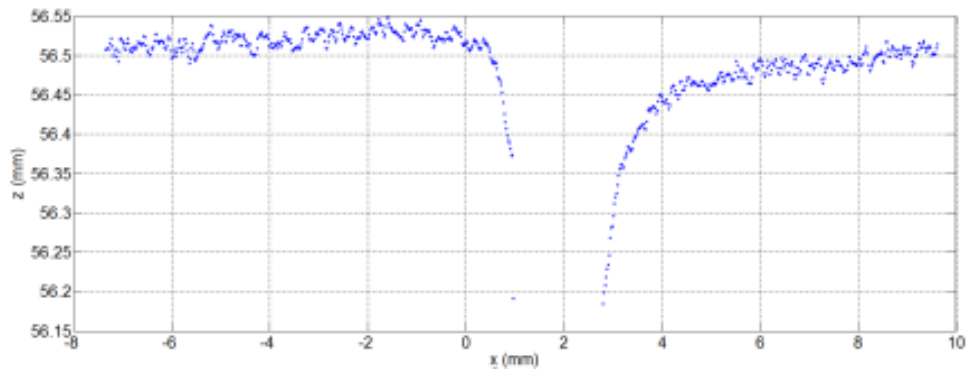
Figure 6.11 (a)
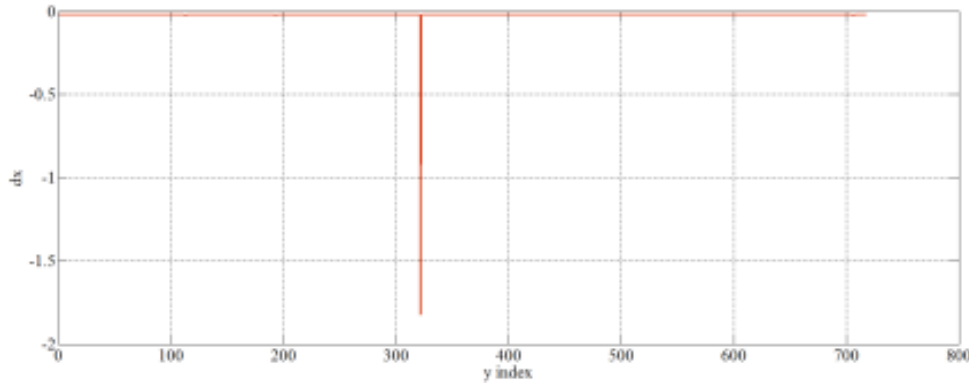
Figure 6.11 (b)
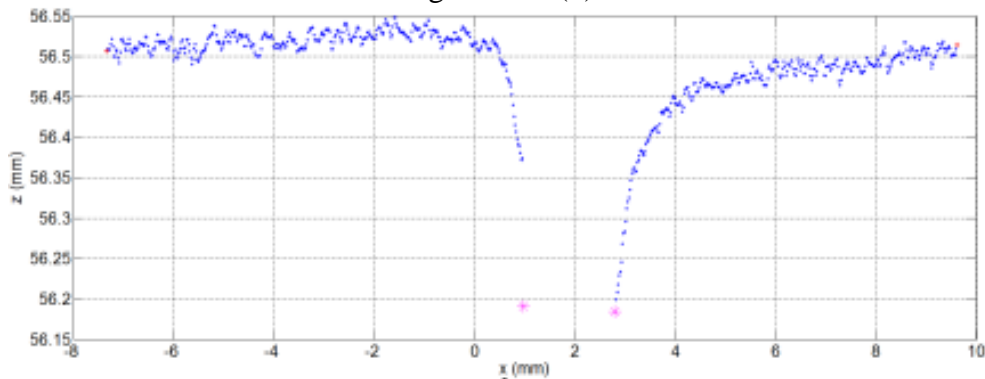
Figure 6.11 (c)

Figure 6-11: Feature extraction of a I-butt joint (a)raw data, (b) dx, (c) Detected points (∗)

The raw data obtained from an *I*-groove can be seen in Figure 6-11 (a). The horizontal offset which was measured between two consecutive laser points is shown in Figure 6-11 (b). The gap is present where the maximum offset between two consecutive laser points is detected. Therefore, Point *B* and *C* can be located where the peak is detected in the Figure 6-11 (b). It should be noted that in an *I*-groove, Point *A* coincides with Point *B* and Point *D* coincides with point *C*.

It can be seen from Figure 6-11 (c) that the extracted points are 0.3mm below the actual points. This is a constant error which exists along the *I*-groove. Therefore this constant, systematic, error was always added to the *z* co-ordinate of the extracted points. It should be noted that this effect was only in the case of the *I*-groove. Gaps of 1mm, 1.5mm,

132

2mm and 5mm were examined and the algorithm always returned a 0.3mm offset in point detection. This led the author to conclude that the error is a constant value due to the sample shape and does not vary based on the sample thickness.

6.4 Post-processing algorithm for filtering

As observed in Chapter 5, the surface characteristic (reflectivity) of the weld sample influences the quality and repeatability of the data. It was also found that laser scanners tend to return noisy data if the surface is highly reflective or if there was any change in angle between the scanner and the surface. Any spurious points detected due to the inaccuracy of the laser scanner or the extraction algorithm used can lead to unexpected behavior (such as faulty detection of a feature point) in the welding run. This can affect the welding position between the samples and consequently the mechanical properties of the weld. Hence a suitable filtering method was applied to eliminate the outliers in the extracted points.
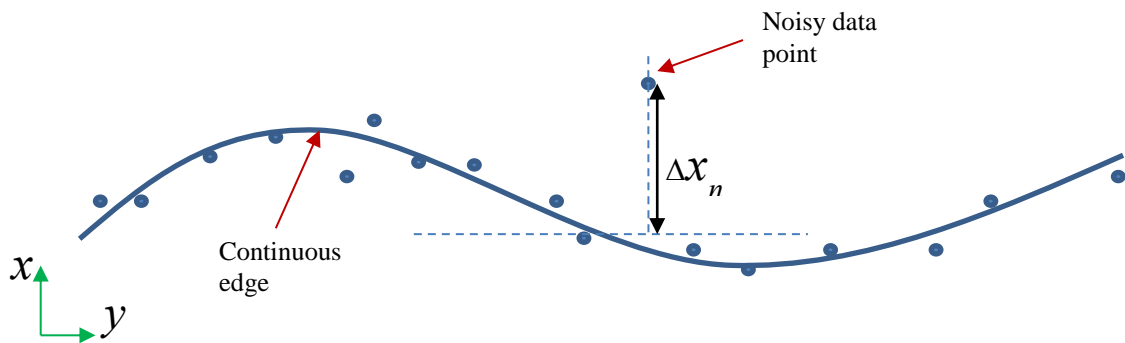
Figure 6-12: Continuous weld groove edge and detected noisy data point

A noisy data point in the *x-y* plane has been illustrated in Figure 6-12. The maximum distance between two consecutive laser points in the *x* direction (ΔX) should be close to the laser scanner's lateral resolution as a well machined weld groove does not have sudden changes in the *x*-direction. Therefore, if any point has a significantly larger horizontal offset than the previous point it could be an outlier. A threshold value was defined to filter any point which had an offset more than the specified threshold value of 0.1mm (this is the accuracy of the gap detection). This filtering method was used to remove high amplitude outliers in both the *x* and *z* directions separately. Equations 6.7 and 6.8 define the horizontal and vertical offsets between two consecutive points respectively.

$$\Delta X_n = X_n - X_{n-1} \qquad\qquad (6.7)$$

$$\Delta Z_n = Z_n - Z_{n-1} \tag{6.8}$$

The "Smooth" function in Matlab was then used to filter outliers within less than 0.1mm. The "Smooth" function assigns lower weight to outliers in the regression. Using this method a zero weight was assigned to data outside six mean absolute deviations. The filtering sequence described above has been shown graphically in Figure 6-13.
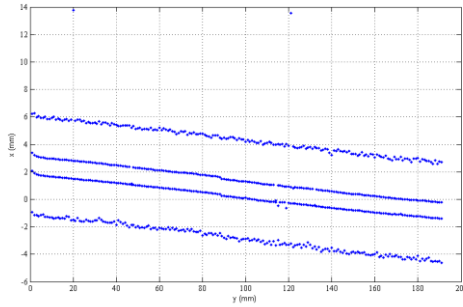
Figure 6.13(a)
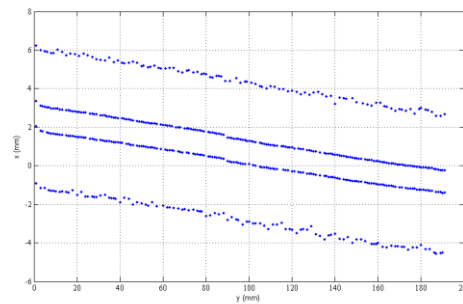
Figure 6.13(d)

Figure 6.13(b)

Figure 6.13(e)
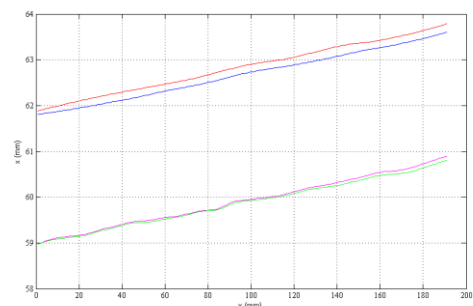
Figure 6.13(c)

Figure 6.13(f)

Figure 6-13: Filtering applied in both x and z axis separately (a) x-y raw data, (b) x-y data after filtering, (c) x-y data after fitting, (d) y-z raw data, (e) y-z data after outlier removal, (f) y-z data after fitting

The features detected from the raw data in the *x-y* and *y-z* planes respectively are shown in Figure 6-13 (a) and (d). As can be seen from the figures raw data contains spurious points. After applying equations 6.7 and 6.8, the results can be seen in Figure 6-13 (b) and (e). The resulting data is then filtered again using the "Smooth" function in Matlab

134

which results in the data displayed in Figure 6-13 (c) and (f). As can be seen from the figure, the fully processed and filtered data contains a low number of noisy data points.

Figure 6-14(a) shows the extracted raw points (*A, B, C* and *D*) plotted in *3D* and Figure 6-14(b) shows the fitted points. As can be seen from the figure the processed data is more error-free compared to the raw data. This re-assures that the filtering method implemented is functioning to reliably perform gap sensing and seam tracking.
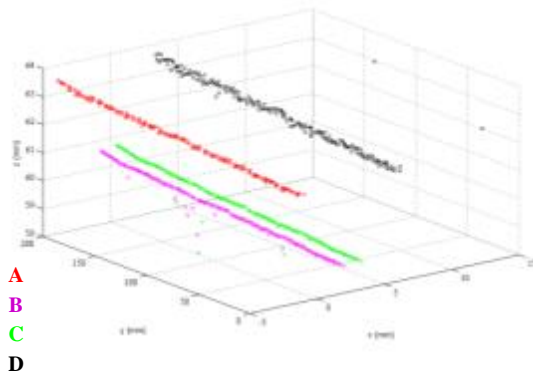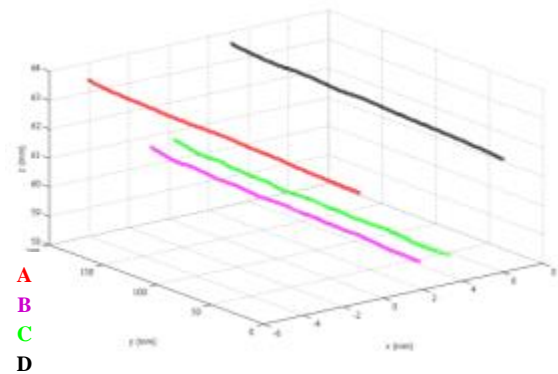
Figure 6.14(a)   Figure 6.14(b)

Figure 6-14: Extracted feature points (a) raw data, (b) fitted data

6.5   Joint fit-up quantification

In an industrial automated welding system, setting up the part is still carried out by the manual operator. However, manual operators do not have the high repeatability that an automated system does and, therefore, setting up the parts can have fit-up errors. Some of the possible joint configurations, due to part fit-up for a simple butt-joint can be seen in Figure 6-15 (These configurations were selected based on the experience of manual operator).

Roll   Pitch   Yaw

Horizontal offset   Vertical offset
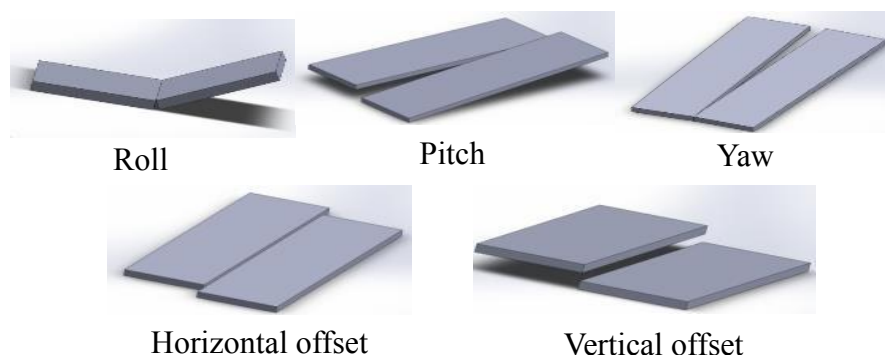
Figure 6-15: Possible joint configurations

Based on the part fit-up, any automation system should either adapt to the variation caused by the operator or make an intelligent decision whether the weld joint should be

135

re-adjusted. Quantification of joint fit-up will enable the system to correctly position the welding torch so that the desired weld quality can still be achieved. This will reduce the cost and time associated with set-up and therefore improves productivity of robotic welding.

In the work presented in this thesis, the horizontal offset configuration is not investigated as it is assumed that the effect of the horizontal offset is minimal in an industrial weld setting. In this section, joint fit-up has been quantified for the three different joint types (*I*, *U* and *V*) under consideration. The following sections only describe how the joint fit-up was measured for a *V*-groove. The same method was implemented for the both *I* and *U* grooves.

6.5.1 Quantification of roll angle

The method of measuring the roll angle (α) between the parts is shown in Figure 6-16(a) and geometry is shown in Figure 6-16(b). The angle between the horizontal edges defines the role angle per single cross sectional profile. In order to quantify the roll angle, two lines are to be fitted to the horizontal edges of the samples.
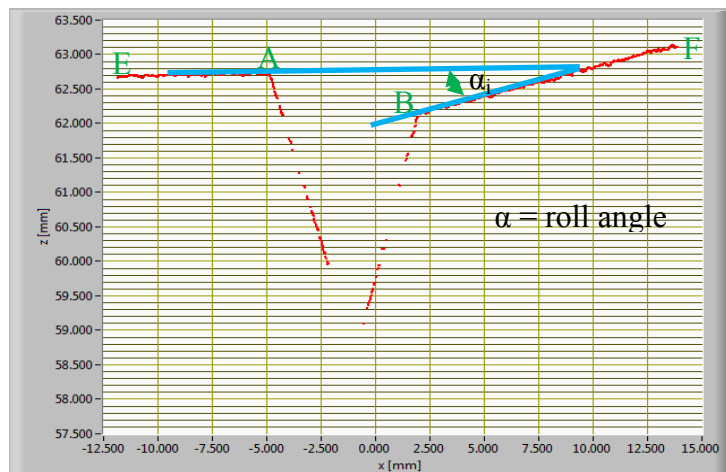
Figure 6.16(a)   Figure 6.16(b)

Figure 6-16: Roll angle measurement (a) physical set-up, (b) roll angle

The method of identifying Point *A* and *B* has been described in Section 6.3.1. However, in order to fit lines to the horizontal edges of the samples, Point *E* and *F* should also be identified, namely the outside points of the scanned laser line. This was accomplished by finding the coordinates of the points which have the maximum and minimum *x*-coordinates of a particular cross sectional profile. The angle between the lines *EA* and *BF* therefore defines the roll angle and it has been calculated using equation 6.9.

136

$$\alpha = \tan^{-1}\left|\frac{m_{EA} - m_{BF}}{1 + m_{EA}.m_{BF}}\right| \qquad (6.9)$$

where, m_{EA} and m_{BF} are the gradients of the lines *EA* and *BF* respectively. Also it should be noted that $0 \leq \alpha \leq \pi/2$.

The average roll angle has been calculated by extracting the division between the summation of the roll angles for the complete scan and the number of profiles as shown in Figure 6-17. The set value for the graph shown was 3° and the measured average value is 2.85°.
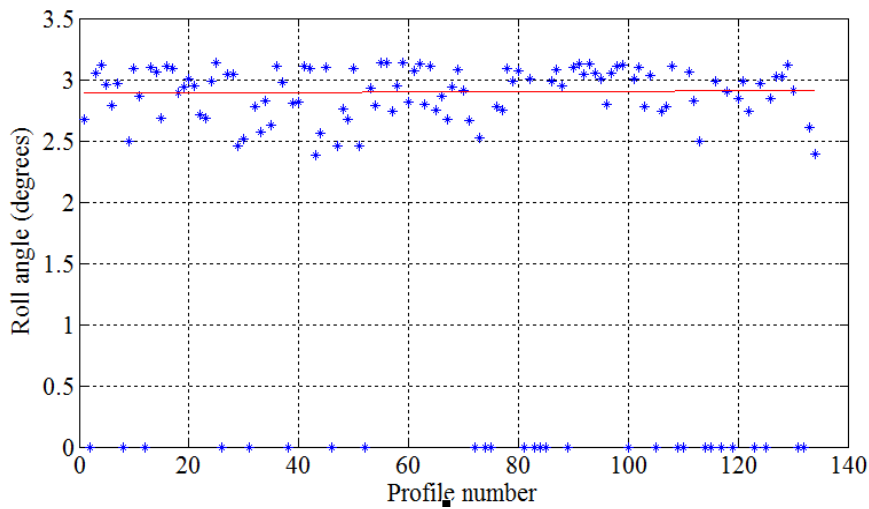
Figure 6-17: Roll angle measurement along the weld joint

6.5.2 Quantification of pitch angle

The pitch angle (β) between the two samples is shown in Figure 6-18(a) and the geometry is shown in Figure 6-18(b). The angle was created by keeping a slip gauge underneath one sample as shown in the figure. The pitch angle was then measured in the *y-z* plane of the point cloud data. This angle was measured between the lines fitted along the top edges of the groove (i.e. along Point *A* and Point *D*). Equation 6.9 was then used again to quantify the angle. The extracted points (*A* and *D*) in *y-z* plane and the lines fitted to the raw data are shown together in Figure 6-19.
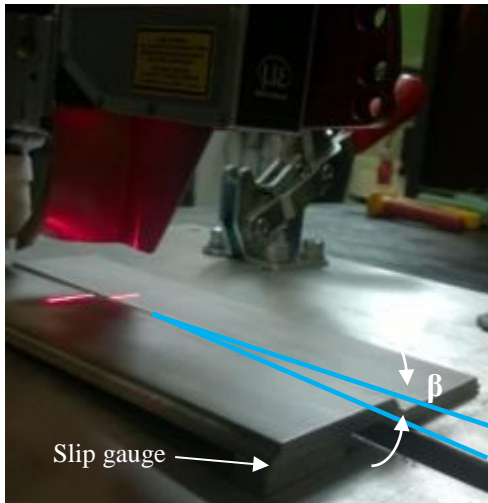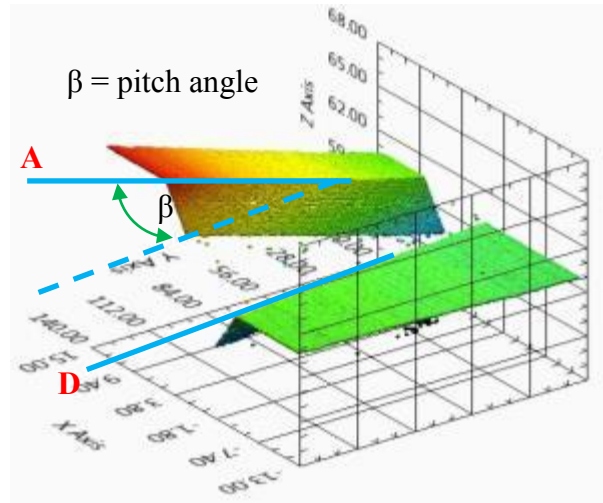
Figure 6.18(a)   Figure 6.18(b)

Figure 6-18: Pitch angle measurement (a) physical set-up, (b)pitch angle
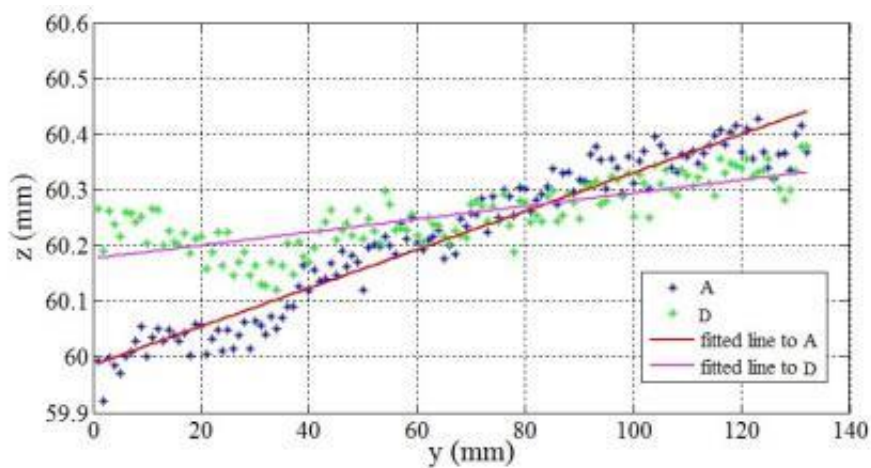
Figure 6-19: Line fitting for pitch angle measurement

6.5.3 Quantification of yaw angle

The yaw angle (μ) between two samples can be seen in Figure 6-20 (a) and the geometry is shown in Figure 6-20(b). Yaw angle is measured in the *x-y* plane of the point cloud data. This angle was measured between the lines fitted along the top edges of the groove (i.e. along Point *B* and Point *C*). Equation 6.9 was used again to quantify the angle. The extracted points (*B* and *C*) in *x-y* plane and the lines fitted to the raw data can be seen in Figure 6-24. As can be seen from the figure the line fitting process fits the best line along the raw data and attempts to overcome the errors caused by outliers.
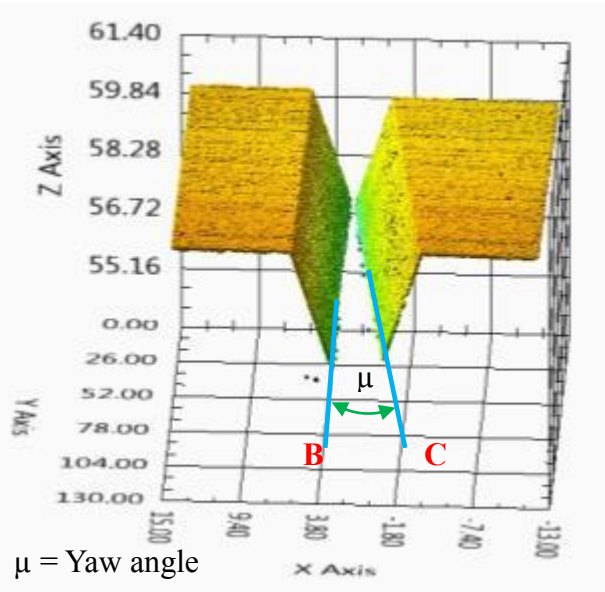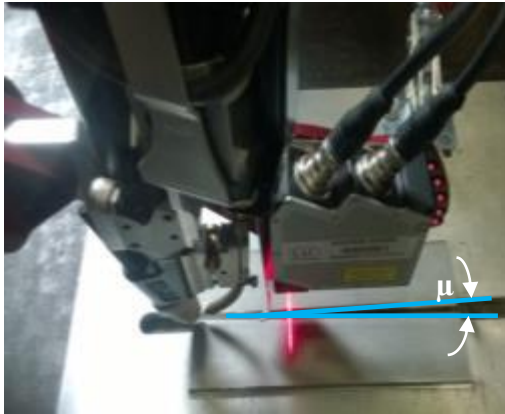
<table>
<tr><td>Figure 6.20(a)</td><td>Figure 6.20(b)</td></tr>
</table>

Figure 6-20: Yaw angle measurement (a) physical set-up, (b) yaw angle
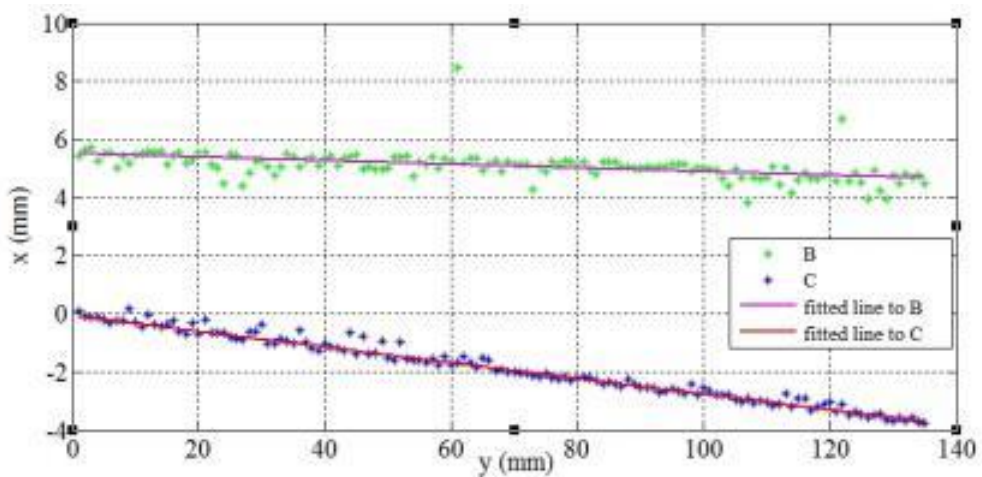
Figure 6-21: Line fitting for yaw angle measurement

6.5.4 Quantification of vertical offset

The vertical offset (v) between the two samples is shown in Figure 6-22(a) and the geometry is shown in Figure 6-22(b). This was measured between the fitted lines along the top edges of the groove (i.e. along Point *B* and Point *C*).

A profile by profile vertical offset calculation along the weld joint is shown in Figure 6-23. The average vertical offset was quantified by taking the division between the summation of vertical heights of the entire cross sectional profiles and the total number of profiles acquired. The set value for the graph shown was 1.5mm and the measured average value is 1.61mm.
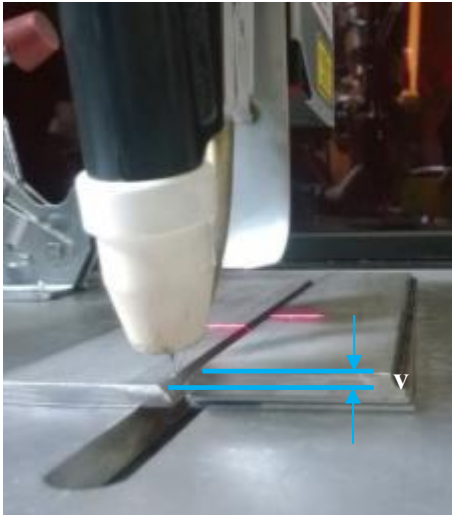
v = Vertical offset
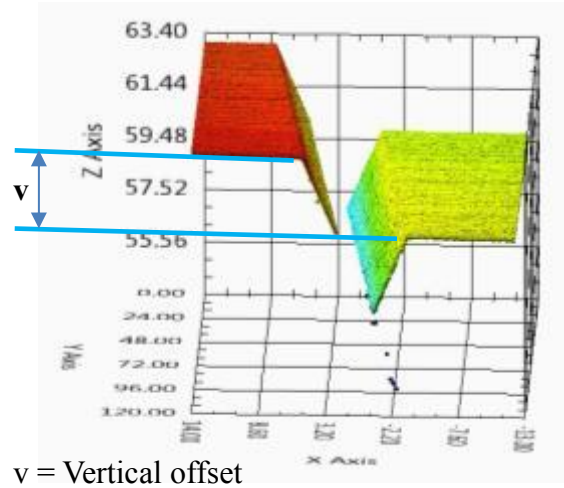
Figure 6.22(a)   Figure 6.22(b)

Figure 6-22: Vertical offset measurement (a) physical set-up, (b) vertical offset
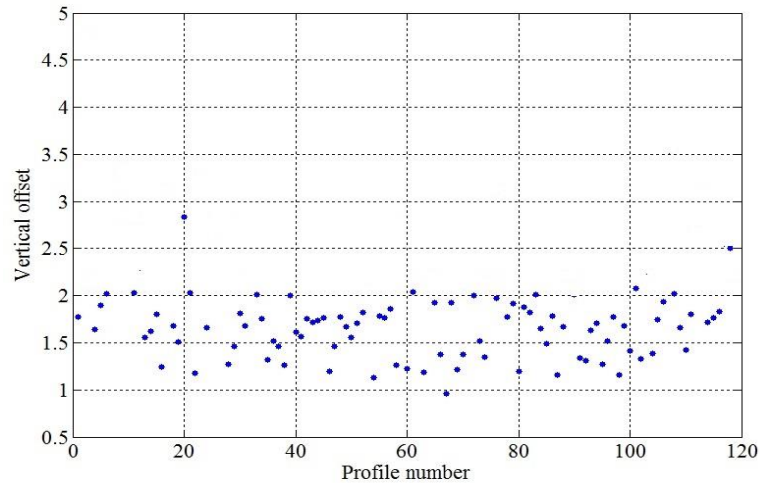
Figure 6-23: Vertical offset measurement along the weld joint

6.6   Results and validation

This section describes the results obtained using the feature detection and joint fit-up identification algorithms. Experiments were carried out to investigate the performance of the feature detection algorithm and gap sensing. Each experiment was repeated three times to assure repeatability.

6.6.1   Extracted features for different joint types

According to the methods described in Sections 6.3 and 6.4, feature points of three different joint configurations were extracted. The extracted points, displayed in blue, have been overlaid onto the raw *3D* point cloud data in Figure 6-24. As can be seen from the figure, the data extraction algorithm functions as it was designed to, irrespective of the joint configuration. The algorithm is also robust enough to overcome

issues such as missing data points and noisy data points. The settings identified for the 'best' performance of the laser scanner identified in Chapter 5 assisted in the reduction of spurious data being output from the laser scanner. Reducing these spurious data helped in improving the accuracy of the algorithm.
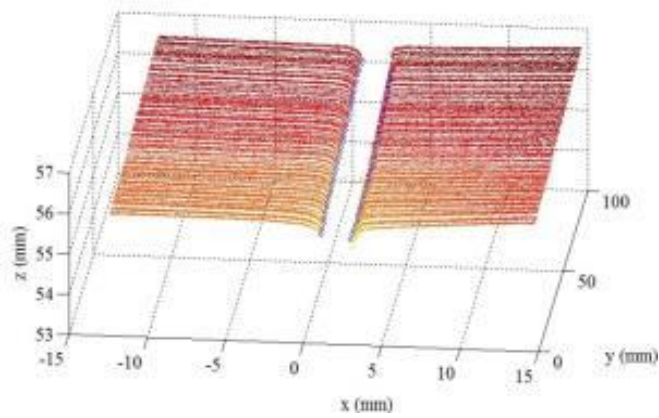
Figure 6.24(a)
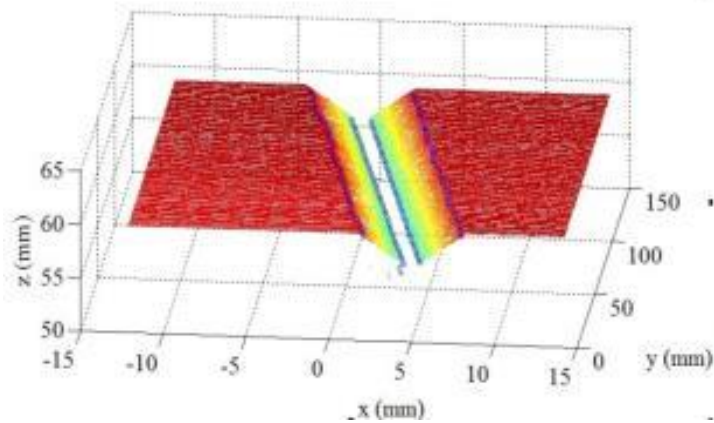
Figure 6.24(b)
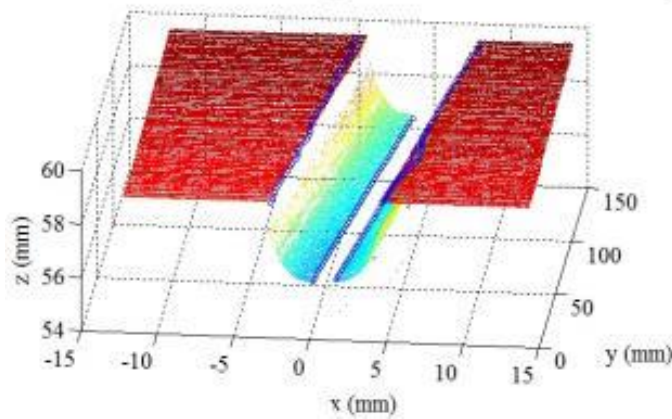
Figure 6.24(c)

Figure 6-24: Extracted features of selected weld joint type (a) I-groove, (b) V-groove, (c) U-groove

6.6.2 Validation of feature detection algorithm

In order to validate the accuracy of the algorithm, randomly selected points (out of 150 points) from the final result (for three different joint configurations) were compared against the corresponding raw data points. The results are listed in Table 6-1.

Table 6-1: Accuracy measurement of feature detection algorithm

	Point	x coordinate			z coordinate		
		Raw data (mm)	Final result (mm)	Error (μm)	Raw data (mm)	Final result (mm)	Error (μm)
I-groove	1	-1.711	-1.698	-13	59.21	59.28	-70
	2	-1.524	-1.511	-13	54.52	54.55	-30
	3	2.351	2.331	20	60.28	60.21	70
	4	3.524	3.541	-17	58.88	58.92	-40
	5	3.574	3.562	12	56.87	56.79	80
	6	0.875	0.888	-13	57.96	57.87	90
V-groove	1	-3.553	-3.512	-41	63.05	62.98	70
	2	1.74	1.739	1	59.71	59.72	-10
	3	-0.499	-0.4984	-0.6	60.18	60.21	-30
	4	3.893	3.896	-3	63.04	63.05	-10
	5	5.674	5.672	2	62.08	62.14	-60
	6	0.779	0.777	2	59.48	59.56	-80
U-groove	1	-3.715	-3.748	33	63.21	63.33	-120
	2	2.545	2.515	30	60.21	60.28	-70
	3	0.552	0.578	-26	58.95	58.71	240
	4	-2.664	-2.598	-66	60.25	60.38	-130
	5	-1.287	-1.278	-9	59.22	59.34	-120
	6	-4.314	-4.375	61	61.35	61.43	-80

The mean square error (MSE) calculated for each groove type in the respective x and z coordinates of the detected point is shown in Figure 6-25. As can be seen from the figure, the MSE is higher in the z-coordinate of an extracted point. It can also be noted

that the *V*-groove returns comparatively lower errors for these randomly selected data points whereas the *U*-groove produces larger errors in the point extraction. This can be attributed to the reduced data acquisition performance of the laser scanner when scanning vertical surfaces (Both *U* and *I* grooves have vertical surfaces where the steepness angle is high, which leads to a poorer performance of the laser scanner (Refer section 5.3.2.2) and consequently reduces the performance of the feature extraction algorithm). Comparatively the *V*-grooves do not have surfaces with high steepness angles and therefore return the lowest *MSE* values in both *x* and *z* co-ordinates.
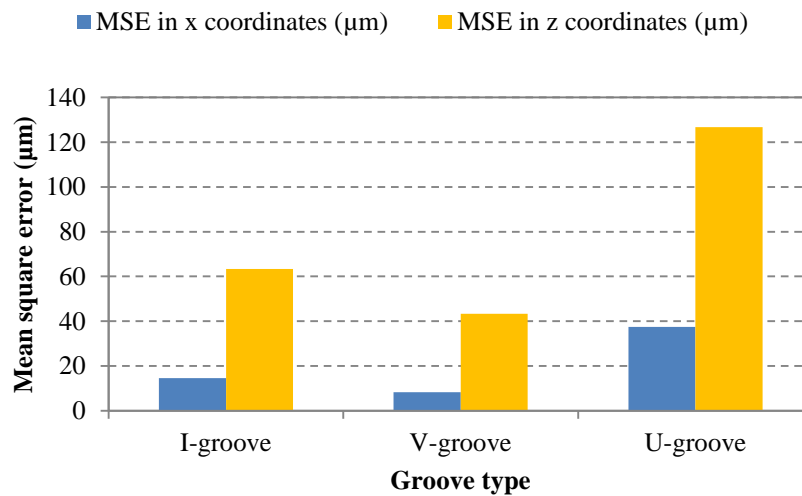
Figure 6-25: Mean square error in detected points for different groove types

6.6.3 Gap measurements and validation

The physical arrangement used to measure gaps is shown in Figure 6-26(a). Metric feeler gauge was in between the samples (in the gap) to set known gap. Then gap measurements was carried out using the developed algorithm which is graphed in Figure 6-26 (b) and (c). Due to the errors in processing the gap between the edges are detected with error in some points. However, as can be seen from the figure, points with errors were eliminated by fitting a line to the raw data.

To estimate the accuracy of the gap measurements, 14 known root gaps were set between the samples (between point *B* and *C*) using a metric feeler gauge in the range from 0.05mm to 1mm. The respective set root gap was then measured using the developed robotic scanning system (real-time gap measurement). The results can be seen in Figure 6-27. The gap measured between the top two edges (*w*) follows the same variation as the bottom gap. The actual horizontal distance between Point *A* and *B* (i.e. *(w-b)/2*) is 2.5mm. According to the results the average respective distance obtained

143

from the algorithm is 2.53mm which is again reassuring that a reliable detection of point *A* and *D* and the top-gap (*w*) measurements is being made. The average error in weld gap measurement is ±28μm. This result is acceptable because the laser scanner's lateral resolution is limited to ±20μm according to the manufacturer.
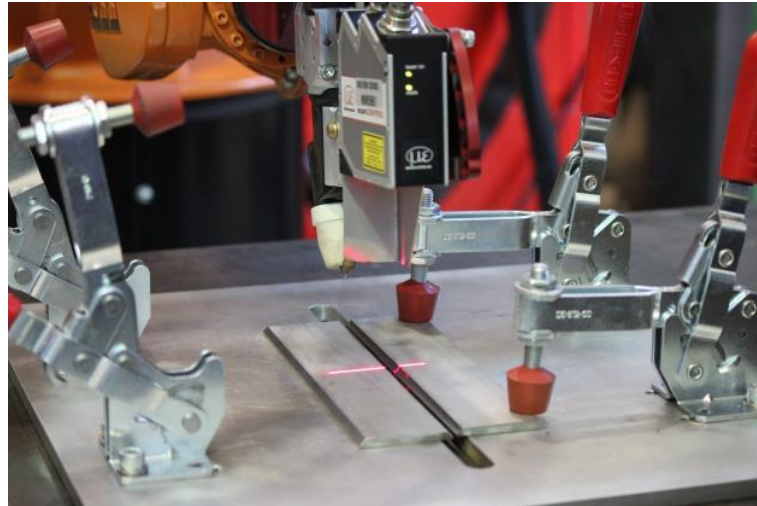
Figure 6.26(a)
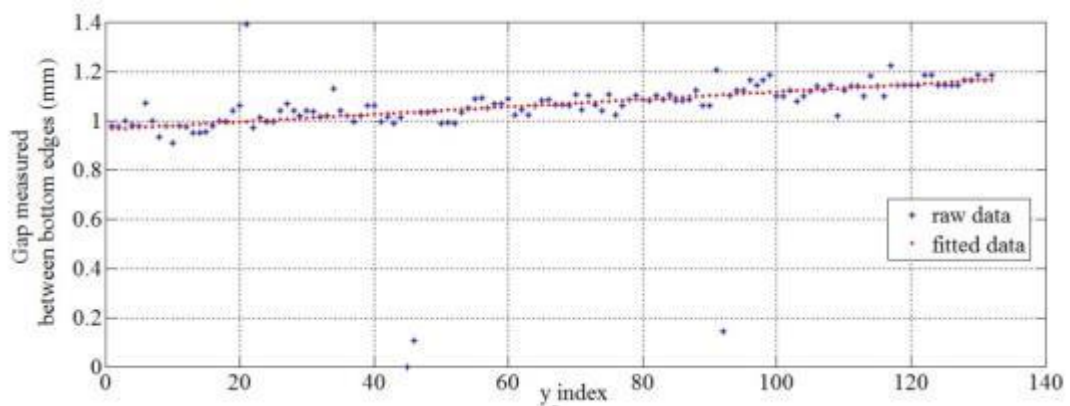
Figure 6.26(b)
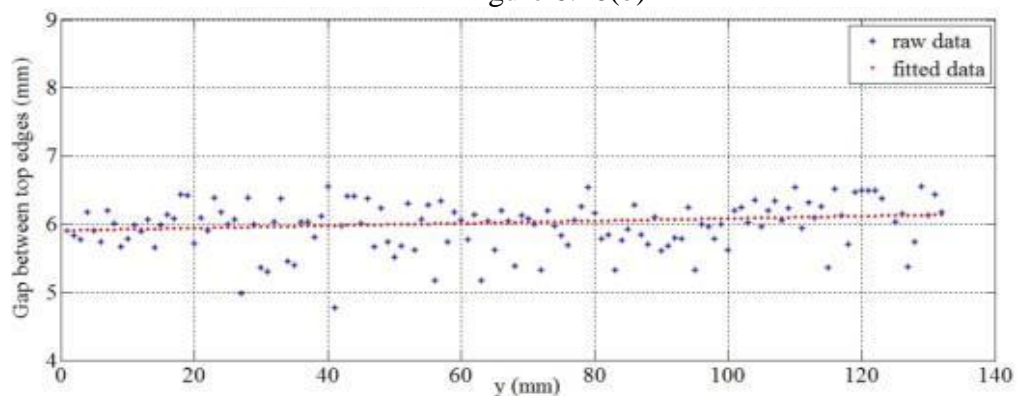
Figure 6.26(c)

Figure 6-26: Gap measurements (a) physical setup (b) gap measured between top edges, (c) gap measured between bottom edges (*b*)
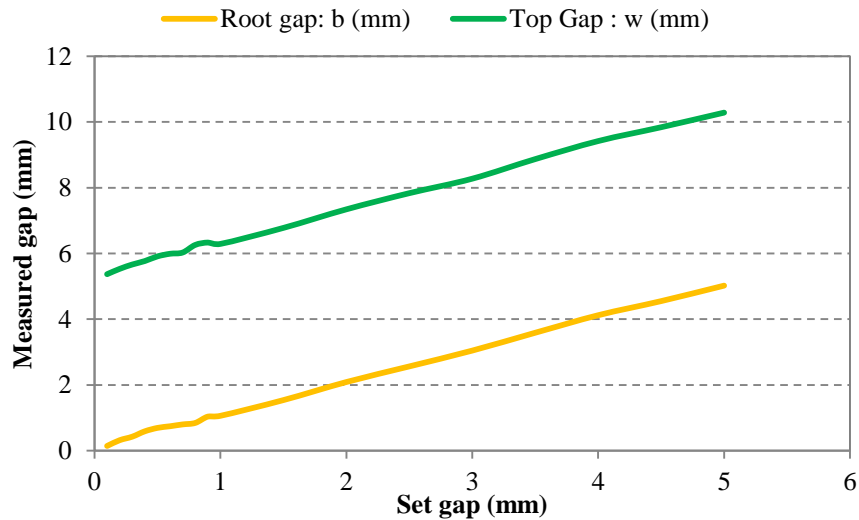
Figure 6-27: Gap measurements using feature detection algorithms

6.6.4 Validation of joint fit-up measurements

In order to assure the robustness of the algorithm, feature extraction has to be successful in all possible joint orientations. Therefore, known parameters for each orientation were set and the feature extraction algorithm was tested. Finally the results were compared against the set values to quantify the robustness. The following sections describe the results in detail.

Roll

The roll angle setup is shown in Figure 6-16. The scanning was carried out with the robot where the *3D* point cloud data is collected. After that, the feature extraction algorithm was used to extract the points. The point cloud data acquired for the roll orientation is shown in Figure 6-28. As can be seen from the figure, the features are extracted as expected. In order to quantify the accuracy of roll angle detection, known roll angles were set using different sizes of slip gauges and were measured using the algorithm. The absolute error in the roll angle measurements against different set roll angles is shown in Figure 6-29(a) and the respective percentage error is given in Figure 6-29(b). As noted from the figure the error increases when measuring larger roll angles. This is attributed to the fact that the feature detection algorithm does not function as expected at higher roll angles. However it is always expected that the machine operator can set up the samples with rolls angle below 3° which assures that the system measures the roll angle with 2% error which is acceptable for the welding process.
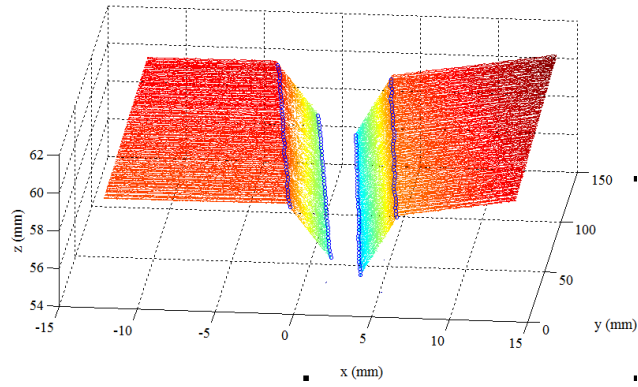
Figure 6-28: extracted points at roll orientation
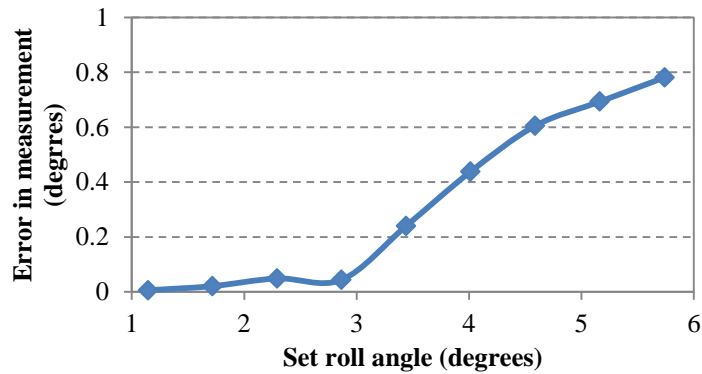
Figure 6.29(a)
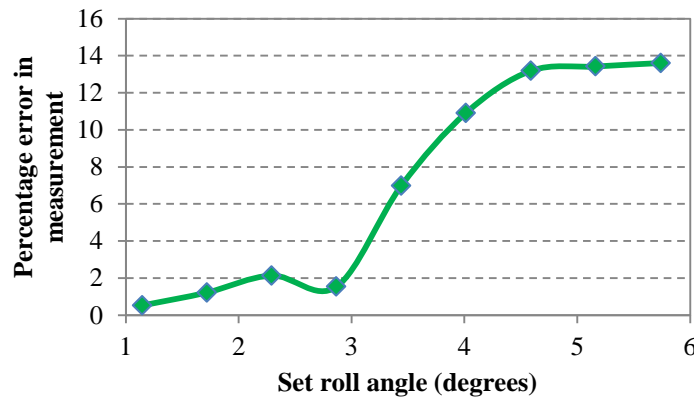
Figure 6.29(b)

Figure 6-29: Average roll angle measurement accuracy (a) absolute error, (b) percentage error

Pitch

The roll angle setup is shown in Figure 6-18. The point cloud data acquired for the pitch orientation is shown in Figure 6-30. As can be seen from the figure, the features are extracted as expected except for some deviation when detecting point *D*. The absolute error in the pitch angle measurements against different set roll angles is shown in Figure 6-31(a) and the respective percentage error is given in Figure 6-31(b). As noted from the figure the error increases when measuring larger pitch angles. This is attributed to

the fact that the feature detection algorithm does not function as expected at higher pitch angles. However it is always expected that the machine operator can set up the samples with pitch angles below 0.5º which assures that the system measures the pitch angle with a 3% error, which is acceptable for the welding process.
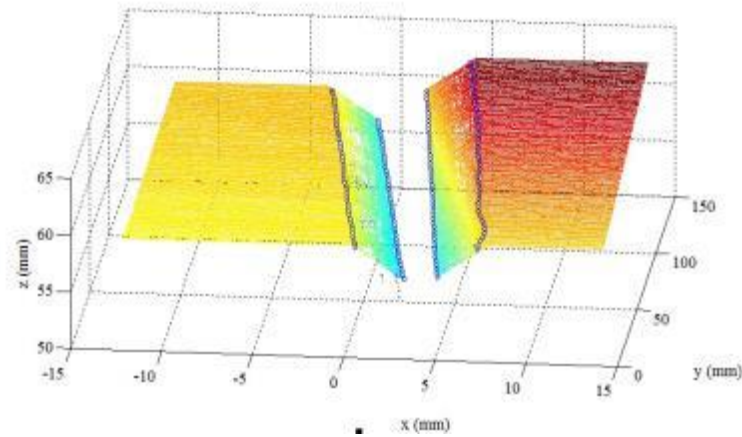
Figure 6-30: extracted points at pitch orientation
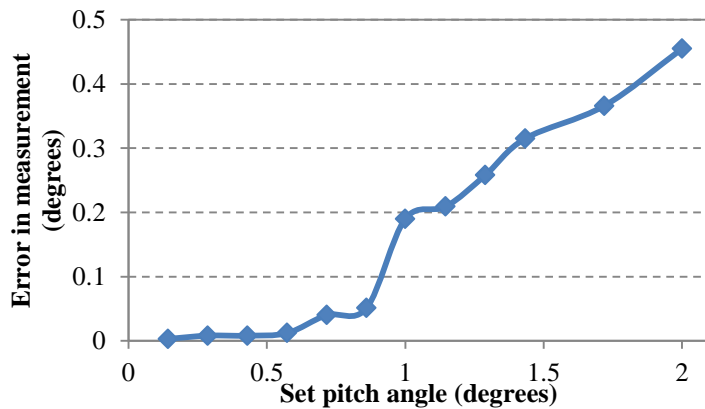
Figure 6.31(a)
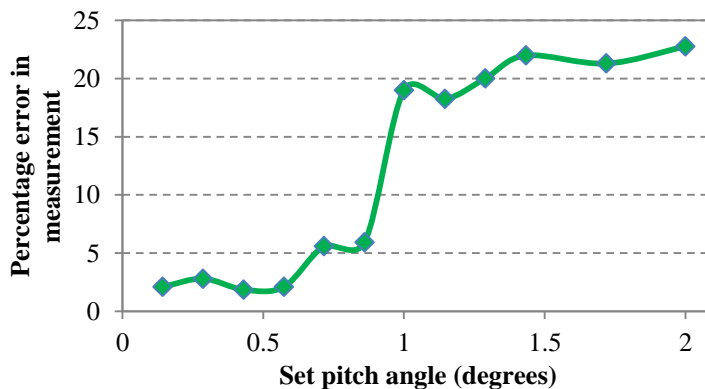
Figure 6.31(b)

Figure 6-31: Pitch angle measurement accuracy (a) absolute error, (b) percentage error

Yaw

The yaw angle setup is shown in Figure 6-20. The point cloud data acquired for the yaw orientation is shown in Figure 6-32. As can be seen from the figure, the features are extracted as expected except for some deviation in detecting point *D*. The absolute error in the pitch angle measurements against different set roll angles is shown in Figure 6-33(a) and the respective percentage error is given in Figure 6-33(b). As noted from the figure the error is lower when measuring lower yaw angles. This has been attributed to the fact that the feature detection algorithm does not function as expected when the parts are too close to each other (zero gap condition). However it is expected that a zero gap condition does not exist within an industrial weld setting, when considering this type of joint fit-up.
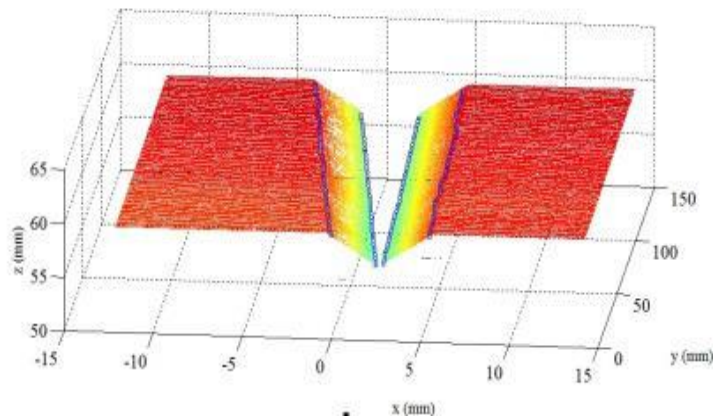
Figure 6-32: extracted points at yaw orientation
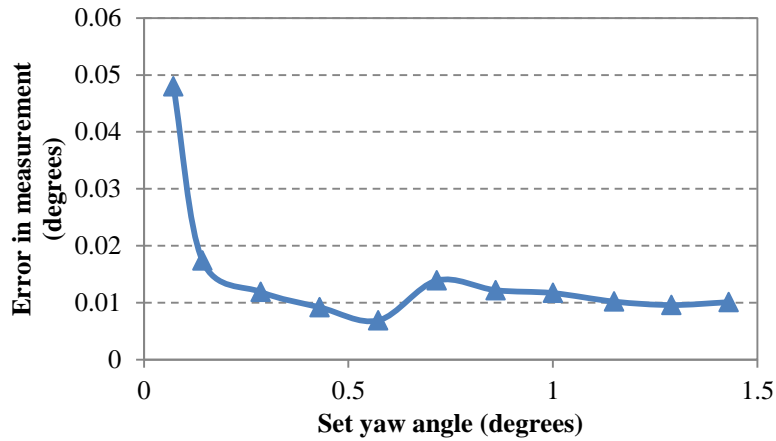
Figure 6.33(a)
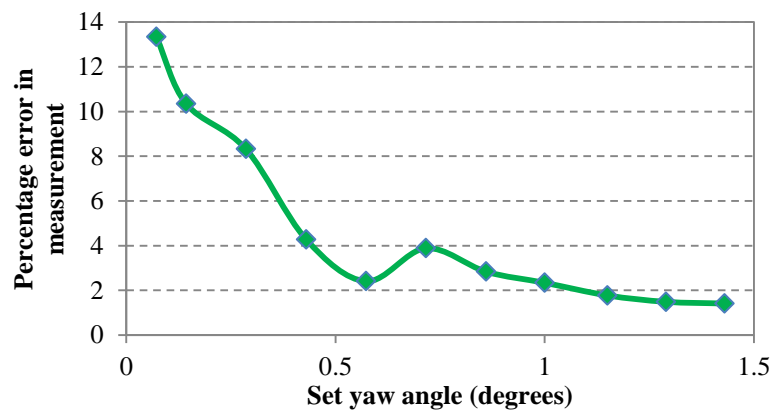
Figure 6.33(b)

Figure 6-33: yaw angle measurement accuracy (a) absolute error, (b) percentage error

Vertical Offset

The vertical offset setup is shown in Figure 6-22 and the resulting point cloud data is shown in Figure 6-34. As can be seen from the figure, the features are extracted as expected except some deviation in detecting point *D*. The absolute error in vertical offset measurements against the different set values is shown in Figure 6-35(a) and the respective percentage value is shown in Figure 6-35(b). As noted from the figure, the error is lower when measuring lower offsets. This suggests that the feature detection algorithm does not function as expected when the parts are too far from each other vertically. However it is expected that an offset not more than 1-2mm can exist in an industrial weld setting where the percentage error in detection is less than 1.5%.
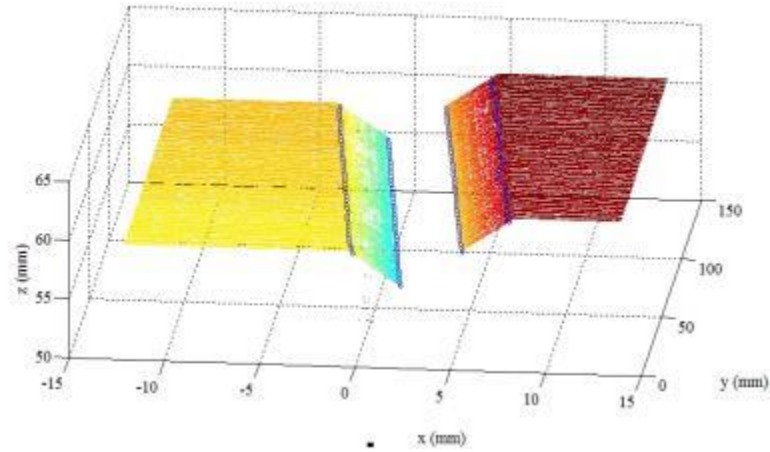
Figure 6-34: extracted points at vertical offset orientation
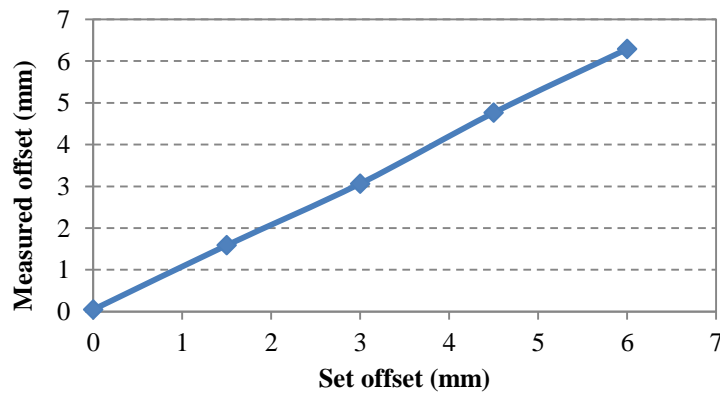
Figure 6.35(a)
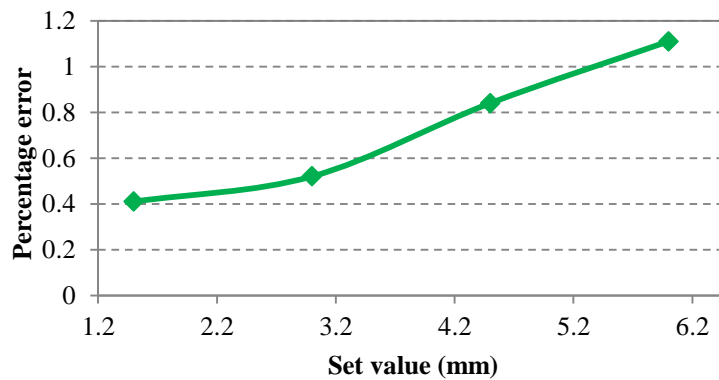
Figure 6.35(b)

Figure 6-35: vertical offset measurement accuracy (a) absolute error, (b) percentage error

In order to satisfy the robustness of the algorithm, the previously described orientations were tested for *I* and *U* joints, with the results obtained shown in Figure 6-36. As can be noted from the figures, the feature extraction algorithm functions as expected in the point detection for all possible orientations of the *I* and *U* grooves. However, it is also noted that the detection of points *A* and *D* in the *U*-groove case has some deviation.

Therefore, it is more robust to use the coordinates of Point *B* and *C* for calculating the middle point which is used for seam tracking (as discussed in Chapter 7).

	I-groove	U-groove
Roll		
Pitch		
Yaw		
Vertical offset		
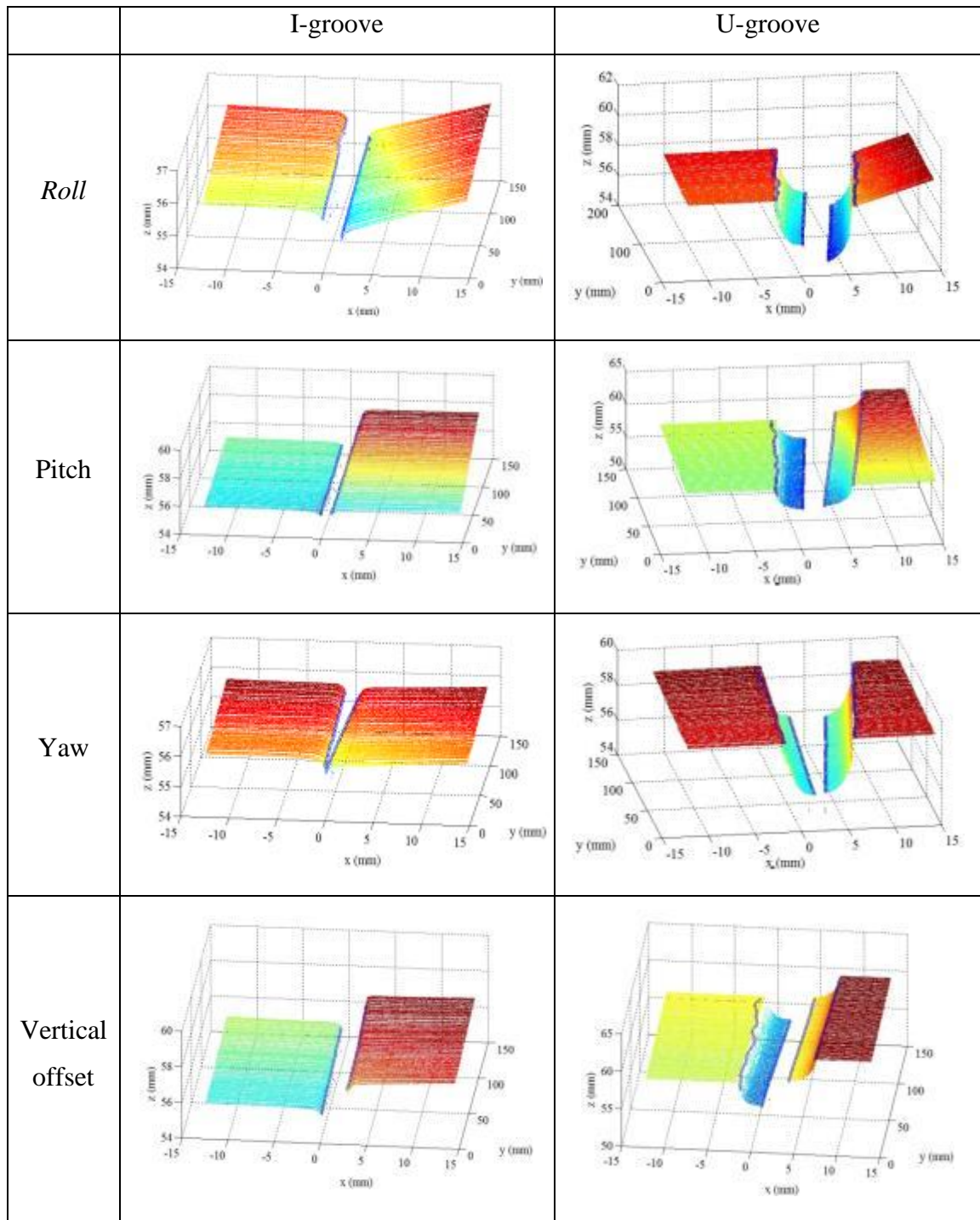
Figure 6-36: Feature extraction in I and U grooves at various joint fit-ups

In the results it is clear that the feature detection algorithm does not work for larger angles. This is because when the larger angles are measured, the points to be extracted moves closer to the outer borders of the laser scanner span. This creates inaccuracies in

feature detection. However, this due to the small laser span and if a laser scanner with larger span is used this can be overcome.

6.7   Summary

This chapter presents a novel algorithm for feature detection of a weld groove with a maximum *MSE* of 38µm and 127µm in the *x* and *z* coordinates respectively. The feature detection algorithm was successfully implemented on the most commonly used weld joint types (*I*, *V* and *U*). The real-time gap measurement algorithm was also able to measure gaps with an accuracy of ±28µm.

Approximation methods were used to remove outliers from noisy data present in the obtained point clouds. Weld joint fit-up in *3D* was quantified and the algorithm developed was robust enough to extract features accurately at all possible joint set ups for all selected joint types.

The algorithm can be effectively used for adaptive weld process control, accurate seam tracking and intelligent decision making for process control which is discussed in the next three chapters.

7 Seam tracking and Robotic Welding

The positioning accuracy of the welding arc with respect to the joint mainly depends on the robot path accuracy and the work piece geometry. In Chapter 5 it was proven that the feature extraction algorithm was successfully able to recognise the most frequently used joint types at all possible fit-up configurations. This chapter presents the work carried out in establishing accurate robot path planning for *3D* seam tracking. This chapter also presents a detailed description of the algorithms and methodology used for *3D* seam tracking.

Work presented in this chapter also includes the initial work carried out in *2D* path tracking using a compact *CMOS* camera. The methodology used for the hand-eye calibration is also discussed. Results obtained during seam tracking and robotic welding is also discussed in this chapter. Despite the complexity of the path being recognised, both the overall accuracy and success rate of the system are close to 95%. The developed system was successfully used for three dimensional seam tracking, and demonstrates an accuracy of ±0.5mm at a tracking a speed of 2mm/s. It proved to be simple, reliable and resulted in a satisfactory accuracy being obtained and allows for automatic tracking of *3D* paths.

7.1 Introduction

Seam tracking using vision sensors has been a widely discussed topic over recent years. Welding, spray painting and sealant application have been the leading applications of seam tracking technologies. Basically the seam tracker governs the location of the weld joint and interconnects with the robot control system to track the joint. A good seam tracker should not only consider positional accuracy, but should also be able to orient the welding torch in such a way that the welding quality is maximized. In addition, the seam tracker should be compact so that it can perform seam tracking on complex weld shapes in narrow spaces. It should also be rigid enough to withstand extreme conditions during welding.

Over the years *2D* and *3D* methods have been used with industrial robots to achieve path tracking. *3D* vision sensors are mostly used to track *3D* complex paths whereas *2D*

vision sensors are used to follow simple *2D* paths. *3D* methods easily improve upon the capability of *2D* methods due to the increased capabilities such as the ability to measure *3D* shapes, increased accuracy, robustness, compact size, rugged build, easiness for system integration and reliability. Although it has been found that *3D* laser scanners are the most suitable sensor for this research, initial work was carried out to understand the performance of a *2D* camera for a simple path tracking application.

As presented in Chapter 2, the work carried out in seam tracking can be categorized in to three generations. It is understood that for an assembly line or a continuous production system the third generation solution (real-time seam tracking and welding) is most feasible [15]. However, in aerospace applications most welding is carried out as a job shop production system. Part variety and variability is comparatively higher than in a standard assembly line. Additionally, the required welding quality is also significantly higher. If welding was performed on an erroneously set up joint by the manual operator, the whole part could end up being wasted. This includes a significant amount of cost (due to expensive material, skilled labour, energy, time). Therefore intelligent decision making is essential prior to performing any robotic welding in aerospace applications. In this research the two-pass approach was selected, where the robot surveys the seam along a pre-taught path and makes the decisions before performing welding. In the second pass, welding is performed along the path points generated during the first pass. The main issue in the two pass method is the time taken for pre-surveying. Another drawback is the incapability of the system adapting to the thermal distortions created during welding. However, in this work the main interest is to carry out welding with proper fixtures which involve only a small amount of distortion (the majority of distortion occurs after welding due to thermal stress build up and fixtures). Good quality fixtures used in the aerospace industry help to assure a low amount of distortion during welding. It should be noted that the designed system also could perform surveying and welding in real-time (single pass). However, the core work in this thesis is based on the two pass approach as discussed before.

Section 7.3 presents a hand-eye calibration methodology used for the seam tracking task. The work carried out as part of establishing the seam tracking control methodology between the PC and the robot are also presented within this section. It involves real-time tracking using a *2D* camera (Single pass approach). Section 7.4 presents the two-pass approach carried out for *3D* seam tracking and welding.

7.2   Coordinate system transformation

Normally the transformation matrix (4×4) between two co-ordinate systems can be represented by a rotational component and a translational component. For example, consider point *A* and *B* as two points in 3D space. The relationship between then in 3D can be represented as given in equation 7.1 and 7.2.

$$\begin{pmatrix} x_A \\ x_A \\ x_A \\ 1 \end{pmatrix} = H_B^A \cdot \begin{pmatrix} x_B \\ x_B \\ x_B \\ 1 \end{pmatrix} \tag{7.1}$$

$$H_B^A = \begin{bmatrix} R_B^A & T_B^A \\ 0 & 1 \end{bmatrix} \tag{7.2}$$

In this expression, *R* is the rotational component matrix with a size of 3×3 and *T* is the translational component matrix with the size of 3×3. This has been used for all the transformations between coordinate frames identified in the work presented in this chapter. Figure 7-1 shows the important coordinate systems identified in the robotic welding system.
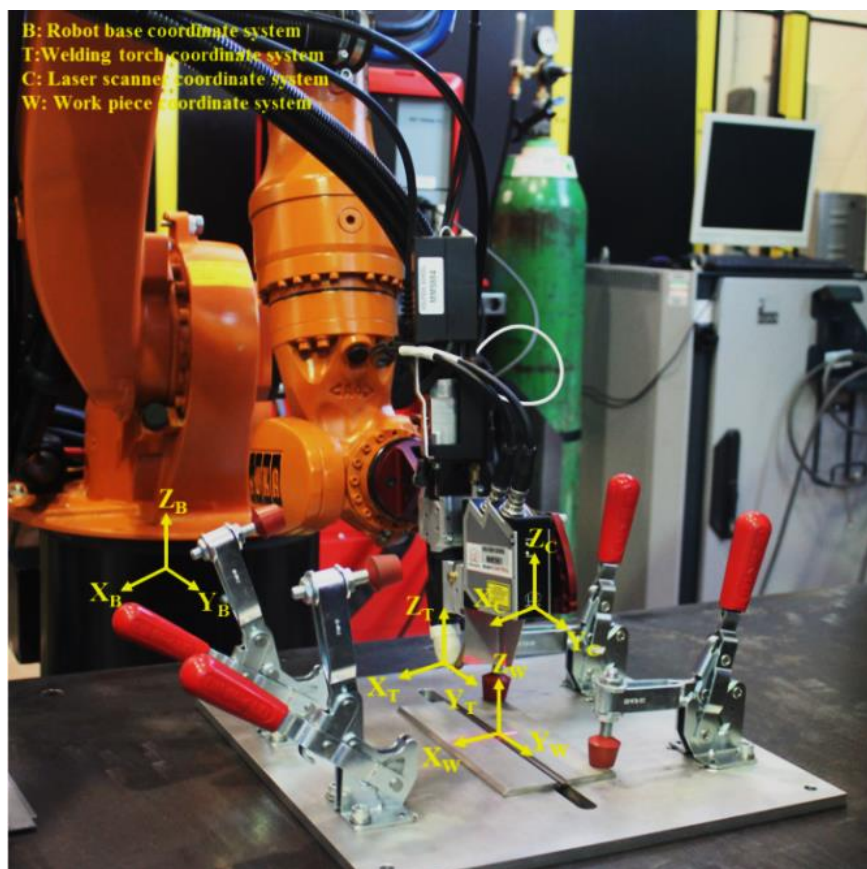
Figure 7-1: Coordinate systems in the robotic welding system

In order to move the robot to perform *3D* seam tracking, it is important to transform the coordinates of a point (for example the middle point of the weld groove) from the laser scanner data in to the robot base co-ordinate frame. This can be represented by equation 7.3 where P_B and P_C are the origins of the base co-ordinate frame and laser scanner coordinate frame respectively.

$$P_B = H_B^E . H_E^C . P_C \qquad (7.3)$$

H_B^E : Homogenous 4×4 transformation matrix from the wrist frame (E) with respect to the robot frame.

H_E^C : Homogenous 4×4 transformation matrix from the laser scanner frame with respect to the wrist frame.

The *3D* hand-eye calibration was carried out by measuring the offsets (between each axis) between each coordinate frames and finding out the rotations (between coordinate frames). All rotation elements were established by using the "right hand rule" and the results are tabulated in Table 7-1.

Table 7-1: Coordinate system transformation values

Transformation	T_x	T_y	T_z	R_x	R_y	R_z
H_B^E	Obtained from the robot (variable throughout the process): x, y, z			-90	0	-90
H_E^C	ΔX	ΔY	ΔZ	-90	0	0

ΔX, ΔY and ΔZ are physically measured distances from the wrist centre to the laser scanner coordinate frame. x, y, and z are robot positions, directly read from the robot.

According to the values in Table 7-1, the following two matrices were obtained.

$$H_E^C = \begin{bmatrix} 1 & 0 & 0 & \Delta X \\ 0 & 0 & 1 & \Delta Y \\ 0 & -1 & 0 & \Delta Z \\ 0 & 0 & 0 & 1 \end{bmatrix}$$

$$H_B^E = \begin{bmatrix} 1 & 1 & 0 & x \\ 0 & 0 & 1 & y \\ 0 & -1 & 0 & z \\ 0 & 0 & 0 & 1 \end{bmatrix}$$

Multiplication of these two matrices (according to equation 7.3) returns the total transformation (*H*) from the laser scanner to the robot base frame. This result can be used to determine any point found (using feature extraction algorithm) from the laser scanner data with reference to the robot frame.

$$H = \begin{bmatrix} 1 & 1 & 0 & x + \Delta X \\ 0 & -1 & 0 & y + \Delta Z \\ 0 & 0 & -1 & z - \Delta Y \\ 0 & 0 & 0 & 1 \end{bmatrix}$$

7.3 2D seam tracking

The experimental setup for the *2D* tracking work, which includes a *2D* industrial camera and the KUKA KR16 robot, is shown in Figure 7-2. It illustrates the main coordinate frames associated with the robot, work piece and the camera. The camera and the robot were connected to the PC according to the method described in Chapter 3. Software development was carried out using LabVIEW and its vision acquisition software package.
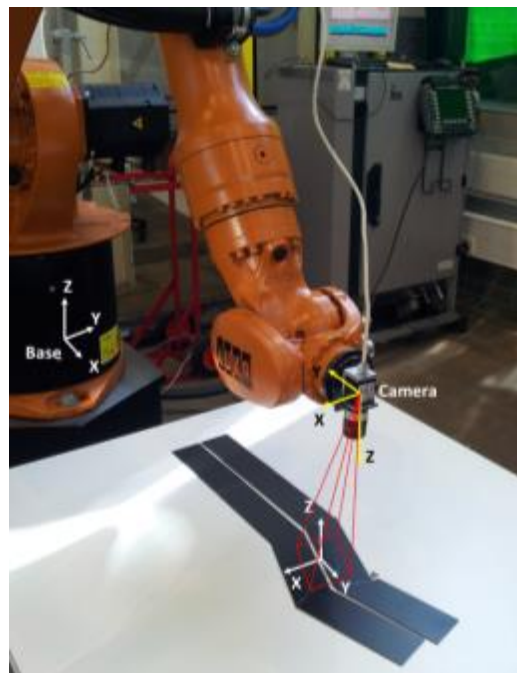
Figure 7-2: *2D* seam tracking setup

The sequence of operations performed for *2D* robotic seam tracking is presented in Figure 7-3. Initially, the robot is moved to its home position where the path tracking is started. At the home position, the camera is triggered and an image is captured. Image processing is carried out (50ms cycle time) to find the position of the centre of the gap which is then issued as the next position (advancement in the *x*-coordinate of the robot)

157

of the robot. The step advancement in *y*-coordinate is the look-ahead distance of the camera which is measured to be 46mm. This sequence is repeated so that the robot is continuously tracking the path until it reaches a pre-determined stop position specified by the user.

```
                          ┌─────────────┐
                          │    Start    │
                          └─────────────┘
                                 │
                    ┌────────────────────────────┐
                    │ Robot move to the home position │
                    └────────────────────────────┘
                                 │
                    ┌────────────────────────────┐
                    │       Capture image        │◄───────┐
                    └────────────────────────────┘        │
                                 │                         │
                    ┌────────────────────────────────┐    │
                    │ Find the edge start point and the end point │
                    └────────────────────────────────┘    │
                                 │                         │
                    ┌────────────────────────────┐        │
                    │ Find middle point of the edge │◄──┐  │
                    └────────────────────────────┘    │  │
                                 │                     │  │
                           ◇ Point found? ◇───No───────┘  │
                                 │                         │
                                Yes                        │
                    ┌────────────────────────────┐         │
                    │ Robot move to the found coordinates │ │
                    └────────────────────────────┘         │
                                 │                          │
                          ◇ Robot stopped? ◇────No──────────┘
                                 │
                                Yes
                          ┌─────────────┐
                          │    Stop     │
                          └─────────────┘
```
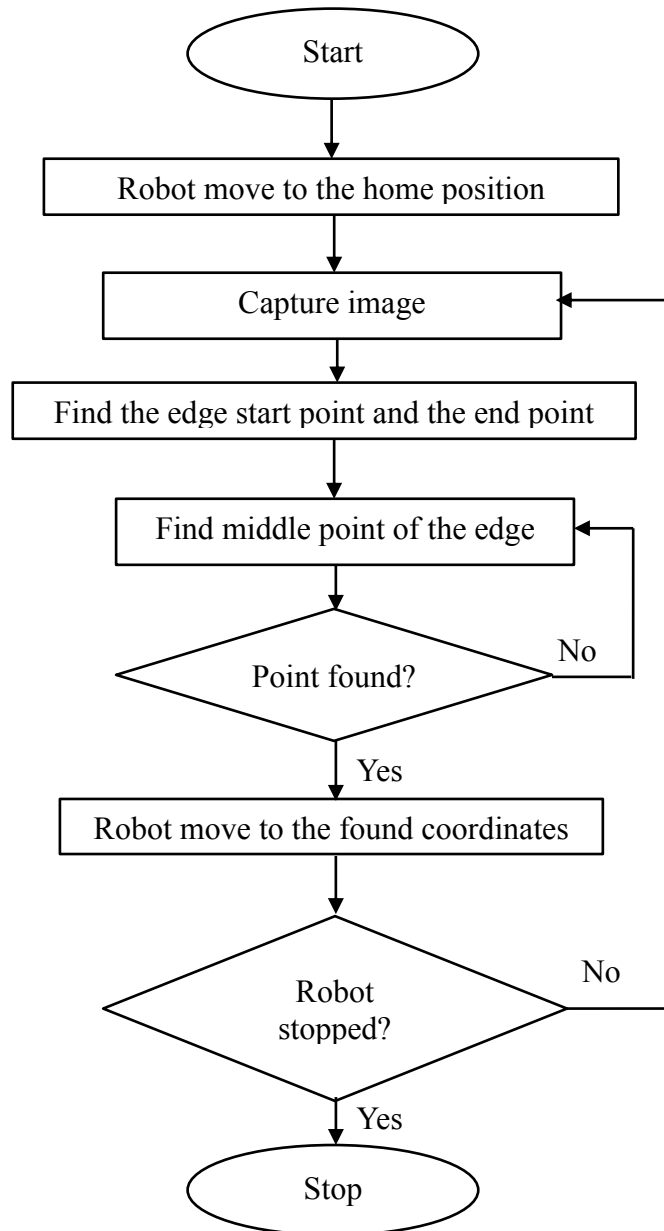
Figure 7-3: *2D* seam tracking sequence

The seam edge detection methodology within the image processing algorithm is shown in Figure 7-4 (a). Initially, the raw image was converted to greyscale which was then followed by thresholding to distinctively separate background from the foreground features. Particle filtering was then carried out which removes all the noise in the image

158

and finally edge detection was carried out which results in Figure 7-4 (b). The middle point calculated between point 1 and 2 was used as the x-coordinate of the next point.
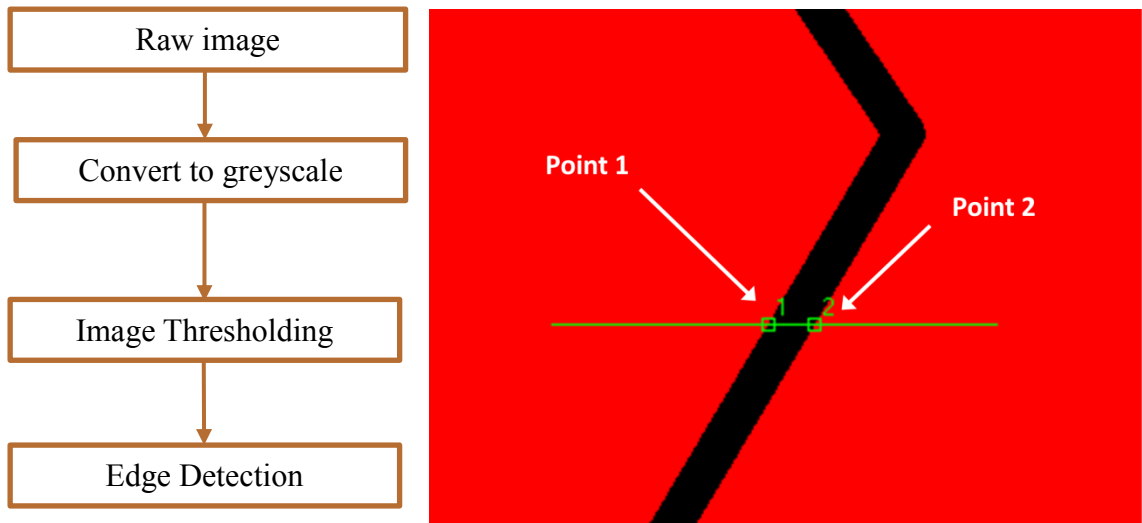
Figure 7.4(a)   Figure 7.4(b)

Figure 7-4: *2D* **image processing for seam tracking (a) image processing sequence, (b) detected edges**

Experimentation

Experiments were then carried out to verify the performance of the system which is described in this section.

7.3.1   Seam tracking accuracy

Figure 7-5 shows the seam tracking results of the sample shown in Figure 7-2.
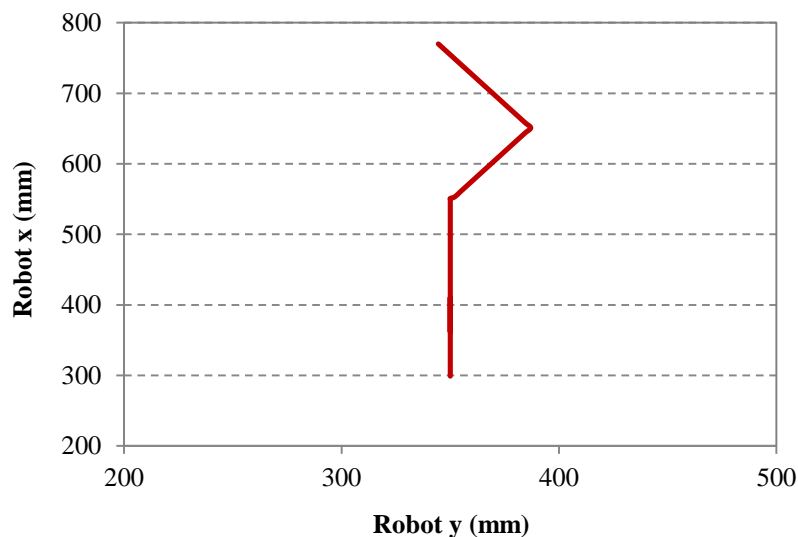
Figure 7-5: *2D* **seam tracking results**

As can be seen from the figure the path has been tracked as expected. The accuracy of the positioning was checked by comparing 10 known points (coordinates) of the

159

arrangement with the respective coordinates of the tracked points. The results obtained are graphed in Figure 7-6 which shows that the accuracy of the tracking process is not as expected for a path tracking application. As can be seen that the error is more than 1mm which not acceptable for a seam tracking application.
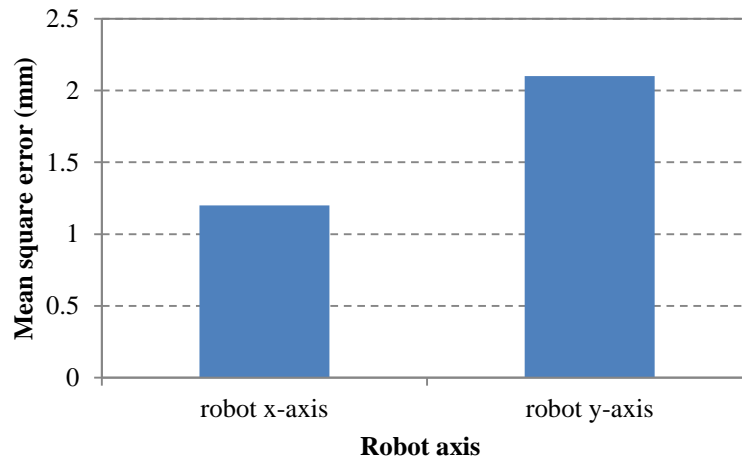
Figure 7-6: Mean square error in *x-y* coordinates in *2D* seam tracking

7.3.2 Gap sensing accuracy

In order to find the gap sensing accuracy, a test sample was created as shown in Figure 7-7 with various known gaps.

Figure 7-7: Setup for checking gap sensing performance

The software was then used with the robot to determine the gap in real-time. The results obtained for absolute measurement error shown in Figure 7-8(a) and its respective

percentage values are shown in Figure 7-8(b). As seen from the figure, the error in measurements is higher when sensing smaller gaps, and as the gap increases the percentage error is reduced.
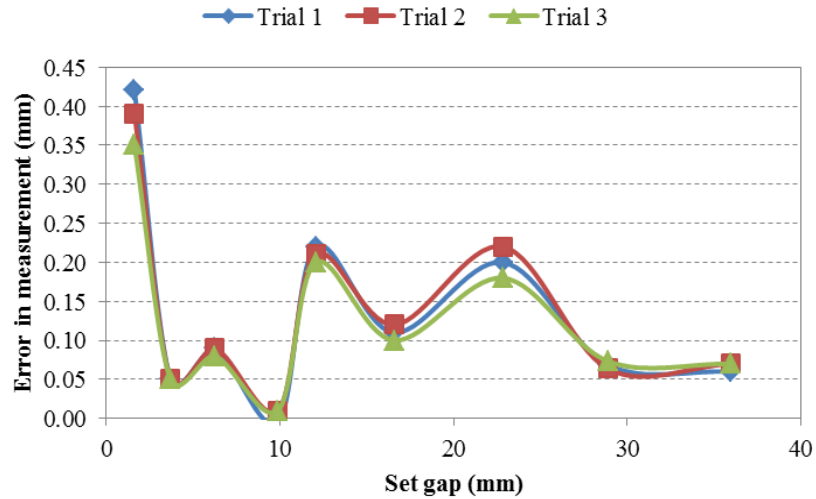
Figure 7.8(a)
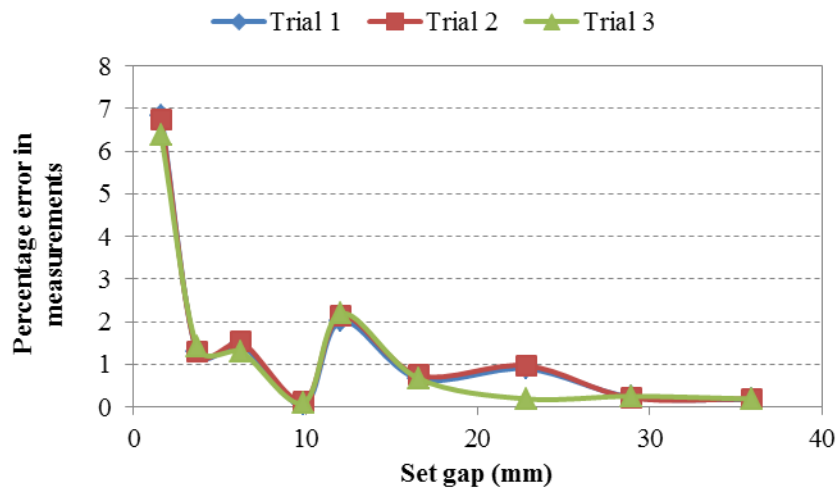
Figure 7.8(b)

Figure 7-8: Results of *2D* gap sensing

These results show that *2D* seam tracking and gap sensing does not provide adequate accuracy for path tracking applications. It was also observed that the edge detection process is affected by ambient lighting conditions and that *2D* methods are incapable of obtaining the third dimension of an object (which is the height information: along the *z*-axis). However, *2D* methods can be useful for tracking simple *2D* paths in applications where the accuracy required is not significantly high.

7.4   3D seam tracking

In the seam tracking process, the path planning has to be performed in *3D* where the Cartesian coordinates of a particular path is to be determined and provided to the robot. Therefore, any point extracted from the laser scanner point cloud data should be transformed to the robot base coordinate frame using the transformation presented in section 7.2. The detailed description of the seam tracking methodology and equations used are presented in this section.

As explained in section 7.1, seam tracking for welding is realized through the two-pass approach. As can be seen in Figure 7-9, initially the robot moved along a nominal path which is denoted as the scan pass (It should be noted that this path can be determined by the user or can be extracted from a CAD file). For each step movement (robot scan step) the algorithm finds the offset in x and z, which are denoted by Δx_j and Δz_j. During the welding-pass, the algorithm is used to calculate the new points by using the offsets calculated during the scanning-pass. The methodology of calculating offsets in the *x-y* plane is shown in Figure 7-9. Similarly, offsets in the *y-z* plane are also calculated.
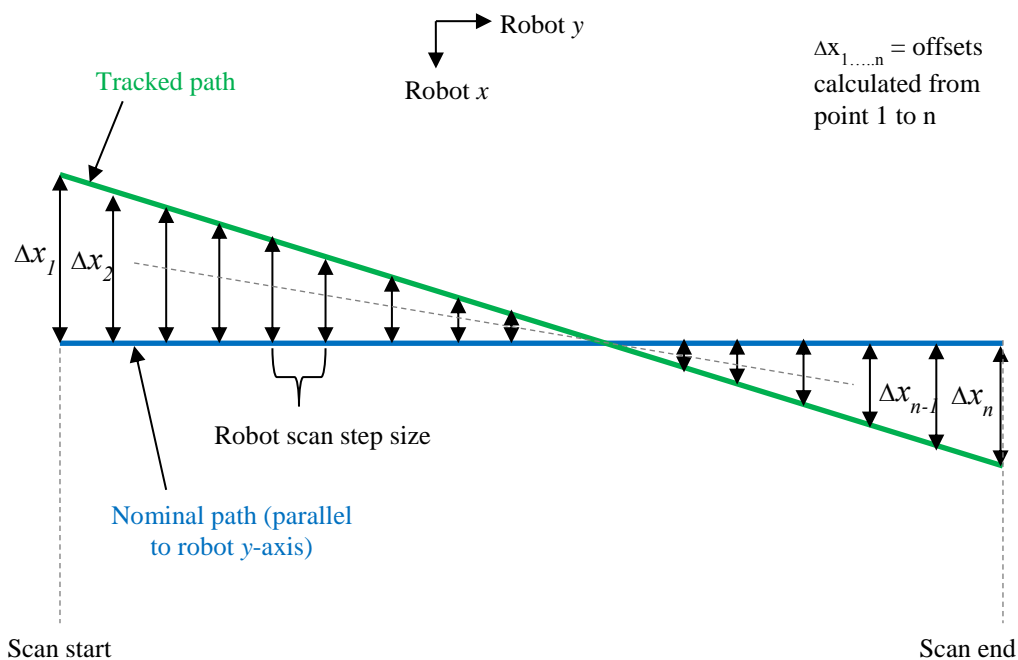
Figure 7-9: Seam tracking methodology in *x*-axis

Figure 7-10 shows the method of measuring the offsets in the *x* and *z* axes respectively. Let point $P(x_j, y_j, z_j)$ be the point to be tracked in the welding run. The coordinates of *P* can then be calculated using equations 7.4-7.6.

$$x_j = x_{j-1} + \Delta x_j \qquad (7.4)$$

$$y_j = y_{j-1} + \Delta y \qquad (7.5)$$

$$z_j = z_{j-1} + \Delta z_j \qquad (7.6)$$

where x_j and z_j are the x and z coordinates of the middle point found of the jth cross sectional profile of the joint. Δy is the robot scan step which is 1mm. Δx and Δz are respective offsets in x and z axis between point P_j and P_{j-1}.
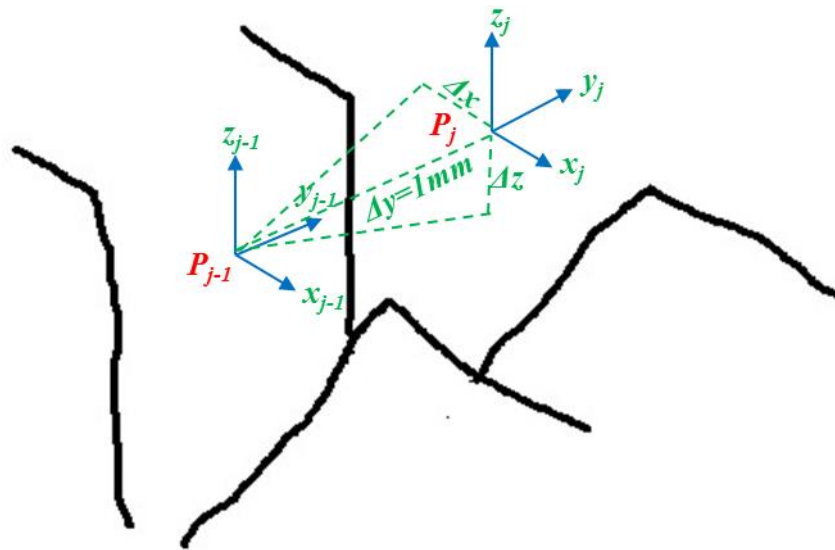
Figure 7-10: Diagram showing the point used for seam tracking

The software sequence of seam tracking is shown in Figure 7-11. During the scanning pass, the robot is advanced by the robot scan step size (for the work presented here, it is 1mm). For each 1mm step, the laser scanner extracts features (from the algorithm presented in Chapter 6) and stores the points in array variables. This array of coordinates is then used to guide the welding torch in the second-pass (tracking/welding pass).
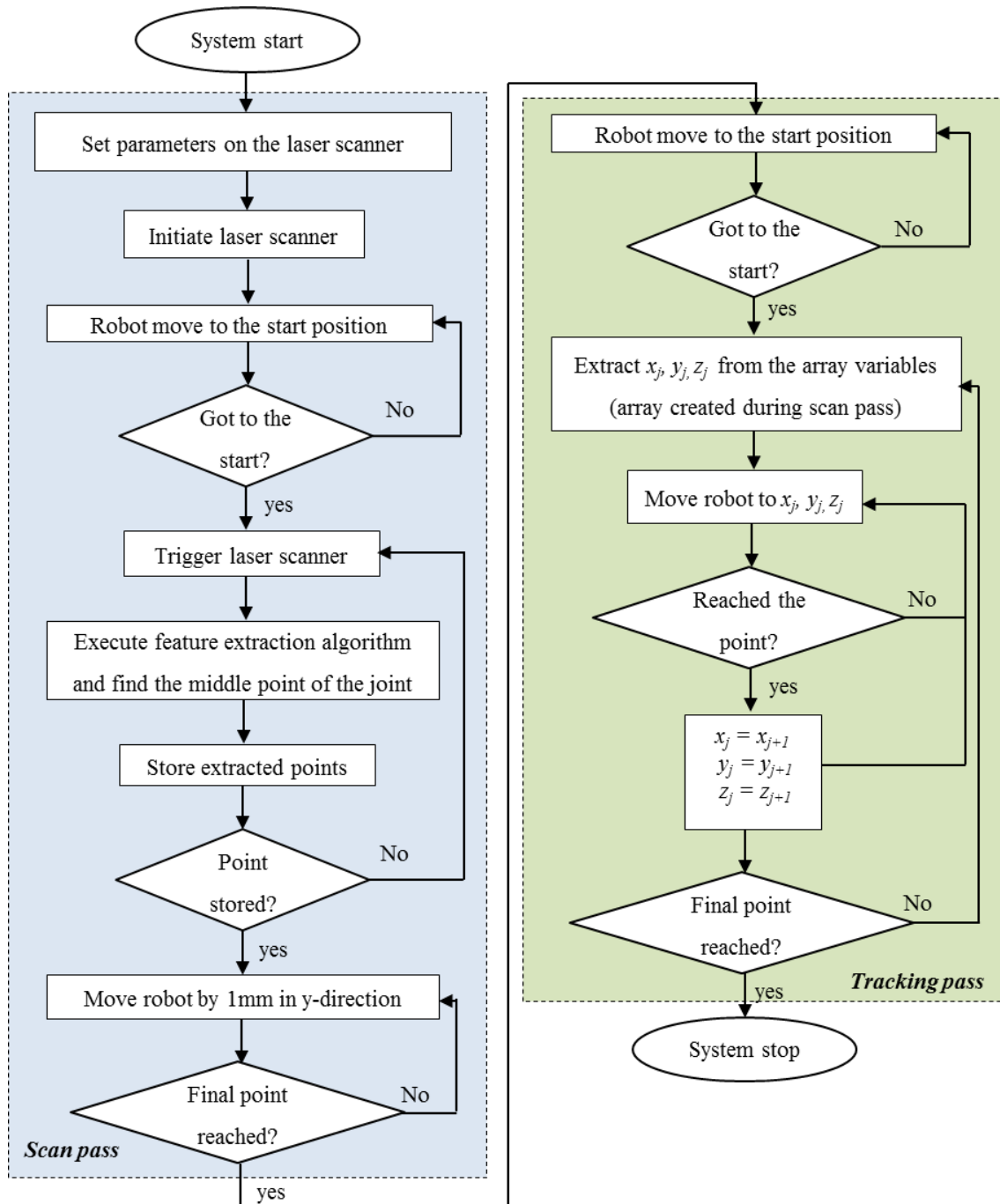
Figure 7-11: Software operating sequence for *3D* seam tracking

It should be noted that the look-ahead distance (the length between the laser line and the welding torch *TCP*) of the laser scanner is added to the *y*-coordinates during the welding pass. The look-ahead distance of the laser scanner is shown in Figure 7-12 and measured to be 70mm.
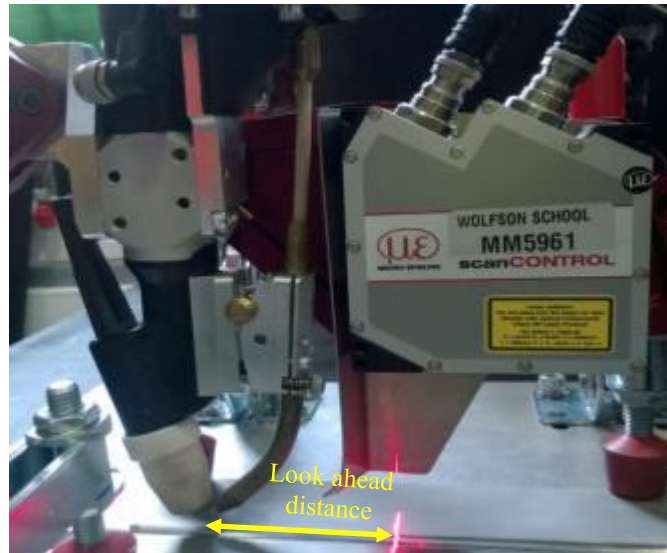
Figure 7-12: Look-ahead distance

It was mentioned in Chapter 6 that the middle point (x_{mid}, z_{mid}) found using the feature extraction algorithm is used as a reference to guide the welding torch. However, in order for the weld to be established completely in to the weld groove, the torch has to be held in such a way that it is slightly higher than the middle point (x_{mid}, z_{mid}). From the manual welding experiments carried out in Chapter 4 it was understood that the torch stand-off distance should be maintained around 3-5mm for better quality. Therefore, it was ensured that the torch tip was maintained at 3mm above the work piece as shown in Figure 7-13. This method assures that welding arc is striking all parts of the joint.
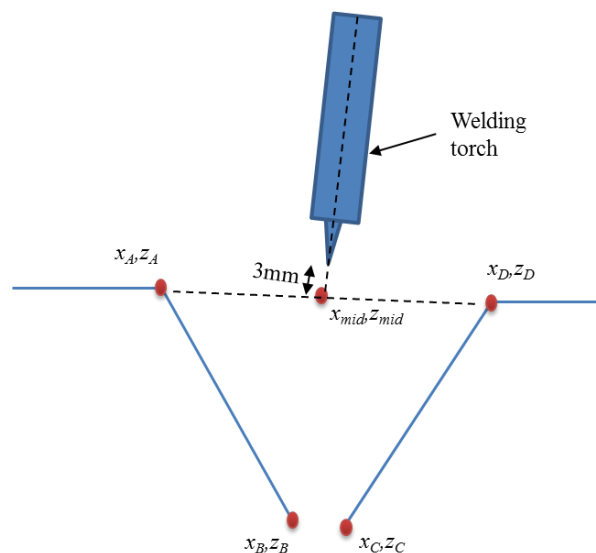
Figure 7-13: Torch placement during seam tracking for robotic welding

In Chapter 6, it was also discussed that part fit-up plays a significant part in the weld quality. It was found, however, that it has only a minor effect on the feature extraction

165

algorithm. Although the robustness of the feature extraction algorithm is proven, the seam tracking performance under all joint types and fit-up configurations has to be established. Also seam tracking performance in *3D* has to be established to realize the validity of the system. Therefore a series of experiments were carried out which are explained in the following sections.

7.4.1   Seam tracking of various joint profiles

The identified points for seam tracking (in dark blue) are graphed on the raw point cloud data for the three different joint types and are shown in Figure 7-14. As can be seen from the figure, the robotic seam tracking system has performed successfully in guiding the welding torch along the joint. In addition, the algorithm has effectively carried out seam tracking irrespective of the weld joint type. In Figure 7-14 (c), it can be seen that there are missing data points within the U-groove. However, it can be understood from the results that the seam tracking algorithm was not affected by those missing data points. This shows that seam tracking can be performed successfully even on shiny components, similar to the expected to be found in industry (especially in the aerospace and automobile industries) which could produce more missing data points.
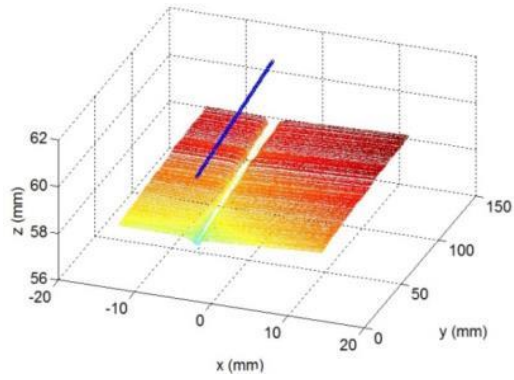
Figure 7.14(a)
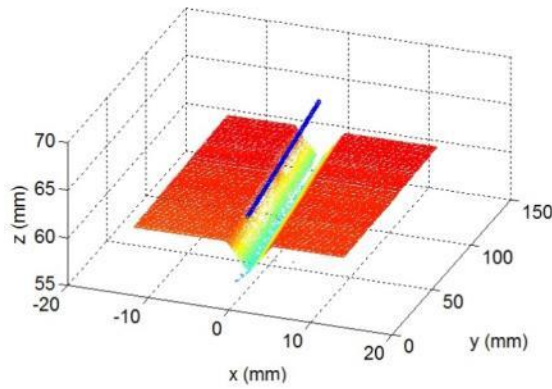
Figure 7.14(b)
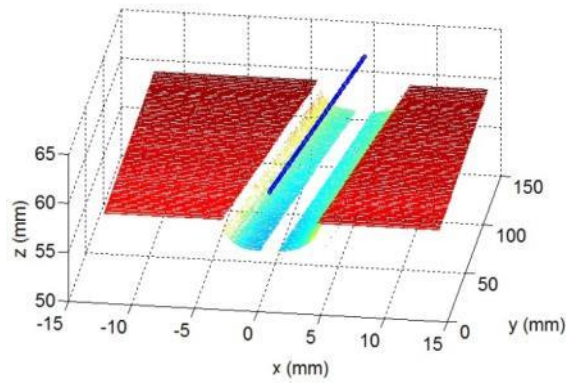
Figure 7.14(c)

Figure 7-14: Points used for guiding the welding torch (a) I-groove, (b) V-groove, (c) U-groove

7.4.2   Seam tracking under various joint fit-ups

As discussed before, seam tracking performance was also tested at all possible joint fit-up configurations that could be present in a welding set-up. The results of the tracked path (in dark blue) are shown on the raw point cloud data in Figure 7-15.
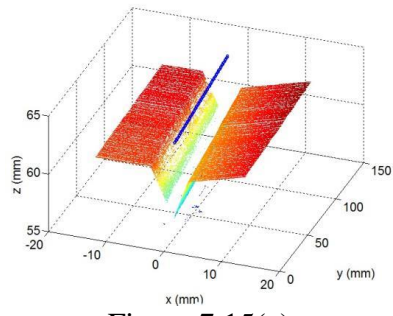
Figure 7.15(a)
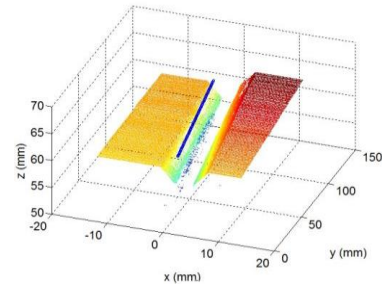
Figure 7.15(b)
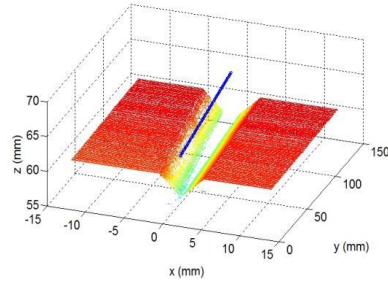
Figure 7.15(c)
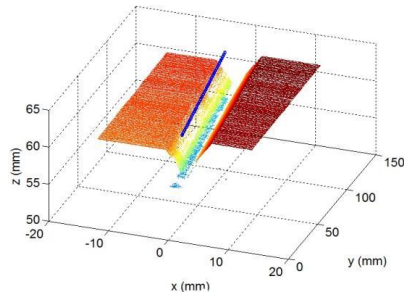
Figure 7.15(d)
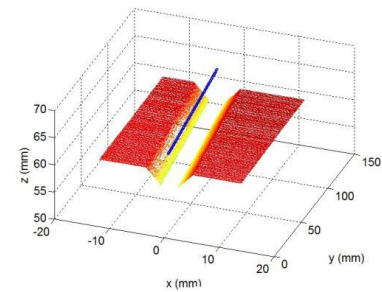
Figure 7.15(e)

Figure 7-15: Seam tracking performed at various joint fit-ups (a) roll, (b) pitch, (c) yaw, (d) vertical offset, (e) horizontal offset

168

As can be seen from Figure 7-15(a)-(e), the seam tracking has been performed successfully for all possible *3D* joint fit-up configurations. This shows that the developed seam tracking algorithm could carry out *3D* seam tracking irrespective of the joint fit-up.

To investigate this further, seam tracking was carried out on each joint configuration by setting up known values for each joint fit-up configuration. For example, known pitch angles were set using slip gauges. Similarly all the other fit-ups were tested for seam tracking performance by setting known values.

The seam tracking performance obtained when one of the samples was moved horizontally and\or vertically by a known distance is shown in Figure 7-16 (a) and (b). The blue line in the figures is the nominal path that the robot was moved.
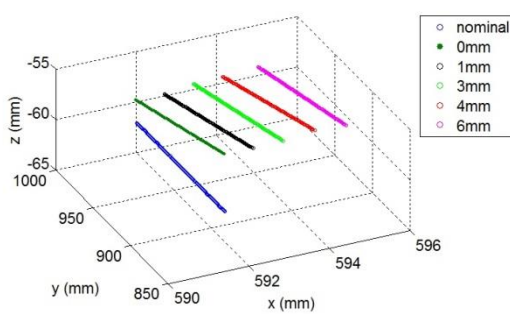
Figure 7.16(a)
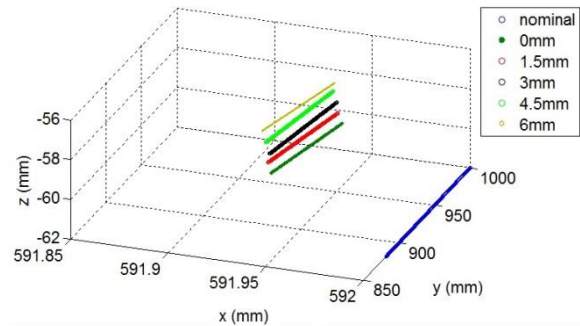
Figure 7.16(b)
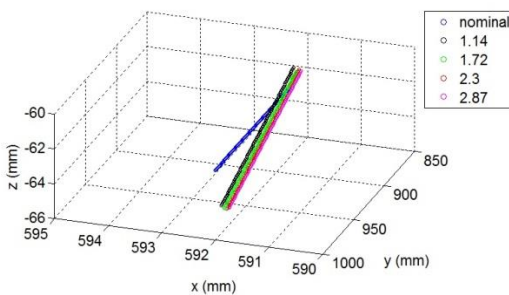
Figure 7.16(c)
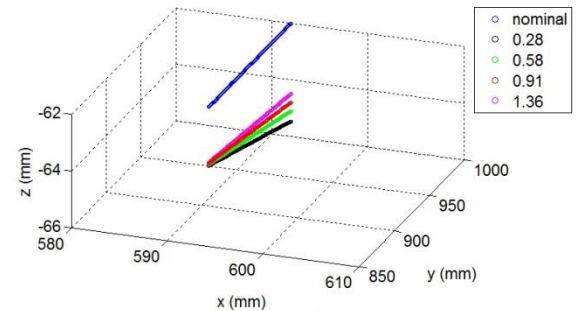
Figure 7.16(d)
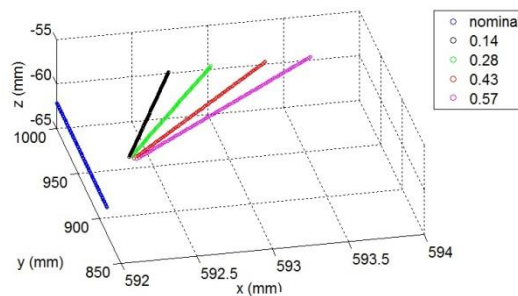
Figure 7.16(e)

Figure 7-16: Seam tracking performance check for possible joint fit-ups (a) horizontal offset, (b) vertical offset, (c) roll, (d) pitch, (e) yaw

It should be noted that if the sample is moved by 1mm the actual seam tracking coordinates will be moved only by 0.5mm for both horizontal and vertical offset configurations because the centre point will be moved by 0.5mm vertically.

Seam tracking performance for the various known angles set for roll, pitch and yaw fit-up orientations is shown in Figure 7-16 (c) (d) and (e) respectively. As can be seen from these figures, the results reveal that the system is sensitive even for small angle deviations around 0.15˚ (Figure 7-16 (e)). This could be useful in an industrial setting because small deviations in fit-up can be addressed with alterations in welding programmes. This can help to improve the final weld quality and strength of the welds.

The results obtained in this section shows that the developed seam tracking algorithm can be successfully used to carry out *3D* seam tracking at all possible joint fit-up configurations.

7.4.3   Seam tracking of selected 3D paths

Previously it was shown that the developed algorithm can successfully carry out seam tracking irrespective of the joint type, joint fit-up or whether there is missing data in the point cloud. This section presents the results of seam tracking performed on some selected *3D* paths (Figure 7-17). These tests were carried out in order show the capability in tracking *3D* paths. As can be seen from the figure, the robotic system successfully managed to guide the welding torch along the *3D* paths. The standard deviation of the tracked path was calculated to be ±54um which is acceptable for the welding process.
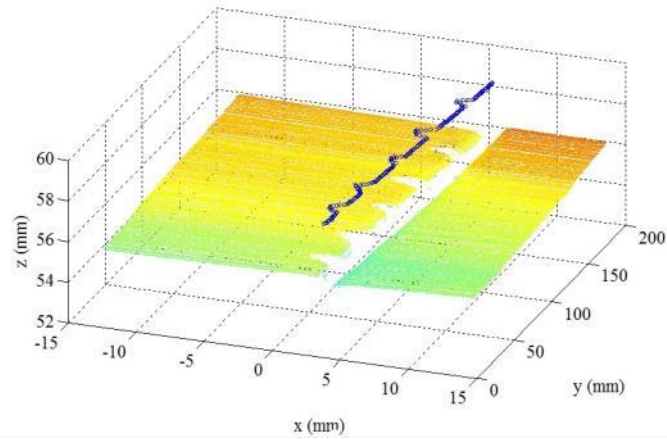
Figure 7.17(a)
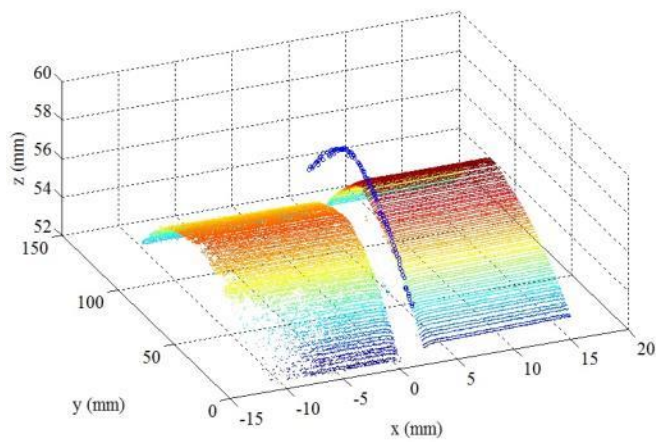
Figure 7.17(b)
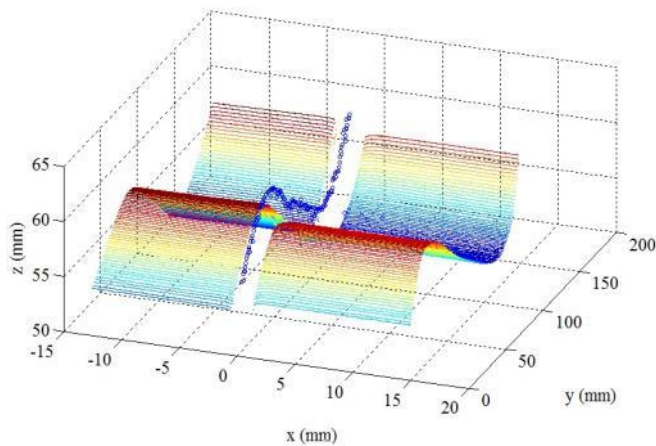
Figure 7.17(c)

Figure 7-17: Seam tracking performed on some complex paths (a) complex 2D, (b) 3D curve, (c) sinusoidal

It should be noted that these paths were selected on the basis that the path was within the laser scanner range (25mm x 25mm) during the nominal path (in this case a straight line in the robot *y*-axis). However, this system can be used to track more complex

171

shapes if the nominal path is provided as an array of *3D* points. This can ideally be derived from a CAD model. Similar to the method discussed before, offsets in the *3D* path can be calculated from the laser scanner data by comparing it with the CAD data to correct the robot path in the tracking pass.

7.5 Robotic welding

The steps involved in carrying out robotic TIG welding are shown in Figure 7-18.
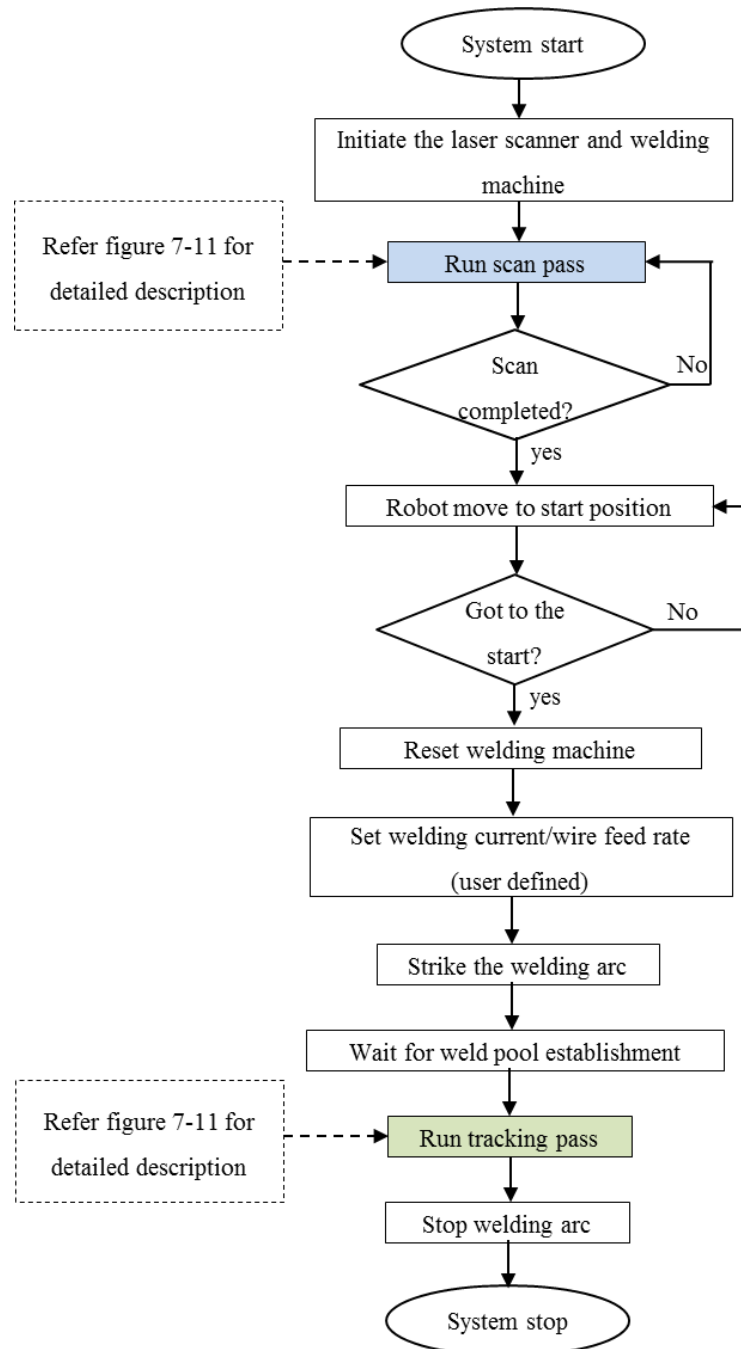
Figure 7-18: Robotic welding procedure

Initially, the robotic welding system carries out the tracking pass as explained in section 7.4. When the robot completes the tracking it returns back to its original start position. At this point the welding machine is reset which is then followed by setting the user specified welding current and wire feed rate values (these are selected based on the experience of human skill knowledge: Chapter 4). After that the welding arc is struck at the starting point. The robot will stay at the start position (while the arc is at its ON state) for a short period to establish the weld pool. The time required for the weld pool establishment is chosen based on the results from human skills capture. Once the weld pool is established, the system carries out the tracking pass according to the method explained in section 7.4.

The robotic welding system set up to perform welding is shown in Figure 7-19.

Figure 7-19: Robotic welding system with fixture

In order to examine the seam tracking and welding performance in *3D* all possible joint fit-ups were tested. 50mm x 200mm x 1.5mm stainless steel (316*l*) plates were set at known joint fit-ups using feeler gauges and slip gauges. Welding was then performed during the tracking pass.

The results of the welding performed with constant parameters of,

- welding current: 80A
- background current: 45A
- pulse frequency: 1kHz

- duty cycle: 60%
- wire feed rate: 0.9mm/s

on all the possible *3D* joint configurations is shown in Figure 7-20. The Figure also shows the numerical set value for each fit-up configuration.

Figure 7.20(a)	Figure 6.20(b)	Figure 6.20(c)
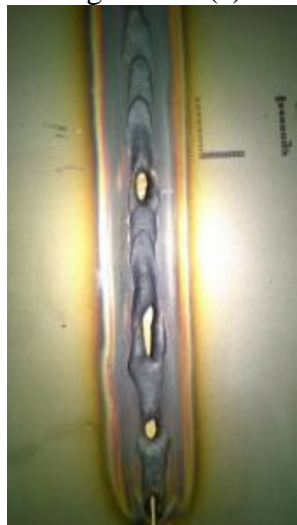
Figure 6.20(d)	Figure 6.20(e)

Figure 7-20: Robotic welding results for all possible joint fit-ups (a) roll angle of 0.5°, (b) pitch angle of 0.5°, (c) yaw angle of 0.5°, (d) vertical offset of 0.5mm, (e) horizontal offset of 0.5mm

According to the results obtained it can be seen that the system seam tracking performance is acceptable since the welding torch has moved successfully along the weld joint centre. However, as can be seen from the photographic views, the visual weld quality is not as desired (especially in yaw and vertical offset set-ups). This is because, the set parameters for the welding current and wire feed rate are not feasible for a weld with a varying geometry (dimensions) along the weld groove. For example, at the "Yaw" configuration, a variable volume is created which must be welded along

174

the weld groove. There is therefore a need for varying the weld machine settings, via adaptable process control, to achieve the required weld quality (discussed in Chapter 9).

The results shown in Figure 7-20, also highlights the need for a method of controlling the weld bead shape (weld pool shape) intelligently. This will help to ensure that the robotic system can intelligently respond to any variability in the joint fit-up. This will be discussed in detail in Chapter 8.

7.6 Summary

The work presented in this chapter has included the results of *3D* seam tracking. A two-pass approach was selected based on the requirement for a decision making process required for the aerospace industry. The developed feature extraction algorithm was successfully used to find the middle point of the weld joint which was then used for the seam tracking process. Seam tracking was successfully carried out on all common weld joint types and all possible joint orientations in *3D* space.

The developed system can be used to track *3D* complex paths and make intelligent decisions whether the joint fit-up is within the suitable tolerances. Such decisions could support improving the welding quality, save cost, time and labour. Robotic welding was performed (with constant parameters) on all the possible joint fit-ups and the resulting welds are not as expected, due to the quality of the weld obtained. Although this might suit a certain scenario (for example a constant gap butt joint), it will not suit a more challenging geometry (such as a variable gap condition: yaw). Therefore it is essential that the parameter selection is carried out automatically. Intelligent algorithms are required to set the welding machine settings based on the joint geometry feedback obtained from the laser scanner data. This will be addressed in detail in Chapter 9.

8 Development of an empirical model for weld quality characteristic prediction

In Chapter 5, 6 and 7, the feature extraction and seam tracking algorithms were presented and the methodology for the two-pass welding approach was established. Experiments were carried out to evaluate and demonstrate the performance of the feature extraction and seam tracking algorithms.

The initial trials on robotic TIG welding with the parameters obtained from chapter-4 were inconclusive with multiple welding defects (low penetration; high HAZ, etc.). Intelligent robotic TIG welding needs a robust experimental database. This chapter (chapter 8) discusses the development of an empirical model to predict the best welding parameters that will give an acceptable weld quality. Welding current, wire feed rate and pulsing parameters (base current, pulsing frequency and duty cycle) were selected as the key process parameters (on the basis of the results obtained from chapter-4) for the work presented in this chapter. Parameters such as welding speed, arc gap, shielding gas flow rate, electrode diameter and torch orientation were kept constant. Statistical approaches such as Taguchi and ANOVA methods were used to find the relationship between the process parameters and their effect on the weld quality characteristics of reinforcement height, penetration, bead width and tensile strength.

Experiments were carried out to derive and validate the proposed methodology. Individual and interaction effects of the input parameters were established. The results obtained show that the developed mathematical model can predict the weld quality characteristics based on the input parameters. The results show that the weld bead width and penetration increased as welding current, background current, duty cycle and wire feed rate increases. An increase in the wire feed rate resulted in an increase of the weld bead height, whereas increases in the welding current, resulted in a decrease of the weld bead height. The effect of pulse frequency on weld bead dimensions was found negligible. Equations were also derived to establish the relationship between selected welding process parameters and the weld quality characteristics. Application of the derived mathematical model for achieving intelligent and adaptive robotic TIG welding process control is discussed in detail in Chapter 10.

8.1 Introduction

In general, the quality of a weld joint is significantly affected by the weld process parameters. To get the desired quality welds, it is essential to have complete control over the relevant process parameters. Typical welding process parameters includes welding current, welding speed, wire feed rate, arc gap, wire diameter, torch orientation, material composition, material thickness and shielding gas type. The typical input and output parameters that can be considered for control are shown in Figure 8-1.
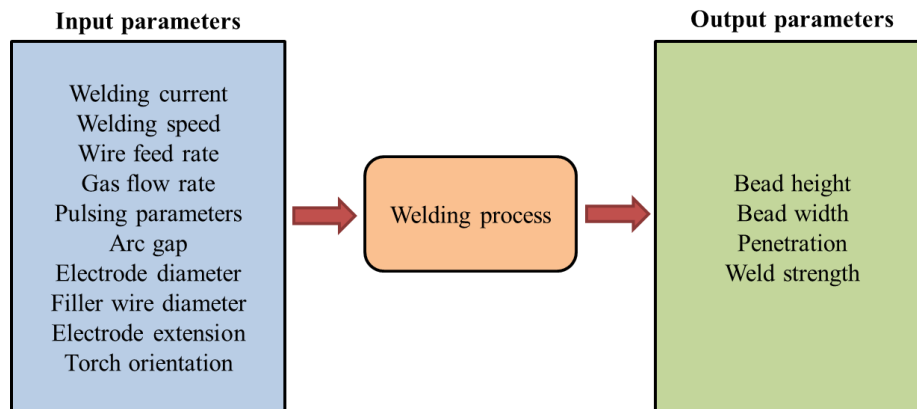
Figure 8-1: Weld input out parameters

In TIG welding, the weld quality characteristics are normally established on basis of weld bead height, width, depth of penetration (Figure 8-2) and strength of the weld.

W : bead width
H : bead height
D : depth of penetration
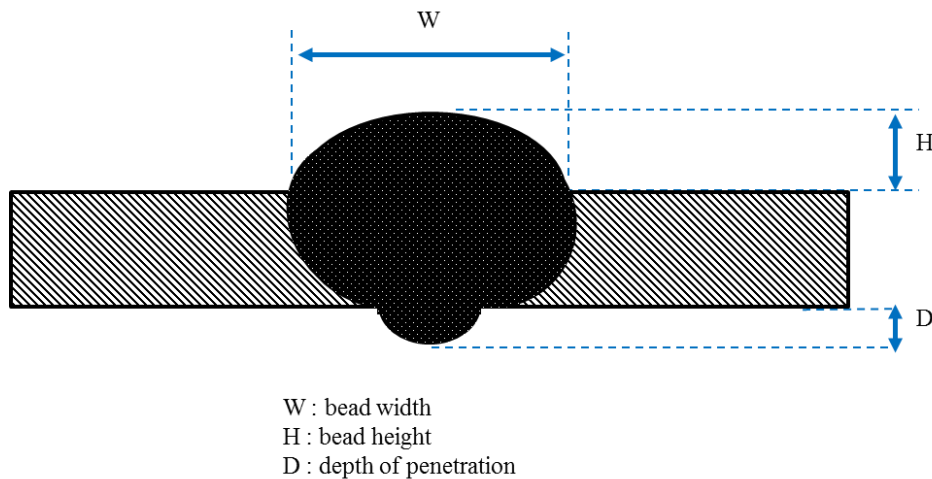
Figure 8-2: Weld bead parameters

It should be noted that in this study it is considered that the depth of penetration is the penetrated amount of weld from the bottom side of the sample.

Compared to other welding processes (such as laser; spot; MIG), the TIG welding process has achieved very low levels of automation, predominantly attributed to the complexities associated with the process (mainly due to wire feeding method).

Previous work carried out on finding the relationships between the process parameters and the bead geometries in arc welding processes can be grouped in to two distinct categories. One method is to use empirical methods based on experimentation [119] and the other is using theoretical studies based on heat flow concepts [125][55]. The Former is identified to be more practical for implementation as the latter involves a significant amount of computation which could be difficult to implement in an automated system. Over the years, many empirical modelling methods such as statistical methods, Artificial Neural Networks (ANN) and Fuzzy logic was attempted [119]. However, due to the easiness of implementation at industrial settings, statistical methods are often preferred by engineers [137].

Sensitivity analysis is a method to quantify the effect of the process parameters on the weld quality characteristics in a manufacturing process [124]. It can be used to rank the process parameters in the order of significance. This study provides the understanding of which input parameter should be prioritized in developing the control solution.

Most of the previous work undertaken on the development of mathematical models to control TIG welding (robotic), are based on bead-on-plate technique, which is not an accurate representation of the actual TIG welding scenario. Bead-on-plate welding is performed with a single plate (no seam present) without considering the joints. This might establish a similar pattern but does not necessarily represent the actual conditions because in an industrial setting a gap always exists between the samples. Existence of a gap affects the weld bead shape. Therefore the bead-on-plate technique could not be the ideal technique for implementing intelligent control on a practical solution for an industrial welding robot.

Use of a pulsed current (see Figure 8-3) for TIG welding is a relatively new technology used in industries especially for the welding of thin sections. Past literature has established the significance of a pulsed current on weld bead shape [128]. However, not much work has been carried out to quantify the affect the weld bead shape or the weld quality characteristics.
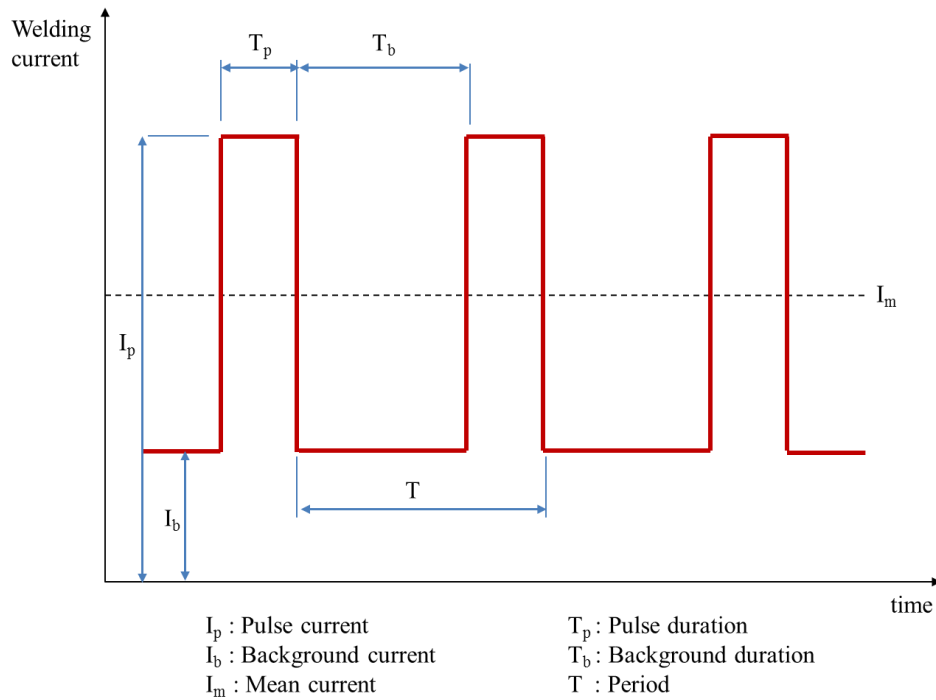
Figure 8-3: Pulsing parameters

Equation 8.1 and 8.2 are used to calculate the pulse frequency and duty cycle respectively for pulsed operation. The Pulse frequency determines the number of pulses per second and it does not affect the heat input (for constant duty cycle, I_p and I_b). Duty cycle determines the amount of time that the welding current signal stays at its high value and therefore has a direct impact on the heat input. High background current increases the mean current and therefore increases the heat input. Therefore pulsing parameters can be used to control the heat input to the weld joint which could be vital when considering welding thin sections.

$$Pulse\ frequency = \frac{1}{T} \tag{8.1}$$

$$Duty\ cycle = \frac{T_p}{T} \times 100 \tag{8.2}$$

8.2 Methodology

As mentioned in the introduction, the TIG welding process is complex and many input parameters influence the weld quality. Studying the effect of all the input parameters is beyond the scope of this study, however, the key process variables that significantly affect the weld bead shape need to be established. The following parameters were considered less significant and were kept constant through the experimentation.

- Gas flow rate : 0.8 l/min
- Arc gap : 0.5 mm
- Weld angle : 90˚
- Welding speed : 2 mm/s
- Electrode diameter : 2.4 mm
- Filler wire diameter : 0.8 mm

The Identified key process parameters for this study are welding current, wire feed rate, pulse frequency, duty cycle and background current. The following sections in this chapter focus on identifying the effect of these parameters on the weld quality characteristics and development of the empirical model to be used with the robotic welding system.

The experimental materials were 200 x 50 x 1.5 mm stainless steel (316 *l*), 5% thoriated electrode (2.4mm) with a stainless steel filler of diameter 0.8mm. It should be noted that the selection of the welding electrode and filler wire size was based principally upon matching the mechanical properties and physical characteristics of the work material, weld size and recommendations from the skilled welders. Prior to carrying out any experimentation, the edges of both samples were prepared using a file and the surfaces of the samples were cleaned to eliminate any dirt or oxides.

The weld bead dimensions (bead width, reinforcement height and penetration) were measured using the Micro-epsilon laser scanner as shown in Figure 8-4 (a).
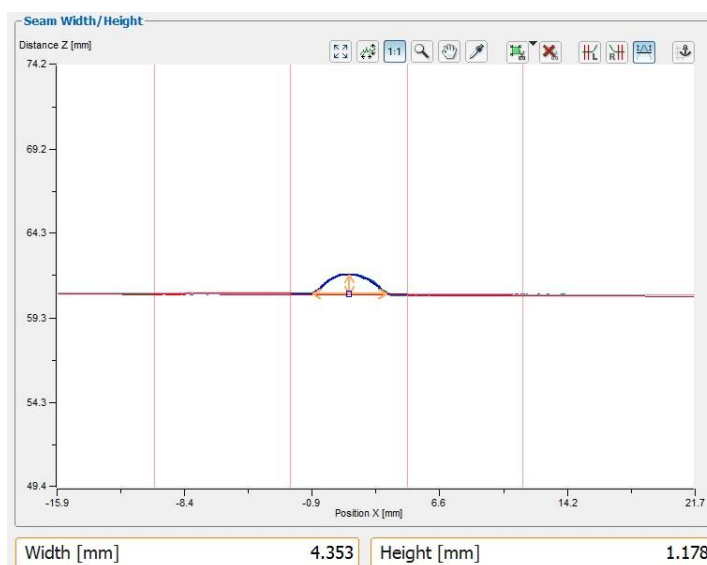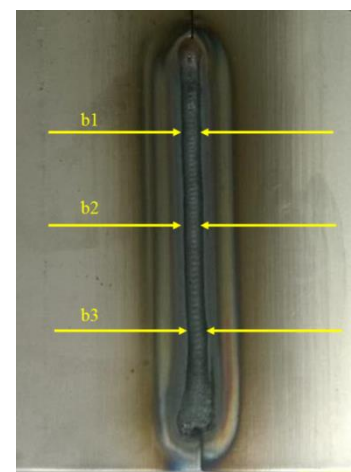
Figure 8.4(a)   Figure 8.4(b)

Figure 8-4: Method of measuring weld bead parameters (a) measurement of bead parameters from Scan-control software, (b) method of obtaining average value

Three positions of the weld were tested for each weld bead parameter and the average was recorded to minimize the error. The three positions were selected by random sampling. Figure 8-4 (b) shows how three positions were measured to obtain the average bead width. Similarly the average values for bead height and penetration was also obtained.

In addition to the weld bead shape it is also important to investigate the strength of the weld to get the full understanding of the effect of the process parameters on the weld quality. An INSTRON 8081 tensile testing machine (shown in Figure 8-5) was used to measure the tensile strength of the weld and to establish the fracture zone. In order for the work pieces to be used with the tensile testing machine, the samples were prepared then (laser cut) into ISO standard (ISO 6892) size which is shown in Figure 8-6. To avoid any machine errors, the sample was held straight and in the middle of the jaws of the tensile testing machine.

Figure 8-5: Tensile testing machine

Figure 8-6: Specimen preparation for tensile testing

During the tensile testing process, the load was increased from zero in 100N steps until the specimen is broken. A load-extension graph was obtained for each sample. From the graph, the load at the maximum tensile extension, the maximum load and the load at the break point was recorded which are shown in Figure 8-7.
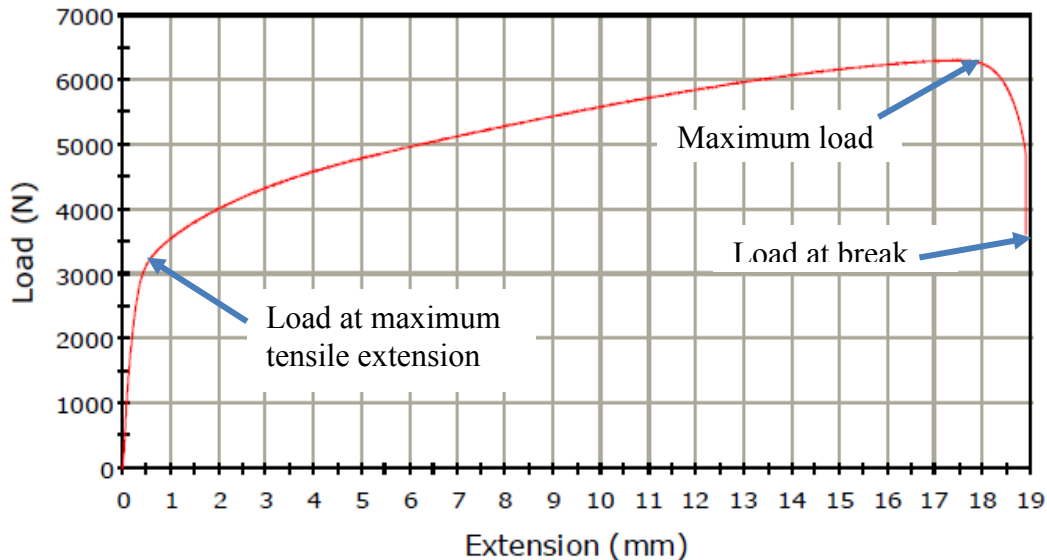
Figure 8-7: Load-extension graph and important parameters extracted

8.3   Identification of important influencing parameters

To study the effect of each parameter on the weld quality characteristics, experiments were carried out by changing one parameter at a time whilst keeping all the other parameters constant. This enabled a better understanding of the effect as well as the boundaries of a particular process parameter to achieve a good weld.

The constant values selected (based on the results from the manual welders' knowledge) are as follows,

- Welding current   :   90 A
- Background current   :   45 A
- Pulse frequency   :   1 kHz
- Duty cycle   :   60 %
- Wire feed rate   :   1 mm/s

The effect of welding current on weld bead dimensions is shown in Figure 8-8. As noted from the figure, the bead width and penetration increase with an increase in welding current whereas the bead height decreases with an increase in welding current. This is attributed to the increase in heat input with an increase in the welding currents.
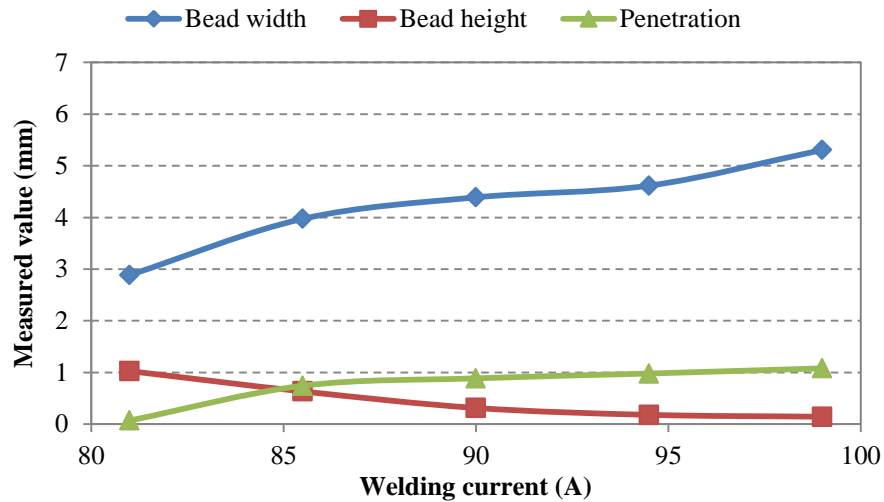
Figure 8-8: Weld bead measurements against welding current

The average weld bead dimensions with changing background current are shown in Figure 8-9.
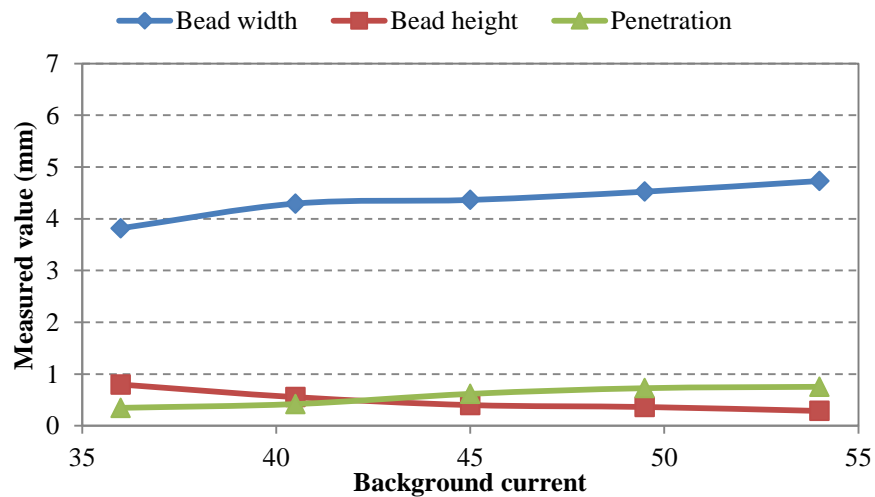
Figure 8-9: Weld bead measurements against background current

As can be seen from the figure, it shows similar variation as the welding current. However the influence of background current on weld bead shape is lower compared to the welding current, which implies that the background current has a comparatively lower effect on the weld bead parameters than the welding current.

The effect of the weld bead shape dimensions with a change in the pulse frequency is shown in Figure 8-10. As noted from the figure, the pulse frequency does not have a significant effect on the weld bead shape. Even though it does not have an effect on the bead size, it might have an effect on the strength of the weld which will be discussed later.

183
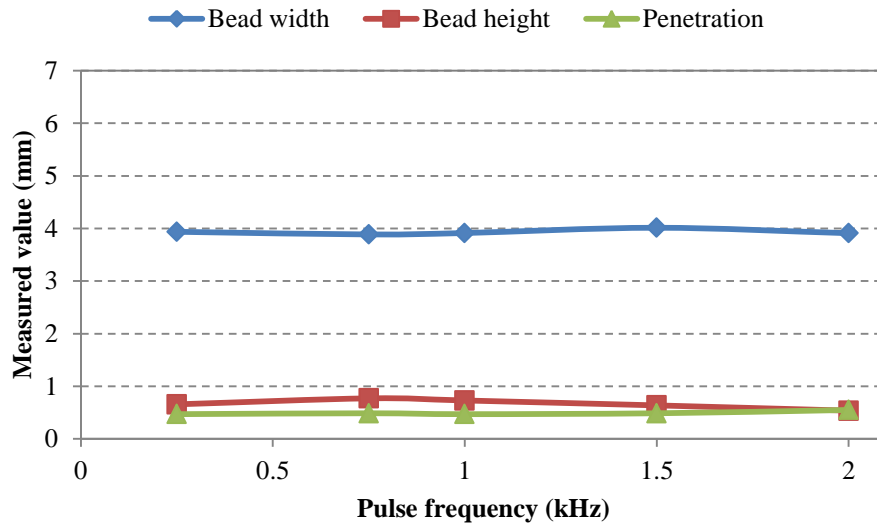
Figure 8-10: Weld bead measurements against pulse frequency

The effect of weld bead dimensions with varying duty cycle is shown in Figure 8-11.
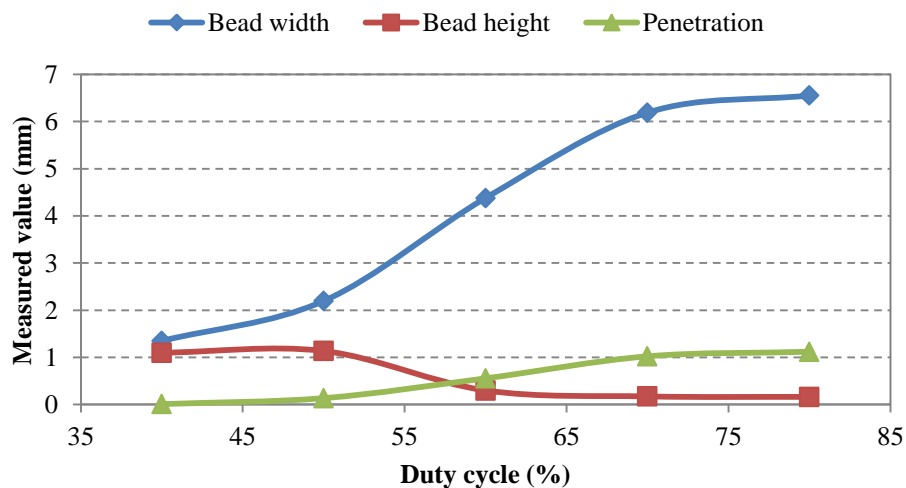
Figure 8-11: Weld bead measurements against duty cycle

As noted from Figure 8-11, the duty cycle has a significant effect on the weld bead width compared to other parameters. The effect of duty cycle on the weld bead height and penetration has a similar variation as the effect of welding current.

The variation of bead parameters against the wire feed rate is shown in Figure 8-12. As can be seen from the figure, the bead width increases with the wire feed rate, but not as much as is observed with the welding current or duty cycle. It also can be noted from the figure that there is a marginal increase in the bead height with an increased wire feed rate. However, the wire feed rate has no significant effect on penetration.
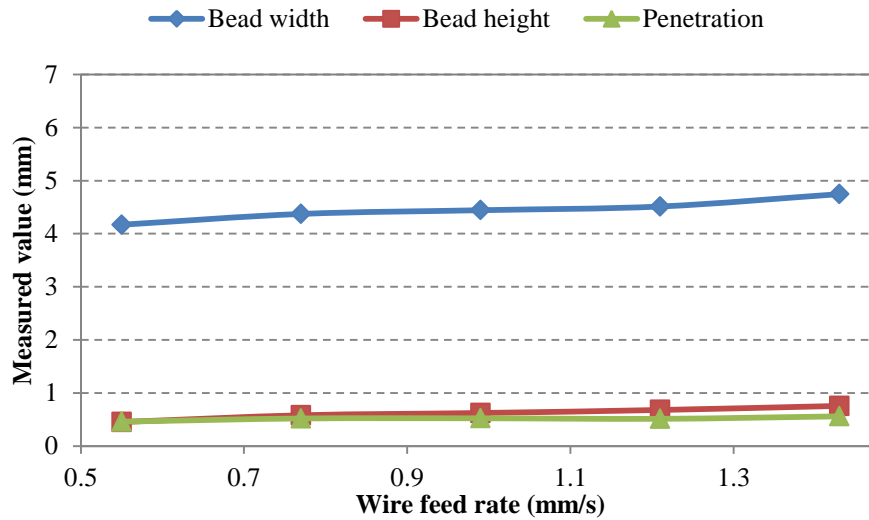
Figure 8-12: Weld bead measurements against wire feed rate

The effect of each selected process parameter on the weld bead geometry and tensile strength is quantified in section 8.4.3.

8.4 Empirical modelling

This section presents the methodology for mapping the relationship between the welding process parameters (input) and the welding performance (output). As explained before, some of the process parameters were kept constant during the experiments as they are less significant.

The response function representing any weld quality characteristic can be represented by equation 8.3.

$$Y = f(X_1, X_2, X_3, X_4, X_5) \tag{8.3}$$

where,

Y is the response (bead width, bead height, penetration, welding strength)

X_1 is the welding current

X_2 is the background current

X_3 is the pulse frequency

X_4 is the duty cycle

X_5 is the wire feed rate

The steps involved in the empirical model development are shown in detail in Figure 8-13.

```
┌─────────────────────────┐
│   Determine the factors │
└─────────────────────────┘
            │
            ▼
┌─────────────────────────┐
│   Identify test conditions │
└─────────────────────────┘
            │
            ▼
┌─────────────────────────┐
│  Design the matrix experiment │
└─────────────────────────┘
            │
            ▼
┌─────────────────────────┐
│ Define the data analysis procedure │
└─────────────────────────┘
            │
            ▼
┌─────────────────────────┐
│    Conduct experiments  │
└─────────────────────────┘
            │
            ▼
┌─────────────────────────┐
│      Analyse data       │
└─────────────────────────┘
            │
            ▼
┌─────────────────────────┐
│    Predict performance  │
└─────────────────────────┘
```

Individual factor contribution	Factor interaction	Determining optimum levels	ANOVA and S/N analysis	Models for prediction

```
            │
            ▼
┌─────────────────────────┐
│    Validate experiments │
└─────────────────────────┘
```
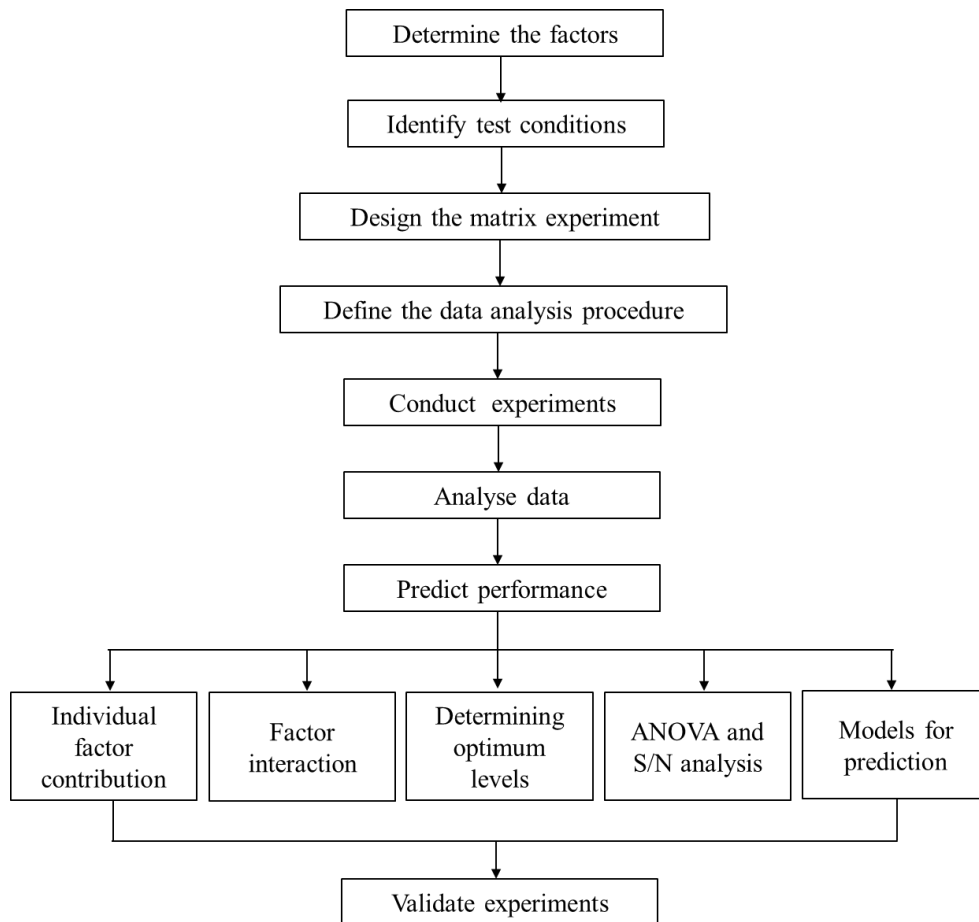
Figure 8-13: Mathematical model development procedure

Initial experiments were used to find the boundaries of the process parameters that will produce an acceptable weld quality. These experiments were carried out by varying the process parameters and the resulting output parameters were measured. Specific methods (Taguchi method and results from ANOVA) were used to reduce the number of experiments. Different statistical algorithms were then tested for developing the empirical model for predicting the output characteristics. The developed empirical models were compared and the best model for prediction was selected. Additional validation experiments were carried out to validate the developed empirical model. The following sections will discuss these steps in detail.

8.4.1 Delimitation of variable boundaries

In the present study, five levels of process parameters are considered. The value of each process parameter at the different levels is listed in Table 8-1.

Table 8-1: Process parameter levels

Process parameter	Units	Level 1	Level 2	Level 3	Level 4	Level5
Welding current (X_1)	A	80	85	90	95	100
Background current (X_2)	A	35	40	45	50	55
Pulse frequency (X_3)	kHz	0.25	0.75	1	1.5	2
Duty cycle (X_4)	%	40	50	60	70	80
Wire feed rate (X_5)	mm/s	0.50	0.75	1.00	1.25	1.50

8.4.2 Design of the experiments

As noted from Table 8-1 there are five process parameters and five levels. A full factorial study therefore would require 5^5 (3125) experiments, which is a costly and time consuming task. The Taguchi method was used to reduce the number of experiments. The Taguchi method uses a special design of orthogonal arrays and is used extensively in engineering fields (such in machining) for the optimization of process parameters maintaining the required quality with minimal cost or time. The main advantage of the Taguchi method is that it can be used to study the whole process parameter range with significantly smaller numbers of experiments. With the implementation of Taguchi's method, the total number of experiments can be reduced to 25 in this work.

In the Taguchi method, the deviance between the experimental value and the anticipated value is calculated by defining a loss function. The value of the loss function is further converted in to signal to noise ratio (S/N). Three categories exist in the quality characteristic optimization in the analysis of the S/N ratio which are:

- lower the better
- higher the better
- nominal is the better

In all of these categories, a better quality characteristic is achieved when the S/N ratio is larger. Therefore in the Taguchi method, the best level of a particular process parameter is the level with the highest S/N ratio.

The signal-to-noise ratio for the case, "Nominal target is best" is given in equation 8.4. It should be noted that for this study, the middle value of the range of a particular weld bead dimension was selected as the nominal value.

187

$$\frac{S}{N_i} = 10 \log_{10}[\frac{1}{n}\frac{\frac{(\sum_{j=1}^{j=n} y_{ij})^2}{n} - \sigma_i^2}{\sigma_i^2}] \tag{8.4}$$

where,

i is the experiment number;

j is the repeated trail number for experiment i;

y_{ij} is the value of each repeated trial for experiment i;

$\overline{y_{ij}} = \frac{1}{n}\sum_{j=1}^{j=n} y_{ij}$ denotes the mean value of j trials for experiment i, where n is the number of repeated trails;

$S_{mi} = \frac{(\sum_{j=1}^{j=n} y_{ij})^2}{n} = n(\overline{y_{ij}})^2$ denotes the sum of the squares of the mean;

$\overline{y_{ij}}^2$ is the mean square;

$\sigma_i = \sqrt{\sigma_i^2}$ is the standard deviation, showing the ability of the welding system to provide closely similar indications for repeated evaluation of the same measurement under the same conditions of measurement;

$\sigma_i^2 = \frac{(\sum_{j=1}^{j=n} y_{ij}^2 - S_{mi})}{n-1} = \frac{1}{n-1}[\sum_{j=1}^{j=n} y_{ij}^2 - \frac{(\sum_{j=1}^{j=n} y_{ij})^2}{n}]$ denotes the experimental variance.

8.4.3   Analysis of variance (ANOVA)

Statistical analysis of variance (ANOVA) is a method performed to quantify the process parameters' effect on a particular quality characteristic (such as weld bead dimensions or weld strength). This is achieved using the F-test introduced by Fisher [124]. According to his findings the F value is larger if the process parameter has a larger effect on the quality characteristic. The ANOVA method also can be used to find whether there are any interaction effects among the welding process parameters.

8.4.3.1   **Enumerating the effect of process parameters on weld bead dimensions**

In section 8.3, the effect of each process parameter on the weld bead dimensions was presented. However the amount of effect has to be quantified and ranked. In order to rank the order of the process parameters and its effect on any weld bead dimension, initially a two factor design was carried out. The maximum and minimum possible

188

levels of each process parameter were selected as the levels for the design (from section 8.3). Table 8-2 shows the experimental data and their relevant resulting weld bead shape dimensions (these are the average value of three trials for each experiment).

Table 8-2: Experimental data and results for ANOVA method

Experiment number	Inputs					Outputs		
	Welding current (A) : $X1$	Background current (A) : $X2$	Pulse frequency (kHz) : $X3$	Duty cycle (%) : $X4$	Wire feed rate (mm/s) : $X5$	Bead width (mm) : $Y1$	Bead height (mm) : $Y2$	Penetration (mm) : $Y3$
1	75	35	0.75	40	0.50	2.45	0.05	1.02
2	75	35	0.75	70	1.50	3.52	0.60	0.78
3	75	58	1.5	40	0.50	2.82	0.05	0.92
4	75	58	1.5	70	1.50	3.81	0.44	0.92
5	100	35	1.5	40	1.50	3.60	0.12	1.21
6	100	35	1.5	70	0.50	6.64	2.10	0.10
7	100	58	0.75	40	1.50	2.90	0.05	1.45
8	100	58	0.75	70	0.50	7.74	1.78	0.05

The collected data was entered into Matlab and the ANOVA was carried out for each output weld bead dimension. The results from Matlab are given in Figure 8-14.

Source	Sum Sq.	d.f.	Mean Sq.	F	Prob>F
X1	11.305	1	11.305	10.75	0.0817
X2	0.3081	1	0.3081	0.29	0.6425
X3	0.021	1	0.021	0.02	0.9005
X4	13.2355	1	13.2355	12.59	0.0711
X5	4.366	1	4.366	4.15	0.1784
Error	2.1025	2	1.0513		
Total	31.3382	7			

Figure 8.14(a)

Source	Sum Sq.	d.f.	Mean Sq.	F	Prob>F
X1	2.6565	1	2.65651	69.98	0.014
X2	0.0055	1	0.00551	0.15	0.7398
X3	0.0231	1	0.02311	0.61	0.5169
X4	5.3301	1	5.33011	140.4	0.007
X5	2.1945	1	2.19451	57.81	0.0169
Error	0.0759	2	0.03796		
Total	10.2857	7			

Figure 8.14(b)

Source	Sum Sq.	d.f.	Mean Sq.	F	Prob>F
X1	0.10811	1	0.10811	1.64	0.3287
X2	0.02531	1	0.02531	0.38	0.5986
X3	0.09031	1	0.09031	1.37	0.3624
X4	0.70211	1	0.70211	10.65	0.0824
X5	0.72601	1	0.72601	11.01	0.08
Error	0.13183	2	0.06591		
Total	1.78369	7			

Figure 8.14(c)

Figure 8-14: Results from ANOVA test for two L8 table for weld bead dimensions (a) Bead width : *Y1*, (b) Penetration : *Y2*, (c) Bead height : *Y3*

As discussed previously, the larger the *F*-value the better the effect on the quality characteristic. The *F*-values are graphed against the relevant weld bead parameters in Figure 8-15. As noted from the figure, the weld bead width and penetration are mostly affected by welding current, duty cycle and wire feed rate whereas the bead height is mostly affected by the duty cycle and wire feed rate. All three weld bead parameters were not affected by either background current or pulse frequency. This implies that these two control parameters (pulse frequency and background current) do not play an important role in controlling the weld bead dimensions. Table 8-3 lists the ranking of input parameters in controlling each weld bead parameter. These results also substantiate the results obtained in section 8.3.
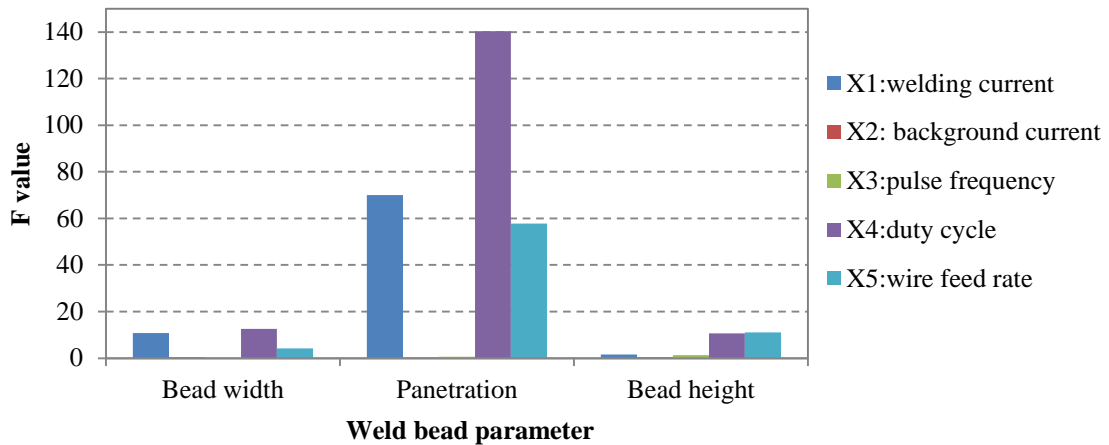
Figure 8-15: F-value obtained from L8 Table

Table 8-3: Ranking of process parameters on bead dimensions obtained using L8 table

Rank	Bead width	Penetration	Bead height
1	Duty cycle	Duty cycle	Wire feed rate
2	Welding current	Welding current	Duty cycle
3	Wire feed rate	Wire feed rate	Welding current
4	Background current	Pulse frequency	Pulse frequency
5	Pulse frequency	Background current	Background current

For the experiments carried out using the two factor method, the maximum and minimum values of each process parameter was used. Since the L8 orthogonal array considers only two levels, an optimum set of input parameters may not be robust enough. Therefore, the work presented in this thesis also included and investigation of an L25 orthogonal array to obtain a more statistically confident dataset for analysis.

According to the findings from the L8 orthogonal array, only three parameters significantly affect the weld bead dimensions. This implies that in further analysis, more levels can be selected for these most significant parameters and less levels can be selected for the least significant parameters, which will save time and cost. Therefore, for the L25 orthogonal array analysis, five levels for the most significant parameters (*X1,X4,X5*) and three levels for least significant parameters (*X2,X3*) were chosen. The values of each process parameter and the resulting bead dimensions (averaged over three trials) at the different levels are listed in Table 8-4.

Table 8-4: Welding process parameters and resulting weld bead parameters

Trial	Input parameters					Output parameters		
	Welding current (A) : *X1*	Background current (A) : *X2*	Pulse frequency (kHz) : *X3*	Duty cycle (%) : *X4*	Wire feed rate (mm/s) : *X5*	Bead width (mm) : *Y1*	Bead height (mm) : *Y2*	Penetration (mm) : *Y3*
1	81	36	0.5	40	0.55	2.86	0.49	0.18
2	81	45	1	50	0.77	2.83	0.64	0.36
3	81	59	1.5	60	0.99	4.07	0.72	0.53
4	81	36	0.5	70	1.21	4.34	0.75	0.77
5	81	45	1	80	1.43	4.91	0.74	0.53
6	86	36	1	60	1.21	3.25	1.26	0.32
7	86	45	1.5	70	1.43	4.46	0.69	0.87
8	86	59	1.5	80	0.55	6.35	0.07	0.54
9	86	59	0.5	40	0.77	2.91	0.67	0.27
10	86	36	0.5	50	0.99	3.18	1.07	0.22
11	90	36	1.5	80	0.77	6.61	0.22	2.11
12	90	45	1	40	0.99	2.66	1.21	0.04
13	90	59	1.5	50	1.21	3.22	1.15	0.14
14	90	45	0.5	60	1.43	3.78	1.42	0.52
15	90	59	1	70	0.55	5.95	0.15	1.10
16	95	36	0.5	50	1.43	2.93	1.58	0.16
17	95	45	1	60	0.55	5.34	0.24	0.91
18	95	59	0.5	70	0.77	6.08	0.13	1.29
19	95	36	1	80	0.99	6.48	0.10	1.52
20	95	45	1.5	40	1.21	2.58	1.55	0.07
21	99	36	1.5	70	0.99	5.72	0.24	0.67
22	99	45	0.5	80	1.21	6.11	0.11	1.06
23	99	59	1	40	1.43	2.69	1.69	0.10
24	99	59	1.5	50	0.55	4.86	0.31	0.91
25	99	45	1	60	0.77	5.27	0.08	1.08

The data listed in Table 8-4 was entered again into Matlab and the ANOVA was performed. The results from Matlab are given in Figure 8-16.

```
Source    Sum Sq.    d.f.    Mean Sq.     F       Prob>F
-----------------------------------------------------------
X1          4.16       4     1.03999     27.19    0.0001
X2          0.0907     2     0.04533      1.19    0.3541
X3          0.1156     2     0.05782      1.51    0.2774
X4         35.4666     4     8.86666    231.82    0
X5          5.0312     4     1.25779     32.88    0.0001
Error       0.306      8     0.03825
Total      48.1895    24
```

Figure 8.16(a)

```
Source    Sum Sq.    d.f.    Mean Sq.     F       Prob>F
-----------------------------------------------------------
X1         0.32327     4     0.08082      1.66    0.2513
X2         0.09503     2     0.04752      0.98    0.4179
X3         0.03168     2     0.01584      0.33    0.7316
X4         2.6678      4     0.66695     13.69    0.0012
X5         3.2284      4     0.8071      16.56    0.0006
Error      0.38983     8     0.04873
Total      6.88226    24
```

Figure 8.16(b)

```
Source    Sum Sq.    d.f.    Mean Sq.     F       Prob>F
-----------------------------------------------------------
X1         0.6827      4     0.17067      1.38    0.3242
X2         0.15672     2     0.07836      0.63    0.5564
X3         0.0386      2     0.0193       0.16    0.8585
X4         2.99103     4     0.74776      6.03    0.0154
X5         1.21076     4     0.30269      2.44    0.1318
Error      0.99285     8     0.12411
Total      6.36418    24
```

Figure 8.16(c)

Figure 8-16: Results from ANOVA for L25 table for weld bead dimensions (a) bead width : *Y1*, (b) penetration : *Y2*, (c) bead height : *Y3*

The *F*-values are then graphed against the relevant weld bead dimension, which is shown in Figure 8-17. As noted from the figure, the weld bead width is mostly affected by duty cycle, welding current and wire feed rate whereas the bead height and penetration are mostly affected by the duty cycle and wire feed rate, although the welding current also has a small effect on them. All three weld bead parameters were not affected by the background current and the pulse frequency which was the same result as in the case for the L8 experiments. Ranking of process parameters obtained using the L25 table is listed in Table 8-5. According to these results, the duty cycle is the main parameter which affects the weld bead shape whereas and the wire feed rate and welding current are the next two most significant parameters. Results obtained using the L8 orthogonal array was therefore fully substantiated from the results of the L25 orthogonal array.
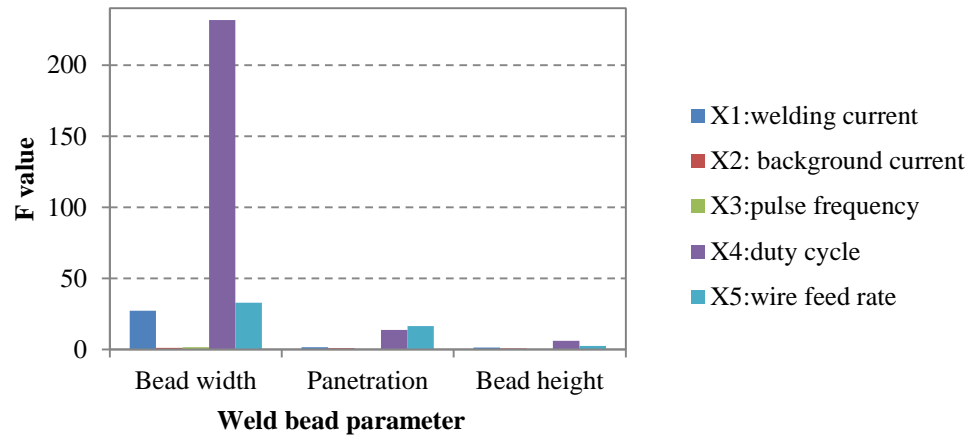
Figure 8-17: *F*-values obtained from L25 table

Table 8-5: Ranking of process parameters on bead dimensions obtained using L25 table

Rank	Bead width	Penetration	Bead height
1	Duty cycle	Wire feed rate	Duty cycle
2	Wire feed rate	Duty cycle	Wire feed rate
3	Welding current	Welding current	Welding current
4	Pulse frequency	Background current	Background current
5	Background current	Pulse frequency	Pulse frequency

According to the results in Table 8-5 the most significant parameters on the weld bead dimensions are the duty cycle, wire feed rate and welding current. The reason for this can be explained as follows: Welding current and duty cycle have a direct effect on the heat input into the system and therefore this increases the size of the molten pool dimensions. A high wire feed rate also increases the weld bead dimensions as more molten material is fed in to the weld pool.

8.4.3.2 **Effect of process parameters on weld strength**

In the previous section, the important parameters which affect the weld bead dimensions were identified and their effect was quantified. However, it is recognised that, although the least significant parameters identified were pulse frequency and background current with regards to the weld bead dimensions, these could be significant when considering the mechanical strength of the weld. In order to investigate this hypothesis, tensile testing was carried out for each sample according to the method presented in section 8.2.

194

The load at maximum tensile extension, the maximum load and the load at break were recorded and tabulated in Table 8-6 (these results are averaged over three trials). The data was entered into Matlab, and the ANOVA was carried out to find the significance of each process parameter on the strength of the weld. The signal-to-noise ratio for this case is the "Maximum target is best" which is given in equation 8.5. This was selected because high strength assures better quality in the weld.

$$n_i = \frac{S}{N_i} = -10\log_{10}\left(\frac{\sum\frac{1}{y_{ij}^2}}{n}\right) \quad (8.5)$$

Table 8-6: Welding process parameters and resulting tensile strengths of welds

| Trial | Input parameters | | | | | Weld strength (N) | | |
	Welding current (A) : X1	Background current (A) : X2	Pulse frequency (kHz) : X3	Duty cycle (%) : X4	Wire feed rate (mm/s) : X5	Load at maximum tensile extension : Y4	Maximum load : Y5	Load at break : Y6
1	81	36	0.5	40	0.55	703	1738	750
2	81	45	1	50	0.77	3760	6411	4960
3	81	59	1.5	60	0.99	3314	5503	3368
4	81	36	0.5	70	1.21	3535	5914	3544
5	81	45	1	80	1.43	3600	6353	5675
6	86	36	1	60	1.21	3777	6404	4035
7	86	45	1.5	70	1.43	3660	6363	4785
8	86	59	1.5	80	0.55	3448	6106	5366
9	86	59	0.5	40	0.77	2032	3398	2050
10	86	36	0.5	50	0.99	2572	4302	2739
11	90	36	1.5	80	0.77	3610	6351	4826
12	90	45	1	40	0.99	1350	2253	1356
13	90	59	1.5	50	1.21	2384	4102	3082
14	90	45	0.5	60	1.43	3700	6295	4973
15	90	59	1	70	0.55	3559	6251	4818
16	95	36	0.5	50	1.43	2262	3850	2314
17	95	45	1	60	0.55	2269	3755	2344
18	95	59	0.5	70	0.77	3532	6250	4661
19	95	36	1	80	0.99	2987	5208	3436
20	95	45	1.5	40	1.21	2450	4087	3242
21	99	36	1.5	70	0.99	3445	6254	5549
22	99	45	0.5	80	1.21	3309	5583	4272
23	99	59	1	40	1.43	1797	2998	1817
24	99	59	1.5	50	0.55	3527	6250	5537
25	99	45	1	60	0.77	3385	6910	5056

The results from Matlab are given in Figure 8-18. The *F*-values are graphed against the relevant tensile strength parameter as shown in Figure 8-19. As can be from the figure, the weld strength is mostly affected by duty cycle. It is also noted that all other process parameters have a lower effect on the strength of the weld. Comparatively the pulse frequency and background current has higher effect on welding strength than it has on weld bead dimensions. The ranking of the process parameters' effect on weld strength is listed in Table 8-7.

Source	Sum Sq.	d.f.	Mean Sq.	F	Prob>F
X1	417371.8	4	104342.9	0.26	0.8941
X2	263050.1	2	131525.1	0.33	0.7278
X3	469902.7	2	234951.4	0.59	0.5763
X4	11568829.8	4	2892207.5	7.27	0.009
X5	1399324.8	4	349831.2	0.88	0.517
Error	3181422.4	8	397677.8		
Total	18352442.2	24			

Figure 8.18(a)

Source	Sum Sq.	d.f.	Mean Sq.	F	Prob>F
X1	1889901	4	472475.3	0.42	0.7877
X2	578643.9	2	289322	0.26	0.7776
X3	2026905.2	2	1013452.6	0.91	0.4407
X4	37865124	4	9466281	8.49	0.0056
X5	5278413.4	4	1319603.3	1.18	0.3872
Error	8915278.8	8	1114409.9		
Total	61016667.4	24			

Figure 8.18(b)

Source	Sum Sq.	d.f.	Mean Sq.	F	Prob>F
X1	2.50953e+06	4	627382.9	0.49	0.7418
X2	1.6315e+06	2	815752.1	0.64	0.5517
X3	2.95875e+06	2	1479376.9	1.16	0.3603
X4	2.56056e+07	4	6401406.3	5.03	0.0253
X5	2.46543e+06	4	616356.8	0.48	0.7475
Error	1.01777e+07	8	1272216.4		
Total	5.13886e+07	24			

Figure 8.18(c)

Figure 8-18: Results from ANOVA for weld strength (a) load at maximum tensile extension: Y4, (b) maximum load:Y5, (c) load at break:Y6
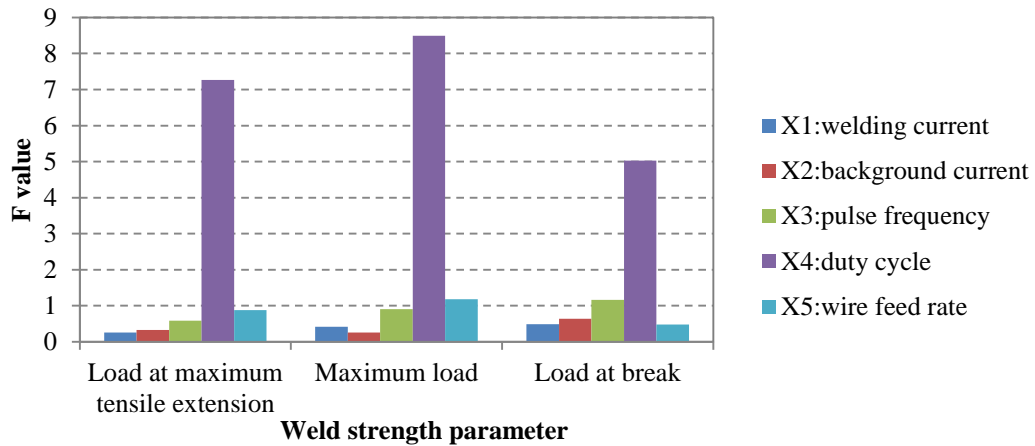
Figure 8-19: *F*-values obtained for tensile strength

Table 8-7: Ranking of process parameters on weld strength

Rank	Load at maximum tensile extension	Maximum load	Load at break
1	Duty cycle	Duty cycle	Duty cycle
2	Wire feed rate	Wire feed rate	Pulse frequency
3	Pulse frequency	Pulse frequency	Background current
4	Background current	Welding current	Welding current
5	Welding current	Background current	Wire feed rate

8.4.4 Development of the empirical model

In the previous section the relationship between the input and output parameters was studied and quantified. In this section, the development of an empirical model to predict the weld bead shape and tensile strength as a function of the identified key process parameters (welding current, background current, pulse frequency, base current and wire feed rate) in the robotic TIG welding system is presented.

Empirical modelling can be carried out using various methods. However, they can be categorized into two main groups:

1. **Statistical methods**: polynomial (including linear, interaction, pure quadratic), curvilinear, logarithmic, exponential, logistic and power.
2. **Other methods**: Artificial Neural Network (ANN), Fuzzy logic.

This study used statistical methods for the development of the empirical model, due to its advantageous of low computational time and easiness in implementing in a robotic welding system. By conserving the relationship between the input and output parameters this study has chosen polynomial fitting for the implementation of the

197

empirical model. The selection of polynomial fitting over other methods is also attributed to fact that other statistical methods may cause an over-fit to occur.

The linear empirical model can be expressed by equation 8.6, where $x_0 = 1$, n is the quality characteristic number (n=1…4) and i is the process parameter number (i=1….5).

$$y_n = \sum_{i=0}^{5} a_i x_i \tag{8.6}$$

The quadratic modelling can be represented by equation 8.7 where $x_0 = 1$,

$$y_n = \sum_{i,j=0}^{5} a_i x_j + \sum_{\substack{i=6 \\ j=1}}^{\substack{i=11 \\ j=5}} a_i x_j^2 \tag{8.7}$$

The interaction modelling can be represented by equation 8.8, where $x_0 = 1$. It should be noted that interaction modelling is different from the interaction effects resulting from the ANOVA method discussed in section XX.

$$y_n = \sum_{i,j=0}^{5} (a_i x_j) + a_6 x_1 x_2 + a_7 x_1 x_3 + a_8 x_1 x_4 + a_9 x_1 x_5 + a_{10} x_2 x_3 \dots$$
$$+ a_{11} x_2 x_4 + a_{12} x_2 x_5 + a_{13} x_3 x_4 + a_{14} x_3 x_5 + a_{15} x_4 x_5 \tag{8.8}$$

The "Interactive response surface modelling tool" (rstool), available in Matlab, was used to obtain the coefficients of each of the three empirical models presented in the above three equations. Tables 8.8-8.10 lists the coefficients obtained for each quality characteristic using the linear, interaction and quadratic models respectively.

Table 8-8: Estimated coefficients of quality characteristics based on linear model

Coefficient	Value of co-efficient			
	Bead width (y1)	Bead height (y2)	Penetration (y3)	Weld strength (y4)
a_0	-5.4045	1.7081	-1.9962	-3.4562
a_1	2.8582	-0.4139	0.9643	3.1123
a_2	0.3568	-0.0327	-0.2575	0.6554
a_3	-0.0004	0.0186	-0.0018	0.0012
a_4	0.8682	-0.2342	0.2573	0.7656
a_5	-1.6774	1.2856	-0.6119	-2.1222

Table 8-9: Estimated coefficients of quality characteristics based on quadratic model

Coefficient	Value of co-efficient			
	Bead width ($y1$)	Bead height ($y2$)	Penetration ($y3$)	Weld strength ($y4$)
a_0	-6.3212	-19.2439	-11.9641	-14.5664
a_1	5.5201	22.8186	10.4981	9.6538
a_2	-0.5055	-4.5866	-0.2158	-2.1134
a_3	-0.2481	0.2114	-0.0444	-0.2245
a_4	0.6395	-0.1595	0.3218	0.4397
a_5	-1.9234	0.0544	0.2654	0.5642
a_6	-0.6583	-5.8031	-2.3831	-3.4532
a_7	0.3945	2.1234	-0.0032	0.1228
a_8	0.0248	-0.0190	0.0040	0.0231
a_9	0.0190	-0.0064	-0.0053	0.0024
a_{10}	0.1334	0.7086	-0.4858	0.4532

Table 8-10: Estimated coefficients of quality characteristics based on pure interaction model

Coefficient	Value of co-efficient			
	Bead width (y_1)	Bead height (y_2)	Penetration (y_3)	Weld strength (y_4)
a_0	-10.0444	2.0056	-3.2167	-4.5643
a_1	6.4829	-1.7296	-0.5174	1.2368
a_2	2.3373	-3.0437	-5.9175	4.6745
a_3	-0.8322	0.2782	1.4412	0.7744
a_4	1.2567	-0.1698	0.3143	0.9885
a_5	-0.4743	6.5824	5.3630	-1.2312
a_6	-1.5082	1.1900	4.8813	-1.4325
a_7	0.1781	0.0434	-0.7053	0.8789
a_8	-0.1984	0.0498	0.3213	0.0643
a_9	-1.6260	-1.0536	-2.6888	-1.8765
a_{10}	0.1170	-0.1281	-0.1294	0.2116
a_{11}	-0.0943	0.1695	-0.6271	-0.4532
a_{12}	1.3483	0.1645	0.0095	1.0065
a_{13}	0.0297	-0.0045	0.0111	0.0231
a_{14}	0.1461	-0.2113	0.0410	0.4213
a_{15}	-0.0157	-0.3797	-0.1734	-0.0324

The coefficient values listed in Table 8-6, Table 8-7 and Table 8-8 can be used with equations 8.6, 8.7 and 8.8 to obtain the empirical model for each quality characteristic. For example, the empirical models for the weld bead width can be represented in equation 8.9 (for the linear model), equation 8.10 (for the interaction model) and 8.11 (for the pure quadratic model). Similarly, the equations for the other quality

199

characteristics (bead height, penetration and weld strength) can be obtained in a similar manner, using their respective coefficients.

$$y_1 = 5.4045 + 2.8582x_1 + 0.3568x_2 - 0.0004x_3 + 0.8682x_4 - 1.6774x_5 \qquad (8.9)$$

$$
\begin{aligned}
y_1 = {} & -10.0444 + 6.4829x_1 + 2.3373x_2 - 0.8322x_3 + 1.2567x_4 \\
& - 0.4743x_5 - 1.5082x_1x_2 + 0.1781x_1x_3 - 0.1984x_1x_4 \\
& - 1.6260x_1x_5 + 0.1170x_2x_3 - 0.0943x_2x_4 + 1.3483x_2x_5 \\
& + 0.0297x_3x_4 + 0.1461x_3x_5 + -0.0157x_4x_5
\end{aligned}
\qquad (8.10)
$$

$$
\begin{aligned}
y_1 = {} & -6.3212 + 5.5201x_1 - 0.5055x_2 - 0.2481x_3 + 0.6395x_4 \\
& - 1.9234x_5 - 0.6583x_1^2 + 0.3945x_2^2 + 0.0248x_3^2 \\
& + 0.0190x_4^2 + 0.1334x_5^2
\end{aligned}
\qquad (8.11)
$$

The adequacy of the mathematical models and the significance of coefficients can be tested by finding the coefficient of determination (R^2) using equation 8.12. The model which results in an R^2 value closest to 1 is the best fitting model for the data. In order to find the most suiting model R^2 values for the three models under investigation (linear, interaction and pure quadratic), the R^2 was calculated for each of the quality characteristics, the outcomes of which are listed in Table 8-11.

$$R^2 = 1 - \frac{\sum_{i=1}^{25}\left[\left(y_{experiment_i} - y_{model_i}\right)\right]^2}{\sum_{i=1}^{25}\left[y_{experiment_i} - \dfrac{\sum_{i=1}^{25} y_{experiment_i}}{n}\right]^2} \qquad (8.12)$$

Table 8-11: R^2 values calculated for empirical models

	Bead width (y_1)	Bead height (y_2)	Penetration (y_3)	Weld strength (y_4)
R^2_{linear}	0.9847	0.8767	0.7185	0.8231
$R^2_{pure\,quadratic}$	0.9867	0.9303	0.7295	0.8114
$R^2_{interaction}$	0.9914	0.9743	0.8809	0.8342

According to the results listed in Table 8-11, the interaction model is best for predicting all four quality characteristics. Figure 8-20 shows the actual and predicted results obtained using the interaction model. As can be seen from the figure, the empirical model returns quite satisfactory results (actual and predicted values lies very close to each other) in predicting the weld bead dimensions.
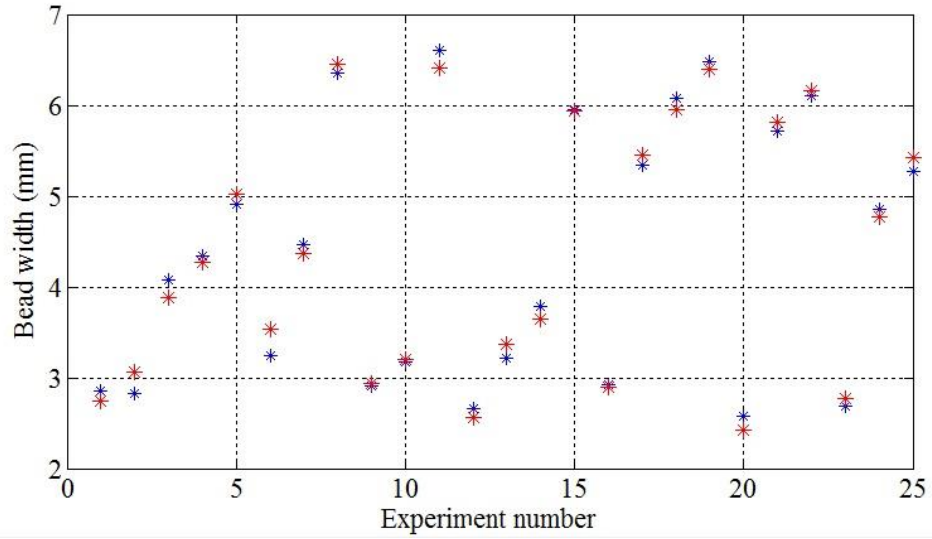
Figure 8.20(a)
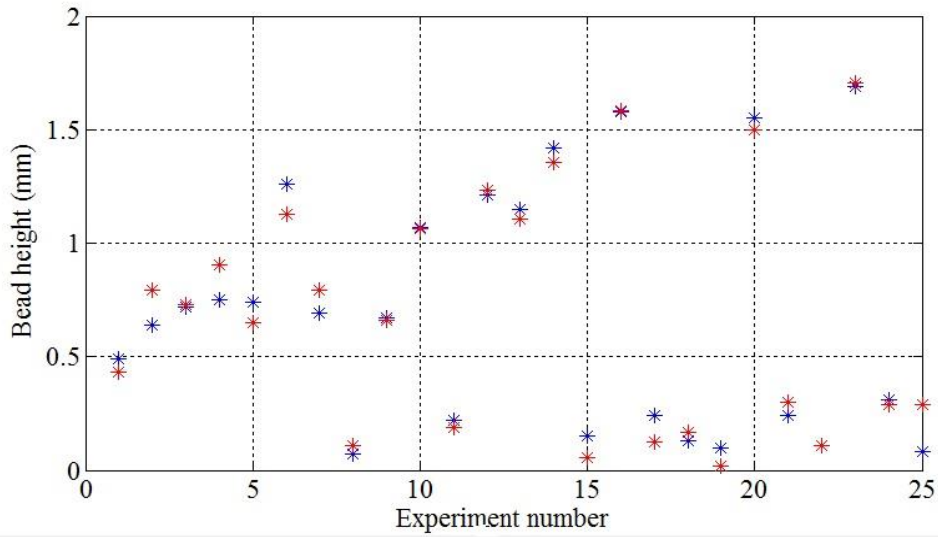
Figure 8.20(b)
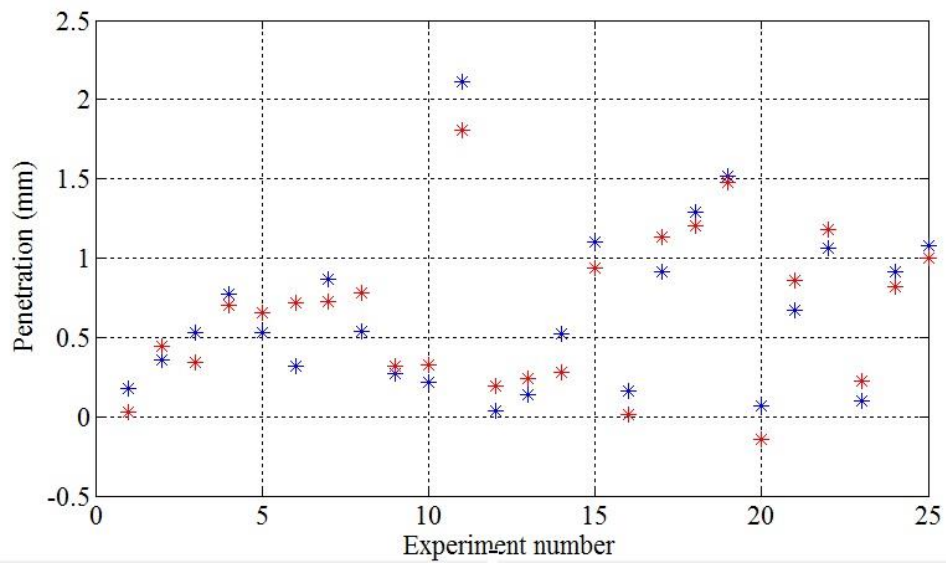
Figure 8.20(c)

Figure 8-20: Actual and predicted results of weld bead dimensions using interaction model (a) Actual (*) and predicted (*) results of weld bead width, (b) Actual (*) and predicted (*) results of weld bead height, (c) Actual (*) and predicted (*) results of weld penetration

Figure 8-21 shows the actual and predicted results obtained using the interaction model for tensile strength (the load at the maximum tensile extension). As can be seen from the figure, the empirical model returns quite satisfactory results.
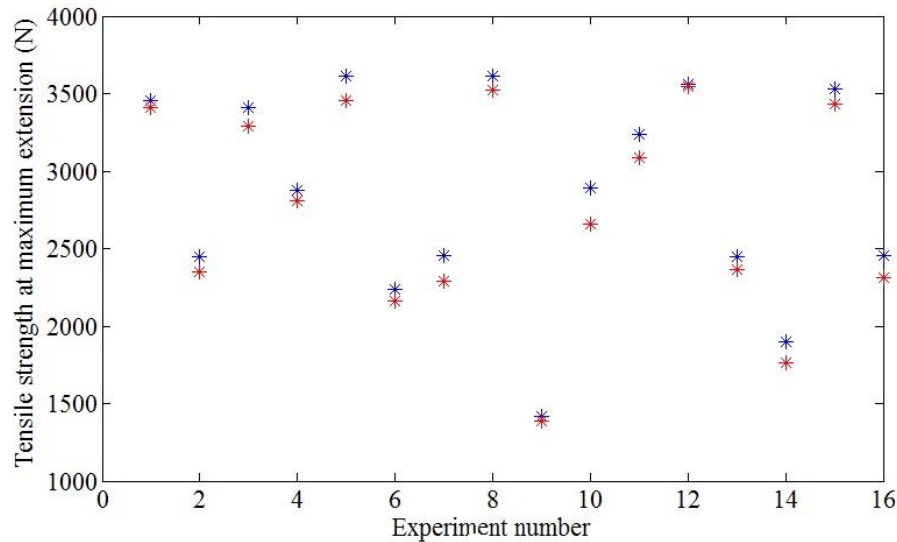
Figure 8-21: Actual (*) and predicted (*) results of tensile strength using interaction model

8.4.5   Model validation

The developed mathematical model and equations must be validated in order to confirm the accuracy of the empirical model. Therefore an additional set of 16 experiments were performed to verify the empirical model. The values of the process parameter sets used for the validation experiments were different from those used for the development of the empirical model. For each validation experiment, the output characteristics were also measured using the same procedure outlined in Section 8.2. Even though the interaction model was selected as the best fit model, in this section the prediction results from the linear and quadratic models are also presented for completeness.

The experimental data and the results for weld bead width are listed in Table 8-12 and graphed in Figure 8-22.

Table 8-12: Measured and predicted results from the validation experiments

Input parameters					Measured bead width (mm)	Predicted bead width (mm)		
Welding current (A) : *X1*	Background current (A) : *X2*	Pulse frequency (kHz) : *X3*	Duty cycle (%) : *X4*	Wire feed rate (mm/s) : *X5*		Linear	Quadratic	Interaction
77	45	1.7	60	1.16	3.67	3.26	3.10	3.23
86	59	1.4	60	1.27	4.50	3.77	3.67	3.84
81	45	0.7	50	1.21	3.13	2.59	2.49	2.67
104	36	1.7	40	1.27	3.85	3.00	2.97	3.04
104	45	1.7	50	1.27	4.90	3.94	3.90	4.01
104	45	1.9	60	1.16	5.53	4.97	5.03	5.12
72	45	1.4	70	1.05	4.17	4.01	3.79	4.04
72	54	1.4	80	1.16	5.14	4.78	4.63	4.90
90	32	1.1	50	1.05	3.94	3.31	3.30	3.29
90	27	1.4	70	1.16	5.03	4.84	4.84	4.81
95	32	0.7	50	1.27	3.76	3.26	3.32	3.16
99	32	0.7	50	1.21	4.12	3.63	3.60	3.54
90	41	1.9	70	1.10	5.49	5.03	5.17	5.04
108	36	1.4	30	1.21	3.00	2.50	2.50	2.47
108	32	1.7	50	1.27	4.52	4.11	4.09	4.28
86	45	1.4	50	0.99	4.02	3.21	3.11	3.21
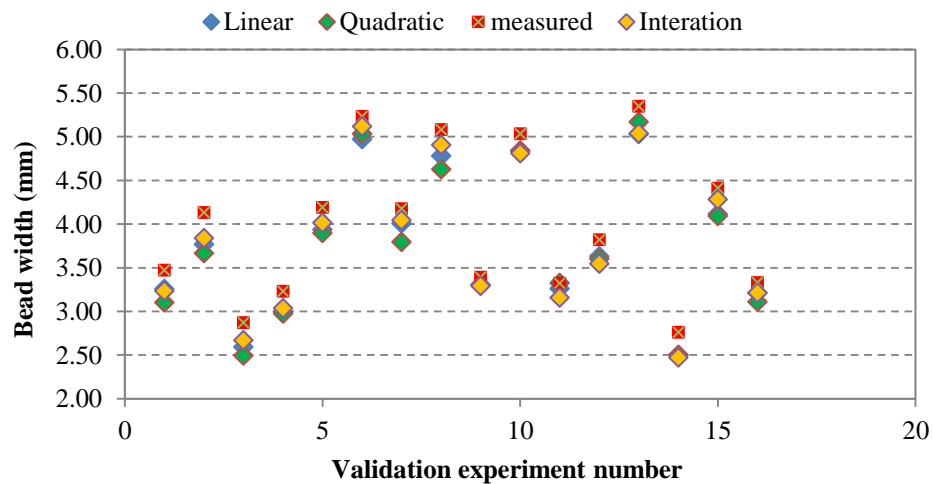
Figure 8-22: Results of bead width prediction from validation experiments

Validation experiments were carried out for the other three quality characteristics and the results are shown in Figure 8-23 (for bead height), Figure 8-24 (for weld penetration) and Figure 8-25 (for tensile strength) respectively. Compared to the bead width, bead height and tensile strength there is more deviation in the prediction results observed for the penetration case (Figure 8-24). This is attributed to a higher

measurement error in penetration due to the smaller values being measured. However, as can be seen from the figures, the interaction model performs satisfactorily in the weld quality characteristic prediction.
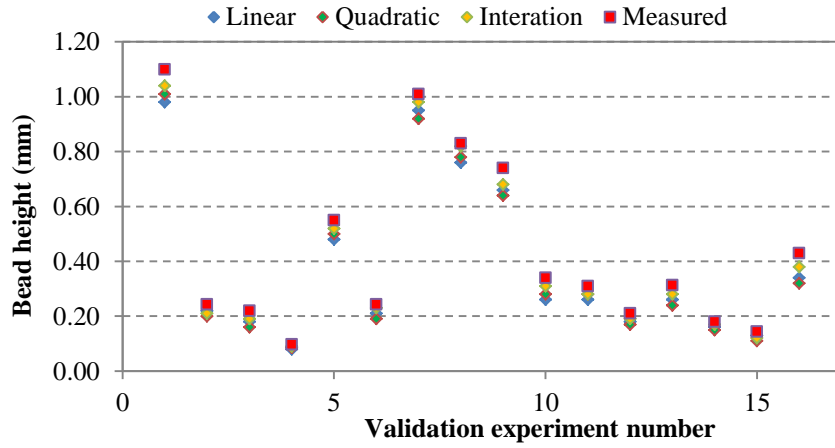
Figure 8-23: Results of bead height prediction from the validation experiments
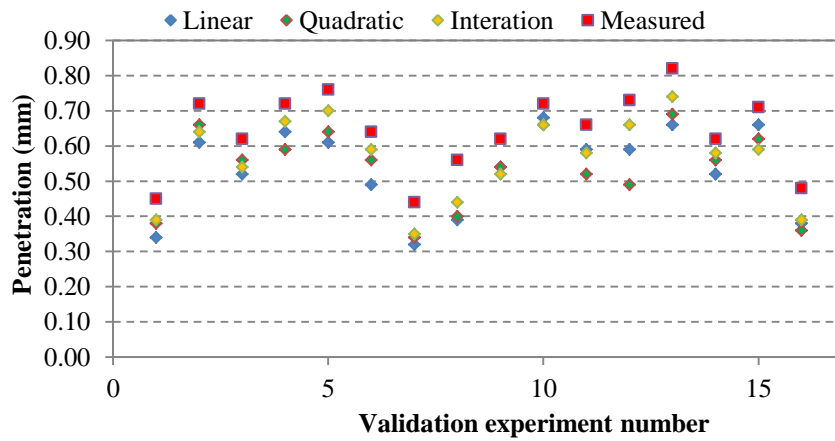
Figure 8-24: Results of penetration prediction from the validation experiments
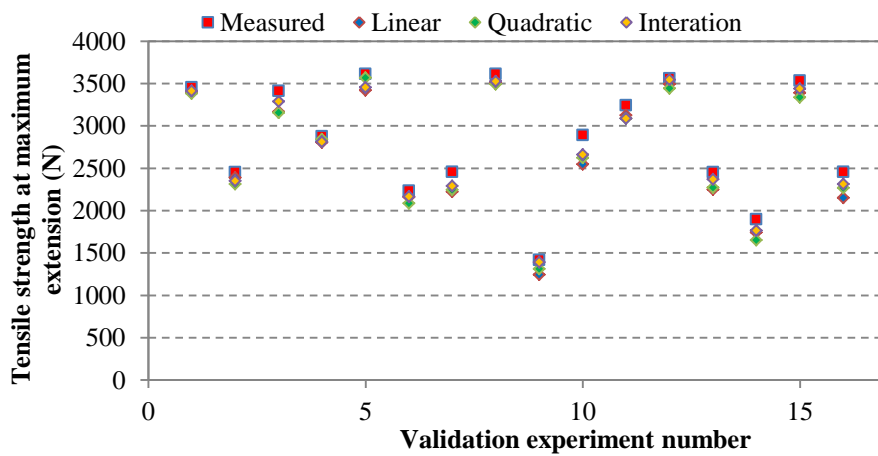
Figure 8-25: Results of tensile strength prediction from the validation experiments

In order to quantify the level of validation, the average percentage error in prediction was calculated using equation 8.13 for all the models considered.

$$Level\ of\ validation = \frac{(y_{experiment} - y_{model})}{y_{experiment}} \times 100\% \qquad (8.13)$$

Table 8-13 shows the quality characteristic and the percentage error in prediction observed for each model. The interaction model can be used in predicting the bead width, bead height and welding strength with a high level of accuracy, compared to the other two models. However, it appears from the results that the developed empirical models are less accurate in predicting the weld penetration. This is because of the high percentage measurement error observed for this variable.

However, the interaction model involves significant computation time compared to a linear model. Therefore for the prediction of the weld bead width and tensile strength, it will be ideal to use the linear model as its level of validation is within an acceptable limit in engineering (<10%). The reduced computation time is also advantageous in implementing the developed empirical model in the robotic welding system.

Table 8-13: Level of validation values

Output characteristic	Linear (%)	Interaction (%)	Pure quadratic (%)	Selected model for prediction
Bead width	5.73	5.15	6.93	Linear (Due to less computational time)
Bead height	13.74	8.44	16.25	Interaction (Due to level of validity)
Penetration	17.47	12.49	16.86	Interaction (Due to level of validity)
Weld strength	6.12	3.87	5.93	Linear (Due to less computational time)

In Chapter 4, it was found that manual welders prioritise the process parameters that can be controlled. They identify the most significant parameters which affect each weld quality characteristic and accordingly adjust them to obtain the optimum weld quality. It was also found that welding current and wire feed rate were the most significant

parameters they used in order to control the welding process while parameters such as welding speed and torch position was not varied significantly by the manual welders.

Similar to the manual welders, the analysis presented in this chapter also returns prioritization of process parameters. It was identified that duty cycle, welding current and wire feed rate are the main parameters that should be controlled whereas base current and pulse frequency do not affect weld quality significantly.

Both these results show the importance of simplifying the control problem by reducing the number of variables.

8.5 Summary

This chapter presented the work carried out on understanding the relationship between the input and output parameters of the developed TIG welding robot. It was highlighted that, although a high number of process parameters affect the quality characteristics of the weld, only certain parameters are significant. These are; welding current, wire feed rate and duty cycle. The work presented in this chapter has considered a real welding scenario where two samples are joined together with the use of seam tracking. This is identified to be novel in robotic welding compared to previous work which has used the bead-on-plate technique.

The effect of each process parameter on the weld quality characteristic was quantified using the ANOVA method. The duty cycle of the welding current signal was the most important parameter affecting weld bead dimensions and weld strength. The welding current and wire feed rate also have a significant effect whereas the effect of pulse frequency and background current is comparatively low.

The design of the experiments conducted was via the Taguchi method to develop an empirical model to predict the output characteristics of the weld (weld bead dimensions and welding strength), using polynomial formulations (linear, interaction and pure quadratic). Equations which map the output parameters with the input parameters were then derived. The results revealed that all three models produced a satisfactory prediction, although the interaction model is comparatively more accurate than the linear or pure quadratic models. However, since the linear model also results in a satisfactory accuracy in prediction is it suggested that using the linear model is better due to the reduced amount of computations.

Quantification of the effect on weld quality is vital for attaining the controllability of the TIG welding process when welding complex shapes, especially in the aerospace industry. This could aid engineers to address challenging welding tasks such as welding of variable welding gaps, volumes, thicknesses etc. Chapter 9 will use the developed model under a challenging welding scenario (variable gap) as a case study to achieve adaptable robotic TIG welding.

9 Intelligent and Adaptable Robotic Seam tracking and TIG Welding

This chapter combines all the knowledge gained throughout this study to demonstrate adaptive robotic TIG welding. As discussed in chapter 4, skilled welders simplify the TIG welding process by prioritizing certain process parameters whilst keeping other parameters constant. In Chapter 8 it was found that three parameters (duty cycle, welding current and wire feed rate) significantly affect the weld bead dimension and hence should control the quality of robotic TIG welding. The first part of this chapter discusses the development of a back-propagation empirical model, which will help to choose the most appropriate welding parameters for the automated TIG welding process. In the second part of this chapter, a comparison was performed between various TIG welding approaches including; a constant parameter approach, a segmented parameter approach, the skilled welder's approach and the proposed adaptive welding approach.

9.1 Empirical modelling for adaptive welding of a variable gap butt joint

This section presents the adaptive control strategy developed using the empirical models, which are discussed in Chapter 8. A back propagation empirical model was implemented to adaptively select the welding machine settings to cater for the variable gap (0.25-2.5mm). Figure 9-1 shows the variable gap scenario used during the TIG welding process.
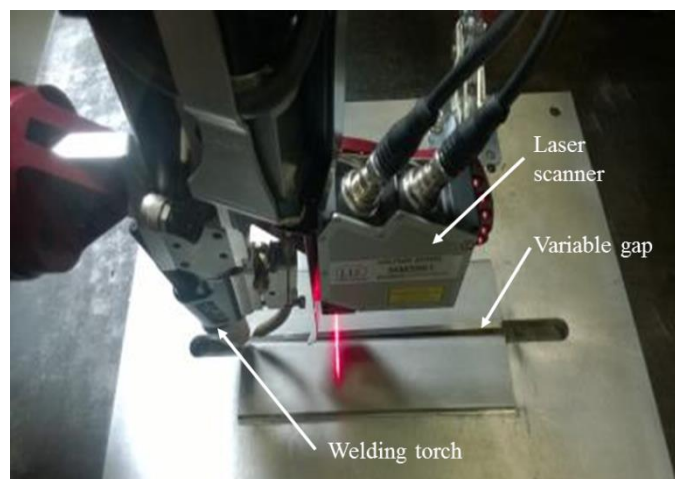
Figure 9-1: Robotic welding system setup to carry out welding on a variable butt gap joint

The key quality characteristic which is to be controlled to carry out welding of a variable gap joint is the weld bead width. Figure 9-2 shows the effect of the process parameters on the weld bead width as derived from the ANOVA method. As can be seen from the figure, duty cycle, welding current and wire feed rate are the most significant process parameters which affect the weld bead width (with the highest F values). Therefore, a constant background current and pulse frequency (less significant process parameters) of 45A and 1kHz respectively were used for all the experiments carried out in this section.
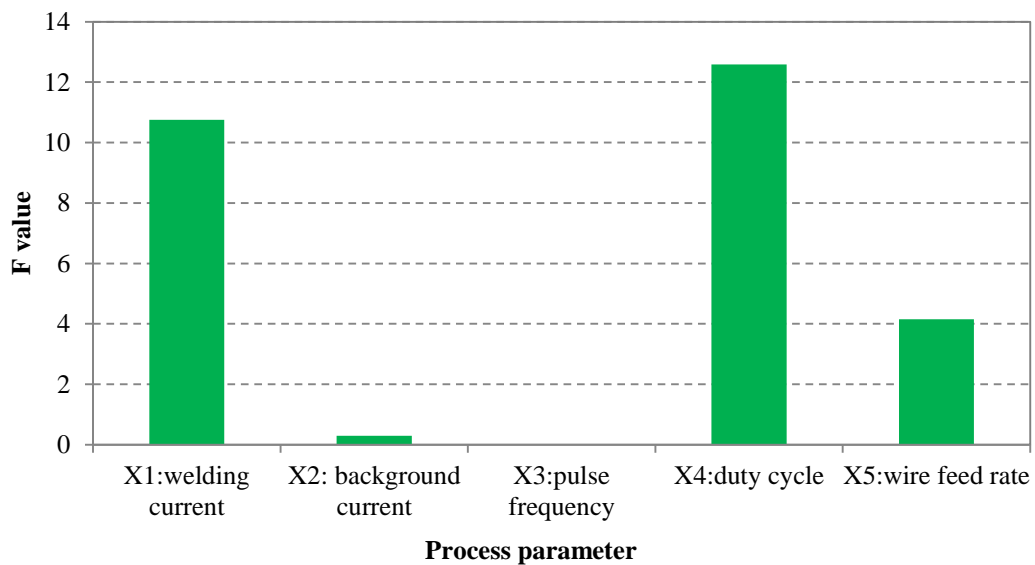
Figure 9-2: Effect of process parameters on bead width

9.1.1.1 Using joint geometry feedback for adaptive control

In this work, the dimensions of the joint geometry was used (from the laser scanner) to control the input welding parameters. Figure 9-3 shows a cross sectional view of a weld joint (It should be noted that the methodology presented in this section is valid for any irregular cross sectional profile). As can be noticed from the figure, two parallel lines of the trapezoidal element represent the respective depth values of the two consecutive laser points. Those two points form a trapezoidal elemental area (dA) on the weld joint profile which can be calculated using equation 9.1.

$$dA_i = \frac{1}{2}(z_i + z_{i+1})\, dx \tag{9.1}$$
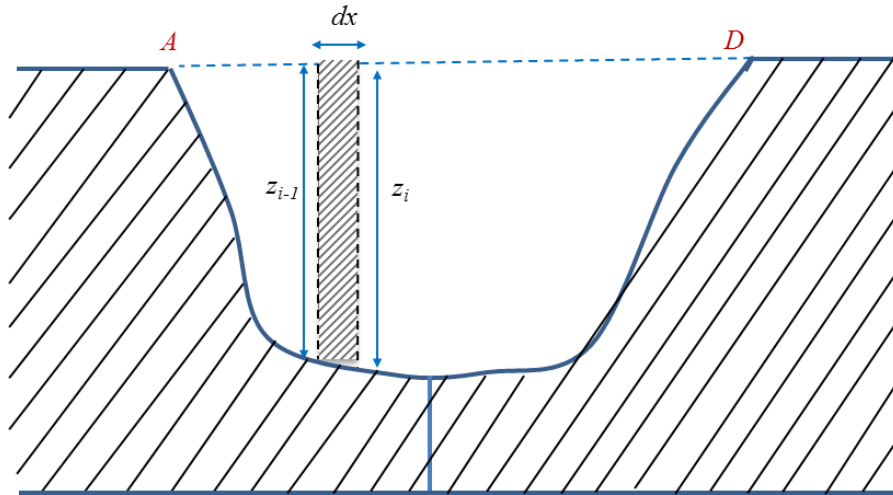
Figure 9-3: Cross-sectional profile of an irregular profile weld joint

By summing all the trapezoidal elements (from *A* to *D*), the total area under a single cross-sectional profile can be calculated (using equation 9.2).

$$Area_i = \sum_{i=1}^{n} dA_i \qquad (9.2)$$

where n is the number of laser points fall within the weld joint (between *A* and *D*)

It should be noted that equation 9.4 and 9.5 can be used in the case of a *U* or *V* or any other irregular shape profile. However, in the case of an *I*-groove equation 9.3 was used to estimate the cross sectional profile.

$$Area_i = Gap_i \times thickness\ of\ the\ sample \qquad (9.3)$$

If *dy* is the distance between two consecutive cross sectional profiles (shown in Figure 9-4), the volume to be welded per robot step movement can be calculated using equation 9.4.

$$dV_i = \frac{1}{2}\ dy.\,(dA_i + dA_{i+1}) \qquad (9.4)$$
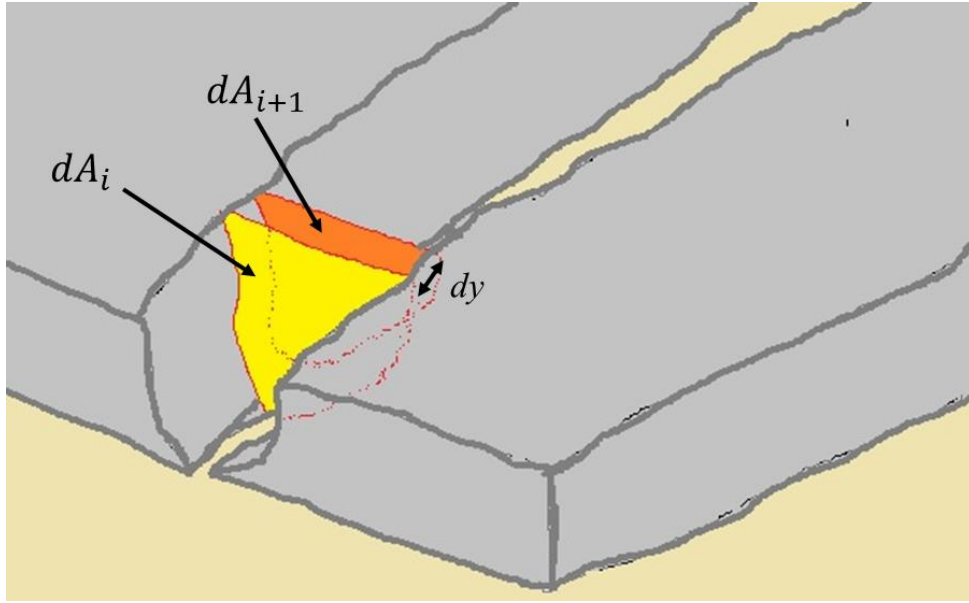
Figure 9-4: Adjacent cross sectional profiles showing respective cross sectional area

9.1.1.2 **Methodology for selection of welding parameters**

An *I*-groove weld configuration with a plate thickness of 1.5mm was used for all the experiments presented in this section. For an *I*-groove, equation 9.4 can be simplified as $dA_i = 1.5 \times Gap_i$. The robot scan step used for the experiments is 1mm. Therefore equation 9.3 can be simplified as follows (equation 9.5):

$$dV_i = \frac{3}{2} \cdot Gap_{avg_i} \tag{9.5}$$

where $Gap_{avg_i} = (Gap_i + Gap_{i+1})/2$ is the average gap calculated between two consecutive profiles and dV_i is the volume of the weld at the ith robot step.

The input value used to control the weld machine is a function of this elemental volume (dV_i). However, from equation 9.6 it is understood that dV_i is proportional to Gap_{avg_i}. Therefore, the final representation for selecting the weld input value can be represented as in equation 9.6.

$$Weld\ input\ values\ = f(Gap_{avg_i}) \tag{9.6}$$

Figure 9-5 shows a schematic of the weld pool and its respective features including the gap between the samples (Gap_{avg_i}) and the expected bead width (y_1). The bead width can be represented as a function of the measured Gap_{avg_i} using equation 9.7.

$$y_1 = k.\,Gap_{avg_i} \tag{9.7}$$
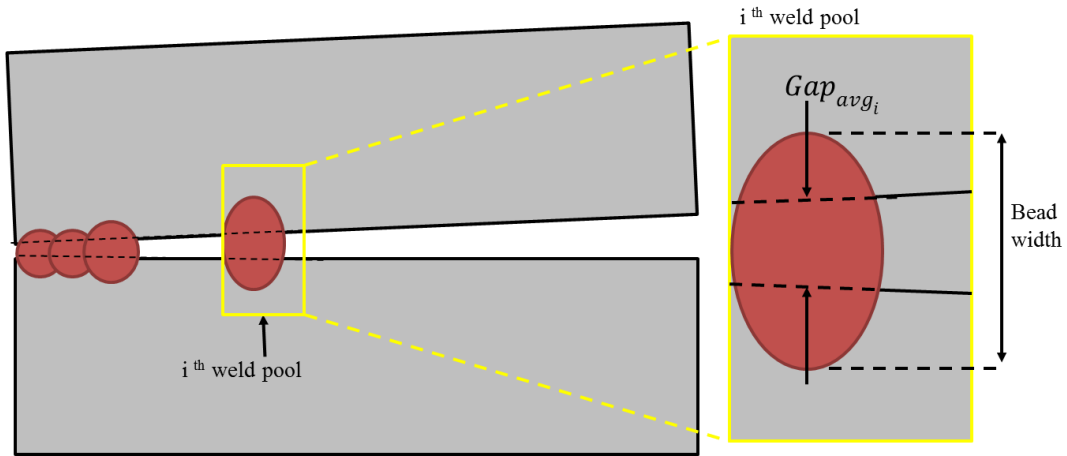
Figure 9-5: Important parameters in the weld pool used for control

Equation 9.8 represents the linear empirical model developed to predict the weld bead width (y_1) (as discussed in Chapter 8). As per the equation, an increase in welding current and duty cycle (x_1, x_4) results in an increased bead width, whereas an increase in the wire feed rate results in a decreased bead width (x_5).

$$y_1 = 5.4045 + 2.8582x_1 + 0.3568x_2 - 0.0004x_3 + 0.8682x_4 - 1.6774x_5 \qquad (9.8)$$

However, it should be noted that for a larger gap, more filler wire has to be used since there is more volume to be filled as the gap increases. Therefore, it is assumed that the wire feed rate has to be increased both for adapting to a variable gap and also to cater for the negative effect on the weld bead width obtained from the linear model.

Using equations 9.6 and 9.7, the following relationships can be obtained.

$$x_1 = k_1 . Gap_{avg_i} + c_1 \qquad (9.9)$$
$$x_4 = k_4 . Gap_{avg_i} + c_4 \qquad (9.10)$$
$$x_5 = k_5 . Gap_{avg_i} + c_5 \qquad (9.11)$$

where $k_1, k_4, k_5, c_1, c_4 \ and \ c_5$ are constants.

9.1.1.3 Intelligent and adaptable weld process control

A set of experiments was carried out with known gaps between the samples and the best combination of the weld input values were selected for each gap. This was used to develop the back propagation model used within this research, so as to select the best weld input values for any gap using interpolation methods. The methodology used for implementation of the adaptive welding process is shown in Figure 9-6.
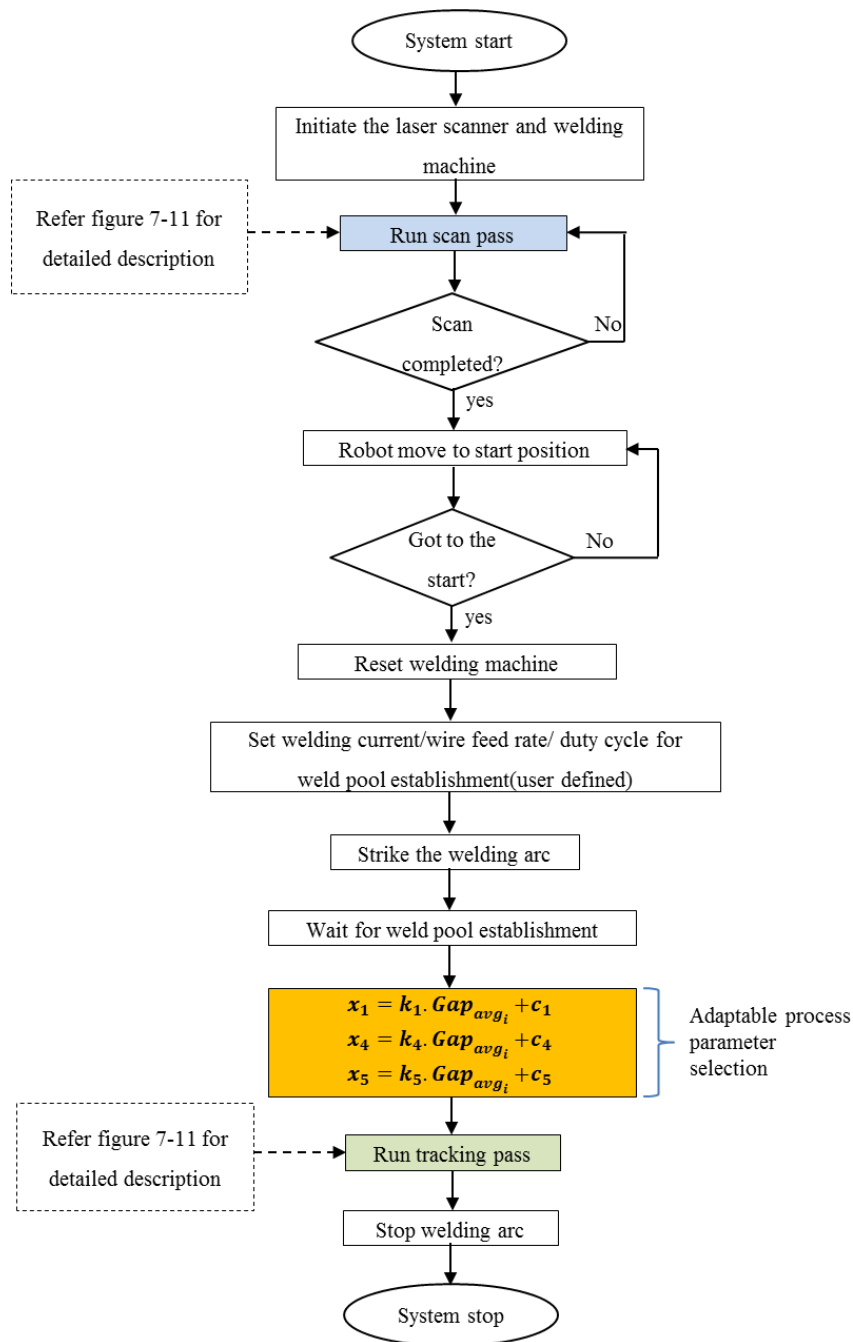
Figure 9-6: Methodology for adaptive welding

As shown in Figure 9-6, the scan pass is carried out using the methodology developed in Chapter 6. The scan-pass gathers the points to be tracked. Then the welding arc is struck with a pre-determined set of process parameters (which are kept constant and are selected based on experience) to establish the weld pool. After that the robot starts moving (the tracking pass) and simultaneously, the adaptive process parameter control algorithm is executed.

To estimate the constant values in equations 9.9, 9.10 and 9.11, a set of experiments were performed using known gaps from 0.5 to 2mm. The experiments were repeated three times to assure repeatability. The gap was set using an industrial grade slip gauge (metric). The best process parameter set for each gap value was established and is given in Table 9-1.

Table 9-1: Results of best combinations of process parameters for known set gaps

Gap (mm)	x1 (A)			x4 (%)			x5 (m/min)		
	Trial 1	Trial 2	Trial 3	Trial 1	Trial 2	Trial 3	Trial 1	Trial 2	Trial 3
0.25	78	76	72	74	80	82	0.69	0.74	0.73
0.5	84	81	78	71	74	78	0.71	0.73	0.82
0.75	83	86	85	63	73	80	0.76	0.83	0.84
1	87	92	81	67	55	74	0.80	0.87	0.92
1.25	92	98	88	59	70	64	0.91	0.96	0.96
1.5	95	97	92	61	67	68	0.96	1.06	1.12
1.75	91	96	96	58	64	66	1.01	1.16	1.24
2	103	99	104	52	57	65	1.06	1.14	1.22

The variation of the process parameters with the set gap is shown in Figure 9-7. As noted from equations 9.12, 9.13 and 9.14, the welding process parameter has a linear relationship with the welding gap.
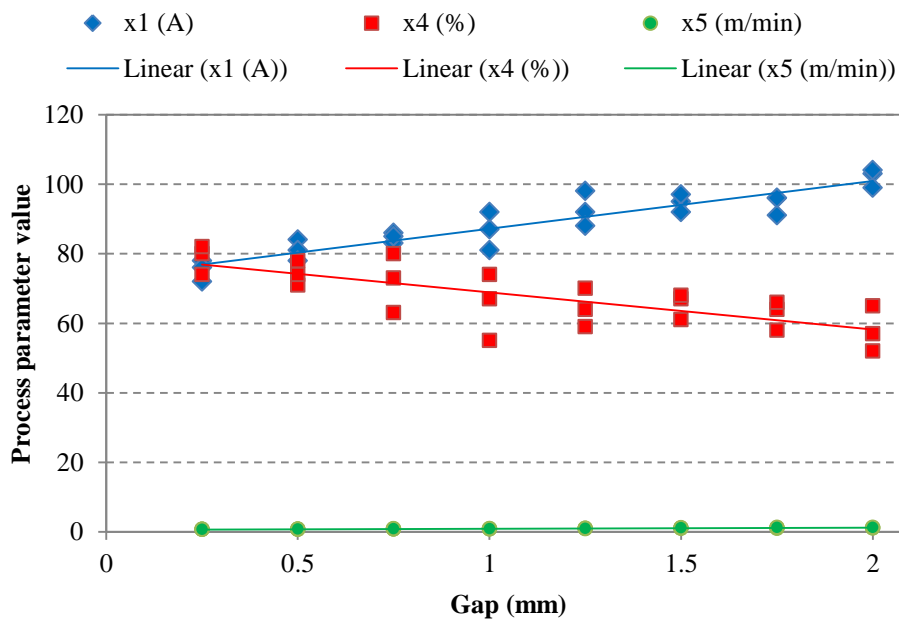
Figure 9-7: Best process parameters obtained against set gap

Therefore, a linear trend was fitted to the data and is shown in Figure 9-7. Coefficients for each equation were obtained from the equation of the relevant trend line. Equations

214

9.9, 9.10 and 9.11, which provided the relationship between the gap and input parameters were then modified as per the trend-lines, and the final derived expressions are given in equation 9.12 (for welding current), 9.13 (for duty cycle) and 9.14 (for wire feed rate).

$$x_1 = 13.76. \, Gap_{avg_i} + 73.43 \qquad (9.12)$$

$$x_4 = -10.67. \, Gap_{avg_i} + 79.58 \qquad (9.13)$$

$$x_5 = 0.268. \, Gap_{avg_i} + 0.625 \qquad (9.14)$$

The above empirical model was used in the robotic system and welding was performed on a variable gap butt joint. The parameters used by the adaptive system for the welding of the varying gap samples are shown in Figure 9-8. The initial constant parameter of the figure corresponds to the establishment of the weld pool (shown in Figure 9-8 (a)) and the varying curve corresponds to the values used during welding.
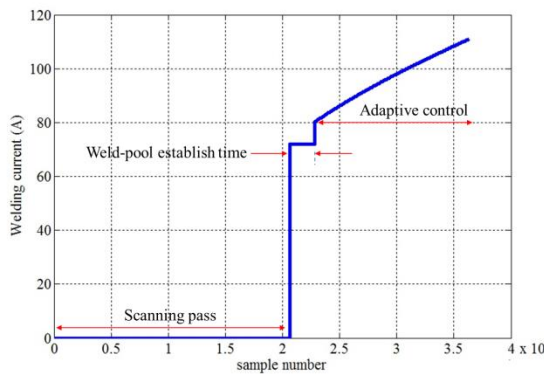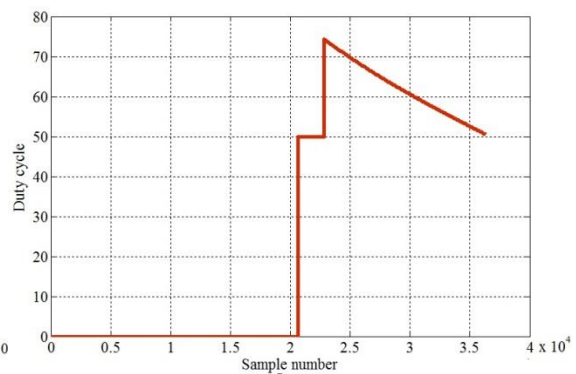
Figure 9.8(a)   Figure 9.8(b)
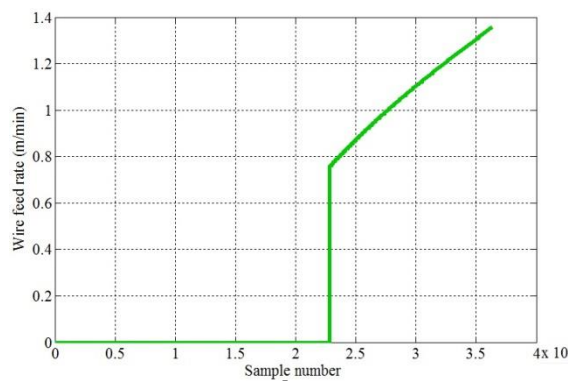
Figure 9.8(c)

Figure 9-8: Adaptive weld process parameter control (a) welding current, (b) duty cycle, (c) wire feed rate

215

9.2 Performance evaluation of different approaches in welding a variable gap butt joint (Case study)

This section considers the welding of the variable gap butt joint (0.25-2.5mm) as a case study for proving the concept of adaptive welding. The methodologies of four different approaches, which can be used to carry out this task, are as follows:

1. Constant weld parameter approach
2. Segmented parameter approach (Used by many industries)
3. Skilled welder's approach
4. Varying parameter approach (Adaptive welding: presented in section 9.1)

9.2.1.1 Constant process parameter approach

The use of constant weld parameters is the most fundamental method that can be adopted with robotic welding. In this case, constant weld parameters are used from the start to the end of the joint. For the purpose of this research, the selected values were, welding current: 90A, Duty cycle: 60%, Pulse frequency: 1kHz, Background current: 45A, Wire feed rate: 0.9mm/s. These values were selected based on the skilled operator's experience.

9.2.1.2 Segmented parameter approach (industrial approach)

The segmented approach for welding of a variable gap joint is achieved by having different welding programmes along the sample. To demonstrate this, the weld joint was divided into four regions as shown in Figure 9-9. For each region a different set of process parameters were selected as listed in Table 9-2.
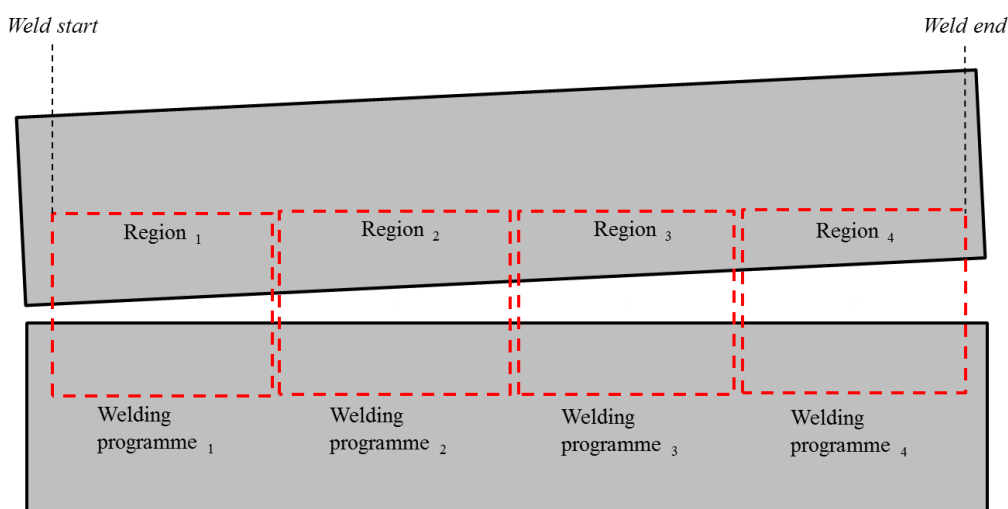
Figure 9-9: Selection of regions for robotic welding

Table 9-2: Different welding programmes selected for welding regions

	Region 1	Region 2	Region 3	Region 4
Welding current (A)	80	84	88	92
Wire feed rate (mm/s)	0.75	0.90	1.05	1.20
Welding speed (mm/s)	1	1.2	1.6	2

9.2.1.3 Skilled welder's approach

The skilled welder uses his/her experience to adapt to the change in either the process or the geometry of the weld. The factors used to calculate the process parameters used by the skilled welder is shown in Figure 9-10.

Welding current was recorded from the welding current sensor. The data obtained from the current sensor is with respect to time rather than sample length. However, since the length of the weld is known (L=150 mm), the time span can be scaled to fit along the length of the weld so that welding current is obtained against the length of the sample. A video of the experiment was recorded which was used to find the welding speed and wire feed frequency. The average welding speed ($Speed_i$) at $position_i$ can be found using equation 9.15 where Δd is selected as 10mm and Δt_i is measured from the videos.

$$Speed_i = \frac{\Delta d}{\Delta t_i} \tag{9.15}$$

L	: length of the weld
Δl_i	: length of the weld from start to the point of interest
Δd	: known distance used to find average speed at point of interest
Gap_1	: gap at start
Gap_n	: gap at end
Δt_i	: time taken to travel through position i
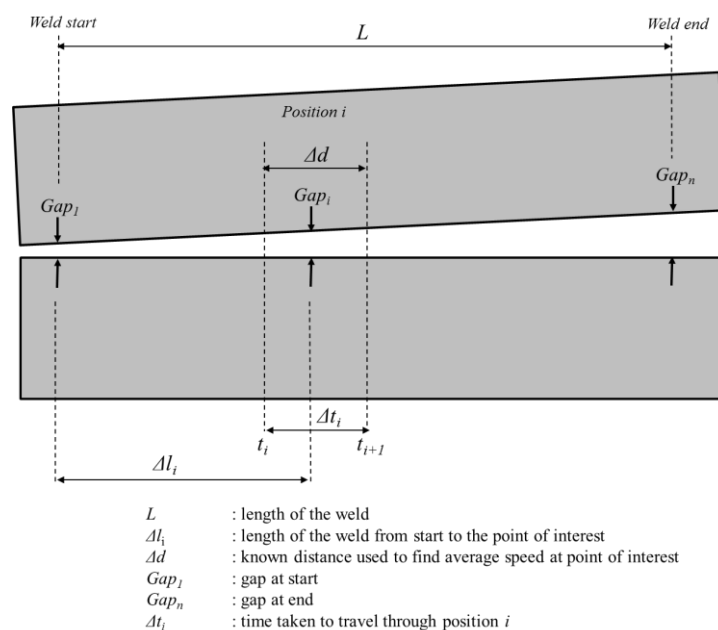
Figure 9-10: Methodology of finding weld process parameters

The number of wire feeds (m_i) between $t = t_i$ and $t = t_{i+1}$ was counted from the videos. Hence, the wire feed rate at *position_i* can be calculated using equation 9.16.

$$Wire\ feed\ rate_i = \frac{m_i}{\Delta t_i} \tag{9.16}$$

Gap_i at *position_i* was calculated according to trigonometric rules using equation 9.17.

$$Gap_i = \frac{Gap_n}{L} \times \Delta l_i \tag{9.17}$$

where $Gap_n = 2.5mm$

The effect of the process parameters (welding current, wire feed rate, arc gap and welding speed) on a varying gap between the samples is shown in Figures 9.11 to 9.13. As can be seen from Figure 9-11, the skilled welder has gradually decreased the welding current with an increase in gap. This is to reduce the heat input with the increase in gap.
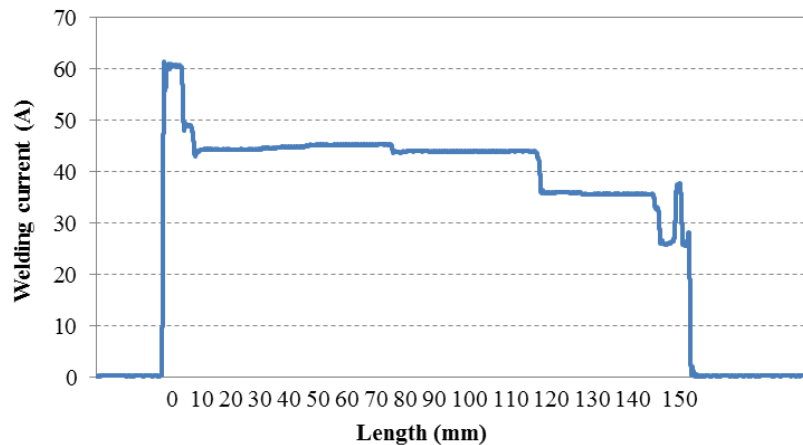
Figure 9-11: Welding current variation along variable gap

As can be seen from Figure 9-12, the skilled welder has gradually increased the wire feed rate with an increase in the weld gap. The increase in wire feed rate helps to address the increase in volume of the weld joint to be filled.
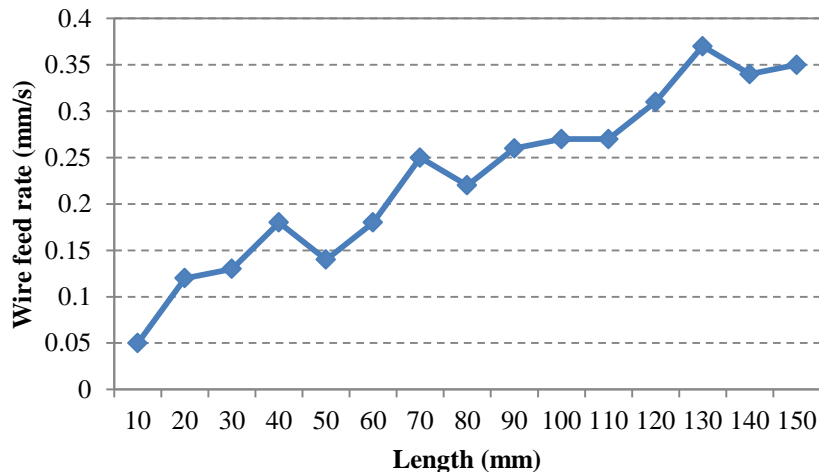
Figure 9-12: Wire feed rate variation along variable gap

As noted from Figure 9-13, the skilled welder has not significantly varied the welding speed (compared to other parameters). This again shows that the skilled welder has prioritized welding current and wire feed rate over welding speed to cater for the geometry variation.
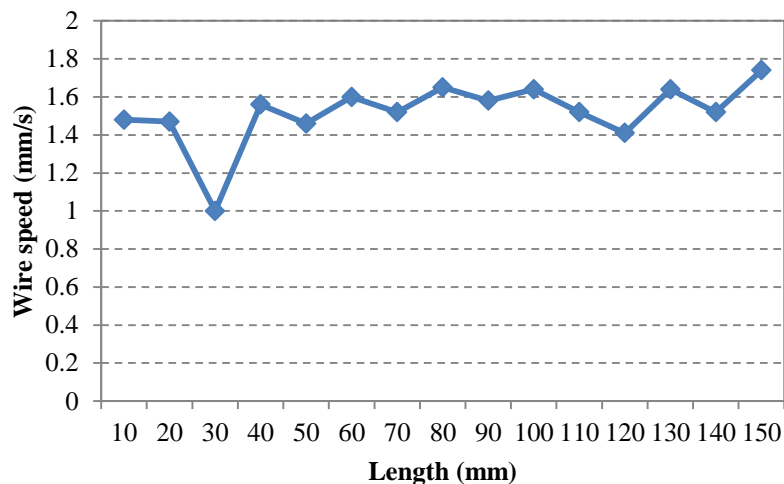
Figure 9-13: Welding speed variation along variable gap

9.3   Comparison of various approaches used for welding of the variable gap joint

The top view of the TIG welded samples obtained from various approaches described in section 9.1 and 9.2 and are shown in Figure 9-14. It should be noted that these images are from the first trial. Images of other two trials are presented in Appendix 8.

As seen from Figure 9-14 (a), the constant parameter approach fails to achieve a continuous weld along the joint. The industrial approach resulted in a better weld than the constant parameter approach but shows a significant heat input at places where two regions meet (during the change of parameters) as seen from Figure 9-14 (b). This may result in varying mechanical properties, such as mechanical strength, along the weld.

219

Figure 9-14 (c) and (d) show the respective welds completed by the skilled welder and through the proposed adaptive control approach. As seen from the images, both methods produce a satisfactory visual weld quality. However, the adaptive control approach shows a more consistent weld bead width compared to the skilled welder. It can also be seen that the adaptive control approach shows a consistent heat affected zone in the weld whereas the other three approaches failed to achieve this.

Figure 9.14(a)

Figure 9.14(b)

Figure 9.14(c)

Figure 9.14(d)

Figure 9-14: Photographic views of the representative welds carried out using different approaches (a) Constant process parameter approach, (b) Segmented parameter (industrial) approach, (c) Skilled welder's approach, (d) Adaptive control approach

The load-extension graphs for the welds carried out using the four different approaches are shown in Figure 9-15. The error bar represents the other two samples from each approach. As can be seen from the figure, the load-extension characteristics of the weld obtained using the adaptive control approach follows a similar trend to that of the weld produced by the skilled welder. It also can be seen from the figure that the maximum extension (at break point) of the samples welded by the skilled welder's approach and novel approach is higher (~20mm) than the segmental and constant parameter approaches. It also can be seen from the figure that skilled welder and the novel approach returns comparatively low (~400N) variation in its respective strength values for the all three trials completed which assures repeatability.

These results demonstrate that the developed adaptive robotic TIG welding system is capable of producing a high quality weld similar to that of a skilled welder.
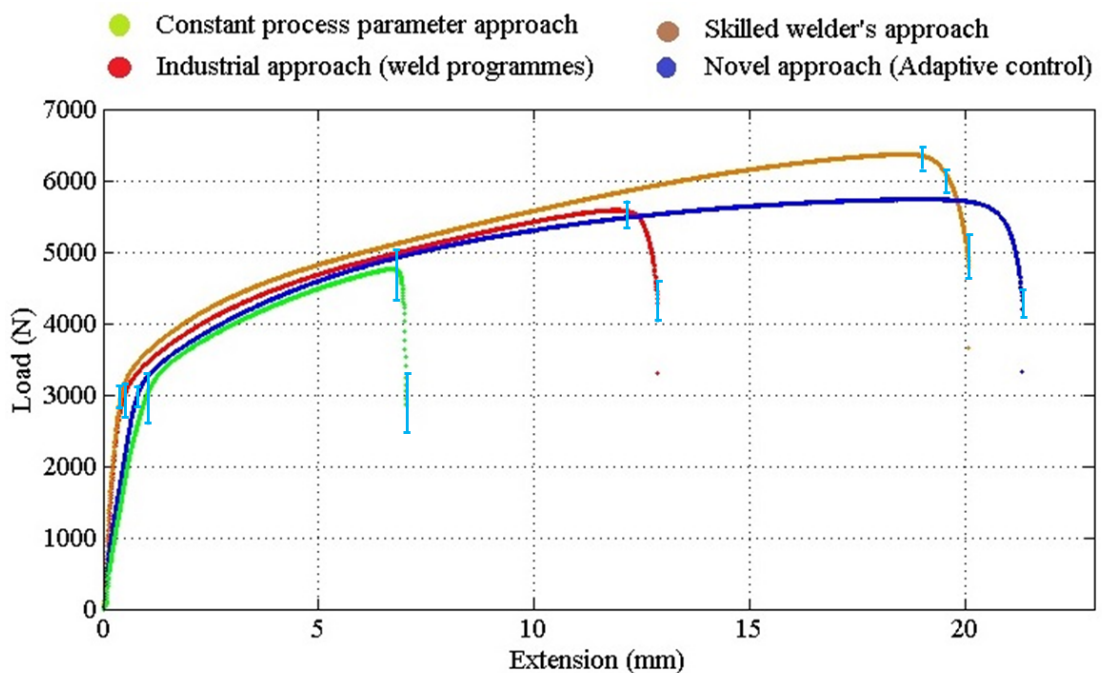
Figure 9-15: Load-extension graphs obtained for welds carried out with industrial approach and continuous welding

9.4   Summary and conclusions

Robotic TIG welding needs an intelligent and adaptable welding approach that is capable of predicting the joint geometry and controlling the process parameters accordingly. This chapter presented the methodology for the development and implementation of adaptable process control in robotic TIG welding of a variable gap

butt joint. A back propagation empirical model was successfully developed and adopted in the robotic TIG welding system.

Various approaches, the constant process parameter approach, the segmented parameter (industrial) approach, the skilled welder's approach and the adaptive control approach, used for the joining two plates into a butt weld were evaluated and reported. The constant parameter approach and segmented approach resulted in poor weld quality. The proposed adaptive control approach returned similar results as the skilled welder. A similar strategy should be used to obtain adaptable robotic welding of complex shapes, especially in the aerospace industry.

10 Conclusions and Future Work

10.1 Conclusions

A novel TIG welding robot (Figure 10-1) with intelligent seam tracking and adaptive weld process control has been created in this thesis.
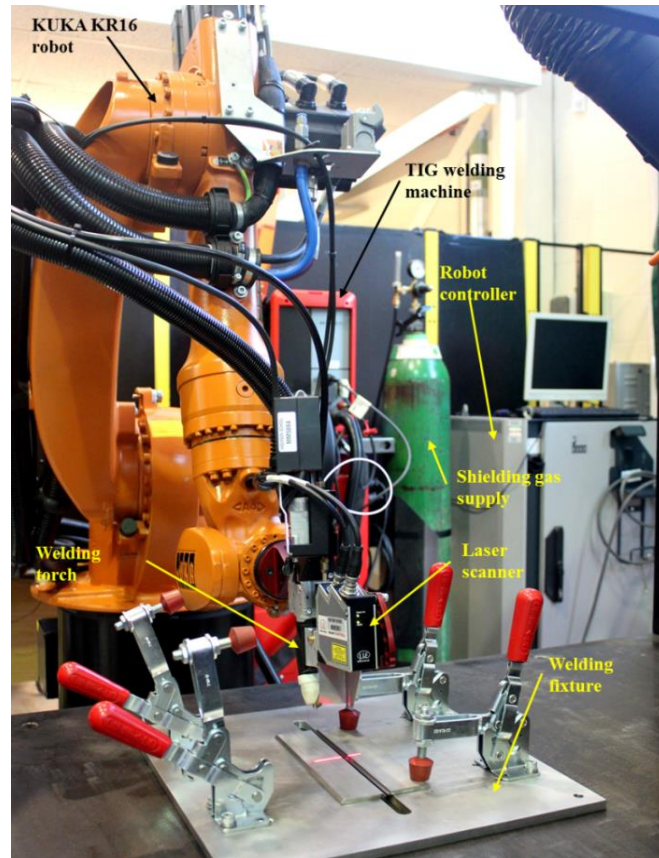
Figure 10-1: Developed robotic TIG welding system as part of the work carried out for the PhD

With reference to the aims and objectives identified in Chapter 1 (section 1.2), the key conclusions based on this research are as follows:

MCRL 3 system integration for robotic welding

It was identified in section 1.1, that an MCRL 3 robotic welding solution was required for the industrialists to transfer research findings to MCRL 4-7. Therefore, work was carried out to complete the system integration of a KUKA KR16 robot, a Fronius Magicwave 4000 welding machine, HKS welding sensors, a National Instruments DAQ system, a Micro Epsilon laser scanner and an IDS camera with a PC. Software was

developed in LabVIEW as part of the work to achieve complete automatic control of the equipment. The software capabilities are as follows:

- Gather information about the welding process using the HKS welding sensors.
- Collect information about the joint geometry, process this information then implement a feature detection algorithm to find the important joint features in real-time (irrespective of the joint profile type, orientation in *3D* or presence of missing data points).
- Point cloud processing algorithm to find joint fit-up and orientation in *3D*.
- Decision making capability based on the joint fit-up.
- Empirical model to predict the Weld quality characteristic.
- Back propagation algorithm for the intelligent selection of the machine settings based on joint geometry.

The developed system is novel and was able to carry out robotic welding with similar weld quality as the skilled manual welder.

Human behaviour analysis for intelligent automation

The work carried out on human skill capturing was focused on understanding the manual TIG welding process, in the context of TIG welding automation. The simultaneous control of key parameters is essential in manual TIG welding to achieve a good weld quality. Welding current and wire feed rate are the most significant parameters that need to be controlled and prioritised to account for variations in joint geometry. By prioritizing the process parameters in a similar manner to the skilled manual welder, it was possible to simplify the control problem in automation. The results collected have indicated that adaptive control of these parameters is vital for successful TIG welding automation. In addition to the prioritisation of the process parameters, the Critical tasks in manual TIG welding were found to be; establishing the weld pool, feeding the filler wire to the weld pool and maintaining a constant weld pool shape. These tasks are mostly controlled by visual observation. It was found that feedback control on the basis of visual information from the weld pool is essential for successful automation of TIG welding.

Evaluation of performance of a laser scanner

A methodology to evaluate the performance capability of a *3D* laser scanner before its use has been introduced. It was found that,

- Stand-off distance, steepness angle, angle of incidence and surface reflectivity were the main variables that affect the data quality obtained from the micro-epsilon scanner.

- The actual work-span of the laser scanner was found to be different from the manufacturer specified values.

- The measurement accuracy of the scanner reached its maximum at the middle of the laser span.

- It was found that ambient lighting affects measurement performance.

- Laser scanners have a critical incidence angle range and a critical steepness angle in which the data acquisition is affected.

A similar experimental procedure can be used for evaluating the performance of any laser scanner prior to its industrial use so that the errors in measurements can be minimized.

3D feature extraction

This thesis also presented a novel algorithm for feature detection of a weld groove with a maximum mean square error (MSE) of 38μm and 127μm in the x and z coordinates respectively. The feature detection algorithm was successfully implemented on three of the most commonly used weld joint types. Further, the real-time gap measurement algorithm was able to measure gaps with an accuracy of ±28μm. Approximation methods were used to remove outliers from noisy data present in the point clouds. Weld joint fit-up in *3D* was quantified and the algorithm was robust enough to extract features accurately at all possible joint set ups for all the selected joint types.

Seam tracking

The feature extraction algorithm was successfully used to find the middle point of the weld joint which was used for the seam tracking process. Seam tracking was

successfully carried out on the three common weld joint types and all possible joint orientations in *3D* space. The developed system can be used successfully to track *3D* complex paths and make "intelligent" decisions about whether the joint fit-up is within suitable tolerances.

Mathematical model development for weld quality prediction

This thesis has been focused on real welding scenarios where two samples are joined together. This is novel compared to previous work which has used a bead-on-plate technique. From the results obtained as part of this work, the relationship between the input and output parameters of the developed TIG welding robotic system was established. It was identified that the duty cycle of the welding current signal is the most important parameter affecting the weld bead dimensions and weld strength. Welding current and wire feed rate also have a significant effect whereas the pulse frequency and background current effects are low. The effect of each process parameter on the weld quality characteristics was quantified separately using ANOVA and equations which map the output parameters with the input parameters were derived. Results have indicated that the interaction model is comparatively more accurate than linear or pure quadratic models.

Adaptable weld process control

It was found from the literature that a limited amount of previous work has successfully implemented an empirical model on a robotic welding system to select the required machine settings intelligently. Therefore, a back propagation algorithm was developed as part of this research and implemented in the software to select the required weld machine settings based on joint geometry feedback. A variable gap weld joint was welded according to four distinct approaches, namely; the constant process parameter approach, the industrial approach, the skilled welder's approach and the novel proposed approach. It was found that the proposed novel algorithm was successful in achieving similar (welding strength and weld bead shape) weld quality as the skilled welder.

In summary, the work presented in this thesis has shown that it is possible to automatically weld butt joints with varying gap. The primary research aims and objectives have also been met through the demonstration of the potential of the developed system (at MCRL 3) and the methodology for intelligent and adaptive

robotic TIG welding to satisfy the industrial needs which have been discussed in sections 1.1,1.2, 2.2 and 2.3.

10.2 Recommendations and future work

The work presented in this thesis has successfully demonstrated the capability of adaptive process control for the improvement of robotic TIG welding. Such an approach can be applied in the welding of aerospace components. Although the work included within this thesis demonstrated adaptive welding according to the feedback from the joint geometry, it can be further developed to be sensitive to other material characteristics such as material type and thickness. Also the work within this thesis has been successfully demonstrated within the constraints of consumables and the hardware/software capabilities. Exploring different equipment (such as different welding machines and robotic equipment) with a similar approach and comparing this with the results presented within this thesis is essential. Gaining access to more complex weld shapes directly from industry could demonstrate the full capability of the developed welding robot.

On-line monitoring of the weld pool and adjusting the robot path or part orientation accordingly to maintain the weld pool at the centre of the seam has a high potential for future research. More investigation on the science of welding needs to be carried out. A detailed study on the factors affecting weld quality is essential to improve the algorithms developed as part of this work. Implementation of heat flow theory and Artificial Intelligence methods to optimize the weld process parameters to further increase the weld quality is another important research area to be prioritised as further work. Selecting the best strategies to reduce deformation in welding of aerospace components could also be derived from applying heat flow theory and finite element methods (FEM).

A mathematical model of the skilled welder has been proposed for development and implemented in the LabVIEW software. This is expected to be used as an error correction model for the welding robot when welding more challenging shapes. In order to achieve this, further in depth study of the manual skilled welder must be undertaken.

A smaller torch and laser scanner is preferred for welding in the aerospace industry. Therefore future work also should be carried out on developing welding end effectors and laser scanners which are more compact in size. Optical systems should be

developed so that the data acquisition performance of the laser scanner is not affected by ambient lighting and shiny components (though the feature extraction algorithm developed in this thesis functions with "inappropriate" data of this type). Moreover, a velocity based control system is proposed for more real-time control instead of the present position based control system.

References

[1] G. Bolmsjo, A. Loureiro, and J. N. Pires, *Welding robots technology, system issues and applications*. Germany: Springer, 2006.

[2] S. B. Chen and J. Wu, *Intelligentized Methodology for Arc Welding Dynamical Process*. Springer Berlin / Heidelberg, 2009, pp. 221–273.

[3] A. Blomdell, G. Bolmsjo, T. Brogardh, M. Isaksson, R. Johansson, M. Haage, K. Nilsson, M. Olsson, Olsson T., A. Robertsson, and J. Wang, "Extending and industrial robot controller," *IEEE robotics and Automation Magazine*, pp. 85–90, 2005.

[4] B.-B. Mathieu, "Top 5 Robotic Applications in the Aerospace Industry," 2014. [Online]. Available: http://blog.robotiq.com/bid/70043/Top-5-Robotic-Applications-in-the-Aerospace-Industry.

[5] "Variations of Jet Engines," 2009. [Online]. Available: http://lyle.smu.edu/propulsion/Pages/variations.htm.

[6] P. Sages, "Adaptive control techniques advance automatic welding," Richmond, Calif, 2010.

[7] M. J. Ward, S. T. Halliday, and J. Foden, "A readiness level approach to manufacturing technology development in the aerospace sector: an industrial approach," *Proceedings of the Institution of Mechanical Engineers, Part B: Journal of Engineering Manufacture*, vol. 226, no. 3, pp. 547–552, Sep. 2011.

[8] K. U. Fu, R. C. Gonzalez, and C. S. G. Lee, *Robotics Control, Sensing, Vision, and Intelligence*. Newyork: McGraw-Hill, 1987.

[9] "ISO 8373:2012," 2012. [Online]. Available: https://www.iso.org/obp/ui/#iso:std:iso:8373:ed-2:v1:en.

[10] M. P. Groover, M. Weiss, R. N. Nagel, and N. G. Odrey, *Industrial Robotics*. Newyork: McGraw-Hill, inc, 1986.

[11] S. B. Niku, *Introduction to Robotics Analysis, Control, Applications*, 2nd ed. John Wiley and Sons Ltd, 2010.

[12] B. Williams, "Introduction to robotics," Ohio, 2004.

[13] K. robot Group, "KRC2 edition 2005: Operating instructions," 2008.

[14] Robotworx, "Robotworx: KUKA KR 16 L6 KRC2," 2009. [Online]. Available: http://www.robots.com/kuka/kr-16-l6.

[15] N. Nayak and A. Ray, *Intelligent Seam Tracking for Robotic Welding*. Springer-Verlag, 1993.

[16]   C. Walker, "Stereo vision basics." [Online]. Available:
        http://chriswalkertechblog.blogspot.co.uk/2014/03/stereo-vision-basics.html.

[17]   X. W.F., Z. Li, C. Perron, and X. W. Tu, "Switching Control of Image Based
        Visual Servoing in an Eye-in-Hand System Using Laser Pointer." [Online].
        Available: http://www.intechopen.com/books/motion-control/switching-control-
        of-image-based-visual-servoing-in-an-eye-in-hand-system-using-laser-pointer.

[18]   A. C. Davies, *The science and practice of welding*, 10th ed. Cambridge
        university press, 1993.

[19]   W. Alloys, "What is TIG welding introduction." [Online]. Available:
        http://www.wballoys.co.uk/TIG/what-is-tig-welding.html.

[20]   M. Massoud, *Data Communication and Networking, A Practical Approach*,
        Internatio. Cengage Learning, Inc, 2011.

[21]   B. Komar, *TCP/IP Network Administration*, 3rd ed. Indianna, USA: SAMs,
        1998.

[22]   E. Preston, "Collaborative robotic plasma arc welding of fabricated titanium
        aero-engine structures," University of Nottigham, 2011.

[23]   Advanced manufacturing research centre, "Shaped metal deposition," 2011.
        [Online]. Available: http://www.amrc.co.uk/featuredstudy/shaped-metal-
        deposition/.

[24]   H. Abulrub, "Automated fusion welding," 2013. [Online]. Available:
        http://www2.warwick.ac.uk/fac/sci/wmg/business/capabilities/database/?id=41.

[25]   I. Brat, "Where Have All the Welders Gone, As Manufacturing and Repair
        Boom?," *The wall street journal*, 2006. [Online]. Available:
        http://online.wsj.com/articles/SB115560497311335781.

[26]   G. D. Uttrachi, "Welder Shortage Requires New Thinking," 2007.

[27]   A. B. Ernest, "Practical Welding Today - Automation training for a new
        workforce," *Fabricators and Manufacturers Association (FMA)*, 2008.

[28]   C. E. Nolen, "Automated Welding Conceptual Study University of Tennessee,"
        University of Tennessee, 2007.

[29]   ESAB, "Welding Automation Submerged Arc, TIG, MIG/MAG," ESAB, Italy,
        2011.

[30]   A. R. Inc, "ABB Robots," 2010. [Online]. Available:
        http://labintsis.com/?page_id=116&lang=en.

[31]   G. Bolmsjö and M. Olsson, "Robotic Arc Welding — Trends and Developments
        for Higher Autonomy," Lund University, 2001.

[32] Welding Technologies Group, "Robotic Welding : The new generation 3G Modular Welding Gun," France.

[33] J. Villafuerte, "New Trends in Robotic Welding Technology," *Canadian Welding Association Journal*, pp. 8–9, 2005.

[34] J. M. Pietrasz, "Robots in gas turbine manufacture," *Computing and control engineering*, no. August, pp. 161–165, 1995.

[35] M. J. Pietrasz, "ROBOTS IN GAS TURBINE MANUFACTURE (INCLUDWG ESPRIT PROJECT INTERROB 6457)," London, 1994.

[36] G. Escobar-Palafox, R. Gault, and K. Ridgway, "Robotic manufacturing by shaped metal deposition: state of the art," *Industrial Robot: An International Journal*, vol. 38, no. 6, pp. 622–628, 2011.

[37] S. Zheng, P. Dayau, and K. Min, "Precision welding for edge buildup and rapid prototyping," Singapore, 1999.

[38] Fraunhofer Institute for Laser Technology ILT, "Laser cladding and integrated process chain for blade tip repairs." [Online]. Available: http://www.ilt.fraunhofer.de/en/publication-and-press/annual-report/2010/annual-report-2010-p79.html.

[39] GKN Aerospace, "Automated robotic welding and assembly," 2010. [Online]. Available: http://www.gkn.com/aerospace/products-and-capabilities/capabilities/metallics/automated-robotic-welding-and-assembly/Pages/default.aspx.

[40] G. Bolmsjo, A. Loureiro, and J. N. Pires, *Welding Robots: Technology, System Issues and Application*, 1st ed. Springer, 2006.

[41] Lincoln Electric, "Surface Tension Transfer."

[42] J. Villafuerte, "Understanding Contact Tip Longevity of Gas Metal Arc Welding," *Welding Journal*, pp. 29–35, 1999.

[43] T. W. Eagar, "Automated welding-research needs," Cambridge, Massachusetts, 1981.

[44] R. Kovacevic, Y. M. Zhang, and S. Ruan, "Sensing and Control of Weld Pool Geometry for Automated GTA Welding," *ASME Transactions*, vol. 117, pp. 201–222, 1995.

[45] K. A. Pietrzak and S. M. Packer, "Vision-Based Weld Pool Width Control," *ASME Transactions*, vol. 116, pp. 86–92, 1994.

[46] G. Huismann, "Effects during the starting period of the MIG process," in *Proceedings of the 7th International Conference on Welding Research*, 2005.

[47]   Lincoln Electric Company, "Waveform Control Technology-Pulsed Spray Metal Transfer," 2004.

[48]   Yaskawa Motoman Robotics, "Motomount Fixture Mounting System." [Online]. Available: http://www.motoman.com/products/positioners/fixturemounting.php. [Accessed: 12-Mar-2012].

[49]   J. J. Madden, M. P. Stowell, P. Wu, H. Li, and L. He, "Welding Fixture with Active Position Adapting Functions," Huazhong University of Science and Technology, 2007.

[50]   P. Sicard and L. M.D., "An approach to an expert robot welding system," in *IEEE Transactions on Systems, Man and Cybernetics*, 2002, pp. 204 – 222.

[51]   J. Xie, "Dual Beam Laser Welding," *Welding Journal*, pp. 223–230, 2002.

[52]   S. Gao, M. Zhao, L. Zhang, and Y. Zou, "Dual-beam structured light vision system for 3D coordinates measurement," in *I7th World Congress on iItelligent Control and Automation (WCICA)*, 2008, pp. 3687–3691.

[53]   Lincoln Electric Company, "Tandem MIG-Garden State Chassis."

[54]   M. Vural, H. F. Muzafferoglu, and U. C. Tapici, "The effect of welding fixtures on welding distortions," *Journal of achievements in manufacturing and materials engineering*, vol. 20, pp. 511–514, 2007.

[55]   H. Long, D. Gery, A. Carlier, and P. G. Maropoulos, "Prediction of welding distortion in butt joint of thin plates," *Material and design*, vol. 30, pp. 4126–4135, 2009.

[56]   B. Catherine, "What is a Collaborative Robot?," 2013. [Online]. Available: http://blog.robotiq.com/bid/66463/What-is-a-Collaborative-Robot.

[57]   Robotiq, "Collaborative robots for welding?," 2014. [Online]. Available: http://blog.robotiq.com/bid/72421/Collaborative-Robots-for-Welding.

[58]   P. G. Ranky, "A method for planning industrial robot networks for automotive welding and assembly lines," *Industrial Robot: An International Journal*, vol. 29, no. 6, pp. 530–537, 2002.

[59]   T. David, T. A. Siewert, K. Matsubuchi, R. Su, L. Flanigan, and T. W. Eager, "In-Space Welding Visions & Realities," in *Thirtieth Space Congress "Yesterday's Vision is Tomorrow's Reality,"* 1993.

[60]   J. D. Majumdar, "Underwater welding – present status and future scope," *Journal of Naval Architecture and Marine Engineering*, vol. 3, pp. 39–48, 2006.

[61]   A. M. Joshi, "Underwater welding," Bombay, 2007.

[62]   Wikipedia, "Hyperbaric welding," 2014. [Online]. Available: http://en.wikipedia.org/wiki/Hyperbaric_welding.

[63]   K. Watson, "Extra-Vehicular Activity Welding Experiment," alabama, 1989.

[64]   A. Ryberg, M. Ericsson, A.-K. Christiansson, K. Eriksson, J. Nilsson, and M. Larsson, "Stereo vision for path correction in off-line programmed robot welding," in *Industrial Technology (ICIT), 2010 IEEE International Conference on*, 2010, pp. 1700–1705.

[65]   S. Wei, H. Ma, T. Lin, and S. Chen, "Autonomous guidance of initial welding position with 'single camera and double positions' method," *Sensor Review*, vol. 30, no. 1, pp. 62–68, 2010.

[66]   M. Dinham and G. Fang, "Low cost simultaneous calibration of a stereo vision system and a welding robot," in *IEEE International Conference on Robotics and Biomimetics (ROBIO)*, 2010, pp. 1452–1456.

[67]   R. Y. Tsai, "A Versatile Camera Calibration Techniaue for High-Accuracy 3D Machine Vision Metrology Using Off-the-shelf TV Cameras and Lenses," *IEEE Journal of robotics and automation*, vol. RA-3, no. 4, 1987.

[68]   J. Heikkila, "Flexible camera calibration by viewing a plane from unknown orientations," in *The Proceedings of the Seventh IEEE International Conference on Computer Vision*, 1999, vol. 1, pp. 666–673.

[69]   Z. Zhang, "A Flexible New Technique for Camera Calibration," *IEEE Transactions on pattern analysis and machine intelligence*, vol. 22, no. 11, pp. 1330–1334, 2000.

[70]   P. Xu, X. Tang, and S. Yao, "Application of circular laser vision sensor (CLVS) on welded seam tracking," *Journal of Materials Processing Technology*, vol. 205, no. 1–3, pp. 404–410, Aug. 2008.

[71]   M. Dinham and G. Fang, "A low cost hand-eye calibration method for arc welding robots," in *Robotics and Biomimetics (ROBIO), 2009 IEEE International Conference on*, 2009, pp. 1889–1893.

[72]   Y. C. Shiu and S. Ahmad, "Calibration of wrist-mounted robotic sensors by solving homogeneous transform equations of the form AX=XB," in *Robotics and Automation, IEEE Transactions on*, 1989, vol. 5, no. 1, pp. 16–29.

[73]   F. Dornaika and R. Horaud, "Simultaneous robot-world and hand-eye calibration," in *IEEE Transactions on Robotics and Automation*, 1998, vol. 14, no. 4, pp. 617–622.

[74]   L. Suyi and W. Guorong, "Fast Calibration for Robot Welding System with Laser Vision," in *EEE Conference on Robotics, Automation and Mechatronics*, 2008, pp. 706–710.

[75] L. He-xi, S. Yong-hua, W. Guo-rong, and Z. Xiao-xi, "Automatic Teaching of Welding Robot for 3-Dimensional Seam Based on Ant Colony Optimization Algorithm," in *Intelligent Computation Technology and Automation, 2009. ICICTA '09. Second International Conference on*, 2009, vol. 3, pp. 398–402.

[76] P. Komi, "Stereo Imaging and 3D Accuracy Assessment," Loughborough University, 2005.

[77] Y. K. Liu, W. J. Zhang, and Y. M. Zhang, "A Tutorial on Learning Human Welder ' s Behavior : Sensing , Modeling , and Control," Kentucky, 2014.

[78] J. Van Essen, M. Van der Jagt, N. Troll, M. Wanders, M. S. Erden, T. Van Beek, and T. Tomiyama, "Identifying Welding Skills for Robot Assistance," in *IEEE/ASME International Conference on Mechtronic and Embedded Systems and Applications*, 2008, pp. 437–442.

[79] V. Malin, "A new approach to the definition and classification of welding automation," in *2nd International Conference on Development in Automated and Robotic Welding*, 1987, pp. 179–190.

[80] S. B. Chen, D. B. Zhao, Y. J. Lou, and L. Wu, "Computer Vision Sensing and Intelligent Control of Welding Pool Dynamics," in *Robotic welding, intelligence and automation*, vol. 299, T.-J. Tarn, C. Zhou, and S.-B. Chen, Eds. Springer Berlin / Heidelberg, 2004, pp. 25–55.

[81] M. Steve, C. H. L. Raymond, O. Kalin, G. Shixiang, D. David, N. Calvin, and A. Tao, "Realtime HDR (High Dynamic range) Video for Eyetap Wearable Computers, FPGA-based seeing Aids and Glasseyes (EYETAPS)," in *25th IEEE Canadian Conference on Electrical and Computer Engineering (CCECE)*, 2012.

[82] Y. M. Zhang and L. Kvidahl, "Skilled Human Welder Intelligence Modeling and Control : Part II — Analysis and," *The welding journal*, vol. 93, pp. 162–170, 2014.

[83] S. Vaughan, "Taking a closer look at welding robotics and automation - Welding automation is gaining momentum," *The Fabricators and Manufacturers Association (FMA)*, 2002.

[84] S. Tachi, "Robotics Research toward Next-Generation Human-Robot Networked Systems," in *Proceedings of the 35th International Symposium on Robotics (ISR2004)*, 2004, pp. 1–8.

[85] R. Koeppe, D. Engelhardt, A. Hagenauer, P. Heiligensetzer, B. Kneifel, A. Knipfer, and K. Stoddard, "Robot-Robot and Human-Robot Cooperation in Commercial Robotics Applications," *Robotics research-Springer Tracts in Advanced Robotics*, vol. 15, pp. 202–216, 2005.

[86] A. Mahajan and F. Figueroa, "Intelligent seam tracking using ultrasonic sensors for robotic welding," *Robotica*, vol. 15, no. 3, pp. 275–281, May 1997.

[87] E. L. Estochen, C. P. Neuman, and F. B. Prinz, "Application of Acoustic Sensors to Robotic Seam Tracking," *IEEE transactions on industrial electronics*, vol. 31, no. 3, pp. 219–224, 1984.

[88] FANUC Robotics, "Through Arc Seam Tracking (TAST)," 2005.

[89] A. Robotics, "ABB Robotics Introduces a 'Through-the-Arc' Seam-Tracking System," 2010. [Online]. Available: http://weldingdesign.com/equipment-automation/news/abb-robotics-through-arc-seam-tracking-system-0629.

[90] M. de Graaf, R. Aarts, B. Jonker, and J. Meijer, "Real-time seam tracking for robotic laser welding using trajectory-based control," *Control Engineering Practice*, vol. 18, no. 8, pp. 944–953, Aug. 2010.

[91] B. Cyganek and P. Siebert, *An introduction to 3D computer vision techniques and algorithms*, 2nd ed. Wiley Subscription Services, Inc., A Wiley Company, 2009.

[92] J. Wang, Q. Chen, and Z. Sun, "Multi-pass weld profile detection for spherical tank through 'quasi double cameras' stereovision sensor," in *Proceedings of the International Conference on Information Acquisition*, 2004, pp. 376–379.

[93] L. Zhou, T. Lin, and S. B. Chen, "Autonomous Acquisition of Seam Coordinates for Arc Welding Robot Based on Visual Servoing," *Journal of intelligence and robotic systems*, vol. 47, no. 3, pp. 239–255, 2006.

[94] T. De, X., Min, T., Xiaoguang, Z. and Zhiguo, "Seam tracking and visual control for robotic arc welding based on structured light stereovision," *International journal of automation and computing*, vol. 1, no. 1, pp. 64–75, 2004.

[95] T. Borangiu and A. Dumitrache, "Robot Arms with 3D Vision Capabilities," Bucharest, Romania, 2009.

[96] M. J. Tsai, W. Lee, and N. Ann, "Machine Vision Based Path Planning for a Golf Club Head Welding System," *Journal of robotics and computer integrated manufacturing*, vol. 27, no. 4, pp. 843–849, 2011.

[97] P. Kim, S. Rhee, and C. H. Lee, "Automatic teaching of welding robot for free-formed seam using laser vision sensor," *Optics and Lasers in Engineering*, vol. 31, no. 3, pp. 173–182, Mar. 1999.

[98] J. Yu and S. Na, "A study on vision sensors for seam tracking of height-varying weldment. Part 1: Mathematical model," *Mechatronics*, vol. 7, no. 7, pp. 599–612, Oct. 1997.

[99] J. Yu and S. Na, "A study on vision sensors for seam tracking of height-varying weldment. Part 2: Applications," *Mechatronics*, vol. 8, no. 1, pp. 21–36, Feb. 1998.

[100] J. E. Agapakis, J. M. Katz, J. M. Friedman, and G. N. Epstein, "Vision-Aided Robotic Welding: An Approach and a Flexible Implementation," *The International Journal of Robotics Research*, vol. 9, no. 5, pp. 17–34, Oct. 1990.

[101] B. Bahr, J. T. Haung, and K. F. Ehmann, "Sensory guidance of seam tracking robots," *Journal of Robotic Systems*, vol. 11, no. 1, pp. 67–76, 1994.

[102] M. Fridenfalk and G. Bolmsjö, "Design and Validation of a Universal 6D Seam Tracking System in Robotic Welding Based on Laser Scanning," 2006.

[103] R. Modic, "Machine vision system for adaptive robotic welding Product datasheet," 2008.

[104] Servo-robot Inc, "Arc Seam Tracking," 2014. [Online]. Available: http://servorobot.com/manufacturing-solutions/arc-seam-tracking/.

[105] Meta Vision Systems Ltd, "Robotic Seam Tracking." [Online]. Available: http://www.meta-mvs.com/seam-tracking.htm. [Accessed: 02-Apr-2014].

[106] Liburdi Group of Companies, "The Liburdi Seam Tracker," 2014. [Online]. Available: http://www.liburdi.com/LiburdiAutomation/seam-tracker/default.aspx.

[107] V. Welding, "Welding robots." [Online]. Available: http://www.valkwelding.com/en/welding-automation/welding-robots. [Accessed: 08-Aug-2014].

[108] F. R. America, "Adaptive Welding," 2005.

[109] Micro-epsilon, "Laser sensors,IR temperature sensors,Displacement and position sensors,Color sensors," 2010. [Online]. Available: http://www.micro-epsilon.com/index.html.

[110] V. G. Nick, C. Steven, B. Philip, and K. Jean-, "A Performance Evaluation Test for Laser Line Scanners on CMMs," *Optics and Lasers in Engineering*, vol. 47, no. 3–4, pp. 336–342, 2009.

[111] W. Boehler, M. B. Vicent, A. Marbs, and S. Technology, "Investigating laser scanner accuracy," in *The 6th CIPA Symposium at Antalya*, 2003, no. October.

[112] G. E. S. Gerald F. Marshall, *Handbook of Optical and Laser Scanning*. 2004.

[113] D. D. Lichti and B. R. Harvey, "The Effects of Reflecting Surface Material Properties on Time of Flight Laser Scanner Measurements," in *Symposium on Geospatial Theory, Processing and Applications*, 2002.

[114] C. T. Yang S., Cho M., Lee H., "Weld line detection and process control for welding automation," *Measurement science and technology*, vol. 18, pp. 819–826, 2007.

[115] I. Kim, J. Son, S. Lee, and P. K. D. V. Yarlagadda, "Optimal design of neural networks for control in robotic arc welding," *Robotics and computer-integrated manufacturing*, vol. 20, pp. 57–63, 2004.

[116] Computer weld technologies Inc, "ADM IV Arc Data Monitor," 2014. [Online]. Available: http://www.cweldtech.com/product-ADM4.html.

[117] Weldindustry AS, "WeldEye Quality System," 2014. [Online]. Available: http://www.weldindustry.com/index.php/products-topmenu-33/weldeye-quality-system.

[118] ETher NDE, "WeldCheck," 2014. [Online]. Available: http://www.ethernde.com/instruments/flaw-detectors/weldcheck.

[119] X. M. Zeng, J. Lucas, and M. T. C. Fang, "Use of neural networks for parameter prediction and quality inspection in TIG welding," *Transactions of the Institute of Measurement and Control*, vol. 15, no. 2, pp. 87–95, Jan. 1993.

[120] M. Miller, B. Mi, A. Kita, and I. C. Ume, "Development of automated real-time data acquisition system for robotic weld quality monitoring," *Mechatronics*, vol. 12, no. 9–10, pp. 1259–1269, Nov. 2002.

[121] E. Karadeniz, U. Ozsarac, and C. Yildiz, "The effect of process parameters on penetration in gas metal arc welding process," *Material and design*, vol. 28, pp. 649–656, 2007.

[122] G. Singh, K. Singh, and J. Singh, "Mathematical Modeling of the Effect of Welding Parameters on Penetration In Submerged Arc," *International Journal of Engineering Studies*, vol. 2, no. 3, pp. 313–320, 2010.

[123] H. J. Park, D. C. Kim, M. J. Kang, and S. Rhee, "Optimisation of the wire feed rate during pulse MIG welding of Al sheets," *Journal of of Achievements in Materials and Manufacturing Engineering*, vol. 27, no. 1, pp. 83–86, 2008.

[124] I. S. Kim, K. J. Son, Y. S. Yang, and P. K. D. V. Yarlagadda, "Sensitivity analysis for process parameters in GMA welding processes using a factorial design method," *International journal of machine tools & manufacture*, vol. 43, pp. 763–769, 2003.

[125] M. S. Ali and P. V. Kumar, "Affect of Different Input Parameters on Weldment Characteristics in Tungsten Inert Gas (TIG) Welding," *American Journal of Scientific Research*, vol. 12, no. 12, pp. 153–165, 2010.

[126] P. Kumari, K. Archna, and R. S. Parmar, "Effect of Welding Parameters on Weld Bead Geometry in MIG Welding of Low Carbon Steel," *International Journal of Applied Engineering Research*, vol. 6, no. 2, pp. 249–258, 2011.

[127] P. K. Palani and N. Murugan, "Development of mathematical models for prediction of weld bead geometry in cladding by flux cored arc welding,"

International journal of advanced manufacturing technology, vol. 30, pp. 669–676, 2006.

[128] D. W. Becker and C. M. Adams, "Investigation of pulsed GTA welding parameters," in *59th annual meeting of AWS*, 1978, pp. 134–138.

[129] Y. . Tarng, H. . Tsai, and S. . Yeh, "Modeling, optimization and classification of weld quality in tungsten inert gas welding," *International Journal of Machine Tools and Manufacture*, vol. 39, no. 9, pp. 1427–1438, Sep. 1999.

[130] S. C. Juang and Y. S. Tarng, "Process parameter selection for optimizing the weld pool geometry in the tungsten inert gas welding of stainless steel," *Journal of Materials Processing Technology*, vol. 122, pp. 33–37, 2002.

[131] E. Batanouny, "Design and Manufacture of a Control Unit for Monitoring Welding Parameters in Resistance Spot Welding," *International Journal of Engineering & Technology*, vol. 10, no. 1, pp. 36–42.

[132] K. Anderson, G. E. Cook, G. Karsai, and K. Ramaswamy, "Artificial neural networks applied to arc welding process modelling and control," in *IEEE transactions on industry automation*, 1990, pp. 824–830.

[133] A. Jaleel, "Grey-based Taguchi Method for optimization of Bead Geometry in Laser bead-on-plate Welding," *Advances in Production Engineering & Management*, vol. 5, no. 4, pp. 225–234, 2010.

[134] T. Greyjevo, Optimizacija Geometrije, U. Esme, M. Bayramoglu, Y. Kazancoglu, and S. Ozgun, "Optimization of Weld Bead Geometry in TIG Welding Process Unisng Grey-relation Analysis and Taguchi method," *Materials and technology*, vol. 43, no. 3, pp. 143–149, 2009.

[135] K. Y. Benyounis and a. G. Olabi, "Optimization of different welding processes using statistical and numerical approaches – A reference guide," *Advances in Engineering Software*, vol. 39, no. 6, pp. 483–496, Jun. 2008.

[136] I. S. Kim, A. Basu, and E. Siores, "Mathematical models for control of weld bead penetration in the GMAW process," *International journal of advanced manufacturing technology*, vol. 12, pp. 393–401, 1996.

[137] I. S. Kim, K. J. Son, and P. K. D. V. Yarlagadda, "A study on the quality improvement of robotic GMA welding process," *Robotics and computer-integrated manufacturing*, vol. 19, pp. 567–572, 2003.

[138] S. Pal, S. K. Pal, and A. K. Samantaray, "Artificial neural network modelling of weld joint strength of a pulsed metal inert gas welding process using arc signals," *Journal of Materials Processing Technology*, vol. 202, pp. 464–474, 2008.

[139] Q. Wang, D. Xu, and I. Science, "Robust features extraction for lap welding seam tracking system," in *IEEE Youth Conference on Information, Computing and Telecommunication*, 2009, pp. 319–322.

[140] H. Engström and A. Kaplan, "Adaptive process control in laser robotic welding," 2008.

[141] H. B. Chen, T. Lin, S. B. Chen, and J. F. Wang, "Adaptive Control on Wire Feeding in Robot Arc Welding System," in *IEEE Conference on Robotics, Automation and Mechatronics*, 2008, pp. 119–122.

[142] Fronius, "Magic Wave 4000." [Online]. Available: http://www.fronius.com/cps/rde/xchg/SID-C7973E01-C70ABDB8/fronius_international/hs.xsl/79_9115_ENG_HTML.htm#.VGTzyvnGrLk.

[143] N. Instruments, "Parts of a PXI System," 2014. [Online]. Available: http://www.ni.com/white-paper/4811/en/.

[144] HKS-ProzeBtechnik GmbH, "HKS sensors for welding data monitoring: technical data/operating instructions/ calibration certificates," Germany, 2008.

[145] C. Andrew, S. and Daniel, "Cameras for Monitoring Welding," *Welding Design and Fabrication*, 2011. [Online]. Available: http://weldingdesign.com/equipment-automation/main/CamerasForMonitoring/#.UDuXEsdHzBw.mendeley. [Accessed: 27-Jun-2012].

[146] IDS, "IDS uEye XS Series - Ultra compact USB Camera with Integrated Lens and RichFeature Set," 2011. [Online]. Available: http://www.stemmer-imaging.co.uk/en/products/series/ids-ueye-xs/.

[147] X. Wen-Fang, L. Zheng, P. Claude, and T. Xiao-Wei, "Switching Control of Image Based Visual Servoing in an Eye-in-Hand System Using Laser Pointer," in *Motion Control*, F. Casolo, Ed. 2010.

[148] P. Manorathna, P. Ogun, S. Marimuthu, L. Justham, and M. Jackson, "Performance evaluation of a 3D laser scanner for industrial applications," in *IEEE international conference on information and automation for sustainability*, 2014.

[149] Micro-epsilon, "scanCONTROL 2D/3D laser scanner (laser profile sensors)."

[150] KUKA Robot Group, "KUKA KR 16 L6-2," 2014. [Online]. Available: http://www.kuka-robotics.com/en/products/industrial_robots/low/kr16_l6_2/.

[151] KUKA system technology, "KUKA.Ethernet KRL XML 1.2," 2012.

[152] F. Duan, Y. Zhang, N. Pongthanya, K. Watanabe, H. Yokoi, and T. Arai, "Analyzing human skill through control trajectories and motion capture data," in *IEEE International Conference on Automation Science and Engineering*, 2008, pp. 454–459.

[153] The British Psychological Society, "Code of ethics and conduct," 2009.

[154] P. C. Miller, "In search of smarter welding systems," *Tooling & Production*, 1994.

[155] E. Nadernejad and S. Sharifzadeh, "Edge Detection Techniques : Evaluations and Comparisons," *Applied Mathematical Sciences*, vol. 2, no. 31, pp. 1507–1520, 2008.

[156] L. W. S. . Chen, D. B. Zhao, and Y. J. Lou, "Computer Vision Sensing and Intelligent Control of Welding Pool Dynamics," *Robotic welding and intelligent automation*, vol. 299, pp. 25–55, 2004.

[157] L. P. Connor, *Welding handbook volume 1: Welding technology*, 8th ed. American welding society, 1991.

Appendix 1: Fronius MagicWave 4000 specifications

Mains voltage	3 x 400 V
Mains voltage tolerance	± 15%
Mains frequency	50/60 Hz
Primary continuous power	15.5 kVA
Welding current range	3-400A
Welding current range at the electrode	10-400A
Open circuit voltage	90 V
Working voltage range	10.1-26.0 V
Working voltage range at the electrode	20.4-36.0 V
Striking voltage	9.5kV
Degree of protection	IP23
Type of cooling	AF
Insulation class	F
EMC emission class	A
Dimensions	625/290/705mm
Weight	58.2 kg
Mark of conformity	S, CE

Appendix 2: Calibration certificates of welding sensors

Kalibrierschein/
Certificate of calibration

HKS
PROZESSTECHNIK

Datum/Date   17.9.2012

Sensor

Bezeichnung/Name	Prozeßsensor	Typ/Type	P 1000
Fabriknr./Fabrication no.	10212263	Hersteller/Producer	HKS-Prozesstechnik GmbH

Kalibriertabelle des Stromkanals/Calibration table of the current channel

Kalibrator/Calibrator A (DC)	Sensor V (DC)	Anzeigewert/Display value A (DC)	Abweichung/Difference A (DC)
450,0	4,50	450	0,0
300,0	3,00	300	0,0
200,0	2,00	200	0,0
100,0	1,00	100	0,0
50,0	0,50	50	0,0
0,0	0,00	0	0,0
-50,0	-0,50	-50	0,0
-100,0	-1,00	-100	0,0
-200,0	-2,00	-200	0,0
-300,0	-3,00	-300	0,0
-450,0	-4,50	-450	0,0
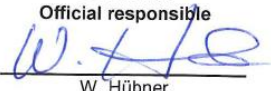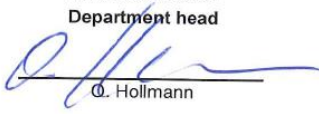
Der Anzeigewert wird durch das Messsystem (WeldQAS, WeldAnalyst) wie folgt berechnet./The display value will be calculated by the measurement system (WeldQAS, WeldAnalyst like followed.

Anzeigewert/Display value =   **100,00**   x Sensor -   **0,00**

Außschließlich der Anzeigewert wird vom Messsystem weiter verarbeitet, z.B. überwacht und abgespeichert./Only the display value will be used for monitor and storage operations.

Kalibrator/Calibrator		Bedingungen/Enviroment	
Bezeichnung/Name	HIOK 7011	Temperatur/Temperature	23 °C
kalibriert/calibrated	12/2011		
Fabriknr./Fabrication no.	70425117		
Anweisung/Instruction	HKS-Kalib 1		

Bemerkungen/Comment

Der Stromkanal des kalibrierten Sensors verfügt über die im Datenblatt angegebene Genauigkeit.   The current channel of this sensor has the precision like written in the technical specification.
Das Protokoll entspricht der DIN EN ISO 9001/9002; DIN EN 729-2 bzw. den DVS-Merkblättern 0714 und 3009./
Certificate of calibration in accordance with DIN EN ISO 9001/9002, DIN EN 729-2, DVS-Flyers 0714 and 3009.

Stempel/Mark	Bearbeiter/ Official responsible	Verantwortlicher/ Department head
HKS-Prozesstechnik GmbH Heinrich-Damerow-Str. 2, 06120 Halle Tel: 0345 68309-0, Fax: -49 www.hks-prozesstechnik.de	W. Hübner	O. Hollmann

HKS-Prozesstechnik GmbH
Heinrich-Damerow-Str. 2
D-06120 Halle

Tel./Phone: 0049 (0) 345 683090
FAX: 0049 (0) 345 6830949
home: www.hks-prozesstechnik.de

Kalibrierschein/
Certificate of calibration

Datum/Date   17.9.2012

HKS
PROZESSTECHNIK

Sensor

Bezeichung/Name	Prozeßsensor	Typ/Type	P1000	
Fabriknr./Fabrication no.	10212263	Hersteller/Producer	HKS-Prozesstechnik GmbH	

Kalibriertabelle des Spannungskanals/Calibration table of the voltage channel

Kalibrator/Calibrator V (DC)	Sensor V (DC)	Anzeigewert/Display value V (DC)	Abweichung/Difference V (DC)
50,00	5,00	50,0	0,0
25,00	2,50	25,0	0,0
20,00	2,00	20,0	0,0
15,00	1,50	15,0	0,0
10,00	1,00	10,0	0,0
0,00	0,00	0,0	0,0
-10,00	-1,00	-10,0	0,0
-15,00	-1,50	-15,0	0,0
-20,00	-2,00	-20,0	0,0
-25,00	-2,50	-25,0	0,0
-50,00	-5,00	-50,0	0,0

Der Anzeigewert wird durch das Messsystem (WeldQAS, WeldAnalyst) wie folgt berechnet./The display value will be calculated by the measurement system (WeldQAS, WeldAnalyst like followed.

Anzeigewert/Display value =   **10,00**   x Sensor -   **0,00**

Außschließlich der Anzeigewert wird vom Messsystem weiter verarbeitet, z.B. überwacht und abgespeichert./Only the display value will be used for monitor and storage operations.

Kalibrator/Calibrator

Bezeichung/Name	HIOK 7011
kalibriert/calibrated	12/2011
Fabriknr./Fabrication no.	70425117
Anweisung/Instruction	HKS-Kalib 1

Bedingungen/Enviroment

Temperatur/Temperature   23 °C

Bemerkungen/Comment

Der Spannungskanal des kalibrierten Sensors verfügt über die im Datenblatt angegebene Genauigkeit. The voltage channel of this sensor has the precision like written in the technical specification.
Das Protokoll entspricht der DIN EN ISO 9001/9002; DIN EN 729-2 bzw. den DVS-Merkblättern 0714 und 3009./ Certificate of calibration in accordance with DIN EN ISO 9001/9002, DIN EN 729-2, DVS-Flyers 0714 and 3009.

Stempel/Mark

HKS-Prozesstechnik GmbH
Heinrich-Damerow-Str. 2, 06120 Halle
Tel: 0345 68309-0, Fax: -49
www.hks-prozesstechnik.de

Bearbeiter/
Official responsible

W. Hübner

Verantwortlicher/
Department head

C. Hollmann

Appendix 3: Sample XML file

```xml
<Robot>
 <Data>
  <ActPos   X="" Y="" Z="" A="" B="" C="" />
  <LastPos  X="" Y="" Z="" A="" B="" C="" />
 </Data>
 <Status />
 <Mode />
 <Complex>
  <Tickcount />
 </Complex>
 <RobotType>
  <Robot>
   <Type></Type>
   <Serial></Serial>
  </Robot>
 </RobotType>
 <Any A="" B="" C="" />
</Robot>
```

Appendix 4: Experiments for real-time video capturing of welding area

As discussed in Chapter 3 there are few techniques that are recommended to use to view the weld pool. Some of those methods were experimented and the results are discussed in this section.

Normal Camera and a Neutral Density Filter

Few researchers have tried using neutral density (ND) filters for weld pool observation. This is the same filter which is being used in manual welding helmets. Therefore it was decided to experiment weld pool capturing using a ND filter with a normal camera. The filter glass was placed in front of the lens and the camera was placed at a stand-off of 30cm.
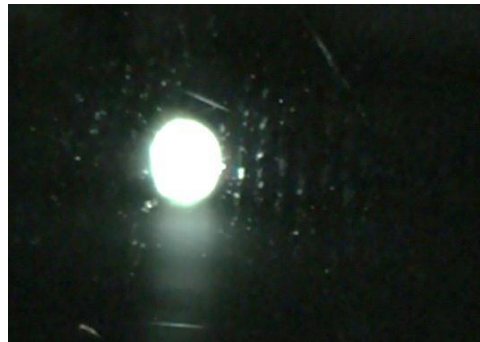
Figure a: Weld area capturing with neutral density filter

The result is shown in Figure a, which does not show satisfactory information. However, this method is not a better solution for viewing weld area since the ND filter naturally filters all frequencies to the same extent and therefore important information such as joint geometry can be lost.

Using High Dynamic Range (HDR) Camera

A HDR camera (120dB) from Stemmer Imaging Technologies was used to directly capture welding area without using any filters or illumination source. Result is shown in Figure b. Welding torch and filler rod is clearly observable. However information of the weld area is missing which can be due to two reasons. First reason can be that since Aluminium was used for the experiment it may have caused more brightness since the surface of the work piece is shiny. Other reason might be the angle of viewing. If viewed from the top it may have caused lesser saturation than viewing at an angle. However this experiment shows the requirement of a filter.
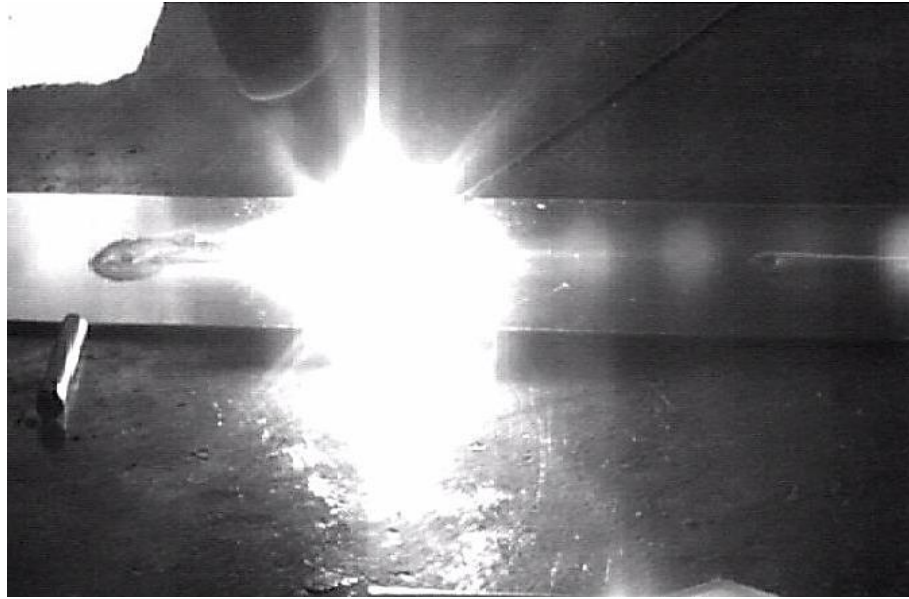
Figure b: Weld area capturing with a HDR camera

High Speed (HS) Camera with a Band Pass Filter and Illumination

After the learning from previous experiments and from literature it was learned that a band pass filter should be used with the camera. However the problem with using band-pass filters is that it filters out most frequencies of the spectrum and therefore some important information also can be lost such as information surrounding the weld point. Therefore additional illumination has to be used at the filtering frequency to aid visualizing for the camera. This technique was experimented with an Olympus HS camera (iSpeed3) and a laser illumination source as shown in Figure c.
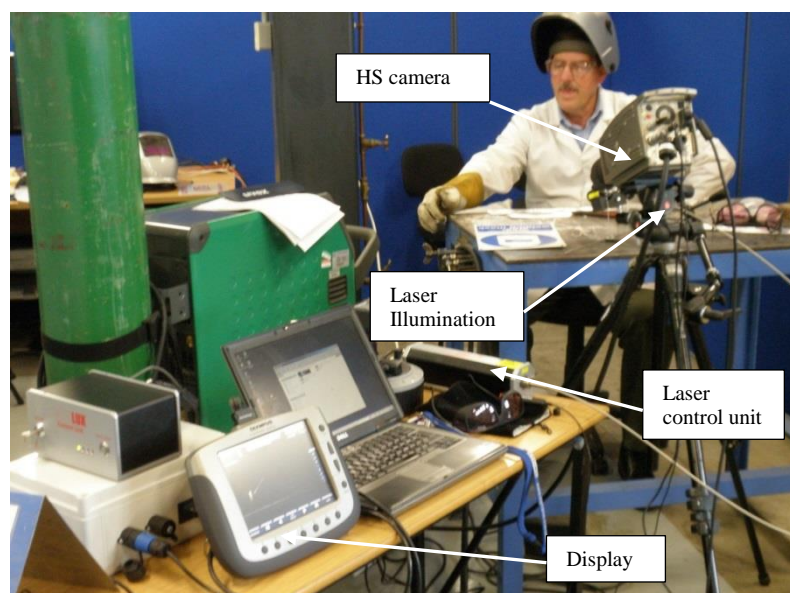
Figure c: HS camera with laser illumination for weld area viewing

Figure d: Weld area capturing using HS camera, band-pass filter and laser illumination

As shown in Figure d, the image was clear and the camera did not get saturated at all. This proves that combination of camera light source and filter is the most appropriate solution for weld area viewing. But, even though the concept is proven still the high speed camera cannot be used in automation due to its bulky size, higher cost and also health and safety issues due to high power laser. In addition there is no flexibility in software modification which limits capability of online processing. Therefore it was decided apply the same concept on a compact, low-cost CMOS camera with a band pass filter and LED illumination array as shown in figure e (a).
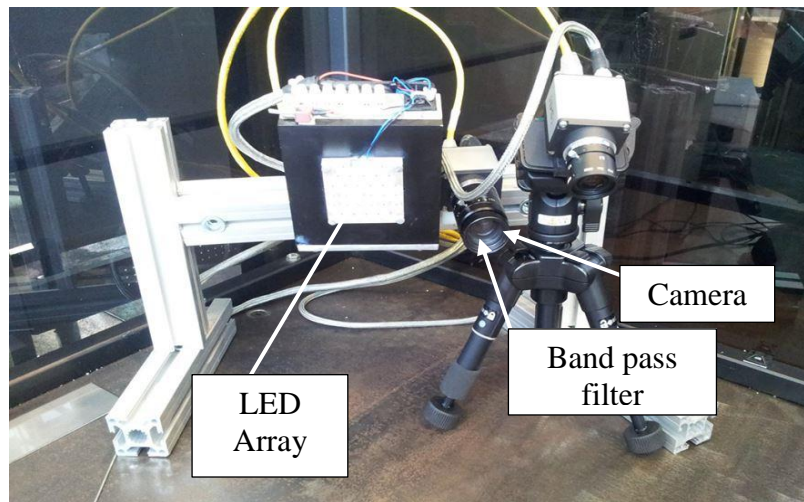
(a)
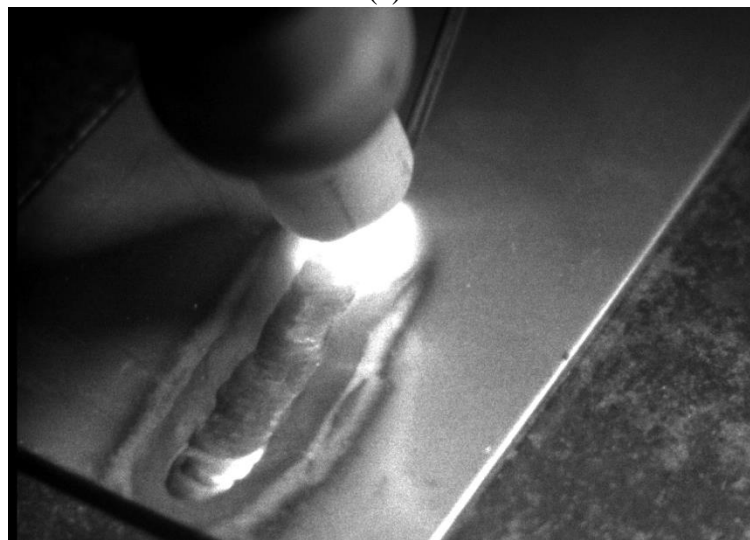
(b)

Figure e: (a) Camera set up weld area viewing (b) results with band pass filter and illumination source

As seen in Figure e (b) there is a clear improvement with this method but still the most important area is saturated with arc light. But the surroundings a much clearer compared to previous experiments. The reason for saturation is that the filtering wave length is lower and for better results it is understood this has to be a higher value. Experiments are planned to use a high power illumination source with a filter at near infrared (NIR) wavelength.

Appendix 5: Relationship between welding voltage and stand-off distance

Stand-off distance between the torch and work piece is vital to maintain the consistency throughout the weld. However as presented in Chapter 4 the method for measuring stand-off distance is by measuring the welding voltage. An experiment was set up as shown in Figure f. Welding torch was held on a retort stand at a known distance from the metal piece. Distance was measured by inserting filler gauges. A stationary weld was carried out for 8 seconds for each stand-off distance and voltage was measured in LabVIEW interface from the welding sensor.
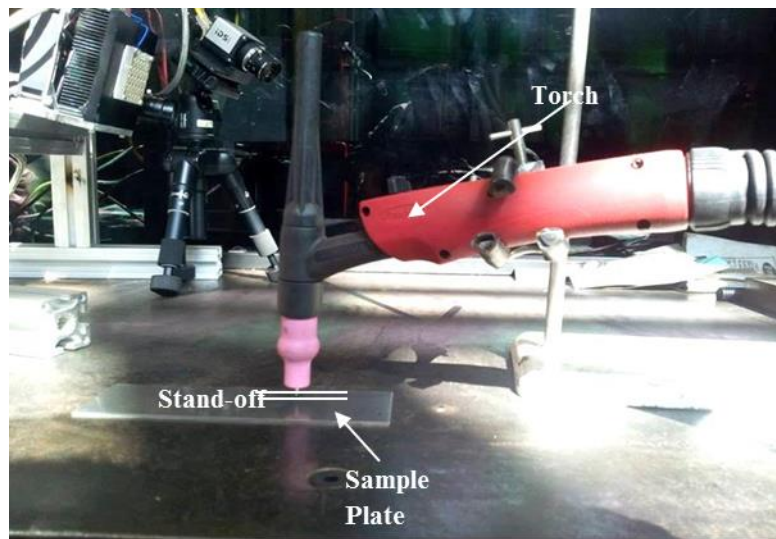
Figure f: test set-up

Figure g shows the voltage measured for different stand-off distances.
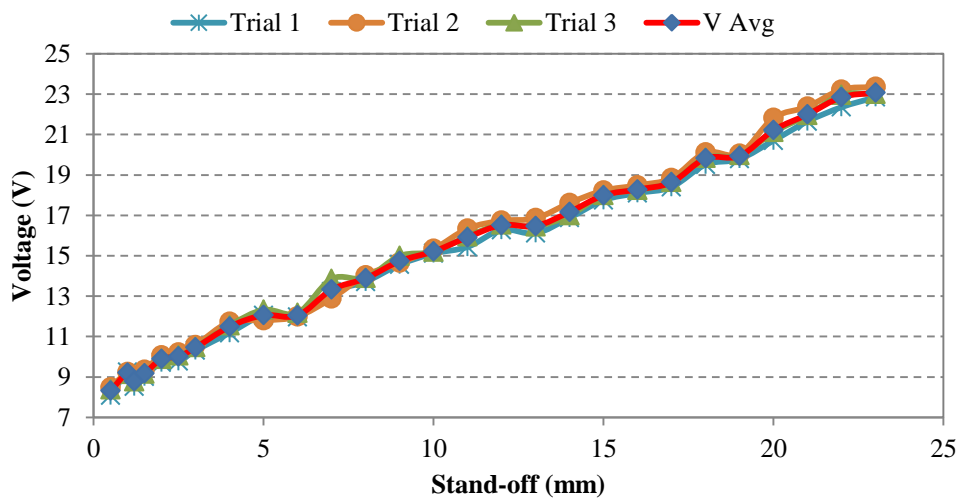
Figure g: Voltage measured for different stand-off distances

As can be seen from the figure, the variation is linear. All three trials were averaged and the trend is observed and the following equation is derived where x is torch stand-off and y is arc voltage.

$$y = 0.6322\,x + 8.5322$$

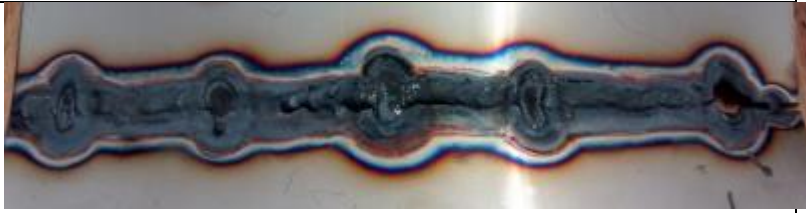Using this equation torch stand-off can be estimated by monitoring arc voltage at a given time.

Appendix 6: Images of the welds completed by manual welder (other than presented in section 4.3.1)

Welder	Image of the weld
N2	
N3	
SS1	
SS2	
S1	
S2	

Appendix 7: Questioner provided to manual welders

1. How experienced you are in welding?
2. What are welding process types you are familiar with?
3. What welding joint type you find more complex out of butt, lap and T-joint?
4. What are weld process parameters which you think will affect the weld quality?
5. What welding parameters will you use for each joint type?
6. What variations did you observe during the welding process?
7. How did you adapt to variations and what parameters did you try to control?
8. What are the main things you look for during welding?
9. How do you assess weld quality while welding?
10. What are the critical tasks in welding? And what is the most important out of that?
11. Did you get any other feedback method than visual feedback?
12. Please comment your experience with a small paragraph.
13. Please suggest any new method that we can use to improve the testing.

Appendix 8: Images of the welds completed by four approaches selected (other than presented in section 9.3)

Approach	Welder	Image of the weld
Constant parameter	Trial 2	
	Trial 3	
Industrial approach	Trial 2	
	Trial 3	
Skilled welder	Trial 2	
	Trial 3	
Adaptive robotic welding	Trial 2	

	Trial 3	